Flexible Discrete Event Simulation Framework for the Development of Integrated Control Strategies Along the Mine-to-Plant Profile

Ryan Wilson

Department of Mining and Materials Engineering

McGill University, Montreal, QC, Canada

August, 2022

A thesis submitted to McGill University in partial fulfillment of the requirements of the degree of Doctor of Philosophy

Abstract

Sustainable mining production is increasingly challenging based on declining global resources of clean ores and current trends in the rates, sizes and grades of new discoveries. This is further compounded by evolving global economics and commodity markets, as well as complex socio-environmental and geopolitical factors. Moreover, ore deposits are subject to wide ranges of geological variability driven by spatio-temporal changes in deposit characteristics, geometallurgical considerations and exploration implications. To improve efficiencies and remain competitive, these operations must adapt their control strategies by optimizing the coordination of inputs and outputs both within and between corresponding process streams. While there are many areas of research and related tool development, pathways for how or when to integrate novel control strategies into existing operating strategies are not clear.

Discrete event simulation (DES) is a computational tool capable of simulating the interplay of important variables and processes within complex mining systems subject to geological uncertainty. Alternate modes of operation are key to the development of effective DES frameworks to model and monitor system performance in response to unexpected changes, e.g. ore feed attributes. The decision to switch between modes is governed by operational policy and is triggered as critical thresholds are crossed, i.e. discrete events. Hundreds of operating days can be simulated to identify potential deficiencies, bottlenecks, or other operational risks. DES is thus useful to support strategic decision-making in the design, development and sustained operation of any mining system.

The current research is focused on the incorporation of a variety of quantitative methods into a DES framework in order to test novel control strategies along the mine-to-plant profile, with a unifying focus on readjustment phases of the mining life cycle. A series of case studies show the utility of a novel flexible and generalizable DES framework towards the evaluation of a broad spectrum of mining system problems spanning commodity markets, operation scales, integration scopes and mine life cycle timing. Common threads between these problems have motivated this research to generalize concepts underlying the integration of mining and downstream processes, to help drive the development of suitable evaluation tools currently lacking in the industry.

Regardless of the data processing technique driving the characterization of ore feeds, the current DES framework acts as a wrapper for the integrated management of downstream processes based on the defined geological variability. For example, Section 4.1 explores the integration of the turning bands geostatistical method for the evaluation of tailings retreatment applications; poorly documented tailings of mixed origin are assessed as a substitute for the clay portion in cement clinker production. Section 4.2 incorporates predictive partial least squares regression modelling to gauge system response for the extraction of bitumen from variably chloride-rich oil sands. A regionalized framework strategy for the processing of low and high-arsenic porphyry copper sulfide ores is developed using Monte Carlo simulation in the Chilean context in Section 4.3. Finally, Section 4.4 integrates multilayer perceptron regression modelling for the regional development of underdeveloped refractory gold systems. In each case, effective control strategies and related operational policies were successfully developed using alternate modes of operation coupled with a combination of stockpiling and blending practices to stabilize/enhance overall plant performance in response to significant levels of uncertainty caused by geological and/or geometallurgical controls.

Résumé

La production durable minière devient plus difficile en raison du déclin des ressources mondiales de minerais propres et des tendances des taux, tailles et teneurs des nouvelles découvertes. Cette situation est aggravée par l'évolution de l'économie mondiale et des marchés des produits de base, ainsi que par des facteurs socio-environnementaux et géopolitiques. Les gisements de minerai sont soumis à de larges variabilités géologiques entraînées par des changements spatio-temporels dans les gisements ainsi que des aspects géométallurgiques. Afin d'améliorer leur efficacité, ces opérations doivent adapter leurs stratégies de contrôle en optimisant la coordination des processus. Bien qu'il existe de nombreux domaines de recherche, l'intégration de nouvelles stratégies de contrôle dans les stratégies d'exploitation ne sont pas claires.

La simulation d'événements discrets (SED) est un outil informatique capable de simuler l'interaction de variables et de processus dans les systèmes miniers complexes soumis à l'incertitude géologique. Les modes d'opération alternatives sont fondamentaux pour le développement de cadres SED pour modéliser et surveiller les performances du système suite à des changements inattendus, par ex. les attributs d'alimentation en minerai. La décision de changer entre les modes est régie par la politique opérationnelle et est déclenchée lorsque des seuils critiques sont franchis, c.-à-d. des événements discrets. Avec la méthode SED, des centaines de jours d'opération peuvent être simulés pour identifier les carences potentielles, les goulots d'étranglement ou d'autres risques opérationnels. La SED est donc utile pour supporter la prise de décision stratégique dans la conception, le développement et l'opération soutenue de tout système minier.

La recherche actuelle se concentre sur l'intégration d'une variété de méthodes quantitatives dans un cadre SED afin de tester de nouvelles stratégies de contrôle le long du profil de la mine à l'usine, avec un accent unifié sur les phases de réajustement du cycle de vie minier. Une série d'études de cas montre l'utilité du nouveau cadre SED flexible et généralisable présenté ici pour l'évaluation d'un large éventail de problèmes de système minier couvrant les marchés des produits de base, les échelles d'exploitation, les portées d'intégration et la synchronisation du cycle de vie de la mine. Les points communs entre ces problèmes ont motivé cette recherche à généraliser les

concepts sous-jacents à l'intégration des processus miniers et traitements ultérieurs, afin de contribuer au développement d'outils d'évaluation appropriés qui manquent présentement.

Indépendamment de la technique de traitement des données pour la caractérisation des charges de minerai, le cadre SED actuel est un emballage pour la gestion intégrée des processus en aval en fonction de la variabilité géologique. Par ex., la section 4.1 explore l'intégration de la méthode géostatistique des bandes tournantes pour l'évaluation des applications de retraitement des résidus. La section 4.2 intègre un modèle de régression prédictif des moindres carrés partiels pour évaluer la réponse du système pour l'extraction de bitume à partir de sables bitumineux à teneur variable en chlorure. Une stratégie-cadre régionalisée pour le traitement des minerais de sulfure de cuivre porphyrique à faible et haute teneur en arsenic est développée à l'aide d'une simulation Monte Carlo dans le contexte Chilien à la section 4.3. Enfin, la section 4.4 intègre la modélisation de régression du perceptron multicouche pour le développement régional des systèmes aurifères réfractaires sous-développés. Dans chaque cas, des stratégies de contrôle efficaces et des politiques opérationnelles ont été élaborées avec succès en utilisant des modes d'opération alternatives associés à une combinaison de pratiques de stockage et de mélange pour stabiliser la performance globale de l'usine en réponse à des niveaux importants d'incertitude.

Acknowledgements

As my PhD studies come to a close, there are many people that I would like to thank for their support over the course of my last three years spent at McGill. First and foremost, I would like to express my sincerest gratitude to Prof. Alessandro Navarra for the opportunity to join the Mining System Dynamics group as his first doctoral candidate. Our fruitful discussions began long before my doctoral residency, and his relentless guidance, motivation, availability and ultimately his trust have been critical to my growth as both a researcher and practitioner in the great and vast world of mining. Over and above your general support, thank you for always finding the time to help steer me back on course. I look forward to continued scholarly discussions, brainstorming sessions and future collaborations!

Great appreciation is owed to all McGill technical and administrative staff for their roles in improving the everyday experience of both staff members and students alike. A special thanks goes out to Barbara Hanley whose dedicated efforts, organizational skills and willingness to help are pivotal to so many of us within the department.

I am grateful to all of my fellow members of the Mining System Dynamics group for all of the discussions, collaborations, successes and failures, and memories that we have shared in the course of our studies. A special thanks to Aldo Quelopana and Javier Órdenes as we each embarked on this journey in a similar window of time, and under similar circumstances – your help, support, and more importantly, your friendships have been greatly valued over these past few years.

I would also like to extend my sincere appreciation to Dr. Patrick H.J. Mercier not only for his collaboration on multiple projects, but also for his valuable guidance, advice and continued support towards my career growth. Your passionate and detailed approach to scientific research is infectious, and I look forward to future discussions and potential collaborations.

A special thanks also goes out to Dr. Tassos Grammatikopoulos for many interesting scholarly discussions and brainstorming sessions over the years. In particular, I thank you for your early guidance and helping set me on this path by way of introduction to Prof. Navarra.

I am ever thankful for all of the great research partners and collaborators I have had the opportunity to work with over these past few years. Without your involvement and contributions,

this body of research likely would have taken a much different trajectory. Specifically, I would like to extend my gratitude to the National Research Council of Canada (NRC), Syncrude Canada Ltd., P.J. Mackey Technology Inc., and Corem for their roles in various research projects. Collaborations with fellow researchers from a number of institutions are also much appreciated, and include Universidad de Chile, Universidad Católica del Norte, University of Antofagasta, Universidad Arturo Prat, and University of Concepción. I believe our diverse backgrounds, experiences and research interests have been indispensable to the formulation of this thesis.

I am much obliged to McGill University and the Department of Mining and Materials Engineering for financial support received through the McGill Engineering Doctoral Award (MEDA) and Graduate Excellence Fellowship programs. Publication support was also garnered through Prof. Navarra by way of the Natural Sciences and Engineering Research Council of Canada (NSERC; grant number 2020-04605). I have also benefitted from a collective partnership with Inspire Resources Inc. and McGill through the MITACS Accelerate internship program; I am thankful for the experience I have gained through this opportunity in addition to financial support in the form of a research stipend.

Finally, I am indebted to my family and close friends as they have been a pillar of strength and support throughout the course of my studies and early career. I thank my parents for their unyielding love and encouragement, as well as their general support in all facets of my life. I owe the deepest of gratitude to my wonderful wife Robyn for her unwavering dedication, love and support. None of this would have been possible without your willingness to explore, openness to change, and steadfast strength. I cannot thank you enough for everything you have done, and the sacrifices made, over these past few very challenging years. I also thank my sons Drew and Nathan for their parts in this journey through both thick and thin. While life is well-known for throwing curveballs, the resilience you have both shown through the changes we have endured as a family is astounding, particularly in light of the adversity brought about by the COVID-19 pandemic. Nothing warms my heart at the end of a difficult day more than hearing your voices and seeing those bright smiles upon your faces. We must always remember that whether side by side, or miles apart, family is always close at heart.

While this thesis represents an end to my PhD studies on the one hand, it also marks the beginning of a truly exciting series of changes in both my career path and life in general. The journey may have felt uncertain and tortuous at times, but the effort and perseverance have been well worth it, and I look forward to a future of interesting and rewarding opportunities and challenges alike.

Contribution of Authors

This thesis is written in a traditional format, and includes work completed between May 2019 and June 2022 as part of the author's PhD studies in mining engineering at McGill University. The work resulted in a series of four peer-reviewed publications, each of which is associated with a specific section in Chapter 4. The author contributions (following the CRediT taxonomy) corresponding to each manuscript are as follows:

Paper #1: Wilson, R., Toro, N., Naranjo, O., Emery, X. & Navarra, A., 2021a. Integration of geostatistical modeling into discrete event simulation for development of tailings dam retreatment applications. *Minerals Engineering,* 164(2021), 106814, pp. 1–11.

Conceptualization, R.W., N.T., O.N. and A.N.; *Methodology*, R.W., O.N., X.E. and A.N.; *Data curation*, O.N.; *Investigation*, R.W. and O.N.; *Formal analysis*, R.W. and O.N.; *Validation*, R.W.; *Visualization*, R.W.; *Writing–original draft preparation*, R.W.; *Writing–reviewing and editing*, X.E. and A.N.; *Supervision*, X.E. and A.N.; *Funding acquisition*, X.E. and A.N.

Paper #2: Wilson, R., Mercier, P. H. J., Patarachao, B. & Navarra, A., 2021b. Partial Least Squares Regression of Oil Sands Processing Variables Within Discrete Event Simulation Digital Twin. *Minerals,* 11(689), pp. 1–30.

Conceptualization, R.W., P.H.J.M., B.P. and A.N.; *Methodology*, R.W., P.H.J.M. and A.N.; *Data curation*, P.H.J.M.; *Investigation*, R.W.; *Formal analysis*, R.W.; *Validation*, R.W.; *Visualization*, R.W.; *Writing–original draft preparation*, R.W.; *Writing–reviewing and editing*, P.H.J.M., B.P. and A.N.; *Supervision*, P.H.J.M. and A.N.; *Funding acquisition*, P.H.J.M. and A.N.

Paper #3: Wilson, R., Perez, K., Toro, N., Parra, R., Mackey, P. J. & Navarra, A., 2021c. Mine-to-smelter integration framework for regional development of porphyry copper deposits within the Chilean context. *Canadian Metallurgical Quarterly,* pp. 1–15.

Conceptualization, R.W., K.P., N.T., R.P., P.J.M. and A.N.; *Methodology*, R.W. and A.N.; *Data curation*, R.W. and A.N.; *Investigation*, R.W. and A.N.; *Formal analysis*, R.W. and A.N.; *Validation*, R.W. and A.N.; *Visualization*, R.W., P.J.M. and A.N.; *Writing–original draft preparation*, R.W., P.J.M. and A.N.; *Writing–reviewing and editing*, R.W., P.J.M. and A.N.; *Supervision*, A.N.; *Funding acquisition*, A.N.

Paper #4: Wilson, R., Mercier, P. H. J. & Navarra, A., 2022. Integrated Artificial Neural Network and Discrete Event Simulation Framework for Regional Development of Refractory Gold Systems. *Mining,* 2(1), pp. 123–154.

Conceptualization, R.W., P.H.J.M. and A.N.; *Methodology*, R.W. and A.N.; *Data curation*, R.W.; *Investigation*, R.W.; *Formal analysis*, R.W.; *Validation*, R.W.; *Visualization*, R.W.; *Writing–original draft preparation*, R.W.; *Writing–reviewing and editing*, P.H.J.M. and A.N.; *Supervision*, A.N.; *Funding acquisition*, A.N.

As previously noted, Ryan Wilson was primarily responsible for study conceptualization, methodological development, investigation and formal analysis via simulation trial work, validation, visualization, and writing of the original manuscripts for each of the case studies listed above. In addition, the candidate was solely responsible for the preparation of the current thesis, including the abstract and all front matter, introduction (Chapter 1), literature review (Chapter 2), overview of integrated DES frameworks (Chapter 3), establishment of discussion points within the mining context and directions for future work (Chapter 5), summary and final conclusions (Chapter 6), and management of the comprehensive reference list.

Oscar Naranjo, under the supervision of Prof. Xavier Emery of the Universidad de Chile, was responsible for the data curation and generation of the geostatistical variability data via the turning bands method in Section 4.1. Elemental, mineralogical and bitumen compositional data for the oil sands study presented in Section 4.2 was collected by staff at the National Research Council of Canada (NRC) in Ottawa, and kindly obtained as part of a joint partnership with NRC and Syncrude Canada Ltd. Prof. Alessandro Navarra assisted with data assembly and simulation trial work for the regionalized smelter study detailed in Section 4.3. Dr. Phillip J. Mackey (P.J. Mackey Technology Inc.) also provided much appreciated feedback and direction for strategy development based on his extensive experience in the smelting sector. Dr. Patrick H.J. Mercier (Corem) provided useful feedback with respect to sensor-based ore sorting technology for the refractory gold study presented in Section 4.4.

Table of Contents

List of Tables

List of Figures

List of Abbreviations

AI	Artificial intelligence	PLS	Partial least squares
AISC	All-in sustaining cost	POX	Pressure oxidation
ANN	Artificial neural network	PS	Peirce-Smith (converting)
AOSR	Alberta oil sands region	QEMSCAN	Quantitative evaluation of minerals by scanning microscopy
ARD	Acid rock drainage	QPA	Quantitative phase analysis
BFS	Bitumen-free solids	REE	Rare earth element
DES	Discrete event simulation	ReLU	Rectified linear unit
FCF	Flash-converting furnace	RMSE	Root mean squared error
FMO	Free-milling ore	RNG	Random number generation
HAC	High-arsenic concentrate	RTO	Refractory type ore
ICP-MS	Inductively coupled plasma mass spectrometry	SD	System dynamics
KPI	Key performance indicator	SGD	Stochastic gradient descent
LAC	Low-arsenic concentrate	SGS	Sequential Gaussian simulation
LS	Least squares	SLO	Social license to operate
MCS	Monte Carlo simulation	SVD	Singular value decomposition
ML	Machine learning	TSL	Top-submerged lance
MLP	Multilayer perceptron	VBA	Visual Basic for Applications
MLR	Multiple linear regression	WD-XRF	Wavelength-dispersive X-ray fluorescence
NPV	Net present value	XRD	X-ray diffraction
OLS	Ordinary least squares		

Chapter 1

Introduction

1.1 Background

With many of the near surface, high-grade ore deposits already identified across most of the easily accessible regions of the world, mining companies are now faced with increasingly challenging prospects. This fact is only magnified by evolving global economics and commodity markets, as well as complex socio-environmental and geopolitical factors. Moreover, mining trends indicate declining rates, sizes and grades of new discoveries among many of the metal sectors; however, this is partly due to companies focusing on brownfields and advanced stage exploration projects, as well as new technologies that have improved the feasibility of processing lower grade material from large-scale open-pit operations (Darling, 2011). Additionally, mining projects are facing increasingly longer start-up timelines related to administrative hurdles, such as obtaining the required approvals and permits from government agencies. Higher levels of undesirable impurities are also being reported from certain ore types, e.g. arsenic in porphyry copper or refractory gold systems; not only are these deleterious elements more difficult (and therefore expensive) to safely dispose of, but they also pose significant health hazards and environmental risks (Perez, et al., 2021).

This collection of trends is causing many mining companies to focus on process optimization and related efficiencies in order to remain competitive. In addition to traditional econometric drivers, there is also a paradigm shift underway to improve energy efficiencies and reduce overall environmental footprints in industrial settings as a matter of importance to community stakeholders and the greater population at large. While there have been rapid advances in technological research and development to meet these goals in the mining industry, equivalent computational tools are lagging behind despite exponential increases in computing power over the past two decades. Indeed, a variety of computational research areas do exist (e.g. Figure 1.1.1); however, pathways on how or when to integrate them with existing control strategies are not clear, and bridges need to be built between academia, government and industry partners.

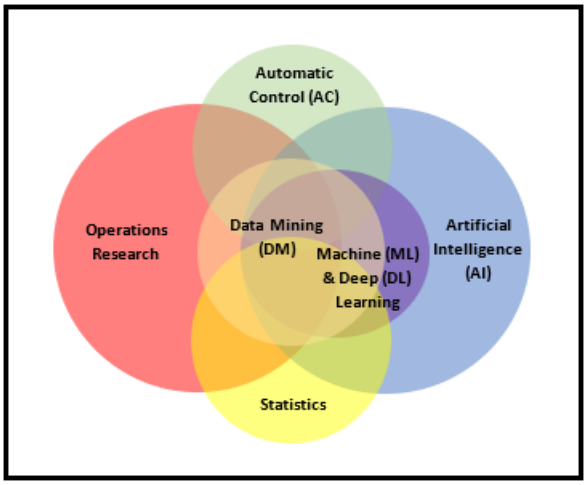

Figure 1.1.1. Venn diagram showing an interpretation of the relationships between various interconnected fields of study at the forefront of process optimization, risk management and automation within industrial and mining system applications.

1.2 Computational Tools for Mining Systems

Mining projects are subject to significant spatio-temporal variability, which can evolve during the course of exploitation or as new characterization data is acquired. As a result, effective control strategies are fundamental to optimize the coordination of inputs and outputs both within and between various process streams, thereby improving overall system efficiencies. However, suitable computational tools are necessary to test new or modified strategies in order to assess the potential effects on system performance prior to implementation, especially for complex industrial systems. The main difference between mining and other industrial systems is the introduction of geological uncertainty, i.e. the random natural variability associated with the abundance and distribution of host-rock mineral assemblages in a given orebody.

System dynamics, often considered a descriptive branch of operations research, is a set of tools and techniques for developing mathematical models of complex systems. The general methodology is useful to identify and quantify causal relationships between variables via simulation modelling to establish critical processes, decision points and parameters within dynamic systems (O'Regan & Moles, 2006; Alpagut & Çelebi, 2003). The approach is thus rather effective in the design and testing of alternative operational policies, relative tradeoffs and resultant system impacts (Alpagut & Çelebi, 2003).

Discrete event simulation (DES) is an important computer-based modelling tool in the implementation of a systems approach because it can simulate the interactions between key processes and parameters in complex systems. Moreover, DES supports the incorporation of random distributions, i.e. it is a form of Monte Carlo simulation (Altiok & Melamed, 2007), and thus can be used to evaluate the system-wide response and sensitivity to unexpected changes in material flows (e.g. ore feed attributes). This is especially useful to mining systems which are commonly subject to significant levels of geological uncertainty; by understanding the potential ranges of variability in upcoming ore feeds, appropriate control strategies can be devised or modified according to the anticipated compositions. As a result, the tradeoffs between available operational policies can be evaluated, as well as the thresholds that prompt the timing of their execution (Navarra, et al., 2019; Saldaña, et al., 2019; Wilson, et al., 2021a). The simulation of extended operating periods allows for the identification of potential deficiencies, such as bottlenecks or other operational risks, in the coordination of unit processes within the target system. DES models are thus useful risk assessment and decision-making tools in the context of any mining system. Moreover, the integration of geostatistical simulations or advanced quantitative methods, such as predictive models built from geometallurgical data collected earlier in the value chain, can further streamline these planning processes.

Given this research falls under the scope of mining engineering practices, it is important to connect the development of novel control strategies along the mine-to-plant profile using DES, as discussed in this thesis, to classical control theory and related automatic control. In some cases, such as mining systems designed around heterogeneous orebodies, it can be difficult (or even impossible) to procure a mathematical dynamical model from physical laws. As a result, internal system state and external input-output relations (i.e. mass balance) are often used to describe the dynamical behaviour of such types of systems (d'Andréa-Novel & De Lara, 2013). In this work, the system state is dictated by different set points (i.e. critical thresholds) for each operational mode, each of which is governed by its own set of operational policies. However, contrary to classical control theory (see d'Andréa-Novel & De Lara, 2013; Evans, 2010), the input-output relations described for the mining systems in this research are not controlled by underlying differential equations but rather by the geological uncertainty inherent to a given orebody. Consequently, these relations cannot be governed by continuously modulated control mechanisms,

such as those used by proportional-integral-derivative (PID) controllers (see Bubnicki, 2005). Instead, system control is thus managed through decision-making logic as defined by the assigned operational policies and related control strategies, e.g. operational buffers such as blending and stockpiling, in response to natural (i.e. stochastic) changes in ore feed attributes, as detected by the system.

The general approach is most suitably compared to modern automatic control theory as described for intelligent agent systems. As shown in Figure 1.2.1, an agent system comprises an agent and its environment; the agent receives stimuli (via sensors) from the environment and executes corresponding actions (via actuators), as necessary (Poole & Mackworth, 2017). The agent is made up of a body and a controller; the body includes transducers that convert stimuli into percepts, and commands into actions, meanwhile the controller receives and sends the corresponding signals from and to the body based on the current system state, operational policy, and/or set goals based on past history, i.e. memories (Poole & Mackworth, 2017). Similarly, when the current DES framework detects a threshold crossing (i.e. a discrete event) for one of the defined control variables, the model decision-making logic is programmed to switch operational modes at the next planned shutdown, or implement a recourse action to provide temporary relief for the stress being experienced by the system (see Section 3.4 for further details). Moreover, both intelligent systems and the current framework can be assembled into hierarchies with the uppermost layers focused on strategic and tactical objectives or goals, with the lowermost layers focused on operational decision-making processes (Quelopana & Navarra, 2021; Poole & Mackworth, 2017).

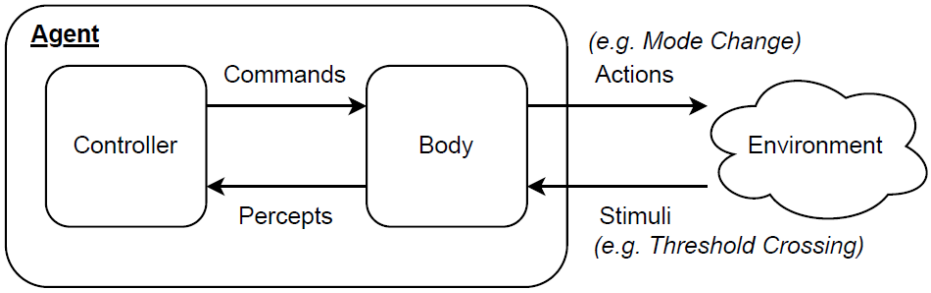

Figure 1.2.1. Schematic diagram showing the relationship of an intelligent agent with its surrounding environment. Similar to the stimuli perceived and actions executed by an automatic control agent, the current DES framework can detect discrete events (i.e. threshold crossings), and implement responsive mode or configuration rate changes in order to achieve a goal (system stability), as governed by the established operational policies (modified after Poole & Mackworth, 2017).

1.3 Research Objectives and Thesis Structure

The key objective of this work is to develop a generalizable methodology to test novel control strategies using integrated DES frameworks. The main advantage of the current approach is the flexibility of the framework to incorporate a variety of data types, quantitative methods, or more detailed models and submodels, as necessary. By breaking down interdisciplinary barriers, this integrated technique is capable of connecting geological attributes (and related uncertainty) to target downstream process parameters for the development of effective operating policies and control strategies. Such a systems approach can lead to improved overall efficiency and/or stability, and thus project sustainability.

In a broader context, there is increasing research interest in ML-assisted operational decision-making processes within industrial systems. However, it is remarkable that there is currently no emerging, unified approach responding to this need within the mining space, particularly for integrated mine-to-mill strategies. There are indeed some excellent highly customized studies that could be better suited to specific functions, but these techniques are often limited by a lack of flexibility. Trying to adapt such methods to new contexts can thus result in a difficult negotiation with the simulation model, rather than fitting the framework around the problem at hand.

To highlight the power of a flexible and generalizable integrated DES framework towards modelling complex mining system dynamics, this research adapts the approach to a broad selection of contexts across the value chain. The remainder of the thesis begins with a high level literature review of the structural controls inherent to mining systems, the general methods used in this research and their scope of applications within the mining sector (Chapter 2). Detailed descriptions of the specific algorithms for each of the integrated quantitative methods, as well as model logic and implementation considerations for the current DES framework, are then provided in Chapter 3. Subsequently, a total of four case studies are developed in Chapter 4; this collection of work focuses on testing novel control strategies along the mine-to-mill (or smelter) profile, with emphasis on the readjustment phases of the mining life cycle. A general discussion draws from the case studies to relate integrated DES frameworks to sustainable mining development within the vein of modern research and development trends, and considerations for future work are also

presented in Chapter 5. Finally, this research work is rounded out with a summary and final conclusions given in Chapter 6. The overall thesis structure is summarized in Figure 1.3.1.

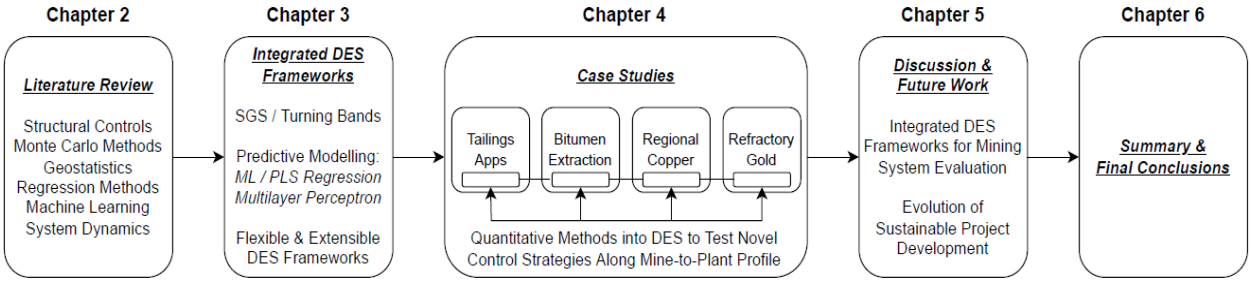

Figure 1.3.1. Schematic flow chart of overall thesis structure.

1.4 Contribution to Original Knowledge

The current thesis has made a number of contributions to original knowledge through the development of a series of case studies focused on the integration of mining (i.e. ore feed supply) and downstream mineral processing. Following earlier work by Navarra et al. (2019):

1. The DES framework was extended to accept different data types, include additional ore types, and stabilize the return to normal mining conditions (i.e. rates) following a required mining surge as a recourse action to ore stockouts.

2. The developed methodology has bridged different data processing techniques with the DES framework in a way not previously reported in the mining literature. Similar architectures have been reported in the manufacturing industry, but this work represents a significant extension; by crossing interdisciplinary barriers, the current approach links the richness of geological descriptions with downstream process management. In this regard, the framework acts as a wrapper that can integrate any selected quantitative method for the characterization of ore feeds and related geological uncertainty.

3. This approach has shown the utility of a flexible and generalizable framework towards addressing a variety of ore supply problems across the mining spectrum, which fills a particular void cited in the literature as key to supporting future innovation, especially for processes driven by artificial intelligence and machine learning. The advantage of an extensible framework also allows for hierarchical detailing, with the capability to

incorporate more detailed models and submodels, as the project advances along the development pipeline.

4. To the best of the author's knowledge, this work represents a first for the incorporation of geostatistical methods (e.g. turning bands) or advanced predictive modelling tools, such as partial least squares or multilayer perceptron regression, into DES in a mining context. This is of high impact to the industry as it allows for the identification of potential downstream processing issues related to supply of distinct ore feed types caused by the significant geological uncertainty inherent to many types of ore deposits.
5. This research also demonstrates a pathway for the development of simulation-based digital twins, which are becoming increasingly important in the age of Industry 4.0 and related Internet-of-Things systems. The current framework is shown to represent a digital model intended primarily for offline use during the design and implementation stages of project development; however, with sufficient data, testing and validation, the framework can be integrated into an online control system.

The overall methodological contribution of the present research is developed and expanded upon in Chapter 3 of this thesis. The approach is then validated in Chapter 4 through the development of novel or improved control strategies along the mine-to-plant profile for a variety of mining problems that span commodity markets, operation scales, integration scopes and mine life cycle timing.

Chapter 2

Literature Review

2.1 Structural Controls of Mining Systems

It is well-known that the incorporation of geological uncertainty is critical to the development of advanced modelling and optimization techniques. However, in order to establish suitable distributions for a given mineralized body, it is important to understand some of the main contributing factors that can drive this variability. Only then can an evaluation tool be used with sufficient confidence to develop and implement robust control strategies capable of stabilizing (and maximizing) system performance in response to unexpected changes. There are a number of structural controls inherent to mining systems and related business development models that can significantly affect how and when ore is mined and processed; this overview is focused specifically on geological and geometallurgical controls.

Geological controls are fundamental to the formation, distribution and ultimately the quality of mineralization in mining systems, and can be determined from the district scale down to individual orebodies and even local mineralized zones. Ore deposits can be characterized in a variety of ways, and improving our understanding of them can help better predict potential spatio-temporal changes in ore feed attributes. Deposit morphology, such as inclination, thickness, depth and geometry, can help in the selection of suitable mining methods (Nelson, 2011). Orebodies can be flat, inclined or steep; mineralization can be massive, tabular, or irregular, and; systems can be hundreds of meters wide, or follow along narrow vein sets (Herrington, 2011). Regardless of the mineralization style, these factors directly affect the planning and scheduling of mine development and production, as well as downstream processing parameters.

The genetic model and deformation history of a deposit are critical to understand the expected composition and location of mineral assemblages, as well as the geotechnical attributes of the host rocks. They also provide clues as to the types and degrees of spatial variation that can be expected within and between mineralized zones, as well as the potential for new discoveries. For example, volcanogenic massive sulfide (VMS) deposits typically form in extensional settings at or immediately beneath the seafloor. Mineralizing fluids ascends along synvolcanic fault systems

from a magmatic heat source at depth, and precipitate metals in predictable zonation patterns based on differing solubilities as the fluids cool (Shanks & Thurston, 2012). In general, higher temperature metals such as copper ± gold drop out of solution first in the core of the hydrothermal system, and lower temperature metals such as zinc, lead and iron precipitate later in more distal areas to the fluid flow. However, these patterns can be obscured and/or altered by later stage alteration and mineralization events as the hydrothermal fluids evolve over time. Long-lived magmatic systems can also produce stacked ore lenses over tens of thousands of year following periods of quiescence and sedimentation that bury each mineralization episode, e.g. the Noranda VMS base metal ± gold camp, Quebec, Canada; see (Franklin, et al., 2005).

Similarly, the distribution and variation of ore deposits are strongly affected by mineralization controls, i.e. fluid conduits and conditions that allow for the accumulation and/or concentration of ore minerals. For instance, mineralized zones can follow along stratigraphic bedding planes, e.g. the Red Dog sedimentary exhalative (SEDEX) Pb-Zn(-Ag) deposit, Alaska, USA (Leach, et al., 2005); concentrate within structural traps such as regional faults and folds, e.g. the Timmins gold camp, Ontario, Canada (Bateman, et al., 2008); or even be transported by post-mineralization processes such as faulting and debris flows, e.g. the Buchans VMS base metal camp, Newfoundland, Canada (Binney, 1987). Chemistry and dynamics of the host rocks and mineralizing fluids are also important to understand mineralogical variation and delimit different mineralized domains for a given deposit type. As an example, oxidation-reduction (a.k.a. redox) fronts are ultimately responsible for the supergene enrichment and related mineralogical variation observed in the world-class porphyry deposits of the Andean copper province (further described in Section 4.3). Similar weathering processes alter the mineralogical assemblages and concentrate metals in the important lateritic nickel ± cobalt class of deposits that form under warm and humid conditions in the tropical regions of the world (Freyssinet, et al., 2005).

From a geometallurgical perspective, there are various factors that can significantly impact operating parameters and related policies for downstream processing, particularly for a heterogeneous ore deposit subject to geological and mineralogical complexities. While some deposits may contain single target ore minerals, e.g. orogenic lode-gold (Dubé, et al., 2017), others can be polymetallic in nature (e.g. base metal deposits). Moreover, complex ores often contain

multiple different mineral phases containing the same target element(s), each with different stoichiometries, crystal structures and/or redox states (i.e. mineral groups) that could drastically affect ore beneficiation process streams based on differing ore characteristics and thus metallurgical responses. As a result, the attributes of the deposit and contained minerals should ultimately dictate the extraction process and related parameters (Grammatikopoulos, 2018). In other words, deposits can exhibit large variations in terms of mineral speciation, abundances, grain sizes and textures, in addition to the liberation characteristics of the target mineral(s), all of which can directly influence final recoveries and product grades. Evaluation of mineral liberation vs. particle size is particularly important for determining the grinding energy (i.e. comminution parameters and related costs) required for beneficiation, flotation or gravity (Grammatikopoulos & Downing, 2020). For instance, certain coarser-grained minerals with particular textures may be well-liberated and exposed through typical comminution practices, but the same parameters applied to fine-grained target minerals, or those with more complex textures, may have little success. In addition to poor recoveries, this latter scenario may also result in undesirable entrainment of gangue minerals that effectively dilute the final concentrate grade (Meng, et al., 2017; Grammatikopoulos & Downing, 2020).

Appropriate mineral speciation and elemental deportment testwork plays a crucial role in helping determine the recovery potential of different ore domains (Grammatikopoulos & Downing, 2020), which is necessary for effective flowsheet development as well as the establishment of robust operational modes and associated policies. For example, in the case of a system with multiple valuable minerals, ideal grade-recovery of the first valuable mineral may require partial to complete rejection of a secondary target mineral (Jordens, et al., 2016; Grammatikopoulos & Downing, 2020). This has clear implications for flowsheet design and related process parameters, such as the potential need for secondary circuits, additional reagents, modified operating conditions, or the like. Moreover, such a scenario would likely have a negative impact on overall plant performance in response to unexpected changes in ore feed attributes caused by geological uncertainty; this underscores the importance of incorporating process mineralogy data into the design of suitable control strategies along the mine-to-plant profile.

While some ores benefit from multiple payable elements, others suffer from high levels of deleterious elements (i.e. impurities), such as arsenic, antimony or mercury, which can be detrimental to both health and the environment. This has significant implications not only for offgas emissions, capture/handling and tailings storage, but also for mining projects that float concentrates with the intention of shipping their product to international smelters and refineries. Because impurities are most often intimately linked to the target valuable minerals, operational risks here include high penalty element costs, or the rejection of the concentrate altogether. Recent reviews have stressed the increasing importance of these issues for global supply and demand chains in the context of the copper industry due to projected increases in arsenic levels associated with a trend towards complex sulfide-rich ores, especially from the Andean Copper Province (Perez, et al., 2021; Flores, et al., 2020). Similar processing challenges associated with arsenic-enriched systems are also abound in the gold sector, particularly with respect to sediment-hosted refractory ores, e.g. (Asamoah, 2021; Wang, et al., 2019; Thella, 2018).

This research will expand on several examples that highlight the effect of ore variability caused by geological and geometallurgical controls on downstream processing, including poorly documented and complex tailings of mixed origin, variable chloride content in oil sands, and complex As-rich copper and refractory gold ores. However, the same concepts hold true across many deposit types and commodity sectors, as indicated by the following (non-exhaustive) review of various recent studies. Peña-Graf et al. (2021) stress the importance of using process mineralogy to delineate chromite ore domains for the development of effective operational modes, particularly with trends towards depletion of high-grade deposits, continued deterioration of ore quality and increasing metallurgical complexities. Due to the variable characteristics of low-grade chromite ores caused by elemental substitutions (e.g. Cr:Fe ratio) and increased silicate gangue minerals, the additional grinding energy required for liberation results in poorer recoveries owing to excess ultrafine particles that report to the tailings stream.

Zhu et al. (2020) show that process mineralogy is critical to the beneficiation of spodumene, an important Li-bearing pyroxene mineral common to (± pegmatitic) granitoid rare earth element (REE) deposits. Results indicate the variable effects of transition metal (e.g. Fe, Mn, Cr) substitutions on crystal surfaces affecting response to froth flotation with sodium oleate (NaOL)

in ores from the Koktokay Mine, Xinjiang, China; this is notable for ore domain classifications given the high potential variability of elemental distributions in REE deposits (Van Gosen, et al., 2017). Similarly, recent work by (Jordens, et al., 2016) couples automated mineralogy (QEMSCAN), geochemistry (ICP-MS) and first-order kinetic modelling with lab-scale flotation testwork to show a spectrum of flotation behaviours for a complex suite of target rare earth minerals in preconcentrated ore from the Nechalacho REE deposit, N.W.T., Canada.

Xie et al. (2022) report on a related class of deposits with a geochronological and geochemical characterization study of the Baishitouwa quartz-wolframite vein-type deposit, Southern Great Xing'an Range tungsten (W) belt, NE China. The work indicates two distinct stages of wolframite mineralization resulting from different crystallochemical substitution mechanisms as the hydrothermal ore-forming fluids evolved during fractionation of the underlying W-rich granitoid source rocks. The ore types are variably mixed throughout the deposit, but can be distinguished based on trace element compositions: wolframite (I) contains notably higher Nb, Ta, Sc, Zr, Hf, Pb and Eu concentrations, but is depleted in Ti, Sn, Cr and Th compared to wolframite (II). Using process mineralogy to delimit ore domains will be especially important for flowsheet development due to the fine-grained nature of wolframite (II) requiring increased grinding for liberation; micro-flotation tests have shown that flotation of fine wolframite and quartz particles can be problematic with activated quartz reporting to, and thus diluting, the concentrate grade (Meng, et al., 2017).

With the proliferation of Industry 4.0 and the clean energy transition, market demand for a number of rare critical metals is increasing at unprecedented rates. As many of these metals are sourced as by-products from complex polymetallic deposits (e.g. ~70% of global cobalt production is sourced from stratiform sediment-hosted As-bearing copper ores of the Central African Copperbelt; U.S. Geological Survey, 2021), there is an abundance of additional examples that could have been described. The key here is that as 'easier' near-surface and giant/world-class deposits of all types continue to be depleted, or as rarer commodities are sought, the industry will be increasingly challenged to source ores from more difficult and complex mineralized systems in order to meet global demand. In addition to technological advancements, it is clear from these recent examples that suitable computational tools are needed to address these issues and help with

project evaluation, as well as the design and implementation of effective control strategies along the mine-to-plant profile in response to geological uncertainty.

2.2 Monte Carlo Methods via Random Number Generation

Random Number Generation (RNG) and related simulation methods (i.e., Monte Carlo) have grown in importance for many scientific fields over the past two decades with explosive advances in computing power and technological frameworks. The generation of random numbers is central to a multitude of statistical and computer-based simulation methods. The most primitive of examples of RNG might include the physical actions of flipping a coin (binary) or rolling a set of dice (combinatorial). However, such methods would be much too cumbersome when large sets of random numbers are required or for the purpose of modelling uncertainty in complex systems.

There are two main types of RNG: 1) those based on physical phenomena (i.e., (sub-)atomic interactions) and linked to entropy derived from the effects of quantum physics (e.g., radioactive decay, electromagnetic noise, etc.), and; 2) those derived from computer-based algorithms (L'Ecuyer, 2017; Knuth, 1998). The former physical type is considered truly random (TRNG) because it depends on natural, fully stochastic processes (in theory) but typically requires a transducer, amplifier and digital converter in order to record the signal. Not only is such a setup highly inconvenient and time-consuming for most practical purposes but the equipment used to capture the data could introduce their own systemic form of bias (L'Ecuyer, 2017). The latter computational form of number generation is considered pseudo-random (PRNG) because it is actually deterministic in nature and generates sequences of pseudo-random numbers that emulate a uniform distribution of independent random variables over the unit interval (0, 1) (L'Ecuyer, 2015; Gentle, 2003). It is from these basic sequences that pseudo-random numbers are derived for other types of distributions (e.g., Poisson, Weibull, etc.) (Gentle, 2003).

Probability theory is a subdivision of mathematics that defines random variables with respect to probability spaces which assign probability measures (between 0 and 1) to sets of outcomes termed sample spaces (L'Ecuyer, 2015). This concept is fairly abstract and therefore the coding of truly random (definite and exact) realizations on a computer has never been clear (L'Ecuyer, 2015), hence the deterministic approach which has been suitable for most applications (Knuth, 1998).

The implementation of RNG is integral to Monte Carlo simulation (and other probabilistic algorithms), which can be loosely defined as a set of methods that use a series of random number 'experiments' to evaluate and approximate the behaviour of systems. As the experimental units are generated at random, there is a strong requirement in the literature that these input data are strictly reproducible given the same initial conditions (Gentle, 2003).

In the mining context, Monte Carlo methods are often used for numerical experimentation with the key goals of performing a sensitivity analysis to validate a model, optimize parameters and/or evaluate risk indicators within a real-world process or system (Kleijnen, 2012). The methods produce output probability distributions, and associated target statistics are calculated to analyze and better understand specific systems.

The application of Monte Carlo simulations in combination with geological sampling campaigns is especially useful in the evaluation of complex mining systems because of the high degree of uncertainty inherent to mineral deposits (geological uncertainty), economic conditions (volatile commodity markets) and potentially unforeseen future cost factors. While conventional methods involve the creation of models that simply evaluate best- and worst-case scenarios, the Monte Carlo approach allows for the analysis of many (e.g. tens or hundreds) equiprobable scenarios that span the entire spectrum of possible feasible outcomes. This allows for the evaluation of the system-wide effects caused by uncertainty via monitoring of key performance indicators (KPIs), such as net present value (NPV) or internal rate of return (IRR); confidence intervals can then be built from the resultant distributions for target variables of interest (Guarnera & Martin, 2011). Monte Carlo simulation can thus be regarded as a form of stochastic analysis in that risks can be weighed, and decisions made based on a robust model that describes the process or system as a whole. This is of particular significance to the development of quantitative frameworks that incorporate geostatistical and/or geometallurgical attributes into strategic planning and decision-making pathways.

2.3 Geostatistical Estimation and Simulation

Geostatistics is a subclass of statistics that describes and estimates unknown values based on spatial $\pm$ temporal characteristics. The development of geostatistical methods and tools originated in the mining industry in the 1950s to early 1960s, particularly to estimate the distribution of ore

in the gold sector of South Africa (Pawar, 2003; Abzalov, 2016). While these methods are based purely on statistical principles and have been applied across many scientific disciplines, the techniques are termed 'geostatistical' due to their early and widespread implementation in geology (Pawar, 2003). Geostatistical methods have wide-reaching applications in mining, including mineral resource estimation, evaluation of model uncertainty, risk quantification, and determination of optimal spatial patterns, such as drillhole and sample spacings (Abzalov, 2016; Wackernagel, 2003).

In the context of resource estimation, an unknown value is assumed to be a random variable with the probability of having a certain value given by the cumulative distribution function at that particular location (Pawar, 2003). Linear univariate geostatistical estimators, such as the popular kriging methods (Krige, 1951; Krige, 1952), model the spatial continuities of regionalized variables and integrate these parameters (e.g. covariance) into regression techniques used for spatial interpolation between sample locations (Abzalov, 2016). Equivalent multivariate techniques, e.g. co-kriging, are used when there are multiple variables of interest to be estimated at each location in order to amalgamate the different data types into a single coherent model (Abzalov, 2016; Wackernagel, 2003).

Initial project evaluations are typically based on geologic block models produced via kriging (or its variants) of the target variable(s) of interest from sparsely distributed sample data collected during exploration or early infill drilling campaigns. However, while a necessary starting point, these localized resource estimates are deterministic in nature and only provide the best estimate (in a least squares sense) from a single set of data points. Similar to other weighted average-based estimators, this results in smoothing effects whereby small values are overestimated and large values are underestimated, a consequence of the *information effect* (Vann, et al., 2002; Journel & Huijbregts, 1978). In other words, the estimated variance is reduced to below that of the true value, and neither the variogram nor the histogram are exactly reproduced (Yamamoto, 2005). Moreover, geological uncertainty cannot be properly assessed as kriging variance is strongly controlled by sampling patterns without taking into account the magnitude of measured values that inform the estimated values (Ortiz, 2020).

To mitigate these issues, a variety of geostatistical simulation methods have been developed that provide probability maps for the variable(s) of interest. The primary aim of these stochastic techniques is to generate a series of equiprobable statistical realizations from which a distribution of possible values can be randomly drawn for the target variable(s) at each unknown location, i.e. they are a form of Monte Carlo simulation. Each realization is either accepted or rejected based on its ability to honour the original sample data values and geological interpretations, and to reproduce the histogram (basic statistics) and variogram (spatial variability) from the measured dataset (Ortiz, 2020). Unlike the estimation methods which aim to reduce overall residual error, this definition of quality results in a set of plausible realizations that cover a range between optimistic and pessimistic scenarios. Therefore, confidence intervals can be built to quantify the geological uncertainty that may be experienced in downstream operating processes in order to conduct appropriate risk assessments.

In practice, implementation of geostatistical simulation requires the specification of a stochastic model, i.e. a random field model that describes the spatial distribution of the regionalized (or co-regionalized in the multivariate case) variable(s) of interest, and an algorithm (Paravarzar, et al., 2015; Chilès & Delfiner, 2012). There are a number of different families of simulation algorithms from which to choose, mainly depending on the nature of the variable(s) under investigation (Ortiz, 2020; Abzalov, 2016; Vann, et al., 2002):

1. Continuous variables (e.g. ore grades, deleterious element concentrations, unit thickness) are typically simulated using Gaussian-based methods such as sequential Gaussian simulation (SGS) or the turning bands method;
2. Categorical variables (e.g. geologic units/structures, faults) are most often modeled using non-parametric methods such as sequential indicator simulation (SIS), and;
3. Object-based variables i.e. defined by location, shape and orientation (e.g. mineral grains) are usually handled using point processes or Boolean methods.

This simplified list is by no means exhaustive as there are many other relevant and emerging simulation approaches that can be applied depending on the specific context; there are a number of great references available in the literature that review the details of the most pertinent and well-

established methodologies in the mining sector, e.g. (Chilès & Delfiner, 2012; Chilès & Lantuéjoul, 2005; Lantuéjoul, 2002).

It is noteworthy that simulation algorithms can also be distinguished based on conditioning to the existing measured data points. A realization is said to be 'conditional' if it reproduces the original sample values at the sample locations (Ortiz, 2020). However, there is a key distinction between methods with built-in conditioning (e.g. sequential methods) and those that require an additional step to condition the simulated estimates to the sample values (e.g. turning bands) (Vann, et al., 2002; Emery, 2008). Further details on the SGS and turning bands methods for the simulation of continuous variables are provided in Sections 3.1.1 and 3.1.2, respectively.

Given the high risk nature of mining projects, it becomes increasingly important to understand the technical, operational, and financial deviations that can result from geological uncertainty as a project progresses from early evaluation towards detailed planning and development (similarly for continuous improvement and reengineering projects). As a result, geostatistical simulation can be an invaluable risk assessment tool by improving the representation of potential variability that might be expected from ore feeds upon extraction. This can have far-reaching implications for ore block classifications and strategic mine planning, as well as other decision-making processes such as development of suitable operational policies and related process control strategies.

2.4 Multivariate Regression Methods

Multivariate statistics is a branch of statistics dealing with methods that examine the simultaneous effect of multiple variables, and which are traditionally classified based on the notion of (co-)dependency between variables (Marinković, 2008). Similar to many other computational-based fields, this area of research has expanded greatly over the past few decades due in large part to significant technological advances in computing power and data frameworks. Unlike univariate and bivariate analyses, which usually focus on simple population estimators (e.g., mean, variance, etc.) or the pairwise relationship between two variables, multivariate techniques are centered around the analysis of covariances (or correlations) that reflect the extent of relationships between three or more variables, as well as similarities indicated by relative distances in n-dimensional space (Marinković, 2008).

There are two main types of multivariate statistical methods (Marinković, 2008):

1. Dependence methods, which aim to explain or predict one or more dependent (response) variables from a set of independent (predictor) variables (e.g. multiple linear regression), and;
2. Interdependence methods, which are less prediction-oriented and seek to provide information about the underlying data structures by simplifying through data reduction and developing taxonomical classifications (e.g. principal component analysis).

Parts of this research touch mainly on the former class of methods, with emphasis on regression techniques. Specifically, multivariate regression analysis aims to predict values of one or more response variables from a set of predictor variable values, and can also be used to assess the relative importance of each independent variable on the resultant predictions (Johnson & Wichern, 2007). In the case of continuous variables, there is a variety of regression methods from which to choose, both linear and non-linear (e.g. polynomial); this overview only deals with the linear methods.

Depending on the nature and number of variables under investigation, as well as the primary objective of the analysis, there are several linear methods that can be applied such as multiple linear regression, partial least squares, and canonical correlation analysis. Regardless of the selected approach, all of these variations belong to the family of least squares (LS) methods, which likely represents the most well-established and popular set of techniques in modern classical statistics. Initially developed at the dawn of the 19th century, the LS methods are now commonly used to estimate the numerical values of the parameters to fit a function to a set of data and characterize the statistical moments of these estimates (Abdi, 2010a). The simplest version is known as ordinary least squares (OLS), from which a number of extensions have been derived including weighted, alternating and partial LS variants.

Multiple linear regression (MLR) is based on OLS, which relies on the *normal equations* to estimate the free parameters (i.e. the intercept and regression coefficients) of the line or plane of best fit, meanwhile respecting a particular set of constraints. The optimal solution (in a least squares sense) is that which minimizes a target metric such as the sum of squared errors, i.e. the residual distances from the regression line or plane. The methodology can be interpreted from a geometrical perspective as an orthogonal projection of the data vector(s) onto the space defined by

the independent variable(s) (Abdi, 2010a). Because MLR is a straightforward extension of simple linear regression, it is relatively easy to understand and implement; as such, the approach has a long history of successful applications across many scientific disciplines.

In the earth sciences alone, MLR has been applied to many varied contexts, such as evaluation of landslide potential from remote sensing imagery (Zhang, et al., 2012), soil characterization studies (Ataee, et al., 2018; Egbe, et al., 2017), water quality assessment (Chenini & Khemiri, 2009), hydrogeologic basic characterization (Lystrom, et al., 1978), land and water use studies (Stokes, et al., 2017), among others. Specific to geology and mining, a number of recent studies highlight the potential for MLR applications across the mineral value chain, including:

- Development of geophysical-based exploration models (Feizi, et al., 2021);
- Hydrocarbon reservoir characterization (Almeida & Carrasquilla, 2017; Eskandari, et al., 2004) and production potential (Niu, et al., 2021);
- Prediction of geomechanical properties (Hu, et al., 2010) and rock fragmentation (Enayatollahi, et al., 2013);
- Blasting dust assessment in coal operations (Roy, et al., 2011);
- Modelling of semiautogenous grinding (SAG) systems (Villanueva, et al., 2020);
- Prediction of geometallurgical ball mill throughputs (Both & Dimitrakopoulos, 2021);
- Analysis of operating parameters and chromite flotation performance (Deniz, 2020);
- Estimation of gold recovery from cyanide leaching (Azizi, et al., 2012), and;
- Metal extraction efficiency through IoT systems (Maheswari, et al., 2020).

However, the implementation of MLR is not without its limitations as it maintains a strong set of statistical properties and related constraints. For instance, the assumption of linearity alone can make it a poor choice for modelling many complex systems, particularly in the mining space where extracted ores undergo a number of sequential unit separation processes, each with their own set of parameters. Nonetheless, an overview of the MLR approach is important to better understand the basis of, and extension to, partial least squares (PLS) regression which is developed in detail for the oil sands case study presented in Section 4.2. Further details on the mathematical basis of MLR models, related implementation considerations, and alternative approaches are provided in Section 3.2.

2.5 Machine Learning Approaches

2.5.1 General Overview

Artificial intelligence (AI) is a branch of computer science focused on the development of 'intelligent agents', i.e. systems that are capable of perceiving their environment and acting in such a way that maximizes the probability of achieving a set of goals (Poole, et al., 1998). Machine learning (ML) is a division of AI concerned with the design of algorithms that aim to optimize the performance of a specific task by learning from examples and/or past history (Alpaydin, 2014). In other words, machine learning comprises a set of techniques that can be used to solve specific problems within a given system. With digitalization and automation trends (e.g. Industry 4.0), coupled with significant improvements in computing power, the increasing availability of large datasets (i.e. 'big data') has driven a recent surge in ML algorithm research and development. As a result, ML approaches are now successfully applied to a variety of classification, regression, clustering, and dimensionality reduction tasks (Schmidt, et al., 2019; Marsland, 2015). In particular, ML techniques are capable of extracting hidden relationships from large multivariate datasets accumulated in complex and dynamic environments (e.g. industrial systems) (Schmidt, et al., 2019; Wuest, et al., 2016). A key advantage of ML algorithms over classic statistical methods, such as multiple linear regression, is the ability to model and learn non-linear relationships. This is particularly important to industrial systems, wherein the final system outputs are usually produced from the initial inputs via a series of coordinated unit processes, each with their own specific operating policies and related parameters.

Machine learning tasks can be divided into three main categories, including supervised, unsupervised, and reinforcement learning techniques (Figure 2.5.1). Supervised learning involves model training with paired data for both input and target output variables (i.e. labeled examples) in order to map relationships between the two spaces; the derived function is then used to classify the example, or predict a continuous value (regression). In unsupervised learning, model training is carried out on unlabeled examples, i.e. input data have no corresponding target output value(s). Unsupervised methods can also be further subdivided into clustering and association tasks. Whereas clustering entails the grouping of examples based on similarities (distance in the sample space), an association rule determines relationships between variables such as the likelihood that

the value of a particular feature can be predicted given that of another feature (Chaudhary, et al., 2020). Reinforcement learning falls somewhere between supervised and unsupervised learning as the algorithm is told when the answer is wrong, but not how to correct it (Marsland, 2015); the technique explores multiple different sequences in order to maximize a reward by combination of optimal or sufficiently good individual actions (Schmidt, et al., 2019). There are also a number of hybrid or ensemble ML methods that combine elements from any of these base model approaches.

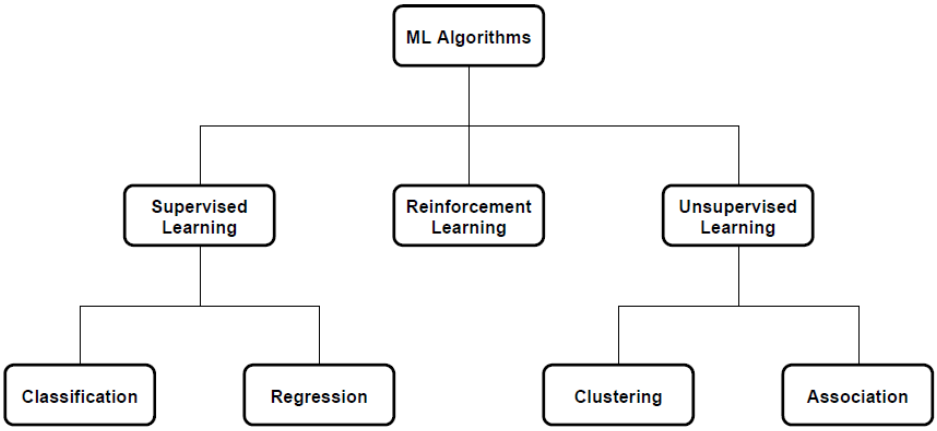

Figure 2.5.1. General classification scheme for different machine learning approaches.

Compared to other industries, the mining sector has been relatively slow to adopt machine learning approaches in common practice (Narendran & Weinelt, 2017; Ali & Frimpong, 2020). Regardless, a recent surge in research and development over the last few years has shown that ML techniques can be successfully applied to a broad spectrum of the mineral value chain, from greenfield exploration through to production, mine closure, and site reclamation. There are a number of review papers available that summarize a variety of ML applications in the mining space, e.g. (Ali & Frimpong, 2020; Jung & Choi, 2021; Dumakor-Dupey & Arya, 2021; McCoy & Auret, 2019; Jang & Topal, 2014), including mineral exploration and resource evaluation, strategic mine planning, machine operations and related automation, drilling and blasting optimization, and ore beneficiation, among others.

However, there is little published work related to the integration of ML techniques into mine-to-plant DES framework strategies. This research intends to employ an artificial neural network, a type of supervised ML algorithm, for the classification of gold ores based on predicted metallurgical response to standard cyanidation and recovery practices from geological data. These

predicted proportions of conventional and refractory ores will then be fed into the current DES framework to evaluate system response to the significant geological uncertainty expected from varied ore sources (see Section 4.4). As discussed above, a specific advantage of this approach over the predictive PLS regression algorithm used in Section 4.3 is the ability to map non-linear relationships, as would be expected for sequential unit separation processes, between the predictor and response variable sample spaces.

2.5.2 Artificial Neural Networks

According to recent reviews, artificial neural networks (ANNs) are among the most popular ML approaches used in many industries, such as manufacturing (Fahle, et al., 2020), maintenance (Carvalho, et al., 2019), solid-state materials (Schmidt, et al., 2019), and mining (Ali & Frimpong, 2020; Jung & Choi, 2021). The underlying concept for ANN models is based on the functioning of the human brain, wherein activated neurons (cell structures) 'fire' to transfer electrical signals (i.e. information) to other parts of the brain via synaptic connections. The term 'ANN' actually refers to a broad umbrella of models that determine mappings between inputs and outputs by composing differentiable functions into any number of directed acyclic graphs (Murphy, 2022). The simplest of these arrangements is a chain called a feed-forward neural network or multilayer perceptron (MLP), which is one of the most suitable ML techniques for structured or tabular data as it assumes the input is a fixed-dimensional vector (Murphy, 2022). Moreover, as a supervised ML technique, MLPs can be applied to a wide variety of classification and regression tasks.

Research into ANN applications in the mining industry has exploded across the entire value chain over the past two decades. Recent reviews have shown that neural networks and deep learning models account for ~25% of all ML approaches used in the mining space, with support vector machines (23%) and ensemble methods (22%) close behind (Jung & Choi, 2021). ANNs have been especially useful in mineral resource estimation, e.g. (Jalloh, et al., 2016; Kaplan & Topal, 2020; Abuntori, et al., 2021), comprising ~46% of the ML techniques used in this area (Dumakor-Dupey & Arya, 2021). Other prominent applications include mineral prospecting and mapping (Leite & de Souza Filho, 2009; Oh & Lee, 2010), geophysics and remote sensing (Du, et al., 2018; Yadav, et al., 2021), ore classification (Xiao, et al., 2019; Yang, et al., 2020), drilling and blasting operations (Lashari, et al., 2019; Al-Bakri & Sazid, 2021), mining method selection,

equipment utilization and production planning (Baek & Choi, 2019; Pham & Phan, 2016), ore beneficiation and mineral recovery (Wang & Han, 2015; Nie, et al., 2021), and mine site reclamation (Amato, et al., 2015; Abaidoo, et al., 2019), among others.

To elaborate from that discussed in the previous section, a case study focused on the regional coordination of refractory gold sources incorporates predictive MLP regression modelling into the current DES framework to evaluate system response to geological uncertainty caused by varied ore sources (see Section 4.4). In this work, gold recoveries predicted from geochemical and mineralogical data are used to classify ores into free-milling and refractory types based on expected metallurgical response. The resultant proportions are then fed into the DES portion of the model for the development of robust operational policies and related control strategies to stabilize plant performance against unexpected changes in ore feed attributes.

2.6 System Dynamics via Discrete Event Simulation

System dynamics (SD) is an approach to conceptualize and quantify causal relationships between variables through model development and subsequent simulations to capture key decision processes within dynamic systems (O'Regan & Moles, 2006; Alpagut & Çelebi, 2003). The methodology is particularly useful in the design and testing of alternative operational policies, associated tradeoffs and resultant short to long-term impacts (Alpagut & Çelebi, 2003). Developed in the 1950s, SD has been applied in many areas of research, including business, medicine, energy and environment, and industrial engineering applications. Despite the many interrelated variables, complex information-feedback cycles within systems, and high degree of uncertainty inherent to any mining operation, SD modelling techniques have not been widely implemented across the mining sector; there have nonetheless been certain niche applications related to production planning and conveyance process capacities (Alpagut & Çelebi, 2003). Some of the earlier research in mining system dynamics dates back to the 1980s in the coal industry and focused on the allocation of manpower and equipment availability to optimize these managerial policies (Alpagut & Çelebi, 2003; Wolstenholme & Holmes, 1985).

The flexibility of discrete event simulation (DES) frameworks is valuable to a system dynamics approach because it allows for the simulation of interactions between critical parameters and processes in response to random variations, e.g. geological uncertainty. Computer-based DES

models are capable of optimizing tradeoffs between available operational policies, and the thresholds that control timing of their implementation (Navarra, et al., 2019; Navarra, et al., 2017b; Saldaña, et al., 2019). A powerful aspect of DES is the ability to assess risk by simulating hundreds or thousands of operating days to identify potential deficiencies or bottlenecks. Strategic decisions can then be made to introduce operational buffers in order to mitigate the identified risk factors.

DES frameworks are critical tools to streamline and support decision-making processes in the design, development and production stages of industrial systems. The distinguishing feature between mining and other industrial systems is the introduction of geological uncertainty, i.e. the natural (random) variability associated with the abundance and distribution of host-rock mineral assemblages in an orebody. DES supports the incorporation of random distributions, i.e. it is a form of Monte Carlo simulation (Altiok & Melamed, 2007), and thus can be used to observe the potential effects of geological uncertainty on mining system dynamics.

Key performance indicators (KPIs) can be monitored within a DES model to simulate and optimize system-wide response to, for example, unexpected trends in the mineral feed characteristics. Sets of testing or validation data can also be simulated in order to build confidence intervals and support strategic decision-making, e.g. changes in operating practices or the installation of new equipment. The key to developing appropriate DES frameworks to model mining system dynamics is the establishment of alternate modes of operation that can be employed under changing conditions or as critical thresholds are crossed (Navarra, et al., 2018; Navarra, et al., 2017a). Distinct geometallurgical domains or units are then defined according to how the various classified mining blocks are expected to behave under each of the available modes (Navarra, et al., 2018; Alruiz, et al., 2009; Suazo, et al., 2010).

Though well-established in many industrial engineering practices, the use of DES frameworks in mining remains in its infancy, with earlier implementations mostly focused on material management (Vagenas, 1999), equipment selection (Awuah-Offei, et al., 2012) and availability (Gbadam, et al., 2015), transport logistics (Greberg, et al., 2016), refuge station planning (Tarshizi, 2015) and continuous mine system simulation (Shishvan & Benndorf, 2014). Some of the earliest mine-to-mill modelling efforts using DES include the coupling of solar radiation with a semi-

autogenous grinding (SAG) mill (Pamparana, et al., 2017) and spectral ore type imaging applications (Nageshwaraniyer, et al., 2018).

Recent work focused on concentrator and smelter dynamics has stressed the importance of coupling alternate modes of operation and mass balance with DES in order to develop a robust framework under changing conditions, or as critical thresholds are crossed (Navarra, et al., 2019; Navarra, et al., 2017a; Navarra, et al., 2017b). The versatility of this approach is further underscored by a number of recent DES studies dealing with heap leach processes (Saldaña, et al., 2019), smelter data acquisition modernization (Navarra, et al., 2020), tailings retreatment (Wilson, et al., 2021a), oil sands processing (Wilson, et al., 2021b), gold extraction reagent control (Órdenes, et al., 2021), rougher flotation cell dynamics (Saldaña, et al., 2021), mine-to-smelter integration for regionalized copper systems (Wilson, et al., 2021c), and mine-to-mill integration for regional development of refractory gold systems (Wilson, et al., 2022a).

Chapter 3

Integrated DES Frameworks

Mining project development carries a substantial level of risk compared to many other industrial systems due to the significant geological uncertainty inherent to all orebodies formed through natural processes. As a result, this uncertainty must be captured by modelling efforts in order to support all levels of decision-making as a project progresses from early scoping through to detailed feasibility level studies, system design and implementation; this is equally critical for continuous improvement and re-engineering of active operations. There are a variety of ways to represent geological uncertainty, including geostatistical simulations as well as other multivariate analytical techniques (via classical statistics or ML algorithms) coupled with Monte Carlo simulation. Regardless of the selected approach, the key is to ensure the resulting probability distributions are properly integrated with system process models such that suitable risk assessment can be undertaken by monitoring system performance in response to deviations from the expected ore feed attributes.

To highlight the concept, this chapter first provides detailed summaries of select geostatistical simulation methods, multivariate regression analysis, multilayer perceptron modelling, and finally discrete event simulation. An ensuing discussion identifies how this research embodies the importance of generalizable and flexible frameworks that can integrate advanced quantitative methods into a DES framework to support the development of novel control strategies in the mine-to-mill (or smelter) profile through a series of developed case studies.

3.1 Geostatistical Simulation

Spatial uncertainty within a model can be evaluated using geostatistical simulation methods that generate a set of equiprobable realizations of the spatial variability of each variable, as well as relationships between variables (Emery, et al., 2016; Emery, 2008; Emery & Lantuéjoul, 2006). To simulate these stochastic realizations, practitioners require a random field model and an algorithm (Chilès & Lantuéjoul, 2005). The most straightforward and commonly used is the Gaussian random field model, which is characterized by multivariate normal distributions (Emery,

2008). There is a multitude of proposed algorithms from which to choose; however, many of these options have limitations on either the number of locations or the spatial configuration of the locations where these random fields can be simulated (Emery, 2008; Emery & Lantuéjoul, 2006).

One way of overcoming these limitations is to use an approximate algorithm (Paravarzar, et al., 2015; Emery, et al., 2016); two of the most suitable such approaches for continuous variables include sequential gaussian simulation (SGS) (Deutsch & Journel, 1998) and the turning bands method (Matheron, 1973). These techniques use random number generation to generate the statistical scenarios independently of each other, and thus are considered a type of Monte Carlo simulation. Both approaches fall within the category of conditional simulation, which implies that each simulated realization preserves the local spatial averages and variances of the original dataset (Navarra, et al., 2018). However, a key difference is that unlike SGS, the turning bands method applies non-conditional simulation as a step towards conditional simulation.

Both the SGS and turning bands algorithms can be used to simulate either regionalized (univariate) or co-regionalized (multivariate) variables of interest. However, a problem with joint simulation (co-regionalized variables) is the need to determine cross-covariance functions that model the relationships between these variables (Emery, 2008). Considering a stationary vector random field, $\mathbf{Y} = \{\mathbf{Y}(\mathbf{x}): \mathbf{x} \in \mathbf{D}\}$, where $\mathbf{D}$ is the defined sample domain and $\mathbf{x}$ is a generic location within $\mathbf{D}$, and assuming random values are mean-centered and multivariate normal, these distributions are described by the matrix of direct and cross-covariances of the components of $\mathbf{Y}$ for a given separation vector $\mathbf{h}$ (Paravarzar, et al., 2015; Emery, et al., 2016):

$$\mathbf{C}(\mathbf{h}) = \mathbb{E}\{\mathbf{Y}(\mathbf{x})\mathbf{Y}(\mathbf{x}+\mathbf{h})^{\mathbf{T}}\}, \tag{3.1.1}$$

in which $\mathbb{E}$ is the expected stochastic value operator. There are many methods to model simple and cross-covariances, but for simplicity purposes this description considers only the linear model of co-regionalization of the form (Emery, 2008; Wackernagel, 2003):

$$\mathbf{C}(\mathbf{h}) = \sum_{n=1}^{N} \mathbf{B}_n \rho_n(\mathbf{h}), \tag{3.1.2}$$

in which $\{\rho_n, n = 1,...,N\}$ represents a set of nested covariance functions, $\{\mathbf{B}_n, n = 1,...,N\}$ denotes a set of symmetric co-regionalization matrices, and $\mathbf{h}$ is the lag separation distance between points.

The stationarity hypothesis can also be weakened to consider generalized covariances instead of ordinary covariances (Emery, 2008).

3.1.1 Sequential Gaussian Simulation (SGS)

Developed by Journel and his graduate students at Stanford in the early 1990s (Deutsch & Journel, 1992; Gómez-Hernández & Journel, 1993; Verly, 1993), SGS has since become one of the most widely used algorithms for conditional simulation. As a natural extension of (co-)kriging estimation methods, the technique has gained popularity owing to its relative simplicity and straightforward implementation (Paravarzar, et al., 2015). In short, SGS aims to generate a series of equiprobable statistical realizations by reproducing the spatial attributes that relate multiple locations as identified by simple kriging. In other words, simulated values are drawn from the local Gaussian probability distribution defined by the expected (kriging) mean and variance for each random variable (Egaña & Ortiz, 2013). Spatial correlation is imposed via Bayesian principles by sequentially conditioning the probability distribution at a given location (i.e. node) on the previously simulated values at other locations (Egaña & Ortiz, 2013; Deutsch & Journel, 1998).

Considering a sample domain $\mathbf{D}$ composed of m locations, the SGS algorithm simulates the vector random field $\mathbf{Y}$ at each successive location $\mathbf{x}_i$ (with $i = 1, \dots, m$), as follows (Paravarzar, et al., 2015):

$$\mathbf{Y}(\mathbf{x}_i) = \mathbf{Y}^{SCK}(\mathbf{x}_i) + \sqrt{\mathbf{\Sigma}^{SCK}(\mathbf{x}_i)}\,\mathbf{U}_i, \tag{3.1.3}$$

in which $\mathbf{Y}^{SCK}(\mathbf{x}_i)$ is the simple co-kriged estimate for $\mathbf{Y}(\mathbf{x}_i)$ acquired using the pre-existing data in addition to the simulated values from previously visited sample nodes, i.e. $\mathbf{Y}(\mathbf{x}_1), \dots, \mathbf{Y}(\mathbf{x}_{i-1})$, as conditioning data; $\mathbf{\Sigma}^{SCK}(\mathbf{x}_i)$ is the variance-covariance matrix of the associated co-kriging errors, and; $\mathbf{U}_i$ is a standard Gaussian vector with independent components.

The overall implementation can be summarized as follows (Egaña & Ortiz, 2013):

1. Decluster sample data to obtain a representative distribution (where applicable);
2. Transform the sample data to a standard normal distribution (i.e. normal or z-scores);
3. Compute the experimental variogram(s) of normal scores and fit a model;
4. Verify that the multi-Gaussian assumption is reasonable;

5. Proceed with the simulation (as defined above) by:
    a. Defining a grid and visiting each of the nodes in a random path;
    b. At each node, simple kriging is performed using the sample data and simulated values from previously visited nodes within a defined search space;
    c. A new simulated value for the current node is randomly generated by drawing from the Gaussian distribution established by the previous kriging step;
    d. Similarly, this new value is used to condition all subsequent nodes, and;
6. Back-transform the simulated values to the original sample space (i.e. distribution).

Despite the clear advantages of a straightforward implementation and successful applications across the mining spectrum, a couple important drawbacks of the sequential approach include a high computational cost and potential accuracy issues. A number of variants have been developed to address the computational aspect, e.g. ($\pm$ collocated) co-kriging in a moving neighbourhood. Such an approach restricts the use of sample and conditioning data to a space defined by a maximal search radius around the target node, as well as a maximum number of data and simulated values to be used for conditioning (Paravarzar, et al., 2015). However, it has been shown that appropriate selection of these parameters is critical to the accuracy and performance of the simulation model (Emery & Peláez, 2011). Other recent studies have also proposed using a constant multigrid path with increased neighbourhood size for generating all realizations in order to accelerate sequential simulation times (Nussbaumer, et al., 2018).

Another alternative is to use a different simulation technique altogether; some studies have shown other methods (e.g. continuous spectral or turning bands) to perform better in terms of accurately reproducing the variogram or covariance matrix, in addition to reducing computational cost and improving numerical stability (Emery & Peláez, 2011; Nazari Ostad, et al., 2018).

3.1.2 Turning Bands Method

Introduced by Matheron (1973) and developed by Journel (1974; 1978), the turning bands method generates simulation results for a *d*-dimensional random field through a series of one-dimensional (1D) simulations along lines that span $\mathbb{R}^d$ space (Emery, 2008; Emery & Lantuéjoul, 2006). Unlike its exact algorithm counterparts, there are no restrictions on the number of random fields to simulate, the number of structures in the co-regionalization model, or the number and

configuration of the locations in the simulation space (Emery, 2008). Some critics dislike the potential for banding artifacts along the 1D lines, but this can be minimized with appropriate selection of the line simulation algorithm and line distribution (Emery, 2008).

Despite being one of the earliest multidimensional simulation techniques, the use of the turning bands method is not widespread in geostatistics and most software packages that do exist are limited in terms of dimensionality (≤2D) or the number of 1D simulation lines that can be used. These factors have motivated the creation of Matlab programs for the conditional simulation of regionalized (Emery & Lantuéjoul, 2006) and co-regionalized (Emery, 2008) models in $\mathbb{R}^3$ using the turning bands method.

Non-conditional simulations are carried out by decomposing each co-regionalization matrix, $\mathbf{B_n}$, as follows (Emery, 2008; Paravarzar, et al., 2015):

$$\mathbf{B_n} = \mathbf{A_n}\mathbf{A_n^T} = \mathbf{Q_n}\Delta_n\mathbf{Q_n^T}, \tag{3.1.4}$$

where $\mathbf{Q_n}$ is an orthogonal matrix of eigenvectors, Δ_n is a diagonal matrix of eigenvalues, and $\mathbf{A_n} = \mathbf{Q_n}(\Delta_n)^{1/2}$.

Given a Gaussian vector random field, $\mathbf{X}_n$, with M independent components (each with covariance function ρ_n), the random field $\mathbf{Y}$ can be expressed as follows (Emery, 2008; Paravarzar, et al., 2015):

$$\forall \mathbf{x} \in \mathbb{R}^d, \qquad \mathbf{Y}(\mathbf{x}) = \sum_{n=1}^{N} \mathbf{A_n}\mathbf{X_n}(\mathbf{x}). \tag{3.1.5}$$

As a result, the simulation of a Gaussian vector random field with cross-correlated components, $\mathbf{Y}$, can be summarized as a set of independent scalar Gaussian random fields in which the N matrix components $\mathbf{X}_1, \dots, \mathbf{X}_N$ are used to predict the M independent random values $\mathbf{Y}_1, \dots, \mathbf{Y}_M$ (Emery, 2008; Paravarzar, et al., 2015). This decomposition is actually the basis of factorial kriging analysis (Goovaerts, 1997; Wackernagel, 2003; Emery, 2008).

An additional step is required in order to generate realizations conditioned to a set of pre-existing data. The realizations obtained by the turning bands (non-conditional) simulation can be

further processed by co-kriging the difference between the simulated values and the actual data values at the corresponding data locations (Emery, 2008; Paravarzar, et al., 2015):

$$\forall \mathbf{x} \in \mathbb{R}^d, \qquad Y_{CS}(\mathbf{x}) = Y_S(\mathbf{x}) + [Y(\mathbf{x}) - Y_S(\mathbf{x})]^*, \tag{3.1.6}$$

in which the subscripts S and CS denote non-conditional and conditional simulation, respectively, and the asterisk specifies the co-kriging weights (Emery, 2008).

Theoretical simulation aspects aside, implementation of the turning bands method requires a similar series of steps as the SGS algorithm, including:

1. Declustering of sample data (where applicable);
2. Transformation of the sample data into normal scores;
3. Calculation of the experimental variogram(s) and model fitting;
4. Verification of the multi-Gaussian assumption;
5. Administration of the simulation algorithm (as defined above), and;
6. Back-transformation of the simulated values to the original sample space.

A key feature of the turning bands simulation algorithm is the ability to parallelize simulations. All variables are simulated simultaneously at each location (irrespective of simulations at other locations), and conditioned by means of a single co-kriging system (Emery, 2008). This results in significant computational savings compared to sequential algorithms, which simulate values in succession conditionally to previously simulated values. As previously described, some studies have also shown the turning bands method to produce more accurate results for a variety of scenarios compared to its sequential counterparts (Paravarzar, et al., 2015).

Potential drawbacks of the approach are mainly related to restrictions caused by the selection of the Gaussian random field model, i.e. the assumption of multivariate normal distributions. Moreover, the fitting of a linear model of co-regionalization to the direct and cross-variograms is common in spatial analysis; however, this simplification may be insufficient for certain temporal or spatio-temporal datasets as no delayed correlation effects are represented (Emery, 2008).

Sample computations for the turning bands method are provided in Section 4.1 as part of a case study focused on development of tailings retreatment applications using an integrated DES framework to evaluate system performance.

3.2 Multiple Linear Regression

3.2.1 Fundamentals and Implementation

Multiple linear regression is a widely used multivariate statistical technique owing to its relatively straightforward implementation as a generalization of simple linear regression. To accommodate multiple independent variables within a single model, each predictor is given a separate slope coefficient. For a system with p distinct predictor variables, the MLR model takes the following form for a single response variable (James, et al., 2013):

$$Y_i = \beta_0 + \beta_1 X_{i1} + \beta_2 X_{i2} + \cdots + \beta_p X_{ip} + \epsilon_i, \tag{3.2.1}$$

in which Y_i is the ith observation of the response variable (with $i = 1, \dots, n$), X_{ij} is the ith observation of the jth predictor variable (with $j = 1, \dots, p$), β_0 denotes the intercept (bias term), β_j quantifies the association between each variable and the response (i.e. the parameters to be estimated), and ϵ is the error term (function of the residual distances) for the model.

In the case of multiple response variables sharing the same set of explanatory variables, the MLR model can be further generalized, as follows:

$$Y_{ij} = \beta_{0j} + \beta_{1j} X_{i1} + \beta_{2j} X_{i2} + \cdots + \beta_{pj} X_{ip} + \epsilon_{ij}, \tag{3.2.2}$$

with observations indexed as $i = 1, \dots, n$ and response variables as $j = 1, \dots, m$.

To estimate the parameters (i.e. regression coefficients), MLR uses the principles of OLS to minimize the sum of squared residuals via the normal equations, such that in matrix form:

$$\hat{\beta} = (X^{\mathrm{T}} X)^{-1} X^{\mathrm{T}} Y, \tag{3.2.3}$$

in which $\hat{\beta}$ denotes the matrix of estimated regression coefficients, X is the $n \times p$ design matrix of independent variables, Y is the $n \times m$ matrix of dependent variables, and the superscript T denotes the transpose of a matrix.

Proof that the obtained matrix of coefficients, $\hat{\beta}$, indeed represents a local minimum is given by the Gauss-Markov theorem, which states that the OLS estimator gives the best estimate of the linear unbiased class of estimators. However, for the theorem to hold true (in which case the

estimates are also maximum likelihood estimates), a number of strict statistical conditions must be met, including (Abdi, 2010a):

1. The data constitutes a random sample from a well-defined population;
2. The population data model is in fact linear;
3. The expected error has a value of zero;
4. The predictor variables are indeed linearly independent, and;
5. The model error is normally distributed and uncorrelated with the predictor variables (i.e. homoscedasticity).

The Gauss-Markov theorem is a well-established cornerstone of linear regression techniques; as such, the reader is referred to any of a great number of references on classical modern statistics, e.g. (Johnson & Wichern, 2007), for details on the mathematical proof and related set of conditions. However, it is notable that when the Gauss-Markov conditions hold, OLS estimates are also equivalent to maximum likelihood estimates (Abdi, 2010a).

3.2.2 Alternative Approaches

Despite its relative simplicity and straightforward implementation, there are indeed some well-known issues with MLR. As with all LS methods, MLR is highly sensitive to extreme outliers due to the exaggeration of the magnitude of differences giving more importance to these observations. Moreover, a key requirement of MLR is that the predictor variables are linearly independent; when there are a large number of predictors compared to the number of observations, the design matrix (i.e. predictor data) is likely to be singular and ordinary regression is no longer feasible due to multicollinearity (Abdi, 2003). In this case, either correlated variables must be removed in order to reduce information overlap and improve the accuracy of regression coefficient determinations, or an alternative approach must be employed.

One possibility is to use principal component analysis (PCA) on the predictor data and use the determined orthogonal components as regressors on the response variable(s), thereby eliminating the multicollinearity issue; however, selection of the optimum subset of predictors remains a problem (Abdi, 2003). Or better yet, other methods such as partial least squares can be used to

identify orthogonal components from the predictor data matrix that are also relevant for the response variable(s).

Partial least squares (PLS) regression is somewhat of a hybrid method as it generalizes features from multiple linear regression, with the objective of predicting a set of dependent variables from a potentially large set of independent variables (Abdi, 2003; Abdi, 2010b). The technique was pioneered in the 1960s by Herman Wold for use in the social sciences (economics) but, with recent and rapid advances in computational frameworks and power, has since gained traction in a variety of fields, including chemometrics, sensory evaluation, neuroimaging and now the engineering sciences (Abdi, 2003; Abdi, 2010b; Hoskuldsson, 1988; Tenenhaus, 1998).

PLS regression is a well-established multivariate statistical technique in many research fields, including economics, chemometrics, sensory evaluation and medical imaging sciences (Abdi, 2003; Abdi, 2010b; Hoskuldsson, 1988; Tenenhaus, 1998). It has also gained recent interest in the bio-environmental sciences with a variety of studies in soil and microbial ecology (Ekblad, 2005; Allen, 2005), biodiversity (Maestre, 2004; Palomino & Carrascal, 2007), paleoclimatological reconstruction (Seppa, 2004), and ecotoxicology (Sonesten, 2003; Spanos, 2008). To the best of the authors' knowledge, there has been very little work done using PLS regression in the areas of mining and system dynamics research to date. The most relatable study successfully developed a predictive model for the amount of kaolinite (clay mineral) in a deposit by linking earlier collected NIR spectroscopic data to confirmatory geochemical data (Huerta, et al., 2019).

Additional details on the fundamentals and implementation of the PLS algorithm are provided in Section 4.2 within the context of a case study focused on bitumen extraction from Canada's oil sands region using an integrated DES framework to model system response.

3.3 Predictive Multilayer Perceptron Modelling

3.3.1 General Overview

There are many great resources that cover the mathematical and probabilistic underpinnings of the MLP algorithm, e.g. (Marsland, 2015; Murphy, 2022; Goodfellow, et al., 2016); as such, this description is presented from more of an applied perspective. At a high level, an MLP can be defined as any feed-forward network comprising at least three layers: the input layer, the hidden

layer(s), and the output layer. While the classification of MLPs is somewhat arbitrary, most practitioners consider networks with just one hidden layer as 'shallow', and those with two or more as 'deep learning' models. Each hidden layer in an MLP is fully connected to the preceding and proceeding layers via a series of nodes, or neurons, as shown in Figure 3.3.1a. The nodes in the input and output layers correspond to the column-wise features in the dataset and the target variable(s) for classification or regression, respectively. Each neuron in the hidden layer(s) acts as an individual perceptron, a local function of its inputs, x_j, and connection weights, w_j (Alpaydin, 2014). Analogous to neurons 'firing' in the brain, the decision to activate an artificial neuron is based on the weighted sum of all inputs (+ a fixed nonzero bias term, b_0), which is then fed through an activation (i.e. threshold) function to determine the output, y_i (Alpaydin, 2014; Marsland, 2015) (Figure 3.3.2b; modified after Emmert-Streib et al. (2020)).

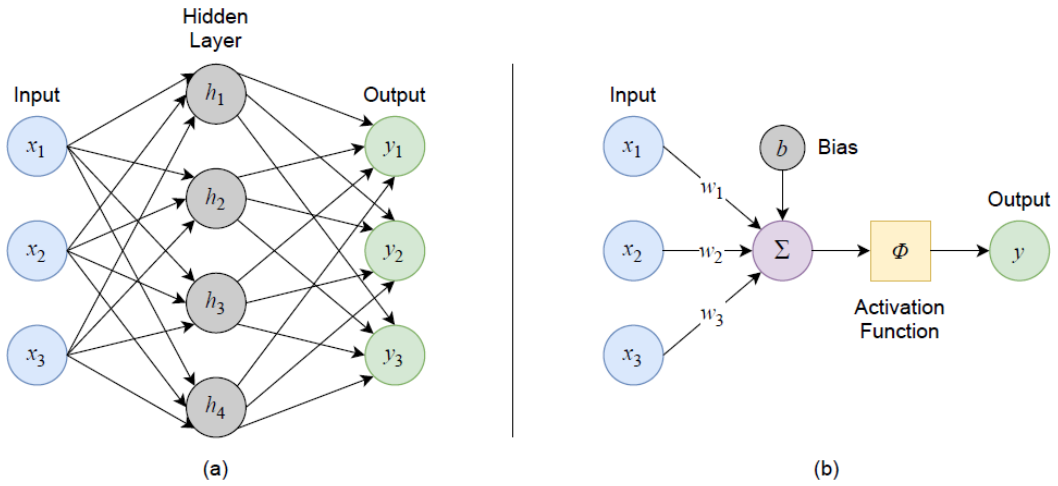

Figure 3.3.1. Schematic diagrams of a feed-forward artificial neural network at the (a) model architecture and (b) neuron levels (modified after Emmert-Streib et al. (2020)).

In general, MLPs can use either linear or non-linear activation functions (Goodfellow, et al., 2016). However, because the final target output is a linear combination of the basis function values computed by the hidden perceptron units, the hidden layers would not be useful if their intermediate outputs were also linear (Alpaydin, 2014). In other words, the hidden units can be thought of as making a non-linear transformation of the initial sample inputs, which are then linearly combined by the final output layer. The basic functioning of the MLP algorithm can be summarized as follows (after Marsland (2015)):

1. A vector of structured data is fed into the nodes of the input layer;
2. The inputs are propagated forward through the network, i.e. there are no cyclic connections that allow direct feedback to current or preceding layers;
3. The inputs and weights to each layer are used to determine whether each node will be activated or not, following the artificial neuron model described above;
4. The final network outputs are used to compute an error metric with respect to the known (labeled) target data;
5. This error is propagated backwards through the network to successively update the weights of each preceding layer prior to the next iteration of sample data processing.

The last step in this sequence, known as backpropagation, is fundamental to the training of the neural network, i.e. it is how the model 'learns'. Backpropagation is an optimization algorithm that aims to minimize a selected loss function by approximating the gradient of the error resulting from the network outputs via the chain rule, and following it downslope (Marsland, 2015; Murphy, 2022). Essentially, a model is said to have 'converged' to a solution once the loss has settled within an acceptable error range, i.e. further training will not improve model performance.

3.3.2 Optimization Approaches

While steepest gradient descent is generally an effective approach to optimization problems, it can only guarantee finding a local minimum. As a result, variations of the algorithm have been developed to help avoid getting stuck in local optima. MLPs were originally designed as a batch algorithm, in which all of the training samples are passed through the network prior to computing the average error; weight updates are thus only carried out once per epoch, defined as one iteration through the entire training set (Marsland, 2015). Alternatively, stochastic gradient descent (SGD) sequentially calculates the error and updates weights accordingly following each individual training sample. Though not as efficient as the batch method, SGD is better at avoiding local minima due to a higher degree of error inherent to each gradient estimate being based on a single input vector (Marsland, 2015). SGD is also not as computationally expensive as the batch approach, which is a consideration for larger datasets. A balanced approach between these two

extremes is to use mini-batches, wherein error computations and weight updates occur following the iterative passing of randomly selected training sample subsets of pre-determined size.

In the basic SGD algorithm, learning rate, α, is essentially the only hyperparameter that can be 'tuned' to improve model performance. The learning rate, i.e. step size, is an important term (generally in the range of 0 to 1) in the weight update rule that controls how fast the network learns. Whereas an overly large learning rate can lead to model instability, an overly small rate can result in underfitting; in either case, the model is likely to fail to converge (Murphy, 2022). A simple approach to select a static learning rate is to begin with a small value (e.g. 0.00001) and increase it by order of magnitude, meanwhile evaluating performance in terms of overall model loss. Once a reasonable range has been established, smaller increments can be tested to identify an 'optimal' value with the lowest loss. However, the learning rate does not need to remain constant; more elaborate methods also implement scheduled or adaptive learning rate approaches (Murphy, 2022).

There are also a number of stochastic optimization variants that can increase the likelihood of finding the global minimum, in addition to accelerating the rate of convergence. One of the most important advances in SGD formulation is the inclusion of a momentum term, β. By analogy, a rolling object is less likely to run out of energy and get stuck in a small valley (i.e. a local minimum) with the extra weight needed to generate enough momentum to get over the next hill. This concept is implemented into the neural network by including a portion from the previous weight change (commonly by a factor of 0.9) to the current update. Not only is the object now less prone to getting trapped in local minima, but it is more likely to find the global optimum by moving more directly to the 'valley bottom' (Marsland, 2015). As shown in Figure 3.3.2, this can stabilize the optimization pathway by reducing the effect of oscillations, thereby improving and accelerating overall convergence.

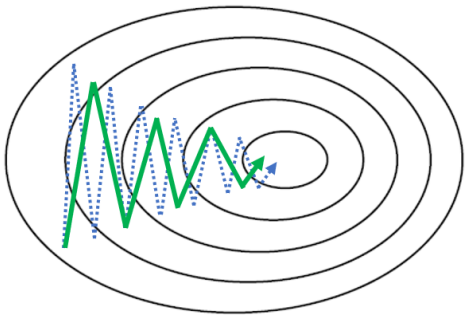

Figure 3.3.2. Schematic gradient contour map comparing SGD without (blue dotted line) and with (green solid line) momentum. Note the reduction in oscillations in the second case, which helps avoid local minima by taking a more direct path to the valley bottom, thus improving and accelerating convergence.

Other well-known extensions to SGD include the adaptive gradient (AdaGrad) (Duchi, et al., 2011), root mean squared propagation (RMSProp) (Tieleman & Hinton, 2012), and adaptive moment estimation (Adam) (Kingma & Ba, 2015) optimization algorithms. Unlike momentum-assisted SGD, which relies on first moment gradient estimates, these methods utilize second moment estimates of the gradients coupled with adaptive learning rates (AdaGrad) and decay rates (RMSProp) to handle sparse data features and speed up convergence, respectively (Kingma & Ba, 2015). The Adam optimizer combines these approaches by using both first and second moment gradient estimates to implement momentum, adaptive learning rates and decay rates; as such, Adam is one of the most popular ML optimization algorithms in use today (Norouzi & Ebrahimi, n.d.). However, while adaptive optimizers have been a recent area of research interest to accelerate model training, they do not generalize as well as momentum-assisted SGD, and may even fail to converge due to certain instabilities and extreme learning rates (Landro, et al., 2021).

3.3.3 Implementation Considerations

There are also a number of other factors to consider in the design and implementation of any MLP. Network architecture, which includes the number of hidden layers and associated hidden nodes, is critical to building a valid and generalizable model. It has been shown that an MLP with just one hidden layer can approximate any continuous function to any target level of accuracy, provided a sufficient number of hidden nodes; this is called the *universal approximation theorem* (Murphy, 2022; Hornik, 1991). However, there are a variety of studies that show deep networks work better than shallow ones because the deeper layers can take advantage of features already learned by shallow layers (Murphy, 2022). There is no steadfast rule to guide depth selection, but

very complex problems may require deeper networks; nonetheless, Occam's razor tells us that we should prefer the simplest model capable of learning the problem set and approximating a solution. Unnecessarily deep networks can actually lead to overfitting of the training data, wherein the model also 'learns' from background noise and therefore becomes poorly generalizable to new data. In terms of model width, i.e. the number of hidden nodes, there is no real theory to guide this selection; there are several rules of thumb in practice (e.g. $\sim 2/3$ between the number of inputs and outputs), but ultimately the choice comes down to trial and error and observing the effect on model performance.

An MLP with a single hidden layer contains $(L+1) \times M + (M+1) \times N$ weights, where L, M, N are the number of nodes in the input, hidden and output layers, respectively (Marsland, 2015). Depending on the problem set, this can result in an exponentially large number of weights; as such, the importance of weight initialization and choice of activation function cannot be overstated. There are a number of non-linear activation functions that can be used in the hidden layers of an MLP, including logistic (sigmoid), hyperbolic tangent (tanh), and rectified linear unit (ReLU) functions. However, the sigmoid and tanh functions are often subject to the 'vanishing gradient' problem. This occurs because the error is propagated through a series of layers which sequentially diminish the gradients towards zero, thereby saturating the weights and causing improper weight updates (Murphy, 2022; Datta, 2020), i.e. the model does not get properly trained, resulting in poor performance.

ReLU addresses this issue by effectively turning off negative inputs and only passing unchanged positive values (Murphy, 2022); it has also been shown to perform significantly faster (Datta, 2020), and is thus the most commonly employed activation function in neural networks. A limitation can occur when a large portion of the inputs are forced to zero, thereby rendering the corresponding neurons inactive, which means a significant portion of the input may not contribute to network training; this is known as the 'dead ReLU' problem. Variants, such as leaky ReLU (LReLU) or parametric ReLU (PreLU), have been devised in response (Murphy, 2022; Datta, 2020). Before training a neural network, the weights must also be initialized to small random values; to this end, there are two methods that are widely used in practice, including Xavier initialization (Bengio & Glorot, 2010) and He (or Kaiming) initialization (He, et al., 2015). Both

approaches can be implemented using either normal or uniform distributions, and have been shown as effective weight initialization techniques for training shallow neural networks. However, He initialization was developed specifically for use with non-linear ReLU activation functions, and is particularly suitable for deeper networks (Datta, 2020; He, et al., 2015).

As noted above, overfitting is a major concern for training any type of neural network. Aside from appropriate model architecture, there are several tools available to limit the effects of statistical noise in training data and improve overall model generalization. Weight regularization is likely the most commonly used approach to control excessive gradient fluctuations. There are two main techniques, namely L1 and L2 regularization, a.k.a. lasso and ridge regression, respectively. In lasso regression, the L1-norm (absolute values) of the weights is added as a penalty term to the error function; in ridge regression, the penalty term is replaced by the L2-norm (squared values) of the weights (Murphy, 2022). In either case, a rate constant, λ, is multiplied by the penalty term, and acts as a hyperparameter that can be tuned by the user to adjust the regularization effect. In practice, lasso regression tends to force the weight coefficients of some features to zero, and is therefore useful for feature selection; ridge regression diminishes the coefficients towards (close to but not exactly) zero more evenly among features, and is thus useful for problems dealing with multicollinear input variables (Murphy, 2022). Moreover, these 'weight decay' methods can also help mitigate the effects of the 'exploding gradient' problem, wherein similar to vanishing gradients, the propagation of error through several layers can amplify the size of gradients to levels that cause numerical instabilities or simply fail to converge (Murphy, 2022).

Another form of regularization common to neural networks is known as 'dropout'. In this technique, nodes and their connections are randomly dropped (i.e. deactivated) from the network during training, which helps prevent co-adaptation (Murphy, 2022; Srivastava, et al., 2014). A tuning hyperparameter allows the user to specify the probability with which outputs are dropped from each layer. As a result, the model learns from a number of thinned networks (akin to sub-sampling), thereby reducing the effects of overfitting to training data noise. The approach has been shown to yield significant improvements over other types of regularization, with state-of-the-art results obtained on many benchmark datasets (Srivastava, et al., 2014).

Finally, training length is also an important consideration to combat overfitting. Neural network training typically involves the splitting of available labeled data into training and validation subsets. These splits should be selected at random, but can also be stratified for datasets with constraints imposed by different sample types. In practice, 80–20 training–validation splits are common, but other techniques, such as k-fold cross-validation, are also widely used to further minimize bias. The training set is used for fitting the model, i.e. learning, meanwhile the validation set is retained for model selection. Training and validation losses are then tracked for each epoch during training. The model continues to learn as long as training loss is decreasing across epochs. Validation loss should follow a similar trend; however, a reversal is a strong indicator that the model is beginning to overfit the training data. It is at this point that the training should be stopped, and the selected model should include the maximum number of training epochs prior to the change in validation loss sign. This final model can then be applied to unseen test sets, keeping the model completely blind to the target output variable labels to evaluate future performance and generalization, or newly generated data altogether.

An example implementation of the MLP algorithm is provided in Section 4.4 as part of a case study centered on development of control strategies for the regional coordination of refractory gold systems using an integrated DES framework.

3.4 Discrete Event Simulation

3.4.1 General Overview

Discrete event simulation (DES) is a computer-based method to develop dynamic quantitative frameworks capable of simulating the interactions between important variables and processes within complex systems. The main difference between mining and other industrial systems is the concept of geological uncertainty, i.e. the random natural variability intrinsic to orebodies and their host geological formations. The flexibility of DES to introduce random distributions thus makes it particularly suitable for a wide variety of mining applications across the entire value chain.

As previously described, the use of DES frameworks in the mining industry has been fairly limited apart from early work focused mainly on equipment and transport logistics. However, recent work has shown the implementation of alternate modes of operation using mass balance and DES modelling as an effective technique to monitor mineral processing system performance,

particularly for concentrator and smelter dynamics (Navarra, et al., 2017b; Navarra, et al., 2019; Navarra, et al., 2020). Moreover, an increasing number of studies have applied a similar approach to other contexts along the mining value chain, e.g. tailings retreatment applications (Wilson, et al., 2021a) and rougher flotation cell dynamics (Saldaña, et al., 2021).

DES modelling is especially useful in the design and evaluation of alternative operational policies and related tradeoffs, and can be applied to any phase of the mining lifecycle. The introduction of alternate operating modes, each with multiple possible configuration rates, allows for adjustments to be made that can stabilize system performance in response to unexpected changes, e.g. ore feed characteristics, caused by geological uncertainty (Navarra, et al., 2019). The timing for switching between configuration rates and/or modes, which is triggered by set threshold crossings (i.e. discrete events), is governed by operational policy. Moreover, key performance indicators (KPIs) can be tracked to optimize the system-wide response by modifying the available operational policies and related thresholds.

DES frameworks are powerful risk assessment tools as they can simulate extended periods of operation in order to identify potential deficiencies, bottlenecks, or other operational risks inherent to mining systems. The key to using DES for modelling continuous processes is to ensure that the number and frequency of discrete events are detected over long time variations; this allows realistic distributions to be captured for appropriate risk assessment. Provided adequate testing and validation, confidence intervals can be generated that support decision-making processes such as modified operating practices that mitigate the identified risk factor, i.e. the implementation of operational buffers (Navarra, et al., 2019; Wilson, et al., 2021a), or the installation of new technologies (Navarra, et al., 2020).

Indeed, there are other approaches to multiobjective optimization in mining systems, e.g. reinforcement learning and bandit algorithms for sequential decision-making (Koch & Rosenkranz, 2020), or integrated sequential mine block selection and smelter feed dopant control using local optimization constraints (Qaeze, et al., 2015). These techniques are no doubt important to their specific applications; however, they do not have the appropriate time resolution to capture the frequency of critical threshold crossings required by the framework strategy presented here.

Instead, the current DES model uses arbitrary time-stepping controlled by system processes in response to geological uncertainty of the ore feeds.

3.4.2 Framework Development

Navarra et al. (2019) identify the notable comparison between a two-mode mining system model and the RQ problem from inventory theory (Winstin & Goldberg, 2004). When an inventory (ore stockpile) level drops below an established 're-order point', R (critical ore level), a replenishment order of quantity, Q, is issued before the inventory is completely depleted (stockout). In the mining context, the critical ore level is directly related to the expected rate of ore consumption and the lead time required to replenish stockpile levels. In practice, however, these factors are both subject to potential random variation. Geological uncertainty of the ore supply could result in shortfalls, requiring a greater than expected consumption rate. Similarly, mining logistics (e.g. a failed stope) could affect the lead time to replenish the ore supply. In either case, there is a risk of stockout. This operational risk can be mitigated by raising the critical ore level, but it is important to note that larger stockpiles typically involve increased operating costs (time and handling) and capital costs (larger equipment and storage areas). The concept of the two-mode framework is therefore fundamental to both risk management (e.g. ore feed stockout) and multiobjective optimization, e.g. balancing throughput vs. stockpile management.

This type of framework can be developed using commercial DES software in order to simulate hundreds of days of operation and evaluate the system-wide response to varied stockpile management strategies. This allows for the monitoring of select KPIs while varying control parameters, such as the critical ore and target stockpile levels. Mode A represents a phase of ore consumption meanwhile Mode B represents a phase of replenishment. Though the consumption mode is typically more profitable in terms of short-term production metrics, it is not sustainable without the application of an alternate replenishment mode due to the risk of stockout (Navarra, et al., 2019). The periodicity of switching between modes is controlled by the operational policy which sets the critical ore level. The replenishment mode is triggered once this threshold is crossed, but it may not be feasible to implement until the next planned shutdown in practice.

It is important to note that when the critical ore level is raised to provide an appropriate security stock, this threshold does not represent a true minimum. In a stochastic mining context,

the ore stock level may continue to decrease even with the onset of the replenishment mode (Navarra, et al., 2019). This can lead to stockout in the event ore levels are insufficient to last through to the next planned shutdown, and highlights the importance of factoring recourse actions into the model, i.e. system flexibility. The current framework incorporates blending practices in response to the geological uncertainty of stockpiles which commonly affects the supply of ore. Two ore types (1 and 2) are blended and processed according to different set proportions under each of the two modes, thereby better controlling the consistency of production feed. This blending allows for the implementation of contingency modes in the case of stockout by adjusting the proportion of ore feed types until the next planned shutdown is reached. At this point in time, operational policy dictates whether to revert to the original mode or switch to the alternate mode.

The current framework considers two control variables in the decision-making process: 1) the critical ore threshold, and; 2) the target total stockpile level, determined as the sum of ore types 1 and 2. A negative threshold crossing for either of these variables represents a discrete event, and triggers a decision (response) in the system. Figure 3.4.1 illustrates the decision-making logic that dictates timing of operational mode changes and loading of new mining parcels following depletion of the previous block. Each simulation run begins in Mode A as it is considered the more productive of the operational modes based on its higher proportion of the more economic ore. Each parcel is described by grade and tonnage attributes, which are implemented as dynamic state variables in the DES model (Peña-Graf et al., 2022). In a mining context, these parcels actually represent the conjunction of mine plans and geological uncertainty, the latter of which is determined through either geostatistical simulation, or Monte Carlo simulation with variability controlled via adjustments to the standard deviation applied during random number generation. When available, the sequencing of the mining parcels can be derived from the geostatistical simulation data (e.g. Taltal tailings rehabilitation case study; see Section 4.1.2); otherwise, the parcel sequence may not necessarily represent a true ‘mine plan’ in the context of a conceptual mining system. However, this information can be readily obtained from mining partners and incorporated into the framework as part of more detailed case studies.

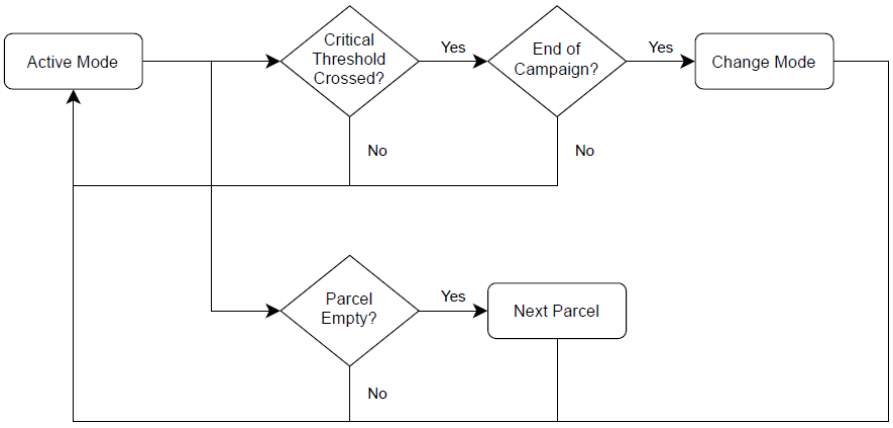

Figure 3.4.1. Generalized flow chart of the DES framework showing decision-making logic for operational mode changes and parcel (i.e. mining block) termination.

The framework also has built-in recourse actions in the event one of the ore types is entirely depleted during a production campaign, i.e. the target total stockpile level decreases below the set quantity prior to a planned shutdown. These actions include contingency modes, which represent a change in configuration rate under the active operational mode, and mining surges. Figure 3.4.2 depicts the decision-making logic for these responses when the system is stressed by inadequate stockpile availability of either ore type. Under Mode A, a total depletion of the critical ore triggers a contingency mode, wherein the configuration rate is reduced and only the available ore type is processed for a period of 1 day to allow the depleted ore to temporarily build back up. On the other hand, a depletion of the non-critical ore calls for a mining surge such that total available ore increases above the target level and is fed directly to the processing plant. These recourse actions are interchanged when corresponding depletions occur during Mode B operation. Regardless, these system responses are undesirable as they can result in significantly reduced production throughputs. Sufficiently high levels must be set for these variables to minimize the occurrence of such events, meanwhile balancing this risk against the elevated infrastructure, equipment and operating costs associated with larger stockpiles (Navarra, et al., 2019; Wilson, et al., 2021a).

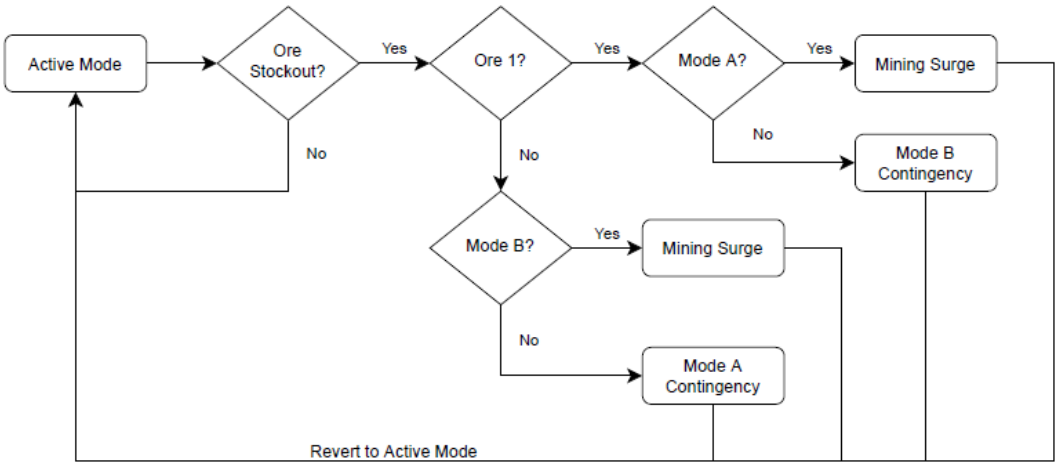

Figure 3.4.2. Generalized flow chart of the DES framework showing decision-making logic for configuration rate changes and mining surges triggered by total depletion of either ore type.

The framework is implemented using commercial DES software (Rockwell Arena©) with Visual Basic for Applications (VBA). Model verification has been carried out by a combination of event checking and debugging, as well as sensitivity analysis through testing a wide range of values for model inputs and parameters. The use of fixed mass balances to assess potential plant performance is standard practice in the mineral processing sector; this work represents a valid extension beyond static modelling by incorporating pragmatic fluctuations in mass and composition flows, i.e. dynamic imbalances, that would be expected from source orebodies.

Though the case studies presented in this research are mainly conceptual in nature, similar techniques have been successfully applied to Chilean smelter operations using real operational data, thus validating the general approach. The framework is calibrated using typical operating parameter values depending on the context, obtained from time-averaged publicly available data; this ensure suitable and valid ranges are used. In practice, operational data would be available to further validate the model and make necessary adjustments to the control parameters.

3.5 Flexible DES Frameworks for Mining Systems

Artificial intelligence (AI), machine learning and other advanced quantitative methods represent the state of the art in research and development trends toward technological advancement and related process automation. Recent reviews specific to mining highlight the current scope of applications in a variety of areas across the spectrum, from exploration to mine planning,

operations and downstream processing. However, these studies also identify a number of key gaps that should be addressed by the industry to support future innovation, including:

1. Development of generalizable models that can be adapted to different problems or contexts (Ali & Frimpong, 2020);
2. Proper integration of ML-acquired data (e.g. soft sensors) into quantitative frameworks that can make use of it (McCoy & Auret, 2019), and;
3. Hierarchical model detailing to improve system performance (Cisternas, et al., 2019).

It is thus clear that a flexible and integrated framework approach to test novel control strategies for operational decision-making along the mine-to-mill (or smelter) profile would be a strong contribution to this void in the mining literature.

3.5.1 Incorporation of Quantitative Methods into DES

The current framework has the capability to incorporate uncertainty using a variety of advanced quantitative methods to characterize mining parcels (i.e. ore blocks) based on expected metallurgical or petrochemical response from geological data collected early in the value chain. The generated distribution of these classified blocks are then fed into the DES portion of the model to analyze system response to potential unexpected changes caused by geological uncertainty. From a broader industrial perspective, there have been other studies that use similar framework architectures, particularly in manufacturing, e.g. (Lidberg, et al., 2020), and food processing, e.g. (Sobottka, et al., 2019). However, the distinction here is that these contexts are not subject to nearly the same degree of variability inherent to natural systems, such as mineralized orebodies, and therefore the resultant formulations do not consider the likes of geological uncertainty.

With geostatistical simulation tools, or other advanced quantitative methods (e.g. machine learning algorithms), acting as the engine driving the characterization of ore feeds, the current DES framework essentially acts as a wrapper (i.e. vessel) for the integrated management of downstream processes based on the defined geological variability (Figure 3.5.1). By incorporating geological uncertainty via stochastic simulation of measured or predicted ore characteristics into a DES framework, one can properly evaluate system response to a range of potential scenarios and develop appropriate operational policies and related control strategies. The inclusion of a

mechanism to introduce uncertainty into a framework is one approach towards improving model generalizability (Shen, et al., 2021). The key is to ensure that file types common to most database systems (e.g. comma-separated values or text files) are supported by the framework either directly, or through suitable interfacing.

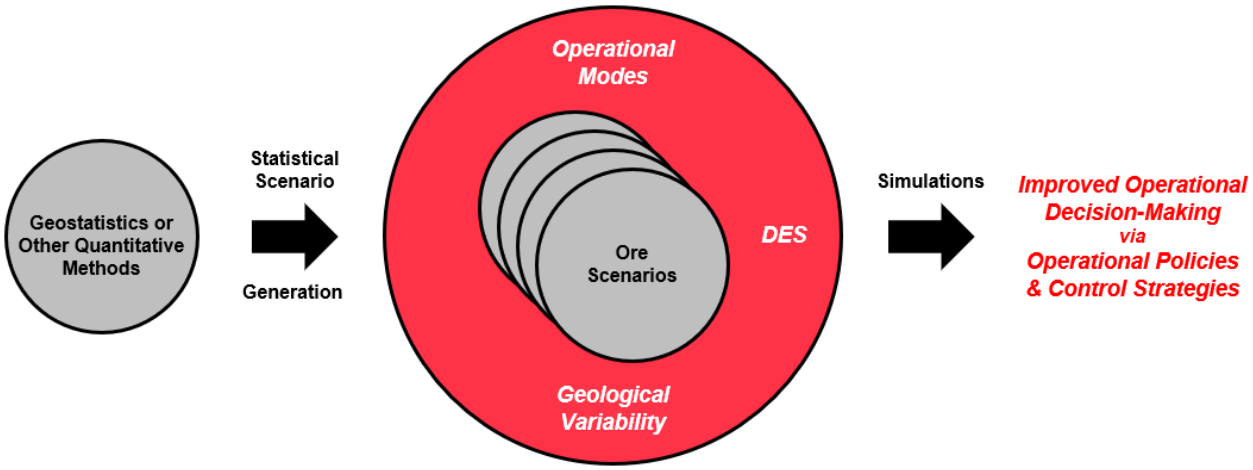

Figure 3.5.1. Schematic diagram illustrating the incorporation of uncertainty via stochastic (i.e. Monte Carlo) simulation of measured or predicted data generated by a variety of advanced quantitative methods into a DES framework to assess system-wide response to unexpected changes in geological attributes. The current framework effectively acts as a wrapper around the selected data processing technique for the integrated management of downstream processes based on the defined geological variability.

Integrated frameworks can benefit from combining state-of-the-art data-driven (i.e. bottom-up) models with process models derived through domain knowledge and physicochemical principles (i.e. top-down approach). However, the development of effective models requires the breaking down of interdisciplinary barriers and improved data sharing, which has been cited as a critical step towards accelerating innovation in the age of big data within the industrial sector (Kusiak, 2017). It is all too common at modern mining operations for geologists, engineers, and operators alike to collect all kinds of vast datasets that are infrequently put to proper use as each department works within their own operational unit. As an example, one might hypothesize through years of experience as to how to connect *these* geological attributes with *those* metallurgical process parameters to increase the competitivity of a given mining project. However, it would remain unclear how a proposed new or modified strategy might affect ongoing operations without appropriate testing using an integrated simulation platform that mirrors the mine-to-plant profile (Peña-Graf, et al., 2022). It is clear that both knowledge and data inputs from all involved

disciplines are critical to develop an accurate and robust framework capable of providing support to the necessary decision-making processes.

3.5.2 Model Extensibility and Adaptability

To deal with changes in mining systems, whether expected (e.g. new feed sources) or otherwise (i.e. geological uncertainty), it is crucial that the resulting frameworks are extensible to handle varying levels of complexity depending on the project scope. This allows for a multi-phase approach in order to improve confidence and justify the next level of investment towards updating control strategies. As the project evolves, so too does the framework as it integrates increasingly detailed models and submodels. By incorporating the incoming data, the effects on system-wide metrics can be assessed, and the necessary adjustments to operating policies and/or related controls can be made to maintain an overall mass balance, thereby improving system stability. This is the key to developing advanced control strategies, driven by the balancing of opportunities and risks towards a sustainable mining system. As shown in Figure 3.5.2, the overall process is by no means unidirectional, with multiple feedback cycles commonly required during model conceptualization, design, testing/validation and optimization stages. Moreover, continuous system monitoring is critical upon implementation of any new or modified strategies, and may indicate the need for further adjustments to the process models and/or operational policies.

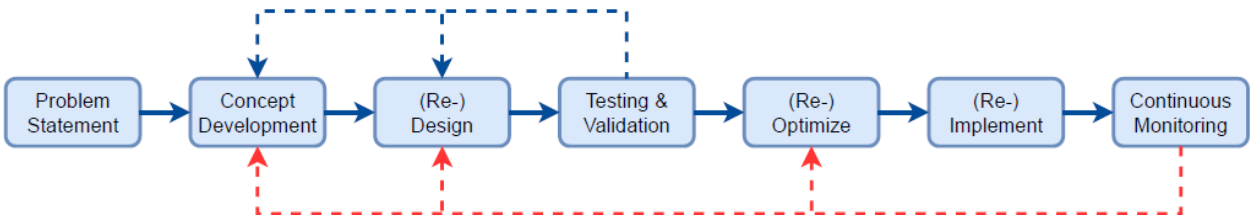

Figure 3.5.2. Generalized flowchart illustrating the importance of a cyclic design and implementation approach to effective development of new or modified process control strategies.

A flexible quantitative framework should also have the capability of being adapted to a range of problem sets and/or temporal scales. Recent system modelling studies have stressed the importance of flexibility towards easy scenario analysis and reusability over the course of mine life for a given project (Upadhyay & Askari-Nasab, 2018). However, this work further extends the concept by proposing that a flexible framework should also be adaptable to a broad spectrum of problems across the mining value chain. By applying the discussed methods to a variety of

different contexts, this research validates the approach of a generalized concept, and highlights its power as a viable tool to plan and evaluate mining system dynamics with a unifying focus on the readjustment phases of the mining life cycle. As shown in Figure 3.5.3, the current methodology is not only useful for initial development planning and design, but also particularly effective towards continuous improvement, re-engineering and post-mine life projects.

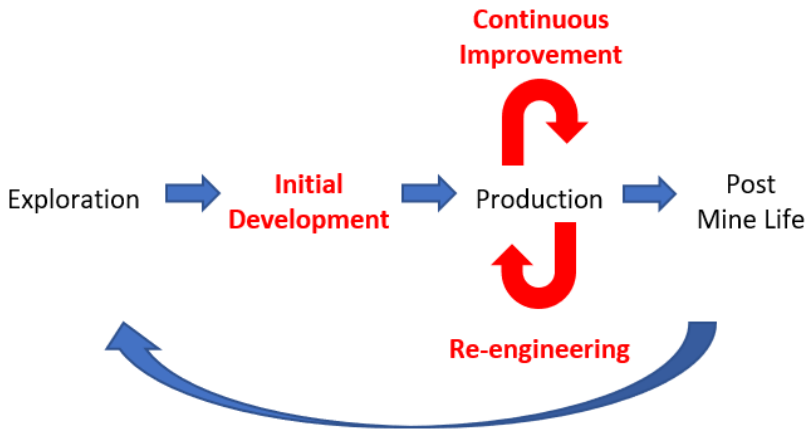

Figure 3.5.3. Schematic diagram of the overall mining life cycle for a given project. The flexible and integrated approach adopted in this research is not only useful for initial development planning and design, but also especially effective towards continuous improvement, re-engineering and post-mine life projects.

The remainder of this thesis is focused on four contexts that adapt a generalized approach to a variety of mining system problems through a series of detailed case studies, including:

1. Tailings retreatment applications (Section 4.1);
2. Predictive modelling of bitumen extraction from oil sands (Section 4.2);
3. Mine-to-smelter integration of regionalized porphyry copper (Section 4.3), and;
4. Mine-to-mill integration for regional development of refractory gold (Section 4.4).

The various contexts were driven by particular needs from research partners and collaborators, but the collection of works is tied together via the unifying principle to integrate advanced quantitative methods into a flexible DES framework to test novel control strategies, evaluate operational risk, and develop suitable operational policies to stabilize system performance. Figure 3.5.4 highlights the adaptability of the current integrated framework by illustrating the breadth of these case studies across the mining spectrum, including commodity type, mine life cycle timing, scope of integration, and implemented data process type.

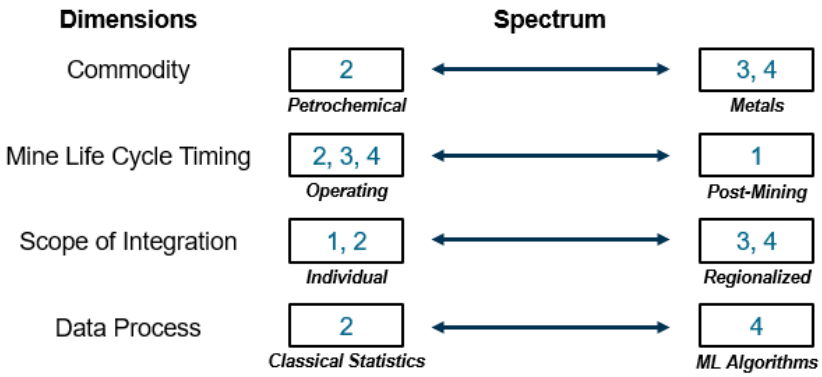

Figure 3.5.4. Schematic diagram highlighting the flexibility and adaptability of the current integrated DES framework to model a broad spectrum of mining contexts and incorporate a variety of data processing techniques by virtue of a series of case studies (numbers correspond to the above case study list) undertaken as part of this research.

Chapter 4

Selected Mining System Applications

4.1 Tailings Retreatment

Mining is fundamental to the development and sustainability of modern society, particularly with respect to the high standards of living that much of the developed world has grown accustomed to. Unfortunately, it is also one of the most detrimental human activities with the potential to cause severe negative impacts on health, safety, and the environment. At the crux of many of these potential side effects is the management strategy, or lack thereof, for waste material and associated tailings residues that result from mining. Mine tailings represent the waste stream following extractive metallurgical processing and are typically stored in tailings dams. As with any structure, these storage facilities have been known to fail over time, causing irreparable damage to human life and communities, fauna and flora, waterbodies and drainage systems, and ecosystems as a whole. Additional risks inherent to tailings storage facilities include the presence of chemical residues and heavy metals, potential acid rock drainage (ARD) and resultant contamination of the surrounding environment, sometimes adjacent to human settlements (Wang, et al., 2014).

Recent estimates for global tailings volumes total over 44.5 billion m^3 in nearly 2,000 storage facilities, and projections total over 55.8 billion m^3 by the year 2025 (GRID-Arendal, 2019). These figures do not include legacy mines which have been abandoned by former companies that were financially incapable, or simply unwilling, to accept the environmental responsibility of appropriate site remediation. Thankfully, increasing environmental awareness and the implementation of stringent mining legislation in most developed nations have limited the conception of new legacy sites. Regardless, these abandoned sites are abundant in mining jurisdictions worldwide, often with little available information; in Canada alone, there are nearly 19,000 orphaned sites of varying scales that have been compiled (NOAMI, 2004). In addition, there is a substantial amount of artisanal mining that is widespread in developing regions, including Africa, Asia, Central and South America, and Oceania (Carvalho, 2017). Artisanal mining activities are small-scale, non-industrial operations typically conducted illegally by large numbers

of people in poverty-stricken rural areas (Carvalho, 2017). These operations are inherently poorly controlled, and tend to leave environmental footprints with waste materials and chemicals haphazardly discarded (Carvalho, 2017). Furthermore, with many of the near surface, high-grade ore deposits already exploited across much of the accessible world, the mining industry is currently geared towards gigantic low-grade, high-tonnage projects that take advantage of recent advances in mechanization and automation (Darling, 2011). These types of operations produce significantly more waste streams and will require increasingly large tailings structures as a result.

Overall, it is clear that appropriate control strategies are needed in order to manage increasing tailings accumulations worldwide. One such strategy that has been gaining traction in recent years is the potential for secondary mining applications. There are currently two main areas of research focused on potential uses for tailings residues: 1) secondary processing for the recovery of metals or elements of interest, and; 2) incorporation into the production of industrial materials. The secondary recovery of metals has long been a consideration, but is inevitably sensitive to market conditions and subject to geological uncertainty; however, there is renewed interest related to the recovery of REEs and increasing demand from the technology sector (Tunsu, et al., 2019). The use of tailings in the fabrication of construction materials (e.g. cement) is a newer concept, but has many potential benefits in terms of site reclamation, in addition to offsetting production costs.

The concept for the current study is focused on the use of tailings for the production of industrial cement. Portland cement is a complex mixture typically made from limestone and clay, thus its primary constituents include CaO (lime) and SiO_2 (silica), with variable amounts of Al_2O_3 and Fe_2O_3, and other minor phases, i.e. MgO, K_2O and Na_2O (Young, 2001; Hurley & Pritchard, 2005). The raw materials are normally ground and heated together in a kiln to a temperature of ~1,400-1,500 ^oC to form what is called clinker (Hurley & Pritchard, 2005). This pyroprocessing step forms the hydraulic calcium silicates that are the active agents in cement (Young, 2001). The clinker is then ground with gypsum ($CaSO_4$) to a fine powder to achieve the desired setting and strength qualities (Hurley & Pritchard, 2005). Since production costs are strongly associated with the fuel consumption necessary to sustain kiln temperatures (Aitcin, 2016), energy-efficient alternatives are highly beneficial to the overall process, and help reduce CO_2 emissions (Gou, et al., 2019). Recent work has shown the ability to use mine tailings as a (partial) replacement for the

aluminosilicate clay component in cement (Gou, et al., 2019; Luo, et al., 2016; Wang, et al., 2019; Qiu, et al., 2011).

The chemical composition of tailings differs greatly across ore deposit types, geological settings, and geographic locations. As a result, not all tailings are suitable for the cement production process, and must be discarded or subjected to additional pretreatment. Examples include those laden with appreciable quantities of metals (potential for ARD), toxic compounds (health and environmental hazards), or elements with deleterious effects on cement quality, for instance, excessive MgO causes disruptive expansion in the hardened paste (Young, 2001). It is therefore important to carry out appropriate chemical characterization of tailings deposits for the potential incorporation into industrial materials (Tripodi, et al., 2019). However, studies have shown that many mine tailings have chemical compositions dominated by SiO_2, Al_2O_3, Fe_2O_3, and CaO, consistent with the natural clay component of most cements (Gou, et al., 2019; Luo, et al., 2016). Moreover, with recent advances in grinding technology for the liberation of primary ore minerals, tailings streams now have a higher proportion of clay-sized minerals.

The vast availability, implied cost efficiencies, and clear environmental implications make the use of tailings an attractive alternative to replace the clay component in cement production operations. However, it is critical to develop models to assess potential risk factors associated with these secondary mining applications. This work introduces a framework capable of integrating geostatistical variability data into discrete event simulation (DES) for the evaluation of system-wide response to geological uncertainty. A case study, using data derived from the Taltal tailings (northern Chile), is presented for a conceptual cement production operation.

4.1.1 Case Study: Taltal Tailings Rehabilitation

The city of Taltal is located along the northern coast of Chile, within the Antofagasta region (Figure 4.1.1). The area has a rich history of mining dating back to the mid-1800s (ancient red ochre, i.e. iron oxide quarries aside). Early mining activities were focused on copper and potassium nitrate deposits (IMT, 2013), but appreciable quantities of gold, silver, nickel and iron have since also been exploited (Tripodi, et al., 2019).

As in many parts of the world, abandoned tailings in Chile continue to pose a threat to human health and safety, as well as the environment. Tracking of these sites was initiated in 2006 by the Servicio Nacional de Geologia y Mineria (SERNAGEOMIN, the Chilean Geological Survey), and recent tallies indicate a total of 740 tailings dams in Chile, 170 of which are abandoned (Tripodi, et al., 2019; SERNAGEOMIN, 2018). More specifically, the Taltal mining district contains the largest number of tailings structures in the Antofagasta region with a total of 24 sites, 10 of which are orphaned (Tripodi, et al., 2019; SERNAGEOMIN, 2018).

Two of these abandoned structures are located along the beach in proximity to both the coast and the surrounding city of Taltal (Tripodi, et al., 2019). This raises concern related to coastal erosion rates and the potential for environmental contamination, as well as health hazards posed by the propagation of fine particulate matter to the nearby population. The present research is based on a conceptual solution to recycle the tailings as a raw material for the production of cement clinker, meanwhile offsetting costs as a tradeoff to replacing a portion of the required natural materials.

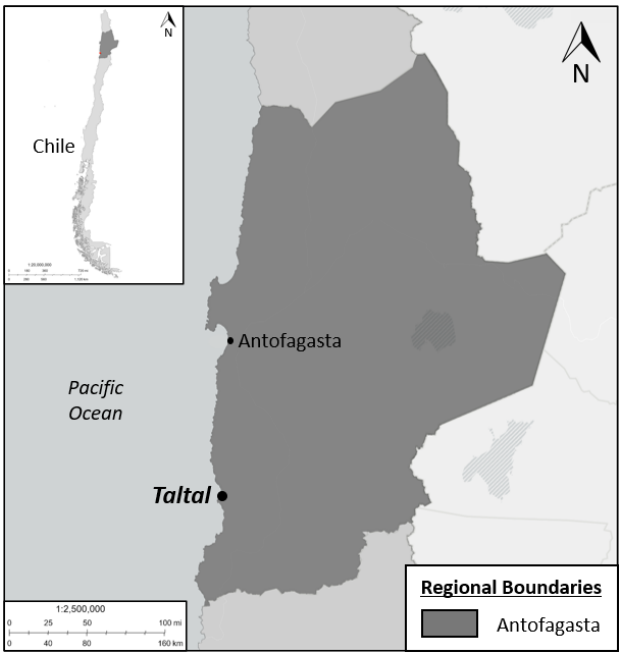

Figure 4.1.1. Location map of case study area, showing Taltal situated in the southern portion of the Antofagasta region. Inset map shows the position of the region relative to Chile. (Map data sources: Esri, HERE, Garmin, FAO, NOAA, USGS, ©OpenStreetMap contributors, and the GIS User Community, Michael Bauer Research GmbH, Instituto Nacional de Estadísticas)

A recent study demonstrated the ability to use iron ore tailings (~45 wt.% SiO_2, ~11 wt.% Fe_2O_3) with minor quartz sand additive to completely replace the natural clay component in a cement clinker (~17% of the raw meal mixture) (Luo, et al., 2016). These iron ore tailings actually increased the burnability and reactivity of the mixture, and promoted the sintering process, resulting in improved cement grindability (Luo, et al., 2016). This acceleration could potentially reduce overall energy consumption and related costs.

Recent mineralogical characterization of the Taltal tailings by Tripodi et al. (2019) indicates high aluminosilicate content (quartz-feldspar-mica-clay) with elevated iron oxides (~8% magnetite-hematite-limonite). Coupled with a particle size distribution dominated by clays and silts (Tripodi, et al., 2019), the tailings appear similar in composition to those used in the iron ore tailing study of Luo et al. (2016). This may support the Taltal tailings as a viable replacement for the natural clay portion in the production of cement clinker. It should be noted, however, that appreciable amounts of gold (~0.25-0.5 g/t) and copper (~0.25-0.5%) were identified, as well as minor contaminants such as arsenic and mercury (Tripodi, et al., 2019). Additional pre-processing may be worthwhile to recover the payable elements and remove the contaminants prior to cement production.

Tailings are complex mixtures of varied mineral and chemical compositions. In the context of potential retreatment applications, it is thus critical to evaluate the operational risks associated with ore feed in relation to geological uncertainty. The current study integrates geostatistical variability data into a DES framework in order to observe the system response to deviations from the expected ore feed. The geostatistical data being used was derived from a database compiled following a drill program completed at the Taltal tailings in 2016 as a collective effort between CSIRO Chile, Universidad de Antofagasta and Chilean state partners. Due to the high variability of the Taltal dataset, the adapted framework implements an alternate mode of operation with select recourse actions in order to improve stockpile management strategies. The primary goal of the model is to maximize throughput to a conceptual cement production facility, meanwhile minimizing total stockpile levels, and mitigating stockout risk. Due to the hypothetical nature of the current study, the process model remains deterministic as no process data could be acquired to assess the system with randomness for pertinent uncontrolled variables, such as tailings deposition, settling and

weathering processes. However, the framework is extensible and submodels can be developed to handle downstream modeling, depending on a given project scope.

4.1.2 Geostatistical Modeling and Simulation

The dataset was compiled from a total of 53 composite samples in 18 holes drilled within an approximate volume of 140m × 70m × 4m (the larger of the 2 tailings structures). Compositional data was acquired by a number of analytical techniques, including x-ray fluorescence (XRF), induced coupled plasma optical emission spectrometry (ICP-OES), and x-ray diffraction (XRD). The study was carried out using 12 variables (elemental concentrations) of interest, including Al, As, Ca, Cu, Fe, K, Na, Mg, Si, Au, Pb, and Hg. For the analysis, the sample volume was divided into 23 nearly equal sized mining parcels. The sparse sampling coupled with spatial heterogeneity imply a high uncertainty in the concentrations at unsampled locations in the volume of the tailings (hereafter referred to as 'geological uncertainty'), which will be modeled through the generation of simulated scenarios (realizations), as explained hereunder.

The methodology begins by computing basic descriptive statistics to summarize the original raw dataset (Table 4.1.1). A variety of tools can be generated to better understand the distribution of each individual variable (Figure 4.1.2) and correlation matrices can also be computed to provide early information on the relationships between variables. The analysis proceeds by transforming the original data of each variable into normal scores, i.e. data with a standard Gaussian distribution. Declustering of the data is unnecessary in this case due to a regular drill pattern, and because the tailings are being considered as a single lithology. An empirical transformation is obtained by associating each original data (grade) with the Gaussian value having the same cumulative frequency. This empirical transformation is then interpolated by a piecewise linear model within the range of the data values and extrapolated by exponential functions beyond the extreme values, following the approach described in Emery and Lantuéjoul (2006) (Figure 4.1.3).

Table 4.1.1. Descriptive statistics for 12 variables of interest from Taltal tailings data (n=53 data).

Element	Mean (%)	Variance (%^{2})	Min (%)	Max (%)
Al	2.44400	0.28350	0.88650	3.70370
As	0.00270	0.00000	0.00101	0.01192
Ca	2.19224	0.81994	0.70930	5.48920
Cu	0.28339	0.02729	0.08507	0.87400
Fe	5.22434	0.99435	3.53050	7.34580
K	0.18597	0.02076	0.06504	0.68490
Mg	1.90226	0.20609	0.60930	3.35710
Na	0.10502	0.00800	0.01000	0.51200
Pb	0.00590	0.00003	0.00150	0.02721
Hg	0.00031	0.00000	0.00001	0.00322
Au	0.00003	0.00000	0.00001	0.00014
Si	87.49	4.49	82.55	93.22

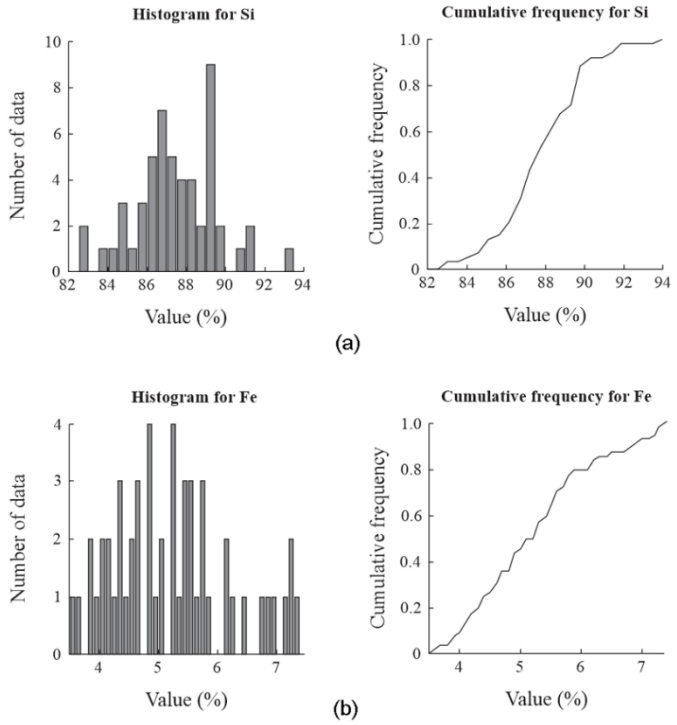

Figure 4.1.2. Histograms and cumulative distribution function plots of Taltal tailings data for (a) Si, and; (b) Fe.

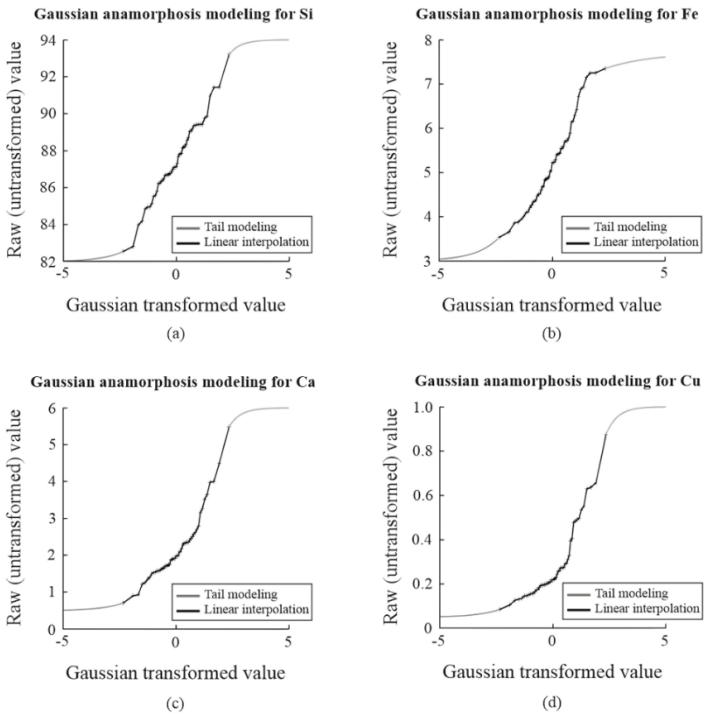

Figure 4.1.3. Gaussian transformation functions relating the original data values (vertical axis) and the normal scores (horizontal axis) for (a) Si, (b) Fe, (c) Ca, and (d) Cu variables.

The experimental direct and cross-variograms (Wackernagel, 2003) are then calculated for the transformed (normal scores) data and fitted with a linear model of coregionalization. Only two directions (horizontal and vertical) were considered for the current study due to the small sample size, as well as the geometry of the tailings structure and the orientation of drilling. Parameters selected for the experimental variography included azimuth and dip tolerances of 90º and 20º, respectively; lag tolerance was set to 10m in the horizontal direction, and 0.3m in the vertical direction. A nugget effect and one spherical variogram model were used to fit the experimental variograms, using a least-square fitting algorithm ensuring the mathematical consistency of the fitted model (Goulard & Voltz, 1992). Examples of direct variograms for Si and Fe are presented in Figure 4.1.4, and both direct and cross-variograms for Ca and Cu are given in Figure 4.1.5.

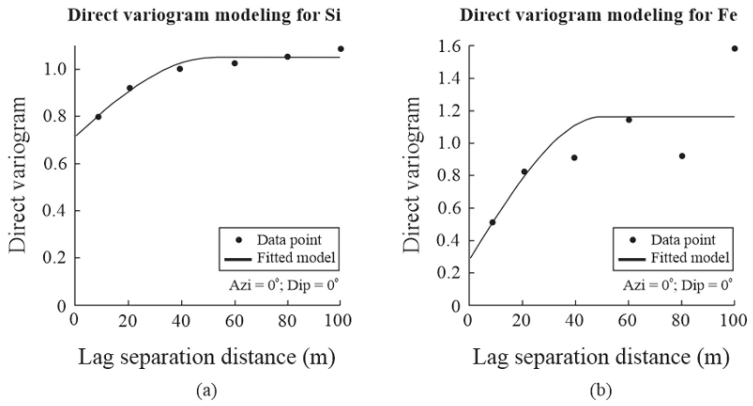

Figure 4.1.4. Representative direct variograms in the horizontal direction for (a) Si, and; (b) Fe.

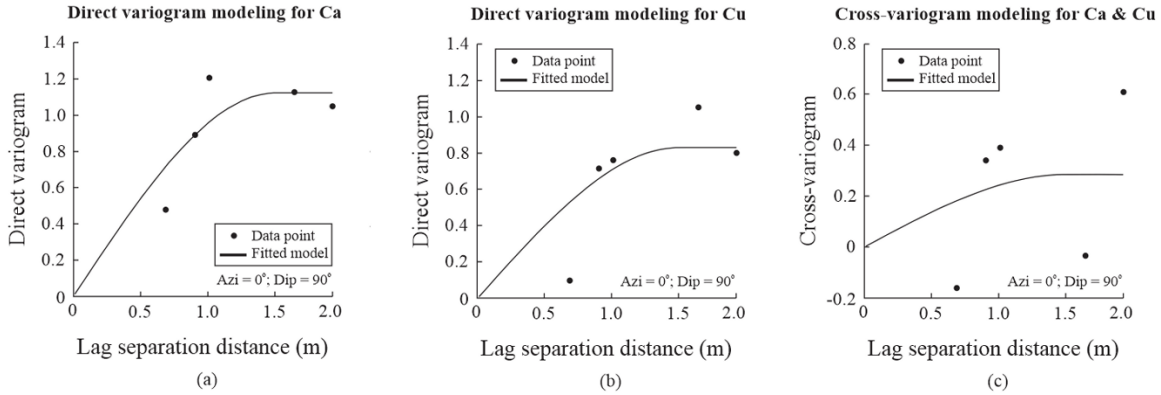

Figure 4.1.5. Representative direct and cross-variograms in the vertical direction for Ca and Cu. The scattered nature of limited data points in the above variography modeling could lead to elevated fitting errors; however, the primary intent at this stage is to identify important spatial features for the attribute, not to perfectly fit the model to the data (Li, et al., 2018; Goovaerts, 1997).

The variables were finally jointly simulated using the turning bands co-simulation program of Emery (2008) with one thousand turning lines. The program takes the normal scores data and the fitted coregionalization model as inputs to compute conditional realizations of the elemental concentrations over a user-defined grid. Data conditioning is performed by ordinary co-kriging, and the supplied transformation functions are used to back-transform the realizations for each variable to its original units (Emery, 2008). A total of 100 realizations were constructed for each variable, which reflect the spatial variability within the volume of the tailings dam as well as the cross-correlations between elemental concentrations. Figures 4.1.6a and 4.1.6b provide examples of the average concentration and variance maps for Fe over all of the realizations. Probability statistics and maps can then be calculated to assess the likelihood that a given variable meets or

crosses critical thresholds, as in Figure 4.1.6c. As discussed in Section 3.4.2, the mining parcels and related sequencing were generated as part of the overall geostatistical simulation process.

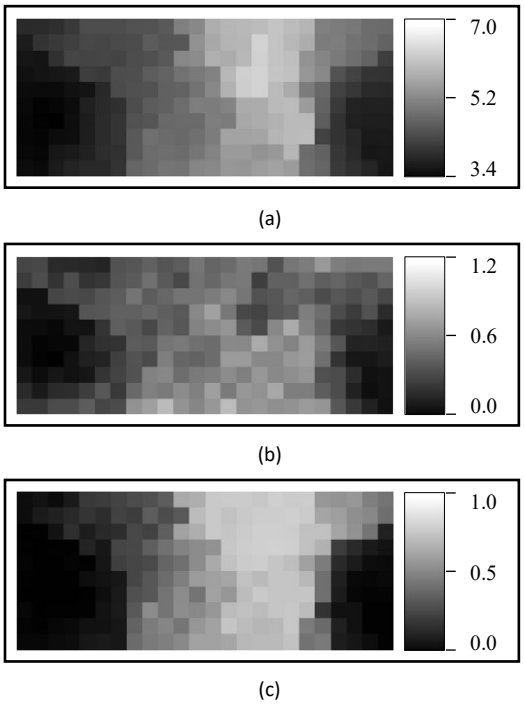

Figure 4.1.6. Average elemental concentration, variance, and probability maps for Fe derived from the consolidated Taltal tailings dataset using the turning bands co-simulation method: (a) local mean distribution map; (b) local variance distribution map, and; (c) probability distribution map of Fe meeting a minimum threshold of 5%. Each image represents a horizontal surface map of the sampled tailings dam, corresponding to an area of 120m (horizontal axis) x 50m (vertical axis). Data have been averaged over 5x5x1m block units, as indicated by individual image pixels.

As described in Section 4.1.1, recent studies have successfully replaced the natural clay component (~17%) in cement clinker with iron ore tailings, and noted the added benefit of increasing burnability and reactivity which promotes the sintering process (Luo, et al., 2016). This could potentially lead to increased energy efficiencies and related cost reductions in the production of industrial cement. Mineralogical and chemical characterization of the Taltal tailings indicate a similar overall composition as the iron ore tailings, with high aluminosilicate content and elevated iron oxides (Tripodi, et al., 2019). As a result, Fe was selected as the primary variable of interest for integration into DES to evaluate the potential system response to geological uncertainty. The framework aims to maximize throughput, enhance stockpile management and mitigate stockout risk for a conceptual tailings pretreatment circuit at a cement production operation.

4.1.3 Discrete Event Simulations

For the DES portion of the study, three material types have been classified according to the geostatistical simulations: 1) ore type 1 (>5% Fe); 2) ore type 2 (between 4-5% Fe), and; 3) waste (<4%). Similar to Navarra et al. (2019), two modes of operation (A and B) are under consideration to balance stockpile levels against 'cement production rates' (akin to milling rates) and incoming ore feed from mining. Despite an overall composition for the tailings deposit estimated at an average blend of 60-30-10 for ore type 1, ore type 2 and waste (respectively), high-level mine planning suggests that the bulk of early excavations could be limited to areas with slightly higher ore type 2 content. As a result, operational Mode A will consist of an approximate 45-55 blend of ores 1 and 2. Longer term forecasts suggest significant distribution variability with a mixture of areas dominated by ore types 1 and 2. Because ore type 2 is generally in shorter supply, a second operational Mode B, consisting of a 90-10 blend of ores 1 and 2, is needed in order to avoid an ultimate shortage. This will allow for seamless production scheduling, stable feed balances and the selection and consistent utilization of mining equipment, all of which can result in decreased operating and capital costs.

Under this conceptual framework, both modes are assumed to exhibit similar downstream performance in the production of industrial cement, except that Mode B requires additional grinding in order to break down the coarser mineral grains associated with ore type 1. Cement production rates under Mode B are therefore set at 80% of those under Mode A. Parameter details for each of the modes are summarized in Table 4.1.2, along with conventions for their algebraic notation. Though Mode A is clearly more productive, its continuous application will inevitably lead to stockouts as the weight fraction of ore type 2 (w_{2A}) is much greater than that of the deposit (w_{2D}). Contingency modes for each of Mode A and Mode B are also included in the event a stockout occurs prior to a planned shutdown.

Table 4.1.2. Description of operational modes in relation to deposit forecast.

		Throughput (t/h)	Ore 1 in feed (%)	Ore 2 in feed (%)
	Algebraic Notation:	$r_{A,ACont,B,BCont}$	$w_{1A,1ACont,1B,1BCont}$	$w_{2A,2ACont,2B,2BCont}$
Mode A	Regular	25	45	55
	Contingency	16.25	100	0
Mode B	Regular	20	90	10
	Contingency	10	0	100
Deposit		-	65	35

A deterministic analysis to balance the respective weight fractions ($w_{1A,2A,1B,2B}$) and rates of throughput ($r_{A,B}$) against the geological forecast ($w_{1D,2D}$) for the two-mode model has been carried out using the following equations (Navarra, et al., 2019):

$$\left(\frac{t_A}{t_B}\right) = \left(\frac{w_{2B}w_{1D} - w_{1B}w_{2D}}{-w_{2A}w_{1D} + w_{1A}w_{2D}}\right)\left(\frac{r_B}{r_A}\right), \tag{4.1.1}$$

in which t_A and t_B represent the time devoted to Mode A and Mode B, respectively. The average throughput is then determined as follows (Navarra, et al., 2019):

$$r = \left(\frac{w_{1A}w_{2B} - w_{2A}w_{1B}}{\left(w_{2B}\left(\frac{r_B}{r_A}\right) - w_{2A}\right)w_{1D} - \left(w_{1B}\left(\frac{r_B}{r_A}\right) - w_{1A}\right)w_{2D}}\right)r_B. \tag{4.1.2}$$

Similar equations can also be derived in order to balance throughputs between each of the regular modes and their corresponding contingency modes (refer to Navarra et al., 2019, for additional details).

Barring the risk of stockout, Eqs. (4.1.1) and (4.1.2) indicate a 50-50 split between modes A and B, with a corresponding average throughput of 22.41 t/h. The objective of the framework is to maximize throughput meanwhile minimizing the target size of stockpiles in order to reduce overall costs. Larger stockpiles require larger storage pads and handling equipment, as well as increased operating costs to manage the lifting and moving of material. In any case, the adoption of an additional mode will likely require certain upgrades to infrastructure and stockpiling equipment.

The framework operates under the assumption that mining rates exceed plant capacity. With the plant thus acting as a bottleneck, stockpiles are required to maintain consistent ore feed. As a result, ore will be mined at 25 t/h under Mode A and 20 t/h under Mode B to sustain the target total stockpile level. Despite a constant total stockpile level, the proportion of ore types 1 and 2 is

expected to fluctuate depending on the mode of operation. Mode A should cause an increase in the proportion of Ore 1 relative to Ore 2, with the reverse effect expected under Mode B. The mode of operation is selected based on individual stockpile levels at the end of a production campaign during planned shutdowns every 5 weeks.

A naïve analysis determines that Mode B should only be selected when the stockpile level for ore type 2 is below a critical threshold of 3,910 t. For the present scenario (Table 2), the Ore 2 stockpile level is expected to decrease by 115 t/day under Mode A. With a production campaign length of 34 days, the critical level for Ore 2 is computed as 115 t/day x 34 days = 3,910 t (recall that the 're-order point' is directly proportional to the expected rate of consumption and the lead time to replenish the stockpile levels). This deterministic calculation does not take geological uncertainty into account, nor the related stockout risk. Specifically, if the actual proportion of a given ore type is lower than expected under a particular mode of operation, there is a real possibility of stockout towards the end of a production campaign (Navarra, et al., 2019). It must therefore be considered whether to raise the threshold for the critical ore type and/or the target total stockpile level (and to what extents) in order to mitigate the potential stockout risk.

If stockout occurs during a production campaign, a contingency mode is implemented wherein only the available ore type is consumed to allow the depleted ore type to build back up before reverting back to the regular mode. For the current scenario, Contingency Mode A only consumes Ore 1, whereas Contingency Mode B only consumes Ore 2 (Table 4.1.2). Because the contingency modes are far less productive than their regular counterparts, the duration of contingency mode segments has been set to 1 day which causes the plant to alternate between regular and contingency until the next planned shutdown. The time segment parameters for production campaigns, planned shutdowns and contingency mode segments are summarized in Table 4.1.3. If the critical ore level remains below the selected threshold at the end of a production campaign, the plant will then switch to the alternate mode of operation in order to re-balance the stockpiles.

Table 4.1.3. Summary of time segment parameters.

Segment type	Duration (days)
Production campaign	34
Planned shutdown	1
Contingency modes	1
Regular modes	Indeterminate

The current framework was implemented, and subsequent computational results (Figures 4.1.7–4.1.9) generated, using commercial DES software (Rockwell Arena©) with Visual Basic for Applications (VBA). The framework can simulate hundreds of days of operation to evaluate the system-wide response to geological uncertainty while varying the critical ore and target stockpile levels as control variables. As previously described, the primary objective of the model is to maximize throughput while minimizing stockpile levels. It should be noted that the simulation model currently assumes that ore is mined to completion from a single parcel at a time.

The framework has the flexibility to incorporate geological uncertainty by reading data from varied external source files. As previously described, the present study integrates geological variability data loosely based on a case study of the Taltal tailings in northern Chile. The model of Navarra et al. (2019) has been scaled down to reflect a tonnage more in line with the Taltal tailings site. The framework has been configured such that 480,000 t of ore are processed within each replica, corresponding to approximately 1,000 days of operation. The model has also been adjusted to handle a third material type as waste. Unlike the ore stockpile levels, this reject material accumulates solely as a function of the mining rate and thus does not take plant production rates into account. A rate of waste accumulation (‘rejectput’) is calculated in addition to the standard ore feed throughputs.

To assess the effects of the set control variable levels on the system-wide response to geological uncertainty, a series of simulations were run to monitor throughputs and potential stockout risk. The first set of simulations were conducted by holding the critical Ore 2 level constant at 3,910 kt, and varying the total stockpile target levels. Five scenarios were considered with total stockpile levels corresponding to 1x, 1.5x, 2x, 3x, and 5x the selected critical Ore 2 level. Simulated results for each scenario are summarized in Table 4.1.4.

Table 4.1.4. Distribution of time spent in each mode type under varied target total stockpile levels.

Scenario:		1	2	3		4	5
Replications:		1	1	1	*100*	1	1
Critical Ore 2 Level (t):		3,910	3,910	3,910	*3,910*	3,910	3,910
Target Total Stockpile Level (t):		3910 (1x)	5865 (1.5x)	7,820 (2x)	*7,820 (2x)*	11,730 (3x)	19,550 (5x)
		Portion of time (%)					
Mode A	Regular	0	48	59	*58*	59	58
	Contingency	0	3	1	*1*	1	1
Mode B	Regular	61	39	37	*36*	37	38
	Contingency	36	7	0	*2*	0	0
Shutdown		3	3	3	*3*	3	3
Throughput (t/h)		16.16	21.53	22.92	*22.51*	22.90	22.90
Rejectput (t/h)		1.10	1.59	1.67	*2.12*	1.65	1.74
Replications with stockouts		-	-	-	*66*	-	-

Consistent with findings by Navarra et al. (2019), the first scenario shows that naïve selection of the critical ore level using the deterministic result, when the total stockpile is also low, causes the simulation to run strictly in Mode B with an average throughput of only 16.16 t/h. Not only is this result significantly lower than the deterministic value of 22.41 t/h computed from Eq. (4.1.2), but the operation also suffered from chronic shortages of ore type 1, as shown in Figure 4.1.7a. Increasing the target total stockpile level by just 1.5x already shows marked improvement in the overall system response. This second scenario produced a near even split between Modes A and B (51-46, respectively), and an average throughput of 21.53 t/h, which are in general agreement with both Eqs. (4.1.1) and (4.1.2), i.e. within 5%. The portion of time spent in contingency modes (10%), however, may still be considered a little too high and suggests the risk of stockout could be further mitigated. Doubling the total stockpile target (Scenario 3) continues to show slight improvement with an average throughput of 22.92 t/h caused by a higher portion of time spent in the more productive Mode A (60%). The overall system response to geological uncertainty was also much smoother with only 1% of the time partitioned to contingency mode segments, as in Figure 4.1.7b. Subsequent increases to the stockpile targets (Scenarios 4 and 5) did not identify any significant changes to the simulated data. This suggests that the total stockpile target is best maintained at levels in the range of twice the selected critical ore threshold value in order to maximize throughput, and mitigate the risk of ore stockout.

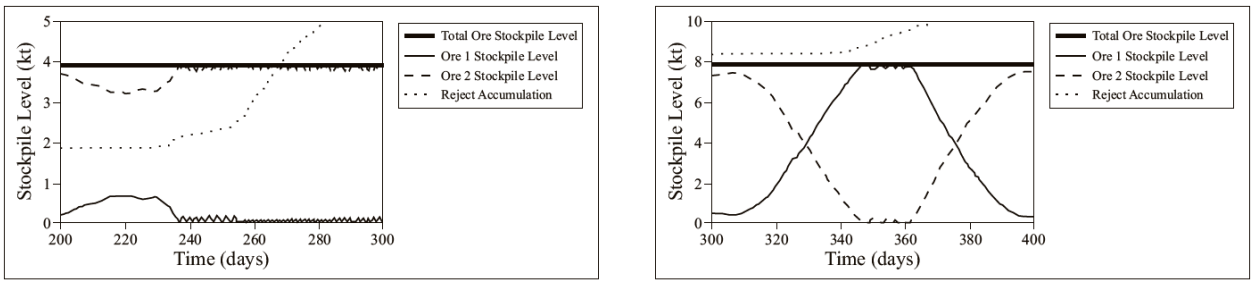

Figure 4.1.7. Simulated operational dynamics of Taltal tailings data in response to geological uncertainty, applying a constant critical Ore 2 level of 3,910 t (deterministic result), and total stockpile target levels of (a) 3,910 t under Scenario 1, and; (b) 7,920 t under Scenario 3. Contingency modes are indicated by the fine jagged saw-tooth pattern resulting from short contingency segment durations of 1 day (Table 4.1.3); note the significant proportion of contingency mode segments in (a) relative to (b).

Based on these findings, the framework was then configured using the parameter values from Scenario 3 to run through 100 replications, corresponding to nearly 100,000 simulated days of operation. The simulated results from this test were nearly identical to the single replication scenario (Table 4.1.4), except that approximately 2/3 of the replications experienced stockouts. This elevated risk of stockout was not apparent in the single replication scenario, and points to the high variability of the source geostatistical data. Some of the stockout periods were relatively frequent and sustained, requiring the implementation of mining surges as a recourse action to supply ore feed directly to the plant to maintain production. A mechanism was built into the framework to decrease mining rates by 25-50% following a surge in order to allow for a smoother transition back to normal mining conditions, as shown in Figure 4.1.8a. Greater reductions to the mining rate cause punctuated mining episodes (Figure 4.1.8b), which are neither conducive to planning nor sustainable for a typical mining operation.

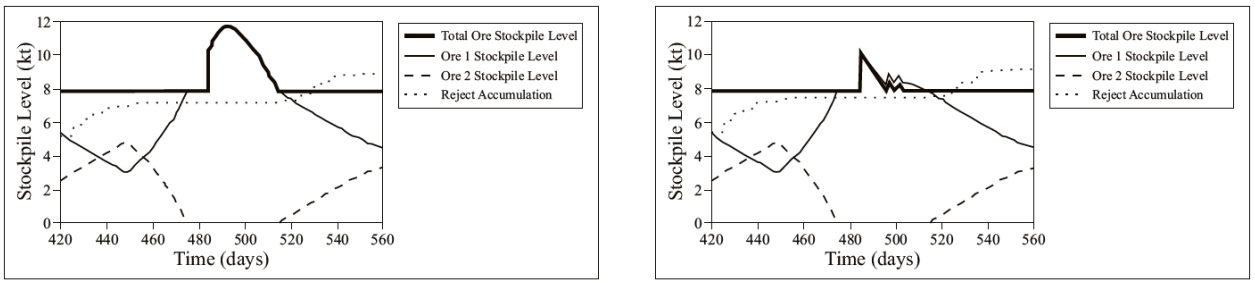

Figure 4.1.8. Simulated mining surges caused by high variability of Taltal tailings data in response to geological uncertainty, applying mining rate reductions of (a) 25%, and; (b) 75%. Surges are indicated when the level of one of the ore types increases above the total ore stockpile target level to provide feed directly to the plant in response to a sustained stockout of the other ore type (~480-510 day range in both images). Mining rate reductions of greater than ~50% following a surge cause multiple punctuated mining episodes in order to sustain plant production, as in (b).

To mitigate the high risk of stockout identified (66% of replications), a second set of simulations were carried out to evaluate the effect of increasing the critical Ore 2 threshold value. Three scenarios were considered with critical ore levels corresponding to 1.5x, 2x, and 3x the deterministic value (3,910 t). Consistent with the above findings, total ore stockpile target levels were set at 2x the selected critical ore value. Simulated results for each scenario are summarized in Table 4.1.5.

Table 4.1.5. Distribution of time spent in each mode type under varied critical ore levels.

Scenario:		6		7		8	
Replications:		1	*100*	1	*100*	1	*100*
Critical Ore 2 Level (t):		5,865 (1.5x)	*5,865 (1.5x)*	7,820	*7,820*	11,730 (3x)	*11,730 (3x)*
Target Total Stockpile Level (t):		11,730	*11,730*	15,640	*15,640*	23,460	*23,460*
		Portion of time (%)					
Mode A	Regular	56	*60*	56	*61*	56	*61*
	Contingency	0	*1*	0	*0*	0	*0*
Mode B	Regular	40	*35*	41	*35*	41	*36*
	Contingency	1	*1*	0	*1*	0	*0*
Shutdown		3	*3*	3	*3*	3	*3*
Throughput (t/h)		22.78	*24.00*	22.82	*24.08*	22.82	*24.19*
Rejectput (t/h)		1.65	*2.40*	1.56	*2.39*	1.64	*2.48*
Replications with stockouts		-	*40*	-	*9*	-	*2*

These results indicate that adjusting the critical ore threshold had no significant effect on throughput rates; however, important decreases in the number of stockout periods were noted when the framework was configured for 100 replications (~100,000 operating days). By doubling the critical Ore 2 threshold value, the number of simulated replications that suffered from ore shortages was reduced to less than 10% (Table 4.1.5). Tripling the critical value decreased the number of replications with stockout periods down to only 2%. This significantly reduces the risk factor for stockouts, but one must also account for the increasing stockpile levels, and related costs, in the decision-making process.

Figure 4.1.9 depicts the time-averaged distribution of operational modes in response to geological uncertainty for 2 different scenarios. Figure 4.1.9a is based on the same data from Scenario 3 over 100 replications (Table 4.1.4), which was configured using a naïve deterministic critical Ore 2 level of 3,910 t. Though a similar analysis concludes a deterministic total ore

stockpile target of 3,952.5 t, early simulation trials indicated nearly chronic ore shortages under such a scenario, and highlighted the high variability of the geostatistical dataset. As a result, the 'naïve' configuration in Figure 4.1.9a used a total stockpile target level set at 2x that of the critical ore level, i.e. 7,820 t. Figure 4.1.9b represents an enhanced framework configuration, making use of conclusions from the first 2 sets of simulations described above. This enhanced operational policy is also based on 100 replications, and used a critical Ore 2 threshold of 7,500 t (nearly 2x the deterministic value) with a total stockpile target of 16,875 t (2.25x the critical value). The distribution of operational modes between the two scenarios is similar, but the enhanced configuration applies Mode A 3% more frequently, and does not include any contingency modes; overall, this results in a slightly more productive operation. Despite similar distributions, both framework applications benefit from the ability to switch between modes relatively freely due to the data variability, and timing for extraction of each mining parcel. The key difference between the two scenarios lies in the potential exposure to stockout risk. The 'naïve' setup is highly sensitive to stockout risk with ore shortages observed in ~2/3 of the simulated replications (Table 4.1.4), whereas the enhanced configuration only identified stockout risk in 3% of trials.

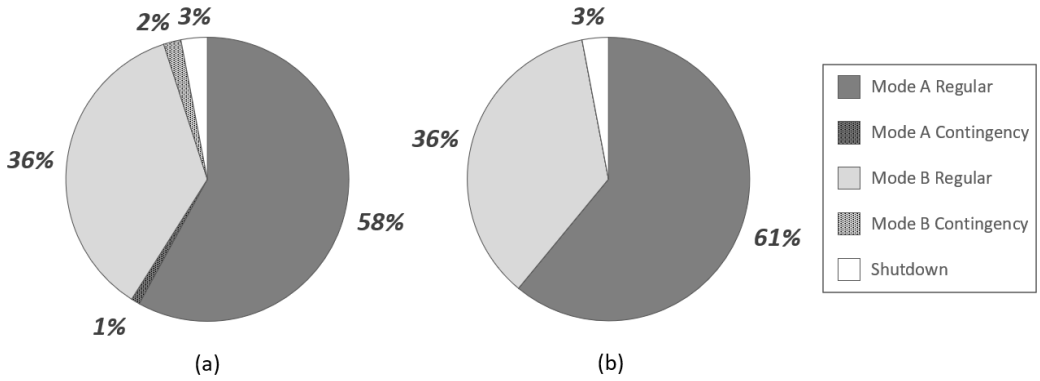

Figure 4.1.9. Time-averaged distribution of operational modes in response to geostatistical variability data from the Taltal tailings in northern Chile, for (a) 'naïve' framework application using a critical Ore 2 threshold of 3,910 t and target total stockpile level of 7,820 t (2x), and; (b) enhanced configuration using a critical value of 7,500 t and target total stockpile level of 16,875 t (2.5x).

4.1.4 Conclusions

The overall results of these simulation studies support the flexibility of the current DES framework to integrate geostatistical variability data in order to evaluate the system-wide response to geological uncertainty. The simulation model is an extension of recent conceptual work by

Navarra et al. (2019) and incorporates a third material type as waste throughput (i.e. 'rejectput'). A case study loosely based on the Taltal tailings site in northern Chile demonstrates how the framework can be adapted to assess risk factors associated with potential secondary mining applications. Simulations using this high variability data indicate the likelihood of ore stockouts at the Taltal site, but the framework provides the means to analyze the effect of adjusting critical parameters and assist with decision-making. Equipment size selection and potential infrastructure upgrades can then be weighed against the additional capital and operating costs associated with larger stockpiles. Such costs could potentially be offset by implementing alternate modes of operation in order to achieve higher throughputs and mitigate the risk of stockouts.

The Taltal data proved to be highly heterogeneous, which points to the fact that tailings deposits are sometimes the result of processing different ore types over different time periods, as was the case here (Tripodi, et al., 2019). This makes the definition of different geometallurgical units especially difficult, and highlights the additional challenges faced by tailings deposits in the context of secondary mining applications. Abandoned tailings deposits are usually poorly documented and require complete mineralogical and chemical characterization, with carefully planned sampling protocols appropriate to the intended end use.

In order to drive and further promote the concept of using tailings as a partial substitution of raw materials in the production of cement clinker, more case studies are required to generate realistic flow sheets and determine the most critical parameters affecting system-wide metrics (Suazo, et al., 2010). In the case of abandoned tailings, wherein the responsibility for site remediation generally falls on the state, synergistic efforts from academic, government and industry partners are likely needed to generate sufficient interest and opportunities for centralized, regional cement production plants.

4.2 Bitumen Extraction from Canadian Oil Sands

With conventional oil and gas reservoirs being gradually depleted worldwide, activity in the research and exploitation of unconventional resources has grown exponentially over the past two decades. Global estimates of in-place bitumen and heavy oil resources are on the order of 5.9 trillion barrels (938 billion m^3), over 80% of which are concentrated in Canada, Venezuela and the United States (Bata, et al., 2019). Boasting the largest collection of these deposits globally with

approximately 1.7 trillion barrels (270 billion m^3) of in-place resources (Bata, et al., 2019), Canada is strategically positioned as an important source of unconventional petroleum products. Of this total, roughly 165 billion barrels (26.3 billion m^3) are considered technically recoverable, and thus correspond to Canada's estimated remaining established reserves (Bata, et al., 2019). Unlike traditional light oil well drilling which will decline over time, forecasts show an overall 12% increase in unconventional petroleum production over the next 30 years, with peak rates reached in 2039 (CER, 2020).

Bitumen and heavy oil reservoirs typically occur in unlithified sand deposits (also called 'bituminous', 'tar' or 'oil' sands); however, heavy oil is also found within porous siliciclastic and carbonate host-rock successions due to its relative mobility (Bata, et al., 2019). These reservoirs are generally heterogeneous, containing a variety of different hydrocarbons across the American Petroleum Institute (API) gravity spectrum (from light oil to bitumen). By definition, heavy oil is marginally less dense than water (0.920 g/mL) and corresponds to API gravities in the range of 10–20°; conversely, bitumen and extra-heavy oils are denser than water with API gravities of less than 10° (Bata, et al., 2019; Hein, 2006). Crude bitumen and heavy oil resources are lacking in terms of lighter distillates, which significantly reduces their market value; consequently, both must undergo upgrading to increase commercial value and marketability. Upgrading to synthetic crude oil products (~20–40° API) involves the addition of hydrogen in order to attain H:C ratios similar to those of conventional crudes, as well as the removal of impurities such as nitrogen, sulphur, oxygen and heavy metals (Bata, et al., 2019).

The current study is concerned with processes specific to the exploitation of oil sand deposits. Typically, economical oil sands contain on the order of 9–13% bitumen (soluble organic matter), 3–7% water, and 80–85% mineral solids and insoluble organic matter (Hein, 2006; Gray, et al., 2009). Generally, 15–30% of the total solids are fines (mainly clays), less than 44 μm in diameter (Gray, et al., 2009). Most deposits are comprised of unconsolidated sand 'bound' by a matrix of bitumen, with or without secondary cements and clays (Hein, 2006). Despite broad acceptance of the origin and emplacement of bitumen reservoirs, oil sand deposits are subject to substantial levels of geological uncertainty in terms of host formation characteristics, ore composition, grade, and overall processability. All of these process variables are strongly influenced by variable and

complex host-formation and hydrocarbon depositional histories, in addition to post-depositional alteration processes such as biodegradation and in situ natural water washing (Algeer, et al., 2016; Fustic, et al., 2015). Each of these contributing factors can lead to significant variability in ore feed particle size distributions, host-formation mineralogy and hydrocarbon chemistry and quality, all of which have direct impacts on downstream processing.

As with many types of mining projects, there are a variety of processes along the oil sands value chain; each of these streams may serve a particular function, but also require coordination of inputs and outputs with both up- and down-stream processes. This coordination can be difficult to maintain at times even for systems that receive relatively stable ore feeds, but is exponentially problematic for projects dealing with heterogeneous ores. For example, blending strategies are common in mining for grade control or to minimize undesirable impurities in ore feeds; however, oil sand operations must also consider factors such as grain size distribution and mineral chemistry in order to regulate the transfer of intermediate products (e.g. slurries or froths) within hydrotransport pipelines. Furthermore, some complex ores may require additional treatment prior to, or between, conventional processing methods. For instance, heavy gas oil phases partitioned by distillation during upgrading are fed to fluid cokers and hydrocrackers to increase H:C ratios and break down long chain molecules (Masliyah, et al., 2011). Similarly, problematic high chloride oil sands, often with elevated clay contents, could require ancillary control strategies (e.g. water content reduction, additives/inhibitors, and blending) to reduce corrosive effects or blockages (i.e. ammonium chloride) related to hydrolysis reactions in downstream processes (Gray, et al., 2008; Kaur, et al., 2012; Li, et al., 2018; Londono, et al., 2009).

Improper process control strategies that do not suitably incorporate the geometallurgical profile of source ore feeds can result in major bottlenecks in mining and processing operations, ultimately leading to increased operating costs, decreased efficiencies, and even potentially important reductions in project life. Several authors have emphasized the importance of establishing alternate modes of operation for mineral processing facilities (Navarra, et al., 2018; Navarra, et al., 2017a). Alternate modes are designed using mass balance and mathematical programming, and the operational decision to switch between modes is triggered by changing conditions or as critical thresholds are crossed (Navarra, et al., 2018; Navarra, et al., 2017a). The

approach is particularly effective for complex mining systems dealing with heterogeneous ore feed and process variables, as demonstrated by recent studies (Navarra, et al., 2020; Navarra, et al., 2019; Saldaña, et al., 2019; Wilson, et al., 2021a). Continuous online material and system process monitoring notwithstanding, a natural and powerful extension is to couple the development of operational modes with robust predictive models that benefit from earlier systematic sampling protocols. This type of integrated approach can lead to improved planning and fine-tuning earlier in the value chain, rather than being forced to make continual reactive adjustments based on process outputs (e.g. bitumen recoveries).

Given the high degree of variability inherent to oil sands mining and processing operations, it is evident that appropriate quantitative frameworks are needed in order to monitor system performance and response under changing conditions. One such computational intelligence tool is the digital twin, which is an integrated multidisciplinary probabilistic simulation of a system that uses the best available data models, updates, and history to mimic the operational life of the corresponding physical system (Boschert & Rosen, 2016; Glaessgen & Stargel, 2012). The development of digital twins using discrete event simulation (DES) is an effective approach because it allows for the simulation of interactions between critical parameters and processes with respect to random natural variations, e.g. geological uncertainty. Furthermore, DES models can also optimize tradeoffs between available operational policies, as well as the limits that dictate the timing of their execution (Navarra, et al., 2019; Saldaña, et al., 2019; Wilson, et al., 2021a). By simulating extended operating periods, potential deficiencies or bottlenecks in the coordination of system processes can be identified; strategic decisions can then be made to adjust operational policies accordingly, thereby pre-emptively assessing and managing risk factors. The drive to improve overall system efficiencies is further amplified by increasingly stringent environmental regulations, industry best practices, and pressure from community stakeholders.

This work introduces an extended framework capable of integrating predictive modelling using partial least squares (PLS) regression incorporated within a digital twin, for the evaluation of system response to geological uncertainty. A case study using data derived from Canada's oil sands is presented for a conceptual surface mining operation to assess the effect of implementing

potential new ore blending schemes. The initial dataset was kindly acquired through partnerships with the National Research Council Canada and Syncrude Canada Ltd.

4.2.1 Geology and Petrochemical Processing

Canada's vast oil sand resources are located almost exclusively in northeastern Alberta, within three core areas, namely the Peace River, Athabasca and Cold Lake deposit regions (Figure 4.2.1) (Masliyah, et al., 2011; Kaminsky, 2008). Collectively, these accumulations span an area of approximately 142,000 km^2 (Masliyah, et al., 2011; ERCB, 2009), the largest of which is the Athabasca region, containing ~75% of provincial reserves (Kaminsky, 2008; Zhao, et al., 2001).

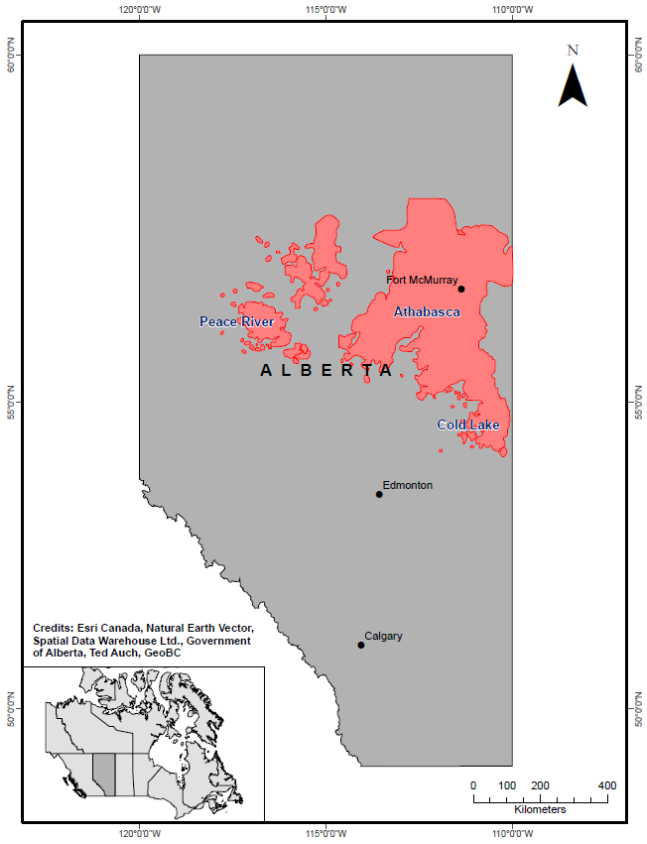

Figure 4.2.1. Location map of the Alberta Oil Sands Region (AOSR), showing the relative positions of the Peace River, Athabasca and Cold Lake oil sand deposit areas.

Generally, the Alberta oil sands have a thin overburden and the deposits are concentrated within the early Cretaceous McMurray Formation (Mannville Group), which has variable thickness related to an original depositional surface defined by karstic features in underlying Devonian carbonates (Hein, 2006; Gray, et al., 2009). The present-day low API oils are the result

of degraded Exshaw Shale sourced hydrocarbons (Hein, 2006; Barson, et al., 2001; Fowler & Riediger, 2000). Ores hosted within the McMurray Formation are subject to heterogeneities and related geological uncertainty, at both regional and individual reservoir scales. Key factors that affect the distribution and chemistry of bitumen include physical reservoir characteristics, mineralogy and mineral chemistry, and fluid distribution and chemistry; these attributes are the result of dynamic host-formation and hydrocarbon depositional histories, as well as complex post-depositional alteration processes (Fustic, et al., 2015). For example, though the predominant host successions are thought to have been deposited in estuarine settings, reservoirs have also been identified in fluvial and shallow marine settings, each with differing host porosities and permeabilities, mineral compositions, grain size distributions, and related bitumen qualities (Hein, 2006; Fustic, et al., 2015; Hein, et al., 2001; Hein, et al., 2000). Moreover, even broadly mappable geologic sequences (e.g. estuarine settings of the Middle McMurray Formation) may actually consist of multiple events overlapping in space and time, with each contributing several hierarchical heterogeneities (Fustic, et al., 2015; Wightman & Pemberton, 1997). Microbial degradation has been strongly linked to the quality of petroleum, having destroyed important proportions of originally emplaced conventional oil through the removal of lighter distillates (Gray, et al., 2009; Fustic, et al., 2015). In situ water washing, which removes the more water soluble distillates through contact with formation waters, is considered the second most important post-depositional alteration process that affects the geochemistry, quality and bulk physical characteristics of petroleum accumulations (Bata, et al., 2019; Algeer, et al., 2016).

Open-pit mining has traditionally been the dominant method implemented in the Alberta Oil Sands Region (AOSR), but in situ production first surpassed surface mining in 2012 and continued this trend into 2013 (Bata, et al., 2019; AER, 2015). For aging open-pit mines to remain competitive with the newer in-situ operations, they must be ready to implement changes to their process and thus adapt to their forecasted feeds. In oil sands surface mining, overburden is stripped and conventional truck-and-shovel methods are used to excavate the ore, followed by a series of treatments to liberate the bitumen from the mineral grains for subsequent recovery and cleaning. First, the ore is crushed and mixed with water and additives to create a slurry, which is then pumped to the extraction facilities via hydrotransport pipelines (Masliyah, et al., 2011; Kaminsky, 2008). Upon exit, the slurry is subject to water addition and gravity-settling separation processes, which

produces a bitumen froth, a middlings stream and a first round of tailings. The aerated bitumen froth (comprising ~60% bitumen, 30% water and 10% fine solid particles) rises to the top of the separation vessel, meanwhile flotation cells are used to recover bitumen from the middlings (Masliyah, et al., 2011). The separated froth is deaerated and then sent to the froth treatment plant, where the addition of a light hydrocarbon solvent helps reduce the viscosity of the bitumen; this allows for more effective separation of any remaining impurities by centrifugation and inclined plate (gravity) settlers. The final product of this froth treatment process is called diluted bitumen (also referred to as 'dilbit'), and is accompanied by another tailings stream.

Depending on the choice of hydrocarbon solvent, the generated dilbit can require further upgrading (typical for naphthenic treatment), or head straight to the refinery market (possible with paraffinic treatment); in either case, the diluent is removed prior to further processing. Lighter hydrocarbon solvents yield cleaner dilbit products by reducing the viscosity of the emulsion, which allows for gravity-based removal of water and solids. Paraffinic solvents promote asphaltene (impurity) precipitation, whereas naphtha cannot do this at practical dilution rates. Upgrading converts viscous, hydrogen-deficient hydrocarbon with elevated impurity levels into high-quality synthetic crude oil products with density and viscosity attributes similar to those of conventional light sweet crude oil (Masliyah, et al., 2011). The process first splits the bitumen into hydrocarbon streams (i.e. light and heavy gas oil) in a vacuum distillation unit. The lighter distillates ('tops') are fed into hydrotreaters for stabilization and impurity removal (e.g. sulphur), meanwhile the heavier phases ('bottoms') are sent to fluid cokers (thermal conversion units) to remove carbon, and to hydrocrackers where hydrogen is added and long chain molecules are broken down (Masliyah, et al., 2011).

4.2.2 Overview of Partial Least Squares (PLS) Regression

Multivariate statistics is a branch of statistics dealing with methods that examine the simultaneous effect of multiple variables (Marinković, 2008). Multivariate techniques extend the approach of univariate and bivariate investigations to include the analysis of covariances (or correlations) that reflect the extent of relationships between three or more variables, as well as similarities indicated by relative distances in n-dimensional space (Marinković, 2008). This area

of research has expanded greatly over the past few decades due to significant technological advances in computing power and data frameworks.

Partial least squares (PLS) regression is a multivariate statistical method that combines and generalizes features from principal component analysis and multiple linear regression, with the objective of predicting a set of dependent variables from a potentially large set of independent variables (Abdi, 2003; Abdi, 2010b). The technique was pioneered in the 1960s by Herman Wold for use in the social sciences but has since gained traction in a variety of fields, including chemometrics, sensory evaluation and neuroimaging (Abdi, 2003; Abdi, 2010b; Hoskuldsson, 1988; Tenenhaus, 1998). It is also becoming popular in the biological and environmental sciences with applications in soil and microbial ecology (Ekblad, 2005; Allen, 2005), biodiversity (Maestre, 2004; Palomino & Carrascal, 2007), paleo-climatological reconstruction (Seppa, 2004), and ecotoxicology (Sonesten, 2003; Spanos, 2008).

The main underlying computation for PLS is the singular value decomposition (SVD) of a matrix, which gives the best reconstruction (in a least squares sense) of the original data matrix by a matrix of lower rank (dimension reduction) while limiting the loss of significance (Abdi & Williams, 2013). The SVD is closely related to the well-known eigen-decomposition for non-symmetric matrices (Abdi, 2007). As a matter of notation, matrices are denoted by upper case bold letters, column vectors by lower case bold letters, and the superscript "**T**" is used to indicate transposition of either. Formally, the SVD of a given matrix, **R**, decomposes it into three matrices, comprising the left singular vectors, the singular values and the right singular vectors, as follows:

$$\mathbf{R} = \mathbf{U}\boldsymbol{\Delta}\mathbf{V}^{\mathbf{T}} = \sum_{\ell}^{L} \mathbf{u}_{\ell}\delta_{\ell}\mathbf{v}_{\ell}^{\mathbf{T}} \tag{4.2.1}$$

where $\mathbf{R}$ is the $J \times K$ correlation matrix derived from the cross-product of the two original data tables, i.e. the transpose $m \times n$ matrix of the independent variables, $\mathbf{X}^{\mathbf{T}}$, and the $n \times p$ matrix of the dependent variables, $\mathbf{Y}$, as:

$$\sum_{k=1}^{n} \mathbf{x}_{ik}^{\mathbf{T}}\mathbf{y}_{kj} \tag{4.2.2}$$

$\mathbf{U}$ is the $J \times L$ matrix of the left singular vectors (L corresponds to the rank of $\mathbf{R}$), $\mathbf{\Delta}$ is the $L \times L$ diagonal matrix of the singular values, $\mathbf{V}$ is the $K \times L$ matrix of the right singular vectors, and $\mathbf{u}_\ell$, δ_ℓ, and $\mathbf{v}_\ell^{\mathbf{T}}$ are the ℓth left singular vector, singular value and right singular vector, respectively (Abdi & Williams, 2013). The non-negative singular values are sorted in decreasing order and represent the maximum covariance between each respective set of left and right singular vectors (Melzer, 2004). Note that both original sets of data are typically made comparable through statistical preprocessing (i.e. mean centering and rescaling each variable).

It is useful to explain the SVD from a geometric perspective as a series of orthogonal axis rotations and scaling of unit matrices about the origin. As shown in the simplified interpretation for a 2×2 matrix (Figure 4.2.2; after (Hern & Long, 1991; Strang, 1993)), the SVD can be summarized as a linear transformation composed of three fundamental actions. These actions include: 1) rotation of the right singular vectors $\{\mathbf{v_1}, \mathbf{v_2}\}$ of matrix $\mathbf{V^T}$ within the original unit sphere; 2) scaling by the singular values $\{\delta_1, \delta_2\}$ of matrix $\mathbf{\Delta}$, which correspond to the length of the principal semiaxes of the new hyperellipse, and; 3) rotation of the left singular vectors $\{\mathbf{u_1}, \mathbf{u_2}\}$ of matrix $\mathbf{U}$, oriented along the same principal semiaxes (Strang, 1993; Trefethen & Bau III, 1997).

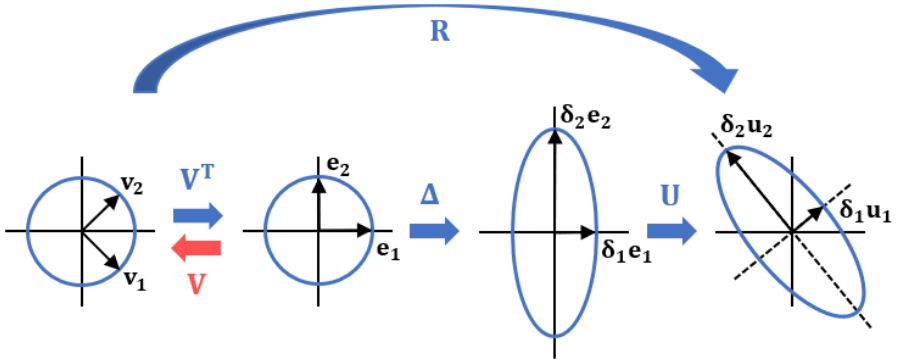

Figure 4.2.2. Geometric interpretation of the Singular Value Decomposition (SVD) for a 2×2 matrix showing the linear transformation induced by matrix R decomposed into three actions: a rotation, a scaling and another rotation (after (Hern & Long, 1991; Strang, 1993)).

The functional basis of PLS is to relate the information in two data tables that gather measurements on the same set of observations (i.e. samples). The method works by deriving linear combinations of the original variables through the SVD of a correlation matrix, such that covariance is maximized between each pair of the defining latent vectors (implied orthogonality) (Abdi & Williams, 2013). These combined variables are also referred to as latent variables,

dimensions or components. In PLS regression, the SVD simultaneously decomposes matrices $\mathbf{X}$ and $\mathbf{Y}$ (by virtue of the correlation matrix $\mathbf{R}$) and iteratively computes sets of orthogonal latent variables and the corresponding regression weights (Abdi & Williams, 2013).

Generally, this entire process is first carried out on subsets of training and validation data (i.e. measured values exist for both independent and dependent variables) to build and evaluate a regression model. The selection of training and validation splits is dependent on a number of factors, including sample population size, the nature and variability of the data, and the scope of the prediction problem. Sample splits should generally be selected at random, but can also be stratified when there are constraints imposed by different sample types (e.g. rock type); 80–20 training-validation splits are common in practice. Other techniques, such as k-fold cross-validation, are also widely popular to further minimize bias; one of these approaches is further detailed in Section 4.2.4. The final regression coefficients are then subsequently applied to a test dataset (i.e. for which data are only available for the independent variables) in order to predict the entire set of dependent variables.

By contrast with standard techniques, PLS regression can be used to predict a whole table of data and can also handle multicollinearity, thereby eliminating the necessity to remove certain predictor variables which may not be linearly independent and would normally cause overfitting (Abdi & Williams, 2013). This is particularly important in the context of mining systems wherein a significant proportion of the data variables used for ore characterization (e.g. geological, geochemical and mineralogical) are intimately linked. For example, ~50% of the variables in the present study are strongly correlated (correlation coefficients > 0.75) with one or more other variables (Appendix 4.2A). This multicollinearity among independent variables renders the classic multiple linear regression (MLR) method inappropriate for predictive modelling in most cases due to difficulties in distinguishing the effects of individual variables (Siegel, 2017). This can lead to the inflation of standard errors, which may cause incorrect variable significance classifications, and/or numerical instabilities related to the inversion of the covariance matrix ($\mathbf{X^T X}$) in the calculation of regression coefficients ($\mathbf{B} = (\mathbf{X^T X})^{-1}\mathbf{X^T Y}$) (Siegel, 2017). In PLS regression, the multicollinearity problem is bypassed by projecting the original variables to latent structures (linear combinations) and forcing orthogonality between the new variables ($\mathbf{t}$ and $\mathbf{u}$). The different

approaches of MLR and PLS are conceptualized in Figure 4.2.3. These attributes make PLS regression a powerful and highly adaptable tool because unlike other methods, it can be used on large datasets with an abundance of variables.

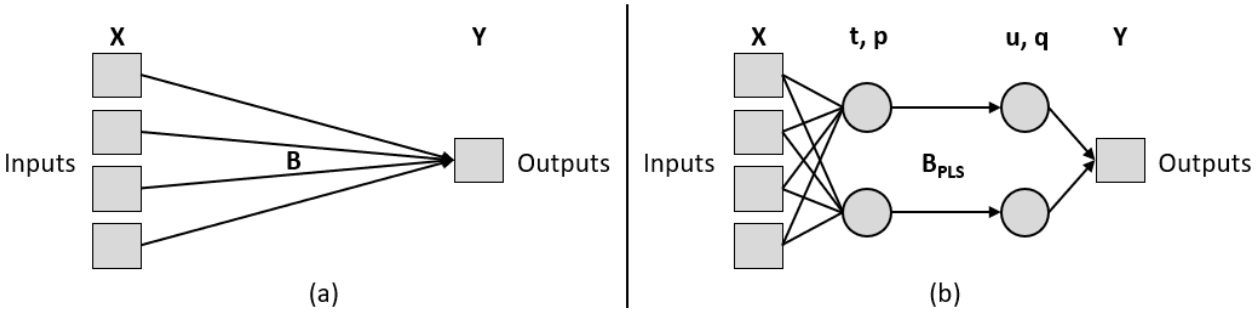

Figure 4.2.3. Simplified schematic comparison of multiple linear regression (MLR) and partial least squares (PLS) regression methods. (a) MLR uses all original variables to directly form a linear combination via the normal equations, and; (b) PLS first transforms the original variables by projecting to latent structures (linear combinations) that maximize covariance (orthogonality) between the new variables (**t** and **u)** (modified after (Egarievwe, et al., 2016)).

4.2.3 Case Study: Predictive Process Modelling of Canada's Oil Sands

An initial dataset derived from Canada's oil sands was acquired through partnerships with the National Research Council Canada (NRC) and Syncrude Canada Ltd. retrieved from the NRC Office of Energy and Research and Development (OERD) database. The set contains elemental, mineralogical and ore compositional data for a total of 60 samples collected from multiple sources in the AOSR. Of the total number of samples, 40 were sourced from various locations at the Syncrude operations, and permission has been graciously granted to include these in the present conceptual study. The remaining 20 samples come from a number of miscellaneous sources as part of smaller studies and are already available to the public domain.

Ore compositions (i.e. bitumen, water and solids contents) were analyzed by the standard Soxhlet-Dean and Stark method (Bulmer & Starr, 1974). Separately, splits from the original sample material were prepared for subsequent analytical determinations using a micronizing procedure recently developed at NRC. In this method, ore samples are first homogenized with a spatula at room temperature; isopropanol (4 mL) and toluene (6 mL) are then added to an aliquot (~2–3 g) and micronized with agate beads in a McCrone micronizing mill. The contents are strained into a weighed petri dish (any remainder is carefully rinsed with isopropanol and toluene) and allowed to dry for 24 hours in a fume hood prior to weighing. Lastly, the dried mixture is

scraped and transferred for further homogenization using a mortar and pestle. Elemental compositions were determined by wavelength dispersive X-ray fluorescence (WD-XRF) using a fusion-based procedure (Patarachao, et al., 2010), and CHNS measurements by combustion technique using an automatic elemental analyzer (Elementar Vario EL Cube) for carbon and sulphur. Mineral phase ratios were acquired by X-ray diffraction (XRD) with Rietveld refinement carried out on random orientation powder mounts. The mounts were prepared using a zero background specimen holder (Si crystal, P-type, B-doped) with a cavity diameter of 20mm and thickness of 0.2mm; a glass slide was used to remove excess powder and create a flat surface. Final mineralogical compositions were based on the combined XRF, CHNS and XRD results, and determined using the NRC-developed quantitative phase analysis (QPA) methodology parameterized with singular value decomposition (SVD), collectively termed SVD-QPA (Couillard & Mercier, 2016).

Basic descriptive statistics were computed to summarize the original raw dataset (Tables 4.2.1 and 4.2.2), which consists of data for 12 elements, 24 mineral phases and compounds, and 4 oil sand constituents (bitumen, water, solids, and proportion of fines).

Table 4.2.1. Summary of descriptive statistics for mineral phases analyzed by X-ray diffraction (XRD) in 60 samples.

	Mineral phase concentrations (wt.%)					
Mineral	Max	Min*	Median	Mean	Standard deviation	Variance ($\%^2$)
Quartz + silica	87.94	33.30	77.43	74.96	11.22	125.82
Illite	25.63	0.01	5.31	5.89	5.20	27.06
Kaolinite	24.09	-1.49	2.18	3.90	5.15	26.48
Chlorite	1.42	-1.09	0.01	0.10	0.37	0.14
Calcite	3.15	-1.06	0.01	0.09	0.50	0.25
Dolomite	8.21	-0.03	0.12	0.83	1.69	2.85
Ankerite	0.98	-0.03	0.01	0.05	0.16	0.03
Siderite	5.09	0.00	0.61	1.04	1.15	1.33
Pyrite	1.05	-0.05	0.04	0.16	0.23	0.05
Zircon	0.44	0.00	0.06	0.09	0.08	0.01
Rutile	0.62	0.03	0.13	0.15	0.09	0.01
Anatase	1.13	0.00	0.11	0.26	0.29	0.09
Ilmenite	0.05	0.00	0.01	0.02	0.01	0.00
Lepidolite	0.05	0.00	0.01	0.02	0.01	0.00
Gypsum	0.29	-0.85	0.01	0.01	0.13	0.02
Bassanite	0.30	-0.90	0.01	0.01	0.14	0.02
Anorthite	3.65	-7.14	0.12	0.22	1.22	1.49
K-feldspar	4.16	-0.35	1.06	1.19	0.86	0.74
Albite	11.38	0.00	0.34	0.96	1.75	3.08

Iron oxide + hydroxide	5.25	-1.75	0.10	0.19	1.07	1.15
Apatite	0.49	0.00	0.05	0.10	0.09	0.01
Cristobalite	0.10	0.00	0.01	0.01	0.02	0.00
Organic carbon	13.15	0.58	8.24	7.63	3.18	10.09
Organic sulphur	1.03	-0.17	0.39	0.38	0.27	0.07

* Negative values are related to the SVD-QPA methodology used for mineralogical composition reconstruction based on combined experimental results from elemental concentrations by XRF (Si, Al, K, Mg, Fe, Ti, Zr, Mg, Ca, and P), carbon and sulphur contents, and mineral ratios determined by Rietveld analysis of XRD powder patterns (Couillard & Mercier, 2016). The vast majority of these are well within tolerance; the anomalous value noted for anorthite (minimum of -7.14) can be linked to a specific sample likely containing Ca-bearing smectite, which was excluded in the QPA due to low overall Ca phases in the analyzed sample population.

Table 4.2.2. Summary of descriptive statistics for elemental and ore compositions analyzed by X-ray fluorescence (XRF) and Soxhlet-Dean and Stark extraction (respectively) in 60 samples.

	Elemental compositions (wt.%)					
Element	Max	Min	Median	Mean	Standard deviation	Variance ($\%^2$)
Na	1.00	0.00	0.03	0.08	0.15	0.02
K	2.00	0.09	0.55	0.64	0.43	0.18
Si	42.01	26.75	38.42	37.98	2.77	7.69
Al	9.09	0.00	1.56	2.22	2.09	4.36
Fe	3.21	0.00	0.54	0.72	0.66	0.44
Mg	1.09	0.00	0.05	0.12	0.22	0.05
Ca	3.49	0.03	0.16	0.30	0.56	0.31
Ti	0.72	0.02	0.20	0.25	0.17	0.03
Zr	0.22	0.00	0.03	0.04	0.04	0.00
P	0.09	0.00	0.01	0.02	0.02	0.00
C	13.29	1.08	8.38	7.86	3.05	9.32
S	1.31	0.05	0.47	0.47	0.28	0.08
	Ore compositions (wt.%)					
Phase	Max	Min	Median	Mean	Standard deviation	Variance ($\%^2$)
Bitumen	16.28	0.00	9.53	9.16	4.48	20.04
Water	19.57	0.41	5.63	6.65	4.37	19.06
Solids	91.25	76.79	83.97	84.42	2.86	8.16
Fines	99.46	1.36	24.80	34.22	27.01	729.80

The data are highly heterogeneous, and reflect ores likely hosted by formations spanning mainly estuarine and shallow marine settings, with a small number possibly from fluvial settings. Because information on sample provenance was fairly limited, assumptions had to be made in order to classify sample points for the sake of this conceptual study. This actually works out reasonably well as it highlights the importance of systematic data collection, and demonstrates the powerful information that can be gained by integrating properly developed geometallurgical profiles into advanced quantitative frameworks, and digital twins.

In positing the depositional settings from which the majority of the oil sand samples came, the data was sorted based on total clay contents (illite-kaolinite-chlorite) and a cut-off level of 6 wt.% was applied; samples with less than this limit were classified as (fluvio-)estuarine, and those with greater as marine. A broad inverse relationship is also evident in the data between total clay and bitumen contents, consistent with previous studies. Given that bitumen contents are generally higher in ores from fluvial and estuarine settings than those from marine settings (Masliyah, et al., 2011), this relationship could serve as a useful check of the viability of assumed provenances. Bitumen contents in the classified (fluvio-)estuarine samples average 11.74 wt.% (standard deviation of 2.81 wt.%), which coincides with the stated range of ~9–13% for economic ores (Hein, 2006; Gray, et al., 2009). The average bitumen content for marine samples is 6.52 wt.% (standard deviation of 4.52 wt.%), consistent with borderline uneconomical ores (Masliyah, et al., 2011; AER, 2016). Overall, the assumed depositional types appear fairly reasonable compared to natural deposit settings and related variations.

The dataset was also expanded to include postulated bitumen recovery data that was mostly unavailable. To this end, batch extraction unit (BEU) test data for 5 estuarine and 5 marine ore samples from previous work (Mercier, et al., 2008; Mercier, et al., 2007) were used to calculate appropriate bitumen recovery distributions for each depositional type. By applying these respective sample population means and standard deviations to a random number generator, reasonable spreads of recovery data were inferred for each sample type. This was deemed necessary in order to classify ore types based on both depositional setting (clay content) and generally related ore processability, for subsequent predictive and system process modelling (Sections 4.2.4 and 4.2.5, respectively). It is notable that the effect of fines on bitumen recovery can vary considerably depending on the type of fines and water chemistry (Masliyah, et al., 2011); studies have shown a depressive effect in the presence of degraded illite or smectitic clays (Wallace, et al., 2004), as well as ultrathin illite (Mercier, et al., 2008) and interstratification (Omotoso & Mikula, 2003).

For the purposes of this study, all samples are being treated as though they were sourced from a single mining project, with each of 20 mining parcels (i.e. blocks) corresponding to a minimum of 3 oil sands samples. The initial concept is to develop effective predictive models using PLS

regression such that bitumen recoveries could be estimated with confidence earlier in the value chain. Subsequent incorporation of this predicted data into DES frameworks would then expedite the evaluation of system response to geological uncertainty caused by heterogeneities in source ore feeds.

To demonstrate the overall concept, the classified ore types are blended according to two different schemes established through mass balancing. Each of these schemes corresponds to a separate operational mode, whereby the primary blend is considered the productive phase, and the secondary blend is considered a replenishment phase. The mining parcel data, classified into proportions of each ore type, is then incorporated into a DES framework to simulate system response to ore feed availability for a designated tonnage of oil sands to be processed; bottlenecks or stockout risk for either ore type can be identified and adjustments made to the potential modes of operation (Figure 4.2.4).

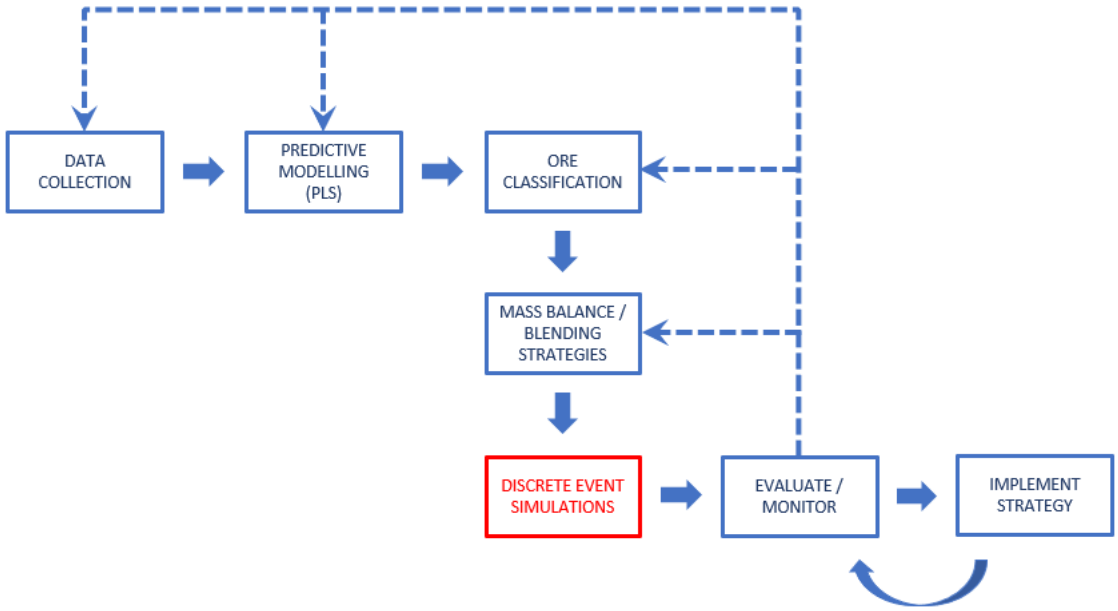

Figure 4.2.4. Generalized diagram showing the implementation of discrete event simulations (DES) in the formulation of blending control strategies and related operational modes.

Notably, since fines content is generally linked to geological setting and processability, a classification scheme based on depositional setting (and predicted recovery) actually runs in parallel to a process recently developed by Syncrude for the control of solids distribution in a bitumen froth (Long, et al., 2020). Under this patented methodology, coarse oil sands (which

normally produce high bitumen recoveries) are blended with high-fines material prior to extraction in order to improve the efficiency of pipeline transport from remote extraction sites to the froth treatment plant (Figure 4.2.5) (Long, et al., 2020). As a result, the current framework could help quantify the effects of different ore blending strategies on downstream system processes, and better guide the implementation of alternate operational modes.

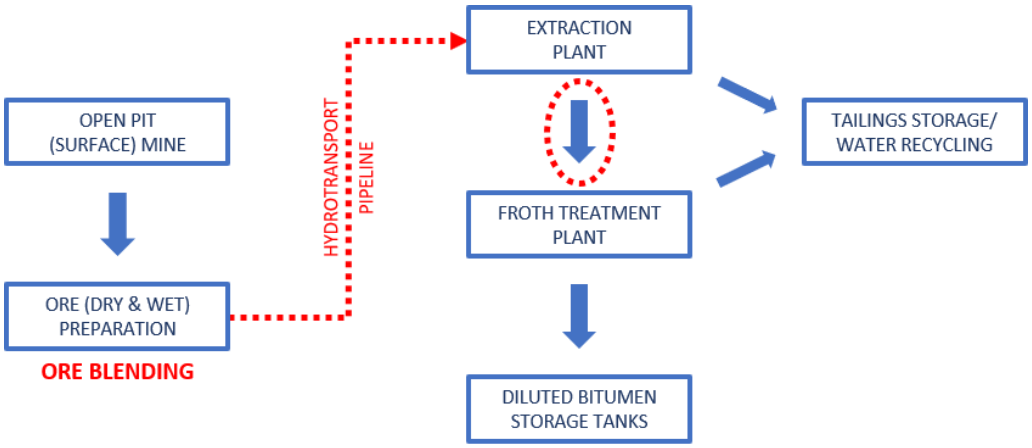

Figure 4.2.5. Generalized flowsheet for the extraction of diluted bitumen ('dilbit') from mined oil sands. Blending should occur during ore preparation (prior to processing) to improve hydrotransport along pipelines (Long, et al., 2020). Red dotted ellipse indicates potential additional point of hydrotransport for remote extraction sites.

This type of integrated quantitative framework allows for well-planned adjustments to process control strategies (e.g. ore blending), thereby streamlining risk-based decision-making, increasing efficiencies, and likely extending operational life through improved mine planning. The approach requires extensive sampling coupled with detailed analytical work initially, particularly in newly discovered or poorly characterized resource areas. With a sufficiently large population of sample points, robust predictive models can then be developed and implemented with confidence; at this stage, the expensive and time-consuming detailed analyses can be replaced with cheaper and faster tests earlier in the planning stages.

4.2.4 Partial Least Squares (PLS) Regression Model

For the predictive modelling portion of the study, elemental, mineralogical and ore composition data, coupled with depositional type, were retained for a total of 46 independent (explanatory) variables including 5 composite variables, e.g. total clays. The depositional setting variable was one-hot encoded to map its categorical data to integer values, represented as a binary

vector (Potdar, et al., 2017). Total bitumen recovery was reserved as the lone dependent (response) variable for the sake of this conceptual study. A PLS regression algorithm was written in Python coding, and follows well-established theory after several authors (Abdi & Williams, 2013; Mevik & Wehrens, 2007; Pell, et al., 2007). The methodology begins by calculating the SVD of the correlation matrix **R**, as described for Eqs. (4.2.1) and (4.2.2), and iteratively computing sets of orthogonal latent variables with the corresponding regression weights.

During each successive iteration, the first left and right singular vectors ($\mathbf{w}_\ell$ and $\mathbf{c}_\ell$) are used as weight vectors to calculate sets of scores ($\mathbf{t}_\ell = \mathbf{X}\mathbf{w}_\ell$ and $\mathbf{u}_\ell = \mathbf{Y}\mathbf{c}_\ell$) for $\mathbf{X}$ and $\mathbf{Y}$, respectively; loadings are then obtained by regressing $\mathbf{X}$ and $\mathbf{Y}$ against the same vector $\mathbf{t}_\ell$ ($\mathbf{p}_\ell = \mathbf{X}^\mathbf{T}\mathbf{t}_\ell$ and $\mathbf{q}_\ell = \mathbf{Y}^\mathbf{T}\mathbf{t}_\ell$) (Mevik & Wehrens, 2007). The last step of the iteration "deflates" the current data matrices (i.e. removes information related to the ℓth latent variable) by subtracting the outer products $\mathbf{t}\mathbf{p}^\mathbf{T}$ and $\mathbf{t}\mathbf{q}^\mathbf{T}$ from $\mathbf{X}$ and $\mathbf{Y}$, respectively (Mevik & Wehrens, 2007). The next component (or latent variable) can then be calculated starting from the SVD of the cross-product of the newly deflated matrices ($\mathbf{X}_{\ell+1}$ and $\mathbf{Y}_{\ell+1}$). The process continues until $\mathbf{X}$ is completely decomposed into L components and a null matrix is obtained. After each iteration, vectors $\mathbf{w}_\ell$, $\mathbf{t}_\ell$, $\mathbf{p}_\ell$, and $\mathbf{q}_\ell$ are stored as columns in their respective matrices $\mathbf{W}$, $\mathbf{T}$, $\mathbf{P}$ and $\mathbf{Q}$. The matrix of regression coefficients ($\mathbf{B_{PLS}}$) can then be calculated as:

$$\mathbf{B_{PLS}} = \mathbf{P}(\mathbf{P}^\mathbf{T}\mathbf{P})^{-\mathbf{1}}\mathbf{Q}^\mathbf{T} \tag{4.2.3}$$

where $(\mathbf{P}^\mathbf{T}\mathbf{P})^{-\mathbf{1}}$ is in fact the Moore-Penrose pseudoinverse for the generalized case of a non-symmetric matrix (Pell, et al., 2007). Finally, the matrix of regression coefficients ($\mathbf{B_{PLS}}$) is multiplied by the original set of independent variables prior to any deflations (matrix $\mathbf{X_0}$) to obtain the predictions of the dependent variables (matrix $\widehat{\mathbf{Y}}$) (Abdi & Williams, 2013). To better highlight the overall programming logic, pseudocode for the PLS regression algorithm developed in Python is shown in Figure 4.2.6. The program makes use of the open-source Pandas and NumPy libraries for data management and matrix operations, respectively.

```
# PLSR Code - written by Ryan Wilson.
# Import pandas & numpy libraries.

# Read data file (same directory as python process).
data = pd.read_csv('dataFile.csv')

# Set up the data (define X and Y matrices).

# Data preprocessing (2 steps).
# 1) Each variable should be mean-centered.
# 2) Column-wise re-scaling to L2 norm of 1.

# Initialize the preprocessed X0 & Y0 matrices.
X0 = np.array(X_scaled)
Y0 = np.array(Y_scaled)

# Initialize iterative storage variables for X0 & Y0.
X0_new = X0.copy()
Y0_new = Y0.copy()

# Assign the number of components for regression.
ncomp = 5

# Initialize summary matrices W, T, D, C, U, P & Q.
# e.g., W = np.empty(ncomp, dtype=object)

# Loop through to pull data into each summary matrix.
for i in range(0, ncomp):
    # Transpose rescaled matrices.
    X0_newT = X0_new.transpose()
    Y0_newT = Y0_new.transpose()

    # Calculate matrix R1 (cross-product of X0T & Y0).
    R1 = np.matmul(X0_newT, Y0_new)

    # Compute SVD of matrix R1 (using numpy).
    # Store singular values(d) & vectors (w, cT).
    W1, D1, C1 = np.linalg.svd(R1, full_matrices=False)
    d1 = D1[:]
    w1 = W1[:, 0]
    C1T = C1.transpose()
    c1T = C1T[:, 0]
    ...
    ...
    # Compute latent variables (T & U scores) & normalize.
    T1 = np.dot(X0_new, w1)
    T1T = T1.transpose()
    T1_norm = np.true_divide(T1, np.sqrt(np.dot(T1T, T1)))
    U1 = np.dot(Y0_new, c1T)
    U1T = U1.transpose()
    U1_norm = np.true_divide(U1, np.sqrt(np.dot(U1T, U1)))

    # Compute loadings (P & Q) by regressing on T1_norm.
    P1 = np.dot(X0_newT, T1_norm)
    Q1 = np.dot(Y0_newT, T1_norm)

    # Compute least squares estimates for X & Y.
    P1T = P1.transpose()
    X1_hat = np.outer(T1, P1T)
    Q1T = Q1.transpose()
    Y1_hat = np.outer(T1, Q1T)

    # Compute deflated matrices X1 & Y1.
    X0_new = np.subtract(X0_new, X1_hat)
    Y0_new = np.subtract(Y0_new, Y1_hat)

    # Store data in summary matrices W, T, D, C, U, P & Q.
    # e.g., W[i] = np.array([w1[:]])

# Stack the summary inputs into single arrays.
# e.g., W = np.vstack(W).transpose()

# Calculate matrix of regression coefficients (Bpls).
PT = P.transpose()
QT = Q.transpose()
PT_Ppinv = np.linalg.pinv(np.dot(PT, P))
Bpls = np.dot(np.dot(P, PT_Ppinv), QT)

# Compute final predicted values (pre-processed space).
X_hat = np.dot(T, PT)
Y_hat = np.dot(X0, Bpls)

# Back-transform predicted values to original sample space.
# i.e., Calculate x_hat_final & y_hat_final.
```

Figure 4.2.6. Pseudocode for the PLS regression algorithm developed in Python using the Pandas and NumPy libraries for data management and matrix operations, respectively.

A number of criteria can also be calculated to select the appropriate number of components to keep while limiting loss of significance, evaluate the quality of prediction and validate the model i.e. cross-validation. Validation is critical to the development of robust predictive models; the quality of prediction must be assessed and model significance also determined. A common measure of prediction quality is called the Residual Estimated Sum of Squares (RESS), and is calculated as follows:

$$\text{RESS} = || \mathbf{Y} - \widehat{\mathbf{Y}} ||^2 \tag{4.2.4}$$

where $|| ||^2$ is the squared matrix norm, and decreases as prediction quality improves (Abdi & Williams, 2013). However, RESS alone is not the most useful metric as it will continue to decrease

until all components are added, i.e. it does not detect overfitting. An improved measure for quality of prediction is the Predicted Residual Estimated Sum of Squares (PRESS), computed as follows:

$$\text{PRESS} = || \mathbf{Y} - \tilde{\mathbf{Y}} ||^2 \tag{4.2.5}$$

where $\tilde{\mathbf{Y}}$ represents a predicted set of values generated from cross-validation, and also decreases with increasing prediction quality (Abdi & Williams, 2013). The selection of the optimal number of components to extract is crucial to avoid overfitting the data. Since prediction quality typically first increases then decreases upon successive component addition, a possible approach is to begin with the first component and stop as soon as the PRESS reverses direction (Abdi, 2010b). A more intricate method is to compute the Q^2 criterion for the ℓth component, as follows:

$$Q_\ell^2 = 1 - \frac{\text{PRESS}_\ell}{\text{RESS}_{\ell-1}} \tag{4.2.6}$$

and compare against an arbitrary critical value (e.g. $1 - 0.95^2 = 0.0975$); only components with a Q_ℓ^2 value greater than or equal to this threshold are generally kept in the model (Abdi, 2010b; Tenenhaus, 1998).

Because the available dataset is limited to only 60 samples, it was decided not to split the data into separate training and validation sets; instead, leave-one-out cross-validation (LOOCV), also called the 'jackknife' method, was utilized. In this technique, each observation is iteratively dropped from the set and the remaining observations then comprise a training set used to estimate the left-out observation. All estimated observations are stored in a final matrix denoted $\tilde{\mathbf{Y}}$, which then serves as the validation set for subsequent prediction quality metrics (e.g. PRESS and Q^2 criteria) (Abdi, 2010b).

The PLS regression model was run sequentially, and a series of quality of prediction statistics were tabulated for each of 1, 2, 3, 4, 5, and 10 component scenarios (Figure 4.2.7). The Q^2 criterion indicates that only the first component should be kept in the prediction model, with a value of 0.28, as all ensuing trials resulted in values less than zero. However, not only was the coefficient of determination (R^2) quite low for the 1 component scenario (0.34), but root mean squared error (RMSE) and mean absolute residual values were also relatively high. Furthermore, the first component alone only accounts for ~88% of the total model variance, as determined by the sum

of squares of the singular values. As a result, the behaviour of the PRESS statistic was tracked upon successive trials to identify an improved fit; ultimately, a total of 5 components was deemed appropriate for building the regression model in relation to the available dataset. This was based upon the fact that the PRESS value trended upwards over the first 4 components but dropped significantly upon addition of the fifth; this reversal also coincided with a much higher R^2 score of 0.72, improved (decreased) RMSE and residual values, and an explained variance of 99.65%. Further addition of successive components (e.g. 10 components) did not greatly improve prediction accuracy or error metrics, resulted in poorer PRESS and Q^2 statistics, and would likely lead to severe overfitting to the present dataset. It is also noteworthy that residuals were consistently greater for marine samples, indicating greater variability in the predicted set for this depositional type (as expected).

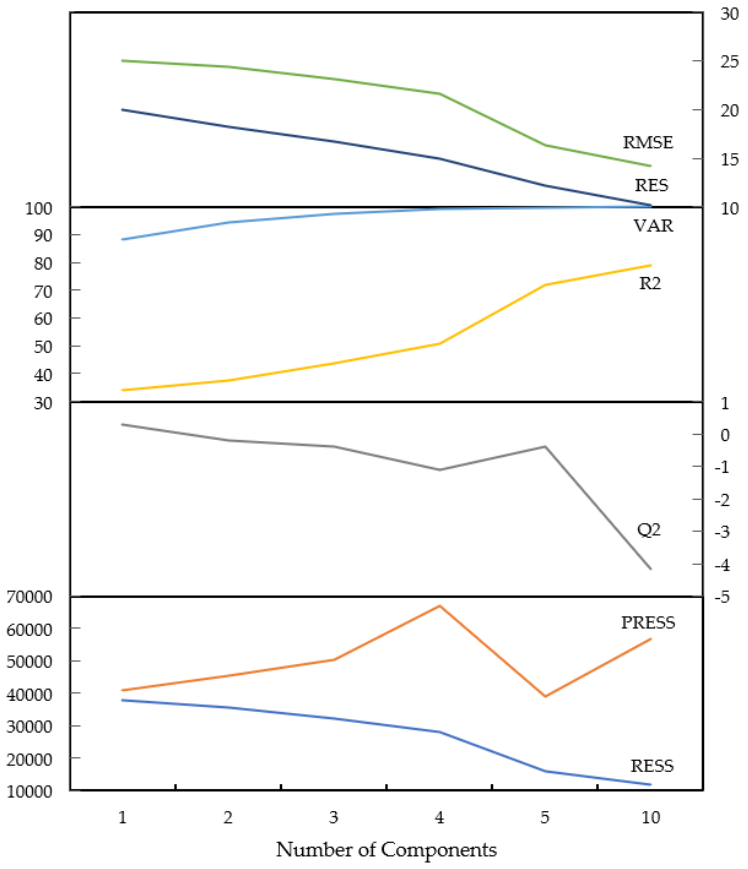

Figure 4.2.7. Stacked panel line chart for a variety of quality of prediction statistics tabulated for each of 1, 2, 3, 4, 5, and 10 component scenarios. Abbreviation definitions: RMSE = root mean squared error; RES = mean absolute residual (all samples); VAR = percentage of model variance explained; R2 = coefficient of determination (×100); Q^2 criterion (as in Eq. (4.2.6)); PRESS statistic (as in Eq. (4.2.5)); RESS statistic (as in Eq. (4.2.4)).

Predictions from the final 5-component model are shown in Figure 4.2.8, and comparative descriptive statistics for the observed and predicted datasets are shown in Table 4.2.3. Estimated bitumen recoveries were capped at 100%, and negative values were set to zero as crossing these thresholds is impossible in practice. The predicted values are generally quite reasonable, within ~11% for the (fluvio-)estuarine samples and ~13% for marine samples on average. This level of error (RMSE of 16.33) is not surprising on account of the assumptions made to finalize the original dataset, in addition to the significant geological variability inherent to oil sands deposits. As expected, the variability in marine sample residuals (standard deviation of 9.89%) is nearly double that of estuarine samples (standard deviation of 5.27%), and can likely be attributed to heterogeneities in clay contents and especially clay types. Overall, the PLS regression model has performed as intended, and with a mere total of 60 samples from unknown and/or different mining projects altogether. This highlights the importance of rigorous sampling campaigns and characterization of appropriate geometallurgical profiles towards the development of robust predictive models, particularly for complex operations dealing with multiple and/or heterogeneous ore feeds. It is postulated that the predictive power of the present model would be greatly increased with these controls in place.

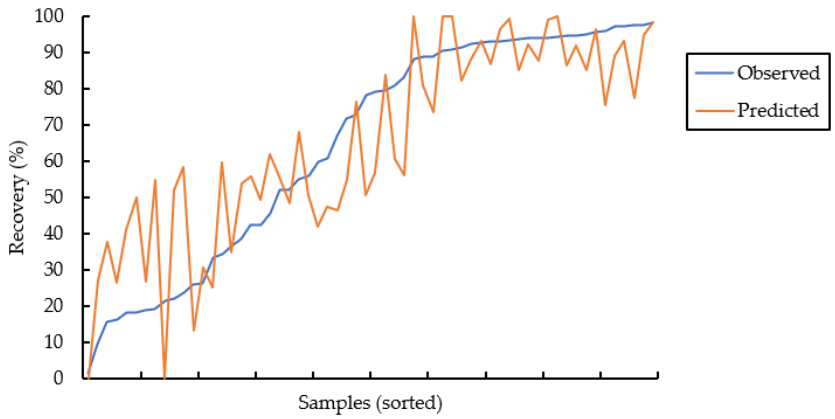

Figure 4.2.8. Plot of predicted vs. observed recoveries from the 5-component regression model. Samples are sorted according to ascending observed values to better reflect residual distances; predictions clearly improve in the middle to upper recovery ranges.

Table 4.2.3. Summary statistics for observed and predicted bitumen recoveries from PLS regression model (5 components).

Metric	Observed values (**Y**)	Predicted values (**Ŷ**)
Max (%)	98.29	100.00
Min (%)	1.55	0.00
Median (%)	78.80	61.27
Mean (%)	64.91	65.17
Standard Deviation (%)	31.14	26.91
Variance (%^{2})	969.95	724.18

Once the regression model has been finalized with the appropriate number of components, confidence intervals for the predicted values can be calculated using the 'bootstrap' cross-validation method. This technique involves the random re-sampling of the original observations with replacement i.e. each observation can be selected zero or multiple times (Abdi & Williams, 2013). This is repeated many times (e.g. 1,000 or 10,000), and regression coefficients and corresponding predictions are computed for each bootstrapped sample set. The distribution of predicted values from all of these iterations is then used to estimate confidence limits for each variable; intervals that do not span zero (positive or negative) are considered significant (Abdi & Williams, 2013). Similarly, bootstrap ratios can be calculated by dividing the mean of each distribution by its standard deviation; akin to a student t-test, if the ratio is greater than a critical value (e.g. >2, corresponding to an alpha value of ~0.05), the variable is also considered significant (Abdi & Williams, 2013).

Table 4.2.4 provides statistics computed from the distribution of 10,000 bootstrap sample sets generated from the 5-component regression model; variable significance was determined based on both bootstrap ratios and 95% confidence intervals. Of the elemental composition variables, only Na, Ca, and Mg were deemed insignificant. Corresponding insignificant minerals include albite for Na; gypsum, bassanite and anorthite for Ca; chlorite for Mg, and; the carbonates (calcite, dolomite and ankerite) for both Ca and Mg. Interestingly, both pyrite and amorphous Fe-oxides/hydroxides were also considered insignificant (oil sands tend to contain significant heavy metals). All remaining elements and mineral phases, in addition to depositional sample type and bitumen recovery, were determined as statistically significant.

Table 4.2.4. Summary of statistics from 10,000 replications of the bootstrap cross-validation method.

Variable	Independent (explanatory) variables					
	No. of observations	Mean (wt.%)	Standard deviation(wt.%)	Bootstrap ratio	Lower CI (95%)	Upper CI (95%)
Sample type	60000	0.57	0.22	2.54	0.20	1.00
Na*	60000	0.08	0.05	1.57	0.03	0.21
K	60000	0.64	0.13	5.12	0.45	0.95
Si	60000	37.97	0.96	39.70	35.30	39.42
Al	60000	2.22	0.64	3.48	1.34	3.99
Fe	60000	0.72	0.24	2.98	0.35	1.42
Mg	60000	0.12	0.10	1.19	0.02	0.48
Ca	60000	0.30	0.31	0.99	-0.02	1.53
Ti	60000	0.25	0.06	3.95	0.15	0.38
Zr	60000	0.04	0.02	2.41	0.01	0.08
P	60000	0.02	0.01	2.40	0.01	0.04
C	60000	7.87	1.00	7.90	5.88	9.67
S	60000	0.47	0.13	3.64	0.25	0.76
Bitumen	60000	8.79	1.36	6.46	6.06	11.16
Water	60000	6.64	1.42	4.69	4.25	9.97
Solids	60000	84.42	1.11	76.29	82.27	86.83
Fines	60000	34.27	7.91	4.33	22.22	52.30
Quartz + silica	60000	74.94	3.46	21.64	64.62	79.82
Illite	60000	5.89	1.66	3.55	3.43	10.21
Kaolinite	60000	3.90	1.83	2.13	1.08	8.58
Chlorite	60000	0.10	0.14	0.73	-0.16	0.41
Calcite (Cal)	60000	0.09	0.28	0.33	-0.24	1.07
Dolomite (Dol)	60000	0.84	0.82	1.01	-0.03	3.67
Ankerite (Ank)	60000	0.06	0.07	0.85	-0.05	0.21
Siderite (Sid)	60000	1.04	0.50	2.07	0.10	2.19
Pyrite	60000	0.16	0.11	1.40	-0.02	0.46
Zircon	60000	0.09	0.04	2.41	0.02	0.17
Rutile (Rut)	60000	0.15	0.04	3.73	0.07	0.22
Anatase (Ana)	60000	0.26	0.10	2.64	0.12	0.49
Ilmenite	60000	0.02	0.00	3.74	0.01	0.03
Lepidolite	60000	0.02	0.00	3.72	0.01	0.03
Gypsum	60000	0.01	0.06	0.19	-0.12	0.11
Bassanite	60000	0.01	0.06	0.16	-0.13	0.10
Anorthite (Ano)	60000	0.22	0.61	0.36	-0.92	1.77
K-feldspar (Ksp)	60000	1.20	0.38	3.17	0.39	1.96
Albite (Alb)	60000	0.96	0.61	1.57	0.29	2.36
Iron oxide/ hydroxide (AFE)	60000	0.19	0.44	0.42	-0.46	1.55
Apatite	60000	0.09	0.04	2.34	0.04	0.22
Cristobalite	60000	0.01	0.00	2.70	0.00	0.02
Organic carbon	60000	7.63	1.00	7.63	5.61	9.41
Organic sulphur	60000	0.39	0.13	2.96	0.14	0.67
Total clays	60000	9.89	3.24	3.05	5.13	19.00
Sid + AFE	60000	1.22	0.49	2.48	0.45	2.52
Rut + Ana	60000	0.40	0.11	3.82	0.24	0.63
Cal + Dol + Ank	60000	0.98	1.01	0.97	-0.05	4.39
Ano + Ksp + Alb	60000	2.37	0.82	2.91	1.09	4.76
	Dependent (response) variables					
Variable	No. of observations	Mean (wt.%)	Standard deviation(wt.%)	Bootstrap ratio	Lower CI (95%)	Upper CI (95%)
Total Recovery	60000	64.84	28.86	2.25	1.52	109.53

* Insignificant variables indicated in red text.

The relationships between the independent variables can be observed visually by plotting the stored **X**-loadings (matrix **P**) for the first two components (Figure 4.2.9). Bitumen content is clearly most strongly linked to elemental carbon and organic carbon (as expected); it also appears in association to silicon (quartz-silica-cristobalite), sulphur (organic sulphur), titanium minerals (rutile and ilmenite), and lepidolite (Li-rich mica). The first dimension also opposes the bitumen group from the clay minerals, water content, and carbonates (siderite). Notably, anatase (metastable form of TiO_2) plots opposite the other Ti-bearing phases. In the second dimension, the organic-related groups (bitumen, carbon and sulphur) clearly oppose the related silicate and oxide minerals; there is also a broad separation between silicates and carbonate + iron-bearing phases.

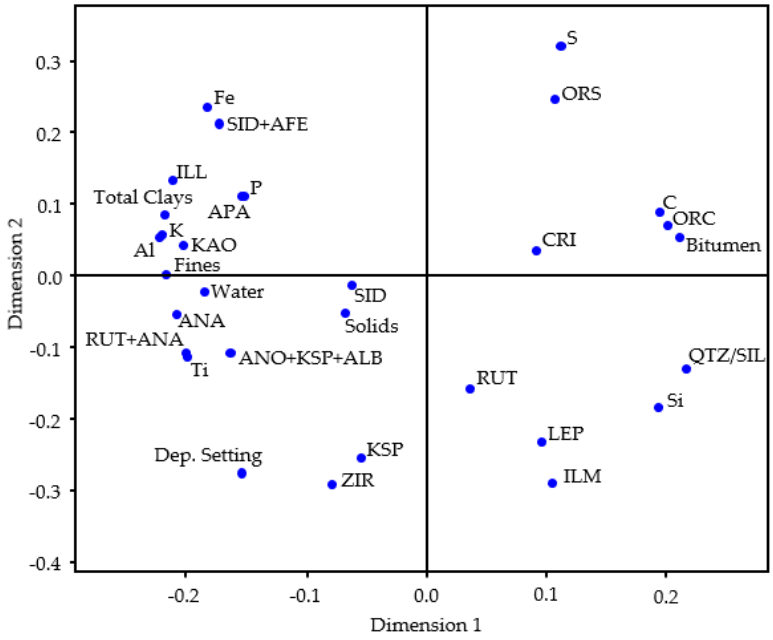

Figure 4.2.9. Plot of the **X** variable loadings (matrix **P**) for the first two components (dimensions 1 and 2).

Overall, the PLS regression model has proven to be a powerful prediction tool, capable of providing additional useful information regarding process variables that can help drive the characterization of geometallurgical profiles, sampling methodologies, and other planning processes.

4.2.5 Discrete Event Simulations

For the DES portion of the study, two ore types were classified according to documented depositional setting and predicted bitumen recoveries from the 5-component PLS regression

model. Ore type 1 consists entirely of marine samples (generally <75% recovery), and ore type 2 includes (fluvio-)estuarine samples (>75% recovery) as well as a few of marine type with recoveries also greater than 75%. Due to the limited nature of the dataset (only 3 samples per mining parcel), natural background noise was added to the relative proportions of ore types 1 and 2 via random number generation with a standard deviation of 5%. Two modes of operation (A and B) are considered here to balance stockpile levels against bitumen extraction rates and incoming ore feed from mining. While the conceptual mine has been operating in areas containing predominantly ore type 2 (favourable due to higher grades and recoveries) for some time, a large expansion of reserves comprising mainly ore type 1 has recently been completed. With the expansion, longer term forecasts suggest an overall deposit composition of 55–45% for ore types 1 and 2, respectively, with increased variability caused by geological heterogeneities; these values correspond to the average proportions determined from ore classification based on the predictive modelling.

In order to sustain the availability of ore type 2, and improve the economics of certain portions of the newly expanded area, the operation is evaluating possible adjustments to current blending strategies, and intends to implement a secondary alternate mode. Based on the geological attributes of ore types 1 (high bitumen, low fines) and 2 (high fines), the new strategy will also serve to control the distribution of solids in ore feeds to the froth treatment plant, thereby improving amenability to transport via pipelines to the upgrader. As a result, operational Mode A will consist of an approximate 40-60 blend of ores 1 and 2. Because ore type 2 will generally be in shorter supply, a second operational Mode B, consisting of an 80–20 blend of ores 1 and 2, is needed in order to avoid stockouts, or an eventual shortage. This will ultimately stabilize feed balances, maximize equipment/infrastructure selection and utilization, and allow for improved production scheduling; collectively, these factors can lead significant reductions in operating and capital costs.

Both modes are expected to perform similarly in terms of downstream bitumen recovery processes, except that Mode B requires a pretreatment stage to control excess chloride ions related to the marine origin and high fines content of ore type 1. Consequently, bitumen extraction rates for Mode B are set 10% lower than those for Mode A; modal parameters for each configuration are summarized in Table 4.2.5. Despite the fact that Mode A is both more productive and

economical, ore stockouts would be inevitable over extended periods of usage because the weight fraction of ore type 2 (w_{2A}) is 15% higher than that of the deposit (w_{2D}). To account for the possibility of stockouts prior to a planned shutdown, contingency modes with adjusted configuration rates have been incorporated for each of Modes A and B.

Table 4.2.5. Description of operational modes in relation to deposit forecast.

		Throughput (t/h)	Ore 1 in feed (%)	Ore 2 in feed (%)
	Algebraic Notation:	$r_{A,ACont,B,BCont}$	$w_{1A,1ACont,1B,1BCont}$	$w_{2A,2ACont,2B,2BCont}$
Mode A	Regular	30,000	40	60
	Contingency	19,500	100	0
Mode B	Regular	27,000	80	20
	Contingency	13,500	0	100
Deposit		-	55	45

After the approach of Navarra et al. (2019), a deterministic analysis (which ignores the risk of stockout) indicates that Mode A should be applied 1.5 times as often as Mode B, with an average throughput of 28,800 t/h. The framework aims to simultaneously maximize throughput and minimize target stockpile levels, thereby increasing production efficiency and reducing overall costs; larger stockpiles necessitate larger storage areas and equipment, as well as increased handling costs.

The current framework is designed such that mining rates exceed plant capacity, hence the plant acts as a bottleneck. To ensure stockpiles are adequately supplied to maintain consistent ore feed to the plant, ore will be mined at minimum rates of 30 kt/h under Mode A and 27 kt/h under Mode B. Target total stockpile level is a control variable that remains constant (except during extended stockout periods); however, the relative proportions of ore types 1 and 2 fluctuate contingent on the active operational mode. Mode A (productive phase) causes a relative decrease in the proportion of ore type 2, meanwhile Mode B (replenishment phase) has the opposite effect. The selection of operational mode is based on the stockpile level of the limiting ore type (in this case, Ore 2) at the end of a production campaign during planned shutdowns every 4 weeks.

Under the present framework (Table 4.2.5), a naïve analysis indicates a critical threshold of 2.916 Mt for ore type 2; this level is computed as a function of campaign length (27 days) and rate of change under Mode A (108,000 t/d; plant capacity of 720,000 t/d × w_{2D} of 45% less relative critical ore 2 throughput from 40–60 blending strategy). Similarly, the analysis indicates a

minimum total target stockpile level (sum of ores 1 and 2) of 4.374 Mt, determined as the maximum rate of change between ore stockpiles 1 and 2 as a function of campaign duration (under either mode). Unexpected fluctuations in ore feed attributes can indeed cause either overages or shortfalls for a given ore type, potentially leading to stockout towards the end of a production campaign (Navarra, et al., 2019). To mitigate this risk, an operational buffer can be introduced by raising the threshold for the critical (limiting) ore type; a similar control measure would be to raise the target total stockpile level.

Because stockouts are nonetheless a real possibility, recourse actions are built into the digital twin to maintain ore feed consistency. As indicated in Table 4.2.5, Contingency Mode A only consumes ore type 1, and Contingency Mode B only consumes ore type 2. These contingency modes are much less productive than the regular configuration rates (65% for Mode A and 50% for Mode B); as a result, the duration of these segments has been limited to 1 day, which causes alternations until the next planned shutdown. If the critical ore level remains below the selected threshold at the end of a campaign, the plant will employ the alternate mode of operation to re-equilibrate stockpile levels. Time segment parameters for production campaigns, shutdowns and contingency mode duration are summarized in Table 4.2.6.

Table 4.2.6. Summary of time segment parameters.

Segment type	Duration (days)
Production campaign	27
Planned shutdown	1
Contingency modes	1
Regular modes	Indeterminate

The current framework was implemented, and subsequent computational results (Tables 4.2.7–4.2.8, Figures 4.2.10–4.2.11) generated, using commercial DES software (Rockwell Arena©) with Visual Basic for Applications (VBA). Extended operating periods can be simulated to assess system performance in response to geological uncertainty, with adjustments made to the critical ore and target stockpile levels as control variables. In its present configuration, the simulation model assumes that ore is mined to completion from a single parcel at a time. For the purposes of this study, geological uncertainty was introduced through Monte Carlo simulation; the proportions of ore types 1 and 2, determined from the classification of mining parcels based on depositional setting and predicted recoveries, were used to generate 100 statistical replicas through

random number generation with a standard deviation of 5%. The model is configured such that 792 Mt of ore are processed within each replica, corresponding to approximately 1,200 days of operation.

A series of simulations were run to observe the effects of the selected control variable levels on throughput and potential stockout risk, in response to geological uncertainty. The first set of trials varied the total stockpile target levels, while holding the critical Ore 2 level constant at 2.916 Mt (deterministic value). A total of 5 scenarios were considered with total stockpile levels set at 1x ("one times"), 1.5x, 2x, 3x, and 5x the deterministic value (4.374 Mt); simulated results for each are summarized in Table 4.2.7.

Table 4.2.7. Distribution of time spent in each mode type under varied target total stockpile levels.

		Scenario:	1	2	**3**		4	5
		Replications:	1	1	**1**	***100***	1	1
		Critical Ore 2 Level (Mt):	2.916	2.916	**2.916**	***2.916***	2.916	2.916
		Target Total Stockpile Level (Mt):	4.374 (1x)	6.561 (1.5x)	**8.748 (2x)**	***8.748 (2x)***	13.122 (3x)	21.870 (5x)
			Portion of time (%)					
Mode A	Regular		45.6	54.8	**59.7**	***60.1***	58.4	59.4
	Contingency		4.9	0.2	**1.6**	***1.4***	0.6	0.6
Mode B	Regular		34.8	37.3	**35**	***34.5***	37.4	36.4
	Contingency		11.1	4.2	**0.1**	***0.4***	0	0
Shutdown			3.6	3.5	**3.6**	***3.6***	3.6	3.6
Throughput (kt/h)			26.5	28.1	**28.7**	***28.7***	28.8	28.8
Replications with stockouts			-	-	**-**	***82***	-	-

Consistent with Navarra et al. (2019) and Wilson et al. (2021a), the results show that naïve selection of the total stockpile target level does not perform well over extended operating periods, with Mode A being applied only 1.1x as often as Mode B for an average throughput of 26.5 kt/h. This is clearly less productive than the deterministic result of 28.8 kt/h (Mode A applied 1.5x more than Mode B), and the simulated operation also suffered from frequent sustained shortages of both ore types (Figure 4.2.10a). Increasing the total stockpile level by just 1.5x (Scenario 2) already improves overall system response; however, with Mode A applied 1.3x as often as Mode B for an average throughput of 28.1 kt/h, this is still worse than expected from the deterministic calculations. Scenario 3, which doubled the deterministic total stockpile level to 8.748 Mt, produced the best overall results with Mode A applied 1.75x more frequently than Mode B for an average throughput of 28.7 kt/h; there was also a drastic reduction in the proportion of time spent in contingency modes (Figure 4.2.10b). Successive increases to the stockpile targets (Scenarios 4

and 5) did not show any marked changes, and system performance was actually slightly worse for both. These results suggest that in order to maximize throughput and mitigate stockout risk, the target total stockpile level is best maintained in the range of twice the selected critical ore threshold.

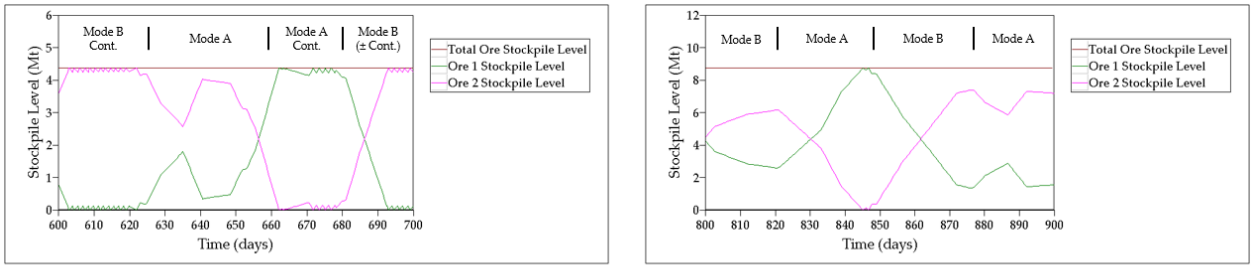

(a) (b)

Figure 4.2.10. Simulated operational dynamics of Canadian oil sands data in response to geological uncertainty, configured with a critical Ore 2 level of 2.916 Mt (deterministic value), and total stockpile target levels of (a) 4.374 Mt under Scenario 1, and; (b) 8.748 Mt under Scenario 3. Contingency modes are depicted by the fine jagged saw-tooth pattern, and result from short contingency segments of 1 day; note the abundance of these ore shortages in (a) compared to (b).

Using the parameter values established from Scenario 3, the framework was subsequently configured to simulate 100 replications, corresponding to approximately 120,000 days of operation. Average results from this test mirrored those of the single replication (Table 4.2.7), but highlighted repeated ore shortages as a significant operating risk under this scheme, with 82% of the replications confronted by stockouts. While not apparent from the single replication simulation, this outcome is directly related to the high variability of the dataset, and is entirely possible in the context of oil sands mining, particularly when dealing with multiple and/or heterogeneous ore feed sources. Frequent and/or sustained stockout periods (especially early in a campaign), require additional consideration; as a recourse action, the possibility for mining surges has been incorporated into the framework in order to supply ore feed directly to the plant to maintain production (Figure 4.2.11).

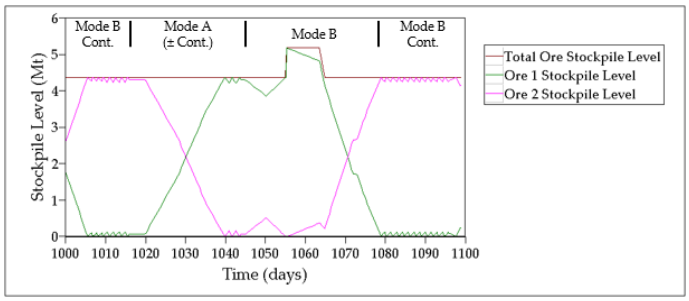

Figure 4.2.11. Simulated mining surge caused by high variability of Canadian oil sands data in response to geological uncertainty. Surges are indicated when the level of one of the ore types increases above the total stockpile target, and are required to provide feed directly to the plant as recourse to a sustained stockout of the other ore type (e.g. ~1,055-1,065 day range).

To attenuate the significant stockout risk observed under Scenario 3, a second set of simulations were executed in which adjustments were made to the critical ore limit while keeping the total stockpile target at 2x this level. Four scenarios were tested with critical ore levels designated at 1.5x, 2x, 2.5x, and 3x the deterministic value (2.916 Mt); results for each simulation trial are summarized in Table 4.2.8. While variations in the critical ore threshold had no meaningful effect on throughput rates or modal proportions, important reductions in the number and frequency of stockout periods were observed with the framework configured for 100 replications (~120,000 operating days). At twice the deterministic value (Scenario 6), the number of replications affected by ore shortages was reduced by 20% (cf. Scenario 3); at 2.5x (Scenario 7), this number decreased to just 5%. Tripling the critical value eliminated simulated stockout periods altogether; however, increased capital and operating costs associated with exceedingly large stockpile levels must be weighed against the risk of stockout in the decision-making process.

Table 4.2.8. Distribution of time spent in each mode type under varied critical ore levels.

	Scenario:	6		7		8	
	Replications:	1	*100*	**1**	***100***	1	*100*
	Critical Ore 2 Level (Mt):	5.832 (2x)	*5.832 (2x)*	**7.290 (2.5x)**	***7.290 (2.5x)***	8.748 (3x)	*8.748 (3x)*
	Target Total Stockpile Level (Mt):	11.664	*11.664*	**14.580**	***14.580***	17.496	*17.496*
Mode A	Regular	58.7	*59.6*	**58.6**	***60.0***	58.6	*60*
	Contingency	0	*0.1*	**0**	***0.05***	0	*0*
Mode B	Regular	37.3	*36.3*	**37.8**	***36.3***	37.8	*36.4*
	Contingency	0.4	*0.4*	**0**	***0.05***	0	*0*
Shutdown		3.6	*3.6*	**3.6**	***3.6***	3.6	*3.6*
Throughput (kt/h)		28.8	*28.8*	**28.8**	***28.9***	28.8	*28.9*
Replications with stockouts		-	*62*	**-**	***5***	-	*0*

The time-averaged distribution of operational modes in response to geological uncertainty can be useful to evaluate the effects of varied control parameters. Figure 4.2.12a represents the naïve approach of Scenario 1, in which the deterministic values for the critical ore level (2.916 Mt) and total stockpile target level (4.374 Mt) were applied; Figure 4.2.12b depicts the enhanced framework configuration established under Scenario 7 (described above). The latter scheme is a significant improvement over the naïve setup, with an 8–9% increase in the proportion of time spent under Mode A, a much lower reliance on contingency modes (~15%), and the virtual elimination of ore stockouts. All of these factors contribute to improved production efficiencies; moreover, the enhanced configuration is also more economical based on higher consumption rates for ore type 2, which boasts higher overall grades and bitumen recoveries. Both framework applications benefit from the ability to switch between modes relatively freely in response to data variability, but the enhanced configuration is much less susceptible to operational risk caused by geological heterogeneities.

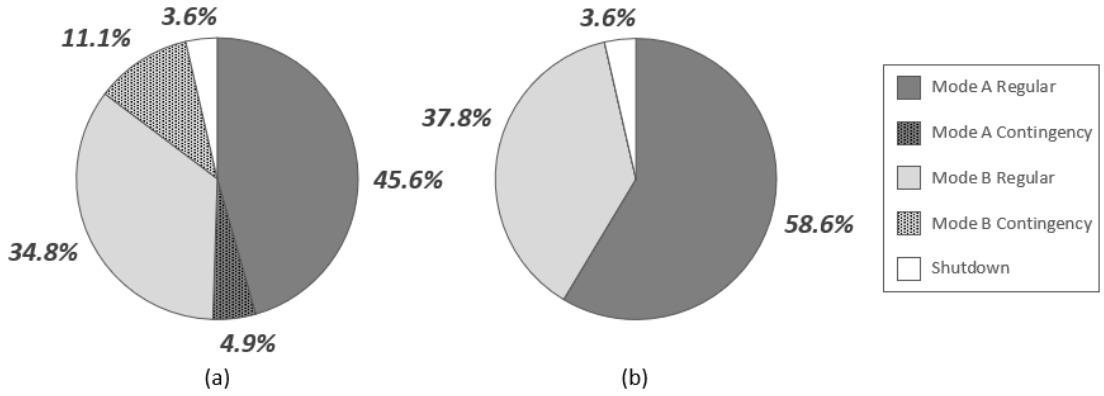

Figure 4.2.12. Time-averaged distribution of operational modes in response to geological uncertainty in the context of Canada's oil sands, for (a) 'naïve framework using deterministic critical Ore 2 threshold of 2.916 Mt and target total stockpile level of 4.374 Mt, and; (b) enhanced configuration using a critical value of 7.290 Mt (2.5x) and target total stockpile level of 14.580 Mt.

4.2.6 Conclusions

Overall, the results from this study support the flexibility of DES digital twins to integrate predictive modelling data generated through PLS regression in order to assess system-wide response to geological uncertainty. This quantitative framework is an extension of recent conceptual work by Navarra et al. (2019) and Wilson et al. (2021a), and demonstrates its adaptation to evaluate operational risk factors associated with potential processing applications for Canada's

oil sands. Simulations indicate that ore stockouts are a very real possibility due to extreme geological heterogeneities inherent to oil sands; however, the current digital twin allows for the analysis of potential adjustments to control strategies at an earlier stage, which can help drive decision-making and mitigate identified risk factors. The blending control strategies described in this study would necessitate significant stockpiling infrastructure and equipment, but these implied costs could easily be offset by higher throughputs, minimized downtime, and extended operational life achieved through the implementation of alternate modes of operation.

The current study focused on ore blending strategies and overall feed management through the integration of predictive PLS regression models into a DES framework within an oil sands context. The results confirm the approach as an effective way to improve and stabilize plant throughput, despite challenges with significant geological variation of source ore feeds. Despite a small sample population and incomplete characterization (i.e. minimal depositional provenance and bitumen recovery data), the integrated quantitative framework made reasonable predictions and demonstrated how appropriate mineral and geochemical characterization could positively impact process control strategies and decision-making earlier in the value chain.

As ore compositional data is routinely collected in the industry via the Soxhlet-Dean and Start method, bitumen free solids (BFS) are readily available for geochemical and/or mineralogical analyses that can be used for predictive modelling. This work proposes that, with adequate sampling and characterization, expensive and time-consuming analytical work (e.g. organic-rich solids separation) can be replaced by faster and cheaper alternatives, such as WD-XRF and XRD executed on BFS streams (Patarachao, et al., 2010). The generation of robust predictive models will require extensive systematic sampling and analytical campaigns to properly characterize ore feeds and related downstream process responses; the degree of sampling is difficult to anticipate in advance, and ultimately depends on data variability as well as the exact problem being addressed. Regardless, the ability to integrate reliable predictions of bitumen processability into a DES digital twin earlier in the value chain is of key importance to assess the effects of heterogeneous ore feeds on system process performance in the design and implementation of any new or modified control strategy.

Like other complex mining projects, oil sands operations are host to a variety of treatments and processes. From mining to slurry and froth formation, froth treatment, upgrading, and pipeline transport (each possibly comprised of multiple sub-systems), there are a large number of moving parts requiring both management and coordination. The interaction of these parts can be a major source of bottlenecks and generate severe deficiencies, which makes the oil sands context an ideal candidate for DES modelling. However, coordinated efforts between academic, government and industry partners are required in order to couple recent advances in quantitative methods with project-specific problems and data; only then can detailed flowsheets, testing, and full system optimization with constraints proceed.

4.3 Regional Mine-to-Smelter Approaches in the Chilean Context

The large Andean Copper Province (Figure 4.3.1), characterized by a series of long and notably linear metallogenic belts, has been identified as one of the most important sources of copper worldwide for over a century (Sillitoe & Perello, 2005). Deposits in the central Andes, from southern Peru to central Chile and adjacent Argentina, are dominated by epithermal-porphyry copper mineralized systems (Sillitoe & Perello, 2005). These magmatic-hydrothermal deposits, which are typified by large tonnages and relatively low ore grades (generally <1% Cu), include both sulfide and oxide minerals precipitated from aqueous solutions at elevated temperatures (Seedorff, et al., 2005). Characteristic mineralization styles include disseminated ore minerals, with lesser vein and fracture-filling formations, within and adjacent to large, altered intrusive bodies (Seedorff, et al., 2005).

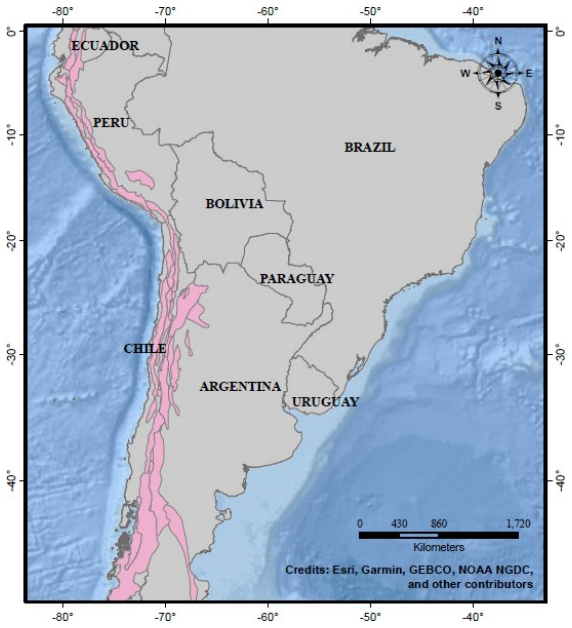

Figure 4.3.1. Map of South America showing the distribution of porphyry Cu tracts (pink) within the elongate, orogen-parallel Andean Copper Province spanning the border between Chile and Argentina, and extending northwards along the coast of Peru towards Central America.

Andean porphyry copper deposits exhibit considerable variation in terms of mineralogical and metal zonation patterns, but commonly include deeper potassic through sericitic (phyllic) zones to overlying advanced argillic lithocaps with propylitic zones (epidote-chlorite) along the margins (Sillitoe, 1995; Sillitoe, 2000; Sillitoe & Perello, 2005). As shown in Figure 4.3.2, primary copper content is greatest in proximity to the central potassic core, and grades upwards and outwards to distal areas with higher contents of auxiliary metals, such as Pb, Zn and Ag (± Au) (Seedorff, et al., 2005). Younger assemblages (e.g. sericitic overprinting of earlier potassic zones) may be dominantly pyritic and effectively barren, or additionally contain a complex variety of high-sulfidation Cu-bearing sulfides including chalcopyrite, bornite, chalcocite and covellite (Seedorff, et al., 2005; Sillitoe & Perello, 2005). It is notable that sulphosalts (particularly enargite) are prevalent in the replacement massive sulfide bodies in the lithocap regions of carbonate-hosted deposits (Sillitoe & Perello, 2005). These mineralogical variations are important to understand the significant geological uncertainty inherent to porphyry-type ore feeds for downstream processing options and related decision-making.

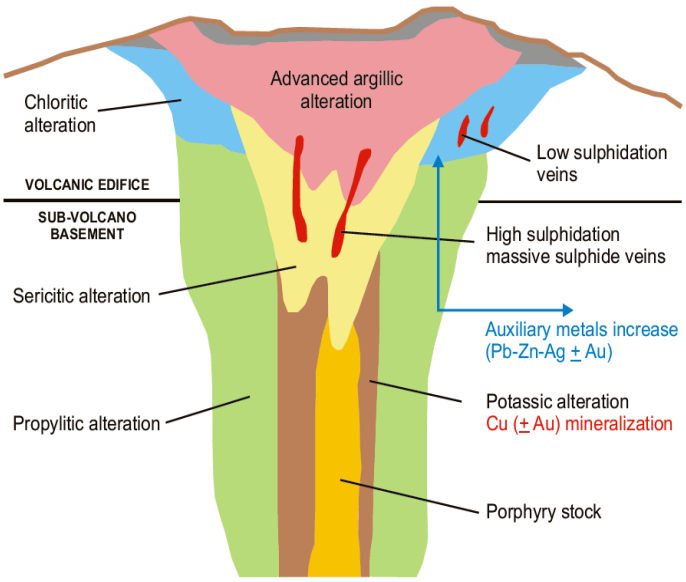

Figure 4.3.2. Schematic diagram of an epithermal-porphyry copper mineralized system, showing idealized alteration mineral and metal zonation patterns (modified after (Sillitoe, 1995)).

Chile is the global leader in copper production, and its vast collection of porphyry and related deposits within the Andean copper belt maintain approximately 23% of current reserves worldwide (U.S. Geological Survey, 2021). As many of the deposits are mined to depth, oxidic copper ores from the upper zones that can be processed via conventional hydrometallurgy technology are being rapidly depleted. In fact, Chilean estimates suggest a potential statewide decrease in the proportion of oxide ores from 31% in 2015 to 12% by 2027 (COCHILCO, 2017; Perez, et al., 2021). A concomitant increase in sulfide-rich ores is projected as these zones are accessed from below the paleo-watertable; these ores are typically only amenable to milling and pyrometallurgical processing (i.e. smelting, converting and anode casting), followed by electrolytic refining. Many copper smelter plants around the globe are world-class operations having an excellent environmental performance. On the other hand, a number of smelters in Chile are still undergoing upgrading to match industry-best standards; outdated technology can contribute significantly to environmental liabilities, such as offgas (e.g. SO_2) emissions and tailings compositions (Nikolić, et al., 2019).

Moreover, forecasts also indicate a trend towards higher levels of deleterious elements, particularly arsenic, from sulphosalt minerals (e.g. enargite) in the sulfide ore assemblages. Despite a growing body of research into the sustainable treatment of As-rich copper ores, there are

many competing interests, each with their own gaps in knowledge and/or limited track records. Even world-class smelters struggle to process so-called 'dirty' concentrates (>0.2% As), and either impose significant penalties or reject the material altogether. As such, conventional pyrometallurgical techniques require that As-rich concentrates first undergo a form of pretreatment to reduce arsenic to acceptable levels. Regardless, As-rich concentrates will likely play an important role in meeting future global copper demand (Tabelin, et al., 2021). Faced with increasingly stringent regulations, as noted, Chile is still in the process of modernizing several of its smelters and related treatment strategies to achieve full environmental control, meet future planned production increases and improve competitiveness in global markets.

With an ever-increasing world population and accelerated modernization and automation practices (as an example, "Industry 4.0"), continued growth of the global copper industry is projected for the foreseeable future. Considered an important crossover material in the clean energy transition (World Bank Group, 2020), estimates show that annual copper demand will increase by nearly 10 Mt over the next 30 years (Tabelin, et al., 2021). While recycled electrical and electronic wastes ('e-wastes'), which represent one of the fastest accumulating waste streams, will be important to help offset this demand, they will not be sufficient to cover the entire gap (Forti, et al., 2020; Phengsaart, et al., 2020; Tabelin, et al., 2021). It is crucial that major copper producing countries, such as Chile, and others within the world-class Andean Copper Province, develop appropriate frameworks to model and test the implementation of new or modified strategies to process complex sulfidic ores within the mineral value chain for years to come.

Discrete event simulation (DES) frameworks are effective computational intelligence tools in the mining space because they can simulate the interactions between critical parameters and processes in relation to random natural variations, such as geological uncertainty. These types of dynamic representations can thus be viewed as extensions of static mass balance models. This is particularly important to porphyry-related copper projects as the processing plant will be subject to significant variability in ore feed characteristics both between and within mineralized zones; a suitable quantitative framework must be able to capture the system-wide effects in response to these changing conditions. Moreover, DES models can optimize tradeoffs between available operational policies, and the bounds that control the timing of their implementation (Navarra, et

al., 2019; Saldaña, et al., 2019; Wilson, et al., 2021a). Deficiencies or bottlenecks in the coordination of unit processes within the system can also be identified by simulating extended periods of operation. As such, DES frameworks are powerful risk assessment and decision-making tools in the design, implementation or modification of any mining system.

This study proposes an integrated mine-to-smelter framework for the regional development of porphyry copper deposits using DES in order to evaluate potential control strategies, such as stockpiling and blending practices coupled with alternate modes of operation. A case study based on the Chilean context is presented that demonstrates the flexibility of the quantitative framework to monitor system-wide response with respect to geological variability and related uncertainty. The paper provides an overview of recent advances in copper extractive metallurgy in relation to modern processing challenges, followed by descriptions of the regional framework development and DES modelling, and finally a set of sample calculations.

4.3.1 Advances in Copper Extractive Metallurgy

Pyrometallurgical techniques, in which sulfidic ores are treated at high temperatures to induce physical and chemical transformations for the extraction of raw metal content, currently account for ~75% of primary copper production worldwide (Price, et al., 2009; Watt & Kapusta, 2019; Navarra, et al., 2020). The remainder of primary copper production is typically handled through hydrometallurgical processing which involves leaching, often in heaps, solvent extraction and electrowinning (Kordosky, 2002; Ochromowicz & Chmielewski, 2011; Navarra, et al., 2020). Though pyrometallurgical techniques clearly dominate the copper sulfide landscape, this trend could eventually change with intensified efforts to develop hydrometallurgical processes for the extraction of copper, particularly for complex ores and concentrates (Hyvarinen & Hamalainen, 2005; Dreisinger, 2006; Ochromowicz & Chmielewski, 2011; Tabelin, et al., 2021).

The high pressure leaching process built by FIM (formerly Phelps Dodge) at Morenci, Arizona in 2007 is the only large commercial hydrometallurgical plant treating conventional copper sulfide concentrates today. The Morenci plant produces of the order of 50,000 t of EW Cu /year by treating 35-40% Cu concentrates. Other “commercial-ready” hydrometallurgical technologies are Glencore’s Albion process (ultrafine grinding and atmospheric sulphate leaching) and Teck Resources’ CESL technology (medium-temperature pressure oxidation). Though well-established

in the gold sector, the Albion process remains under development for copper, with the first industrial-scale facility retrofit to the Sable Zinc Kabwe plant (Zambia) in 2017 with a target throughput of 10 kt/y (Glencore Technology, 2018). Similarly, Vale installed a 10 kt/y CESL demonstration copper plant in the Carajas region of Brazil in 2008 (Defreyne, et al., 2008; Mayhew, et al., 2011). However, given projected mining trends and the current state of smelting operations in Chile, the present paper focuses mainly on commercially available and proven pyrometallurgical approaches. The goal of the study is to develop suitable frameworks capable of modelling system-wide dynamics in response to the implementation of proposed upgrades and/or new processes.

Overview of copper smelter dynamics

Conventional copper smelter operations target the selective oxidation of Fe and S, which are skimmed away as liquid slag and removed as SO_2 offgas, respectively; the final product from this process is a molten metal product, called blister copper (>98% purity) (Schlesinger, et al., 2011; Navarra, et al., 2020). This is achieved via a two-step process, including: 1) *smelting* of the bone-dry concentrate by the exothermic reactions controlling the oxygen mass balance, which produces an intermediate Cu-Fe-S matte phase, and; 2) *converting* of this matte phase through secondary multi-stage oxidation to produce blister copper. Subsequently, a fire refining step precedes the casting of the copper anode product (~99.5% purity), which is then transferred to the electrorefinery for production of the copper cathode product for the market (99.99% purity) (Navarra, et al., 2020).

There are two dominant smelting technologies used today that are principally distinguished based on the method of oxygen delivery to the concentrate. Flash smelting involves the oxidation of concentrate within the refractory-lined reaction shaft of a vertically mounted burner, and currently accounts for ~45% of the global copper smelting capacity (Mackey, 2013; Watt & Kapusta, 2019; Navarra, et al., 2020). In contrast, bath smelting entails the injection of air into the molten bath either via submerged tuyères or by means of a top-submerged lance (or TSL) wherein the bath absorbs the added concentrate which is typically as a filter cake material; this method accounts for ~50% of the world smelting capacity, and this proportion continues to grow due to

new bath smelting technologies recently developed in China (Mackey, 2013; Watt & Kapusta, 2019; Navarra, et al., 2020).

Peirce-Smith (PS) converting is the most enduring (>100 years) and broadly used technology for matte converting, with ~70% of conventional copper smelters using this process and/or its derivatives today (Wang, et al., 2016; Taskinen, et al., 2018; Navarra, et al., 2020). Principal reasons for its long-standing success include that is it a well-established and reliable technology, it is of relatively simple design, ease of operation, and the ability to melt cold recirculated material (Taskinen, et al., 2018). As with all copper smelting operations, the technology typically requires skilled operators as the development and implementation of advanced control systems has been slow across the industry (Navarra, et al., 2020). Some of the most advanced smelters with excellent environmental control employ PS converters, and they have overcome some of the so-called deficiencies in the technology such as fluctuations in SO_2 offgas concentration and potential fugitive emissions if not well designed and controlled (Mackey, 2013).

More recent continuous converting technologies, such as the Kennecott-Outotec flash converting furnace (FCF) or the Noranda Converter (Prevost, et al., 2013), offer the advantage of good conversion rates from a single process unit, in addition to significant environmental and resource/energy efficiencies (Hanniala, et al., 1991; Taskinen, et al., 2018). In flash converting, blister copper and slag are produced via the oxidation and smelting of fine-grained, granulated matte feed within a highly oxygenated environment (Taskinen, et al., 2018). This results in consistently lower offgas volumes that are also richer in SO_2 compared to PS converting; the stability of the offgas stream is thus more amenable to both emissions control and sulphuric acid generation, which can lead to potentially improved system-wide efficiencies and cost savings in the acid plant (Kojo & Storch, 2006; Taskinen, et al., 2018).

New developments in the continuous converting domain include Glencore's ISACONVERT^{TM} process (Figure 4.3.3; after (Edwards & Alvear, 2007; Alvear, et al., 2014)), which uses TSL technology to produce blister copper from solid matte, and represents an extension of the commercially successful ISASMELT^{TM} furnace (Nikolic, et al., 2009; Schlesinger, et al., 2011). This approach remains mostly under development for copper with extensive experimental

and pilot plant scale testwork ongoing; a single commercial unit (~175,000 t of ~60% Cu matte/y) was installed at the Kansanshi smelter in Zambia in 2019 (Glencore Technology, 2021).

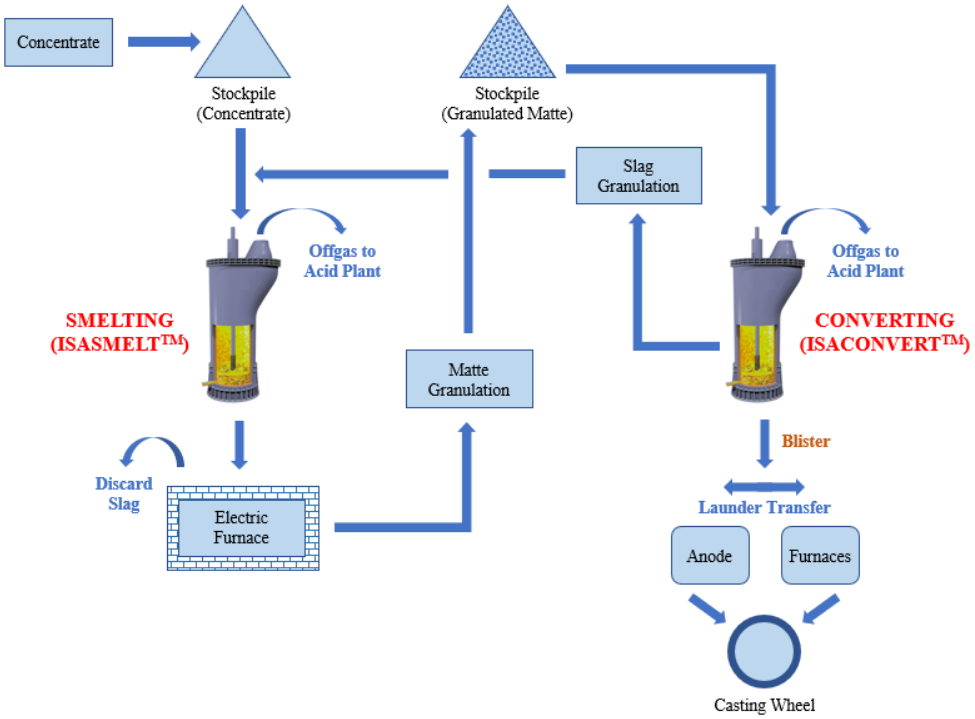

Figure 4.3.3. Schematic flowsheet of copper smelting with ISACONVERT™ for converting (after (Edwards & Alvear, 2007; Alvear, et al., 2014)).

Decoupling of smelting and converting processes

Smelting and converting are the central processes in conventional smelter operations, but together represent a continuous-discrete contrast due to the batch-wise nature of PS systems, which can create major bottlenecks and potentially limit overall production (Navarra, et al., 2016; Navarra, et al., 2020). The advent of continuous converting technologies in the mid-1990s was a major advancement not only in terms of unit smelter operation efficiencies and emissions control, but also towards the development of new and/or modified strategies to coordinate individual processes within the mine-to-smelter profile. As a result, smelting and converting processes can now feasibly be decoupled by means of a matte stockpile replacing the need for a holding furnace, with individual smelting and converting furnaces that operate independently of each other. At the plant scale, this decoupling is significant in that maintenance downtime is reduced as matte can be stored during converter repair and similarly, stockpiled matte can be processed during smelter

furnace servicing (Taskinen, et al., 2018). Though latent heat is lost in the granulation and stockpiling of matte, efficiencies are gained with respect to acid plant production (Hanniala, et al., 1991; Kojo, et al., 2009); however, studies have shown these gains are effectively offset by the high O_2 requirement and related electricity consumption (Coursol, et al., 2010).

An interesting approach is to implement the decoupling concept at the regional scale, whereby individual smelters that produce intermediate matte are located at, or near a collection of, mine sites which collectively feed regionalized converting facilities. Matte products that reach Cu concentrations of 70–78% are called *white metal* (Olper, et al., 2008), hence the term 'white metal economy' can be applied to this type of proposed mine-to-smelter integration. Immediate advantages of the regionalized decoupling concept include: 1) elimination of bottlenecks created by conventional batch conversion cycles, thereby increasing individual smelter availability; 2) the ability to implement control strategies, such as stockpiling and blending practices, in order to mitigate operational risk at regionalized converting plants; 3) a reduction in transportation costs between mine sites and primary smelting operations due to improved feasibility of small-scale plants, and; 4) improved SO_2 offgas capture, acid production and overall energy efficiencies. Additional benefits could also be garnered by keeping primary smelting facilities and related acid plants closer to the source mine sites, particularly when the orebodies are hosted within or proximal to carbonate (limestone) successions which can be used as a neutralizing agent (buffer); however, depending on location, shipment of acid may be problematic.

However, prior to implementing any new strategy, appropriate computational tools are required to properly evaluate the system-wide response to the proposed changes in smelter dynamics and expected changes in ore feed characteristics. Flexible frameworks that can model and simulate such uncertainties are critical to support decision-making processes in the design, development and implementation of multi-phase reengineering projects (Navarra, et al., 2020).

Challenges with high-arsenic copper concentrates

Increasing proportions of deleterious elements in copper concentrates are a growing concern for the metallurgical extraction of copper worldwide. Arsenic levels in particular are already approaching the limits of currently accepted concentrations within which the majority of smelters have elected to function; for instance, Japan recently reported a three-fold increase in As/Cu ratios

in concentrate feeds over a 25-year period, and anticipates breeching the 0.3% mark as new high-As deposits are brought online (Flores, et al., 2020). Similarly, earlier estimates projected total arsenic content in global concentrates to increase from ~85 kt in 2010 to ~218 kt in 2020 (Mayhew, et al., 2011). Stringent environmental and health regulations have led to lower thresholds for arsenic, with concentrates exceeding 0.2% As subject to substantial penalties and those exceeding 0.5% As susceptible to rejection by most smelters globally (Brook Hunt, 2010; Mayhew, et al., 2011; Mean, 2011).

The main cause of increasing arsenic levels in global copper concentrates is the gradual depletion of clean high-grade ores (Chen, et al., 2010). This is especially true of Chile where many of the giant porphyry Cu orebodies are now being mined to depth and beginning to exploit sulfide-rich zones from beneath the paleo-watertable; these complex ore zones commonly contain abundant As-bearing minerals, such as enargite, luzonite and tennantite-tetrahedrite. Arsenic is a challenging impurity for smelter operations to control and properly contain in the environment; moreover, earlier methods of handling and disposal (e.g. lime precipitation) are now poorly tolerated in most non-arid regions of the world due to the formation of soluble arsenic acid and related environmental risks (Riveros, et al., 2001; Mean, 2011). As a result, new control strategies must be adopted to process these complex As-bearing ores.

Research and industry efforts over the past 30 years have focused on a combination of selective flotation applications, hydrometallurgical techniques (± solvent extraction and electrowinning), roasting methods, stabilization of residues, and vitrification in smelting slags (Flores, et al., 2020). A comparison of arsenic levels in ore feeds and concentrates, with current treatment strategies, are summarized for a selection of mining projects from Peru, Chile and Serbia in Table 4.3.1. Of these technologies, collaborative research in Chile has been dominated by the roasting and hydrometallurgical streams. Recent testwork at the pilot plant scale in Chile has shown that dearsenifying (partial) roasting of high-As copper concentrates is an effective technique to eliminate arsenic (>95%), leaving a calcine composed of bornite, chalcopyrite, chalcocite and magnetite (Wilkomirsky, et al., 2020). At temperatures in the range of 600–750°C, arsenic partitions to the gas phase and is subsequently oxidized to arsenic oxide dust (Mayhew, et al., 2011). This technique has also been successfully commercialized at Codelco's Ministro Hales

mine, where the concentrate may contain on the order of 5–6 wt% As, and produced calcine contains in the range of 0.3% As for an elimination factor of ~95% (Caballero, et al., 2016). The volatized arsenic is recovered during wet gas cleaning at the acid plant, stabilized with lime to calcium arsenate, and sent for disposal treatment (Hedstrom, et al., 2016).

Table 4.3.1. Arsenic levels and treatment strategies for selected projects (Candente Copper Corp., 2019).

				Deposit	Concentrate
Company	Project Name	Status	As Treatment	As (ppm)	As (%)
Nevsun	Timok	Development	Blending, Penalties	1700	1.40
Codelco	Ministro Hales	Production	Outotec Roaster	1000	4.00
NEXA	Magistral	Development	-	340	-
Coro Mining	San Jorge	Development	Solvent extraction, Electrowinning	300	-
Rio Tinto	La Granja	Development	Roasting, Hydrometallurgy	250	1.00
Candente	Canariaco	Development	Roasting	240	1.00
Chinalco	Toromocho	Production	Blending (ore)	190	1.00
Chinalco	Galeno	Development	Blending	166	1.20
S. Peru Copper	Michiquillay	Development	TBD	-	-

Notable hydrometallurgical advances include pressure oxidation and ferric arsenate precipitation (Universidad Catolica del Norte), alkaline leach and As stabilization in ceramics (Universidad de Antofagasta/CSIRO), bio-oxidation of Fe(II) and As(III) (Universidad de Chile/Ecometales), and UV-oxidation and ferric precipitation of As (Universidad de Tarapaca). There is also considerable interest in methods that capture As in the formation of scorodite, a stable crystalline form of ferric arsenate (Filippou & Demopoulos, 1997; Nazari, et al., 2017).

4.3.2 Integrated Mine-to-Smelter Framework Development

This work is focused on development of a suitable framework capable of modelling and simulating system-wide dynamics in order to assess potential operational risks associated with a regionalized mine-to-smelter approach loosely based on the Chilean context. The concept is predicated on the decoupling of smelting and converting processes, and aims to evaluate the coordination of site-specific unit smelter operations that supply regional-based continuous converting facilities with granulated intermediate matte or white metal (e.g. Figure 4.3.4). To maximize furnace availability and mitigate stockout risk within the individual smelting and

converting operations, the tactical decision has been made to implement stockpiling practices for both concentrate feed and granulated matte. Similarly, blending control strategies are required in response to geological uncertainty caused by varied ore feeds with evolving attributes (i.e. increasing As levels).

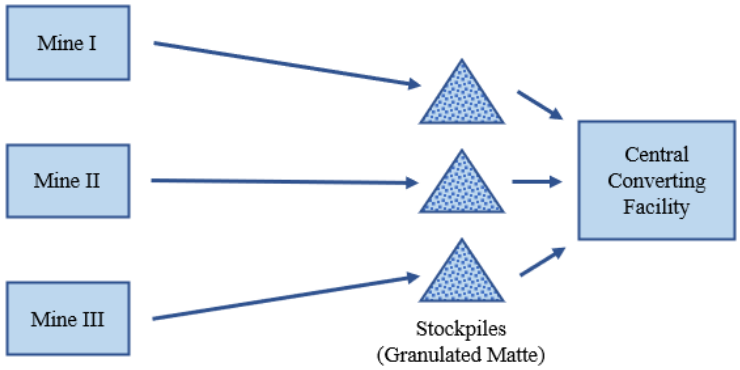

Figure 4.3.4. Generalized diagram illustrating a mine-to-smelter framework with individual mines and site-specific unit smelter operations that supply regional-based continuous converting facilities.

Given the older condition of some current infrastructure and projected mining trends in Chile, this study proposes the following series of upgrades to support the conceptual framework: 1) installation of new technology such as the ISASMELT^{TM} at (or proximal to a collection of) mine sites; 2) investiture in regionalized Kennecott-Outotec flash converting furnace (FCF) facilities that accept granulated matte feed or white metal from the unit smelting plants, and 3) commissioning of partial roasting plants at mine sites afflicted with high-As copper ores.

Glencore's ISASMELT^{TM} process uses TSL bath smelting technology, first commercialized in 1992 at Mount Isa Mines (Glencore, 2015). Compared to other methods, which inject gases into the reaction vessel via tuyeres, this technology allows for the design of a stationary furnace (Bakker, et al., 2009). The lance is submerged in the slag, which creates a turbulent molten bath and permits raw feed materials to quickly react beneath the surface (Glencore, 2015). This technology was selected mainly owing to its proven commercial success (combined smelting capacity exceeding 10 Mt/y; (Glencore, 2015)), flexibility to handle a wide range of concentrate compositions (Burrows, et al., 2012), and scalability (e.g. ~150,000 t/y accepted at the Aurubis Lunen smelter, Germany (even if treating copper scrap as feed) vs. ~1.4 Mt/y processed at the Vedanta Tuticorin smelter, India (Glencore, 2015)).

The many benefits of flash converting systems were described in detail above, but the Kennecott-Outotec FCF technology was also chosen here due to its proven track record; the first commercial operation was commissioned in 1995 at Kennecott's Utah smelter, processing over 7 Mt of copper matte in its existence, and the Xiangguang Copper smelter has produced over 3 Mt of copper since its inception in 2007 (Taskinen, et al., 2018). The partial roasting technique was selected to deal with high arsenic levels in complex sulfidic ores based on ongoing research in this area in Chile, in addition to its successful application at Codelco's Ministro Hales Mine.

The exact nature of the selected technological upgrades is not fundamental to the functioning of the developed quantitative framework because it is based on the mass balancing of target material, energy and/or information flows. The flexibility of the current DES model to handle different data types makes it particularly suitable for the evaluation of different control strategies. For instance, although this study is focused on pyrometallurgical techniques, the framework could easily be adapted to monitor mass flows pertinent to a selected hydrometallurgical approach, or similarly to upstream flotation circuit processes. In fact, as new hydrometallurgical arsenic pretreatment techniques progress from development to commercialization, it would be highly advantageous to adapt the current framework and compare the system response to this roaster-smelter approach using an appropriate set of KPIs.

4.3.3 Discrete Event Simulations

This study extends concepts from recent DES modelling work by Navarra et al. (2019, 2020) and Wilson et al. (2021a, 2021b), which implemented alternate modes of operation with multiple configuration rates in order to optimize the balancing of plant feed types; adjustments were then made to stockpiling and blending practices based on observed system-wide response. The current framework has been adapted to evaluate system performance for a conceptual regionalized mine-to-smelter profile (loosely based on the Chilean context) that involves the decoupling of smelting and converting processes. The concept is to replace aging conventional smelter infrastructure with smaller scale TSL smelting furnaces and modern roasters for the pretreatment of high As feeds. In general, it would be unclear where within the logistical network to place these furnaces and roasters, considering that they may be fed by one or several mines. The resulting slag and white metal could be granulated using novel heat transfer technology following the concept established

by Mucciardi (Navarra, et al., 2016); the high-grade heat could be cycled to assist in roasting. Moreover, the acid could be utilized for the leaching of nearby oxides, while the slag is locally processed as construction and backfill material. Nonetheless the white metal could be shipped to a centralized facility for conversion ultimately into copper anodes; depending on the local energy economy, this larger facility may be integrated with an electrorefinery to produce cathodes.

The current set of calculations focuses on a single roaster-TSL-granulation assembly, i.e. a mini-smelter, designed to accommodate a blend of 60% low- and 40% high-arsenic sulfide concentrates; the low- and high- As concentrates are abbreviated as LAC and HAC, respectively. Moreover, the mini-smelter is integrated with a mine known as "Mine I" that is expected to yield a balance of 70% low- and 30% high-arsenic feed over the foreseeable future, and is subject to geological uncertainty, as described below. Meanwhile, the nearby Mine II has abundant access to high-arsenic ore, and prioritizes sending the resulting high-arsenic concentrate to the mini-smelter whenever it can be accommodated; the overall concept is summarized in Figure 4.3.5.

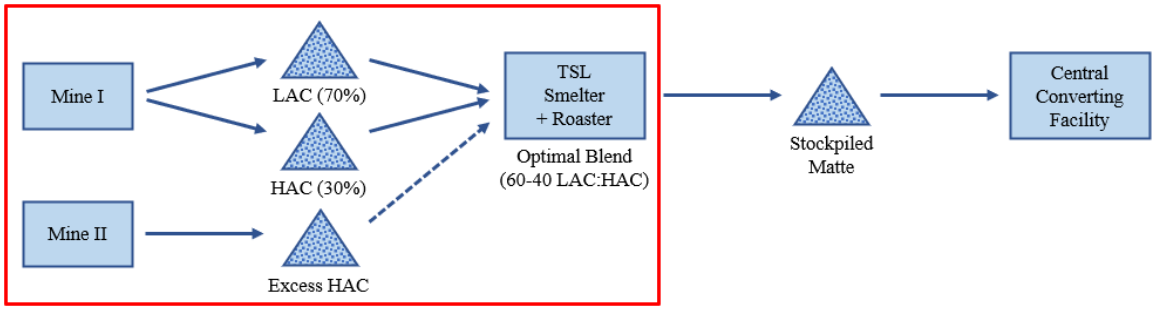

Figure 4.3.5. Diagram illustrating the overall concept for the current set of sample calculations; the red outline highlights the system processes considered by the framework, subject to geological uncertainty.

There are thus two operational modes:

- Mode A: The smelter receives 300 t/d of concentrate from Mine I, and 0 from Mine II
- Mode B: The smelter receives 200 t/d of concentrate from Mine I and 100 from Mine II.

Noting that only high-arsenic concentrate is received from Mine II. The resulting mass balance is described in Table 4.3.2, in which Mode A is expected to diminish the HAC stockpile by 30 t/d but Mode B is expected to replenish the HAC by 40 t/d. The decision to commit to Mode A or Mode B occurs at the end of 5-week production campaigns, and involves a retooling of key equipment which can only be accomplished during the one-day shutdown; having less than 1500

t of stockpiled HAC at the moment of shutdown indicates an opportunity to accommodate HAC from Mine II, through the application of Mode B.

Table 4.3.2. Stockpile balance of low- and high-arsenic concentrate, ignoring geological uncertainty.

	Low-Arsenic Concentrate			High-Arsenic Concentrate			
Mode	From Mine I	Into Smelter	Balance	From Mine I	From Mine II	Into Smelter	Balance
A	210	180	+30	90	0	120	-30
B	140	180	-40	60	100	120	+40

The framework was implemented using commercial DES software (Rockwell Arena©) with Visual Basic for Applications (VBA). As previously noted, model verification has been carried out by a combination of event checking and debugging, in addition to sensitivity analysis by varying model inputs and parameters. The model was calibrated based on typical values in the Chilean context, obtained from time-averaged publicly available data, e.g. (Pradenas, et al., 2006; Perez, et al., 2021), to ensure suitable and valid ranges were used. In practice, operational data would be available to further validate the model and make adjustments to the control parameters.

Figure 4.3.6 illustrates the fluctuations in feed stockpiles over 500 days of operation under the present case study, assuming critical ore and target total stockpile levels of 1500 t and 3000 t, respectively. Deterministic values for these variables were determined following the approach of Navarra et al. (2019), and adjustments were made based on the observed system response. Mode A is in application over the periods in which the HAC stockpile is diminishing and the LAC are increasing. Conversely, Mode B is in application over the periods in which the LAC is diminishing and HAC is diminishing. The alternation of these modes allows the stable functioning of the smelter with its optimal design configuration of a 60-40 blend of the two feeds, even though Mine I is not currently accessing the optimal amount of high-As ore; this presents opportunities for Mine II to periodically offload some of its HAC in the periods of Mode B.

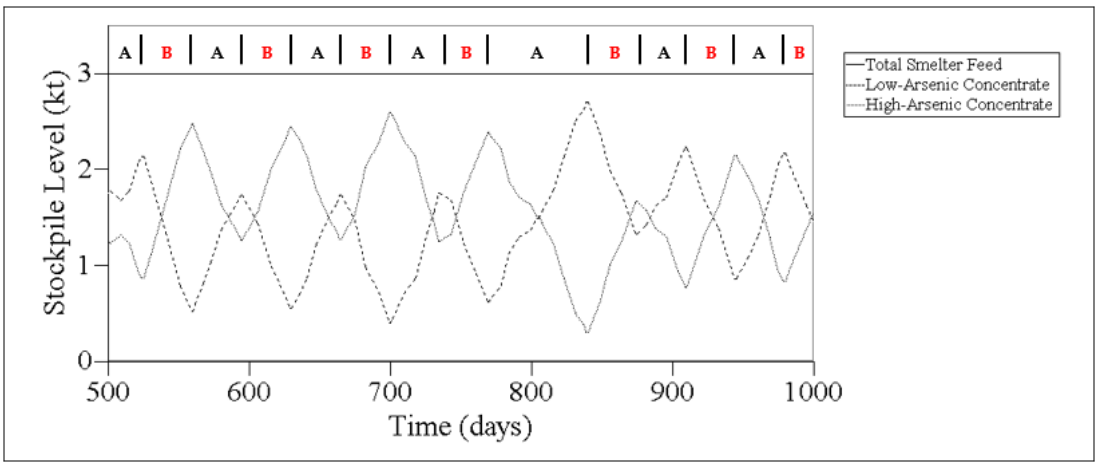

Figure 4.3.6. Graphical output from the DES framework, demonstrating 500 days of operation.

Moreover, Figure 4.3.6 represents the geological uncertainty confronted at Mine I, which is evident by the jagged nature of the line segments. In general, the framework can incorporate geostatistical models (Wilson, et al., 2021a), or other advanced methods such as machine learning algorithms, to classify and determine relative ore type proportions. However, the current set of calculations consider the following simplified Monte-Carlo approach which determines the tonnage of ore, and the portion of ore that is HAC:

- Mine I excavates one parcel at a time; upon completion of the parcel, a subsequent parcel is generated;
- The new parcel contains between 1500 and 2500 t of ore, according to a uniform distribution;
- There is 70% chance that the new parcel is of the same facies as the previous parcel;
- If the new parcel is of the same facies, then the percentage of HAC is within ±1% of that of the previous parcel, according to a uniform distribution;
- Otherwise, if the new parcel is of a new facies, the percentage of HAC is randomly generated according to a Gaussian distribution with mean of 30% and standard deviation of 1%.

The 30% mean is indicative of the 70-30 portions of low- versus high-arsenic ore. Moreover, the potential dissimilarity of two subsequent parcels (i.e. if they belong to two different facies) approximates either the geological discontinuities or the operational decisions to excavate different regions of the mine. In a more elaborate computation, geological uncertainty could also have been represented within Mine II; or more broadly, the framework could represent a network of mines each confronting operational and geological uncertainties, which feed into a network of smelters.

4.3.4 Conclusions

As previously discussed, a number of Chilean copper smelters, which together produce approximately 8% of world smelted copper today, are implementing projects to modernize the plants to best-in-class standards. At the same time, copper ores in South America are more and more complex with mining ore bodies at depth, thus adding to the burden at the copper smelting stage. As part of mine-to-smelter strategies, the concept of a given plant producing white metal for shipping to a second finishing smelter was discussed in the present paper as one economic approach in the modernization process. This was examined using a dynamic DES model, illustrating its utility for coordinating production beyond a single mine.

It was noted that copper demand is expected to grow, driven in large part by great interest in new renewable energy sources and electric vehicles. Studies show that growth in copper demand will be led by China which in 2020 accounted for about 55% of global refined copper consumption. Given that about 80% of refined copper in China is produced by processing imported concentrates – in large part shipped from Chile and Peru at present, and likely with additional material from Africa in the future – the quality of the concentrate shipped will be important moving forward. The present study listed as an example six major copper deposits in Chile and Peru containing elevated levels of arsenic in ore, which based on present technology for milling and flotation, are projected to produce copper concentrates containing of the order of 1% As content. A number of arsenic control strategies to reduce this level for shipping or for handling at a nearby smelter were identified, including roasting (as presently practiced at the Ministro Hales plant in Chile) and hydrometallurgical options. In all cases, the nature of the material expected to be shipped will change – possibly representing a calcine material or a copper residue of some nature.

This work explored a number of mine-to-smelter strategies. Estimates derived from sample calculations loosely based on the Chilean context represent interesting cases for further study of such strategies. The current framework is primarily intended for the design, implementation and monitoring of new or modified control strategies in an ‘offline’ setting. However, future work focused on the incorporation of machine learning algorithms could allow the DES model to be eventually brought ‘online’ by integration with a mine control system, following suitable validation of its ability to mimic responses of the corresponding physical system. It can also be

seen based on the above that research and development efforts by the copper industry need to be strengthened if the targets for expected future copper demand are to be safely met.

4.4 Regional Coordination of Refractory Gold Systems

The rate of new gold discoveries has decreased over the past three decades despite increased exploration spending amidst periods of record gold prices (S&P Global, 2021). This is in part due to companies focusing on brownfields and advanced stage exploration prospects (i.e. known deposits). One must also consider that most of the near surface high-grade gold deposits in easily accessible regions of the world have likely already been found. This notion is reflected in the severe lack of recent world-class gold discoveries, classified as those containing at least 100 metric tons (3.2 Moz) gold. Reports indicate that less than 10% of all gold identified since 1990 can be attributed to major discoveries made over the past decade (S&P Global, 2021). Moreover, average head grades for sizable primary gold deposits (>1 Moz Au) have plummeted from over 10 g/t Au in the 1970s (Schodde, 2011; Mudd, 2007) to less than 1.5 g/t Au at present (Metals Focus, 2020). This significant decrease, however, is partly driven by elevated gold prices and new technologies that have allowed for large-scale open-pit operations, both of which have made mining and processing of lower grade material economically feasible.

Declining trends in rates, sizes and grades of gold discoveries means that new mining projects being brought online are not replacing estimated gold production figures. This assertion is only compounded by volatile market fluctuations, geopolitical and socio-environmental aspects, and related administrative hurdles (e.g. permitting). Furthermore, mining project development pipelines are now facing increased start-up timelines; the average length of time from discovery to commissioning more than doubled between 1995 and 2013 (from 8 to 18 years), and continues to increase (Adams, 2016). While recycling of jewelry and electrical/electronic wastes (a.k.a. e-wastes) will continue to play an increasing role in the supply of gold (World Gold Council, 2021; Tabelin, et al., 2021; Forti, et al., 2020), the reality is that there could be significant imbalance in the supply and demand for gold in the relatively near future. As a result, research and development need to continue exploring options to process more complex and refractory ore types, and tools need to be made available that can improve understanding of potential system-wide effects caused by varied ore feeds and related decision-making processes.

Gold ores can be classified based on their metallurgical response to different processing techniques. Conventional ores are typically considered 'free-milling', meaning they are amenable to direct cyanidation and recovery via carbon-in-pulp/carbon-in-leach processes (Adams, 2016). Certain low-grade or oxide ores have similar characteristics but are only economic by heap leaching as gold tenors are insufficient to justify tank cyanidation. Conversely, refractory ores are not amenable to standard cyanidation practices (or sale of concentrate) and require additional pretreatment prior to leaching and recovery (Adams, 2016).

Refractory gold sources occur in a variety of geological environments, but are most often linked to sediment-hosted deposits with a close association to As-rich sulfide minerals. Though found in many regions of the world, prime examples include the large, disseminated orebodies within the Carlin Trend of Nevada, U.S.A., and along the margins of the Yangtze craton in China. There are three main causes of refractory gold: 1) preg-robbing, which implies adsorption of gold cyanide complexes by carbonaceous material or other minerals in the ore, leading to gold losses that would otherwise bind to activated carbon in the pregnant leach solution (Ng, et al., 2020; Marsden & House, 2006); 2) variably locked or encapsulated gold grains (i.e. inclusions) requiring further particle size reduction in order to liberate and expose the gold to the leaching solution (Baron, et al., 2016), and; 3) 'invisible' gold, which can occur as sub-micron native particles (Au^0) and/or structurally-bound in solid solution (Au^{+1}) within host minerals, most commonly arsenian pyrite and arsenopyrite (Kusebauch, et al., 2019; Reich, et al., 2005). Some severely refractory ores can be afflicted by both preg-robbing and invisible gold, and are thus called 'double refractory'. The strong association of refractory gold with As-rich sulfides and arsenides (or tellurides, antimonides and selenides) also poses additional challenges due to elevated impurity levels and related environmental considerations.

There are a variety of processing options currently available for refractory gold, depending on the nature and level of refractoriness of the ore. Physically-locked gold can be further liberated by fine or ultra-fine mechanical grinding prior to leaching; however, the increased energy costs for this size reduction usually necessitate concentrated ore feeds (e.g. Kalgoorlie CGM, Australia) (Baron, et al., 2016). Oxidative processes are the most common approach to pre-treating sulfidic refractory ores in the industry. Traditionally, high-temperature roasting was used to oxidize iron

sulfides to hematite (Fe_2O_3), the porous nature of which allows for the penetration of leaching solutions (Baron, et al., 2016). Increased environmental awareness and regulations have since led many companies to shift focus to newer technologies due to concerns over offgas (i.e. SO_2) emissions and volatilization of impurities (e.g. As_2O_3) caused by roasting. Pressure oxidation (POX) is now one of the main methods applied to improve recovery by oxidizing iron sulfides to ferric sulfate or other oxides, thereby exposing the gold for leaching (Baron, et al., 2016). Biological oxidation (BIOX) is another leading method, wherein bacteria catalyze the conversion of iron sulfides to soluble ferric iron and sulfur to sulfate and ultimately sulfuric acid (Baron, et al., 2016; Afidenyo, 2008). Both POX and BIOX have limitations when treating carbonaceous sulfidic ores affected by preg-robbing; roasting thus remains the most effective pretreatment option for double refractory ores (Baron, et al., 2016). However, research and development are highly active in this area and new processes continue to emerge, such as oxidation followed by thiosulfate leaching; the first commercial installation of which was commissioned at Nevada Gold Mines' Goldstrike deposit in 2014 (Adams, 2016; Baron, et al., 2016).

Regardless of the processing route, refractory ores contribute significantly to world gold production; for instance, estimates have shown refractory ore sources to generate on the order of 25% of global production (Adams, 2016). Moreover, refractory gold currently accounts for ~24% of classified ore reserves and ~22% of known resources worldwide (McKinsey & Company, 2021). However, the processing of refractory ore requires large capital investments with increased operating costs, often making substantially sizable operations an absolute must. The required installation of infrastructure and equipment to pre-treat the ore presents significant cost barriers to smaller mining projects or companies with less financial liquidity. To this end, there are many companies evaluating newer preconcentration developments in order to improve project valuation.

In particular, sensor-based ore sorting has gained considerable interest in the mining space over the past two decades with many pilot plant and full-scale commercial installations worldwide. Most systems are based on individual particle sorting, and use a combination of sensors to physically separate (accept/reject) material from heterogenous feeds; the approach has also been extended recently to include bulk sorting applications (Wotruba & Robben, 2020). Examples of common diagnostic properties and sensor types include colour, reflection/transparency, X-ray

transmission (atomic density), short-wave or near infrared radiation (mineral detection), and X-ray fluorescence (elemental detection) (Wotruba & Robben, 2020; Robben & Wotruba, 2019; Kern, et al., 2019). The technology is not exactly new to the minerals industry with the earliest and most widespread use in the concentration of diamonds spanning a period of more than 70 years, but most of this development was completed in-house (Wotruba & Robben, 2020). With a lack of confidence towards mineral applications, interest in the technology for other commodity markets did not gain support until the 1990s for industrial materials and the 2000s for base and precious metals (Wotruba & Robben, 2020; Robben & Wotruba, 2019). In the gold sector, many companies report potential mass reductions in the range of 30–60% coupled with 1.5 to 2-fold grade increases and high gold recoveries (>90%) from ore sorting testwork (Tomra Sorting GmbH, 2021; GlobeNewswire, 2021; International Mining, 2021), including sulfidic refractory sources, e.g. (Gowest Gold Ltd, 2015).

This preconcentration of run-of-mine can have a number of benefits, including 1) increased productivity through debottlenecking of milling processes and the potential to raise mining rates equivalent to the amount of ejected waste; 2) reduced mining cut-off grades, which can extend productive mine life or create opportunities to re-process old waste dumps or tailings; 3) decreased tailings generation, which has both economic and environmental implications due to reduced processing and storage of waste materials; 4) decreased capital and operating costs related to equipment and material handling and transportation, and; 5) increased process efficiencies, thereby reducing the environmental footprint through decreased water, energy and reagent consumption rates (Robben & Wotruba, 2019). Such considerations may be less pertinent to certain large-scale operations, but can be especially important to the evaluation of smaller deposits with marginal economics. Regardless, there will likely be a shift towards such pre-concentration technologies in the future by all scales of mining projects due to socio-environmental factors driving the development of more responsible and sustainable approaches to mining.

There are many instances of untapped refractory ores left in the ground, particularly in proximity to active mining operations or processing facilities. Sometimes this is due to the existence of better prospects for project development, but it can also be related to a lack of appropriate tools to evaluate system design, or the effects on existing system processes.

Unfortunately, the latter is all too common among historic or mature mining projects where it could have made sense to extract the material concurrently along with other conventional reserves but would no longer be economical to process on their own. However, there could be opportunities for companies to consolidate these resources within mining camps and process the ore from centralized facilities, or similarly to reprocess waste dumps or tailings to recover initial gold losses from mildly to moderately refractory ores. With recent advances in computing power, the necessary tools can be developed to assess mining system dynamics in relation to proposed new or modified control strategies that can handle varied ore sources, such as refractory gold.

The integration of predictive machine learning (ML) algorithms into DES frameworks can help with decision-making earlier in the value chain; however, it is important to ensure appropriate ore characterization (e.g. gold deportment) is carried out prior to implementing any type of predictive model. This has also been shown as an effective approach towards the development of online, i.e. real-time, simulation-based digital twin models (Atreya & Sridhar, 2019; Greasley, 2020; Lektauers, et al., 2021). A digital twin is a multidisciplinary virtual representation that uses both historic and updated data models to simulate the operational life of the corresponding physical system (Glaessgen & Stargel, 2012; Boschert & Rosen, 2016); such tools are becoming increasingly popular in the age of Industry 4.0 and related internet of things (IoT) systems.

This work proposes an integrated artificial neural network (ANN) and DES framework for the regional coordination of conventional and refractory gold ores feeding centralized processing facilities. In addition to evaluating potential control strategies, such as stockpiling and blending practices using alternate modes of operation, a conceptual case study is presented that also considers the implementation of site-based ore sorting as a form of preconcentration for more distal satellite orebodies. The remainder of this study describes the implemented methods, followed by an overview of the framework development, and finally a set of sample calculations for a conceptual case study.

4.4.1 Materials and Methods

Dataset Generation

In order to develop the framework, a set of geochemical, mineralogical and metallurgical data ($n = 750$ samples) was generated for a conceptual new satellite deposit, reflective of a sediment-

hosted, structurally-controlled orebody. Data ranges for gold and arsenic assays, geochemical elements, mineral phases and potential recoveries were estimated based on data from several studies, e.g. (Patterson & Muntean, 2011; Christiansen, et al., 2011; Li & Peters, 1998; Bao, 2001), in addition to author experience. The geochemistry and assay data were populated via random number generation using normal distributions centered around a suitable mean value for each element. Variability was controlled using standard deviations of 1.0, 0.1 and 0.01 for major, minor and trace elements, respectively, depending on typical detection limits. Mineral phase abundances for a selection of hydrothermal alteration and sulfide minerals common to sediment-hosted gold systems were estimated from whole-rock major element data using the 'MINSQ' least squares fitting method after Hermann and Berry, 2002 (Hermann & Berry, 2002).

Finally, for the gold recoveries, data were sorted according to Au:As ratio and an arbitrary cutoff of 0.02 was applied; values were randomly assigned using a uniform distribution from 80–100% for samples above this level, and from 30–85% for those below. The 0.02 threshold was selected as an extension of the molar solubility limit for solid solution gold contained in As-rich pyrite, as reported by Reich et al. (2005) (Reich, et al., 2005). In practice, bulk metallurgical testwork is an expensive endeavor; instead, recovery data could be acquired via cheaper and faster alternatives, such as shaker table or bottle roll tests, e.g. (Órdenes, et al., 2021), to determine expected metallurgical response to standard cyanide leaching, i.e. level of refractoriness.

A series of basic descriptive statistics were calculated to summarize the original raw dataset, which consists of data for 16 major elements (Table 4.4.1), 50 minor and trace elements (Table 4.4.2), 15 mineral phases and 7 gold-related variables (Table 4.4.3). Of the total 750 samples, 300 were used for training and validation of the ANN model, meanwhile the remaining 450 samples were set aside as an unseen test set to gauge future performance and generalization.

Table 4.4.1. Summary of descriptive statistics for major elemental compositions in 750 samples.

	Elemental Compositions (wt.%)				
Element	**Min**	**Max**	**Median**	**Mean**	**Std. Dev.**
SiO_2	39.80	87.30	62.70	61.60	8.25
TiO_2	0.02	1.56	0.59	0.61	0.35
Al_2O_3	1.43	27.74	14.85	14.26	4.28
Fe_2O_3	0.02	14.76	4.82	5.30	2.92
MnO	0.01	0.82	0.14	0.19	0.17
MgO	0.21	7.08	2.07	2.29	1.22
CaO	0.02	14.09	3.80	4.31	2.62
Na2O	0.17	6.63	1.51	1.71	0.96
K2O	0.11	4.80	2.63	2.60	0.95
P_2O_5	0.01	0.51	0.11	0.13	0.09
Cr_2O_3	0.00	0.12	0.02	0.03	0.03
BaO	0.01	0.17	0.06	0.06	0.04
SrO	0.01	0.13	0.04	0.04	0.03
LOI	0.05	21.30	6.41	6.99	4.26
Total C	0.02	4.49	1.09	1.36	1.02
Total S	0.10	6.60	1.41	1.55	0.92

Table 4.4.2. Summary of descriptive statistics for minor and trace elemental compositions in 750 samples.

	Elemental Compositions (ppm)						Elemental Compositions (ppm)				
Element	**Min**	**Max**	**Median**	**Mean**	**Std. Dev.**	**Element**	**Min**	**Max**	**Median**	**Mean**	**Std. Dev.**
Ag	0.01	53.33	1.24	4.38	9.00	Nd	0.25	72.15	17.97	19.76	12.18
Ba (%)	0.00	0.17	0.06	0.06	0.04	Ni	11.92	199.69	91.40	94.79	47.04
Bi	0.01	2.63	0.58	0.71	0.61	Pb	0.25	254.12	9.59	15.95	38.33
Cd	0.25	2.90	0.25	0.35	0.42	Pr	0.45	18.89	4.56	5.06	3.14
Ce	0.05	148.40	35.62	39.79	25.55	Rb	1.89	141.50	87.29	81.92	30.97
Co	2	80	22	23	12	Re	0.00	0.01	0.00	0.00	0.00
Cr	18	665	161	178	118	Sb	0.02	101.87	11.13	19.14	21.65
Cs	0.3	28.2	13.9	13.3	6.0	Sc	0.25	43.04	13.26	14.23	8.36
Cu (%)	0.00	0.32	0.01	0.02	0.02	Se	0.0	1.4	0.2	0.3	0.3
Dy	0.13	13.28	2.21	2.47	1.85	Sm	0.15	10.64	3.43	3.61	1.67
Er	0.03	8.12	1.26	1.40	1.13	Sn	0.24	2.56	1.01	1.00	0.37
Eu	0.05	2.32	0.81	0.88	0.45	Sr (%)	0.005	0.062	0.034	0.035	0.011
Fe^{3+} (%)	0.01	15.59	3.64	4.18	3.40	Ta	0.05	1.32	0.36	0.38	0.28
Ga	0.5	33.2	20.4	19.5	5.6	Tb	0.01	1.89	0.43	0.47	0.35
Gd	0.87	8.35	2.80	2.96	1.21	Te	0.01	4.33	0.31	0.66	0.88
Ge	2.50	2.50	2.50	2.50	0.00	Th	0.005	6.070	2.882	2.820	1.354

Hf	0.05	4.69	3.23	3.02	0.96	Tl	0.005	0.137	0.039	0.042	0.028
Hg	0.00	0.34	0.01	0.03	0.05	Tm	0.01	1.44	0.17	0.26	0.29
Ho	0.02	2.82	0.51	0.55	0.43	U	0.01	2.00	0.83	0.80	0.45
In	0.00	0.13	0.02	0.03	0.03	V	2.8	319.5	109.3	117.5	63.3
La	0.20	67.08	18.29	18.84	11.75	W	1.00	48.26	13.55	15.21	9.12
Li	5.1	130.7	43.1	48.5	26.5	Y	1.00	81.01	12.16	13.51	10.74
Lu	0.01	1.13	0.15	0.23	0.26	Yb	0.01	5.29	1.14	1.22	0.81
Mo	0.25	28.12	1.06	2.14	4.24	Zn	1.0	1120.5	70.4	179.2	235.3
Nb	1.01	7.24	4.58	4.45	1.22	Zr	2.9	175.6	122.1	115.2	35.9

Table 4.4.3. Summary of descriptive statistics for mineral phase abundances, determined using the MINSQ least squares fitting method, and an assortment of gold-related variables in 750 samples.

	Mineral Phase Abundances (wt.%)				
Mineral	**Min**	**Max**	**Median**	**Mean**	**Std. Dev.**
Quartz	4.80	80.82	39.43	39.23	11.00
K feldspar	0.00	27.54	5.48	6.74	6.77
Albite	0.00	48.98	0.00	1.97	6.06
Muscovite	0.00	39.43	11.24	12.99	11.62
Paragonite	0.00	48.81	19.32	19.31	8.94
Fe Chlorite	0.00	22.89	1.37	3.36	4.64
Mg Chlorite	0.00	20.43	0.24	2.18	3.43
Calcite	0.00	20.49	1.28	2.98	3.97
Ankerite	0.00	41.48	2.32	4.59	6.47
Dolomite	0.00	30.86	3.33	4.67	5.34
Rutile	0.00	1.54	0.58	0.60	0.35
Pyrite	0.00	11.55	2.21	2.44	1.74
Arsenopyrite	0.00	3.64	0.33	0.79	0.91
Chalcopyrite	0.00	0.93	0.05	0.06	0.06
Sphalerite	0.00	0.49	0.04	0.07	0.07
Variable	**Min**	**Max**	**Median**	**Mean**	**Std. Dev.**
Sulfide_Obs (wt.%)	1	14	5	6	3
Sulfide_Calc (wt.%)	0.1	13.8	3.3	3.4	1.9
Au (ppm)	1.0	43.0	5.6	9.3	10.7
As (ppm)	50	16950	1557	3822	4288
Au:As Ratio	0.00	0.52	0.00	0.03	0.06
Au Grain Size (μm)	0.1	18.7	4.7	5.3	4.9
Au Recovery (%)	31.5	99.8	71.9	72.3	15.7

Artificial Neural Network Modelling

For the first portion of the study, a feed-forward neural network, a.k.a. multilayer perceptron (MLP), was developed for predictive regression modelling. The algorithm was written in Python programming language using the PyTorch machine learning library. The elemental, mineralogical and all but one of the gold-related variables were retained for a total of 87 input features for the predictive model; gold recovery was reserved as the lone target output variable. Data preparation consisted of mean centering and rescaling each variable to unit variance (i.e. standardization); this step is critical to make the data comparable and reduce the effects of artificially inflated feature importance caused by large values and/or ranges. This form of data preprocessing also helps deal with any missing values, and can significantly accelerate model convergence.

As noted above, 300 samples were retained for training and model selection, of which 60 samples (20%) were selected via random shuffling for validation purposes. By convention, target labels (i.e. recovery data) were available for both the training and validation subsets; however, the labels are withheld for the validation samples and simply used for metric calculations following prediction. Conversely, though recoveries were generated in building the test dataset ($n = 450$ samples), these were set aside prior to data import to ensure the model was completely blind to testing labels. This allowed for the subsequent calculation of generalization error metrics to better evaluate how the model might perform on new datasets.

A number of model architectures were trialed, but ultimately a fully connected single hidden layer MLP was selected based on correlation and error performance metrics for each of the training, validation and test sets. As shown in Figure 4.4.1, the hidden layer (72 nodes) was arranged sequentially between the linear input (87 features) and output (1 target) layers, and used the rectified linear unit (ReLU) activation function to incorporate an aspect of non-linearity. Accordingly, model weights were initialized using the He (a.k.a. Kaiming) method with a uniform distribution.

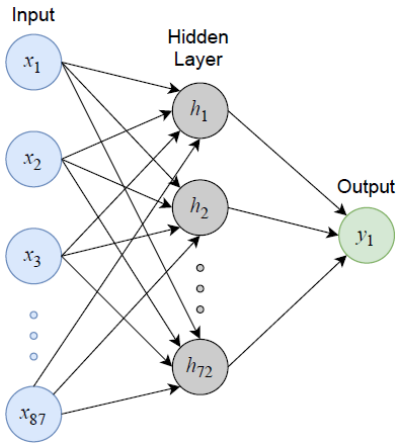

Figure 4.4.1. Schematic representation of the final selected MLP architecture, consisting of one hidden layer (72 nodes) arranged sequentially between the input (87 feature nodes) and output (1 target node) layers.

The loss function used to calculate error and update model weights after each sample batch was based on mean squared error (MSE), which is common for ML regression tasks. Minimization of the loss function was carried out using the Adam optimizer with an initial learning rate of 0.001; this approach is an extension of stochastic gradient descent that uses adaptive learning rates and decay rates. Mini-batches of size 1, 2, 4, 8, 16, and 32 samples were attempted, but it was found the best performance was achieved using single samples. Each training sample 'batch' was randomly selected and loaded into the model via shuffling, which helps reduce overfitting.

While there are many regularization approaches to further prevent overfitting, the current model implements early stopping, whereby the model is automatically stopped when validation loss shows no significant improvement (or begins to increase) over a set number (i.e. 10) of epochs. Dropout with a probability of 0.2 was also used on the hidden layer as an additional regularization control technique.

Discrete Event Simulations

The DES modelling portion of the study was executed using commercial software (Rockwell Arena©) with Visual Basic for Applications (VBA). The model has been verified via event checking and debugging, as well as sensitivity analysis through testing a wide range of values for model inputs and parameters. The use of fixed mass balances to assess potential plant performance is standard practice in the mineral processing sector; this work represents a valid extension beyond

static modelling by incorporating pragmatic fluctuations in mass and composition flows, i.e. dynamic imbalances, that would be expected from multiple mining projects.

Though the current set of calculations is conceptual in nature, similar techniques have been successfully applied to Chilean smelter operations using real operational data, e.g. (Navarra, et al., 2017b), thus validating the general approach. The framework was calibrated using values typical of small to medium-sized underground gold mining and milling operations obtained from publicly available sources to establish realistic and valid data ranges. However, operational data would be available to further validate the model and make necessary modifications to the operational policies in practice. Specifics regarding framework development and related assumptions are further detailed in the context of the present study in Sections 4.4.2 and 4.4.3.

4.4.2 Integrated Mine-to-Mill Framework Strategy

The current framework has been extended to evaluate system performance for a conceptual regionalized mine-to-mill profile in the context of marginal underground gold mining operations. The concept is based on the possible installation of an autoclave (or similar technology) at an existing integrated gold processing facility for the oxidative pretreatment of refractory gold ores. This customization would thereby allow the plant to receive a combination of conventional, i.e. free-milling, and refractory ore feeds from multiple sources in the general area. The framework also considers the notion of installing ore sorting technology at, or near a collection of, satellite orebodies; the intent would be to pre-concentrate classified refractory ores prior to transport to the processing facility. The resultant increase in head grades and waste elimination could render the refractory ore more economical through reduced handling and transportation costs, and increased processing efficiencies, e.g. lower energy and water consumption. The general concept for the study is shown in Figure 4.4.2. For the purposes of this work, pretreatment of the refractory ore is assumed to consist of ore sorting, ultrafine (UF) grinding, and pressure oxidation (POX).

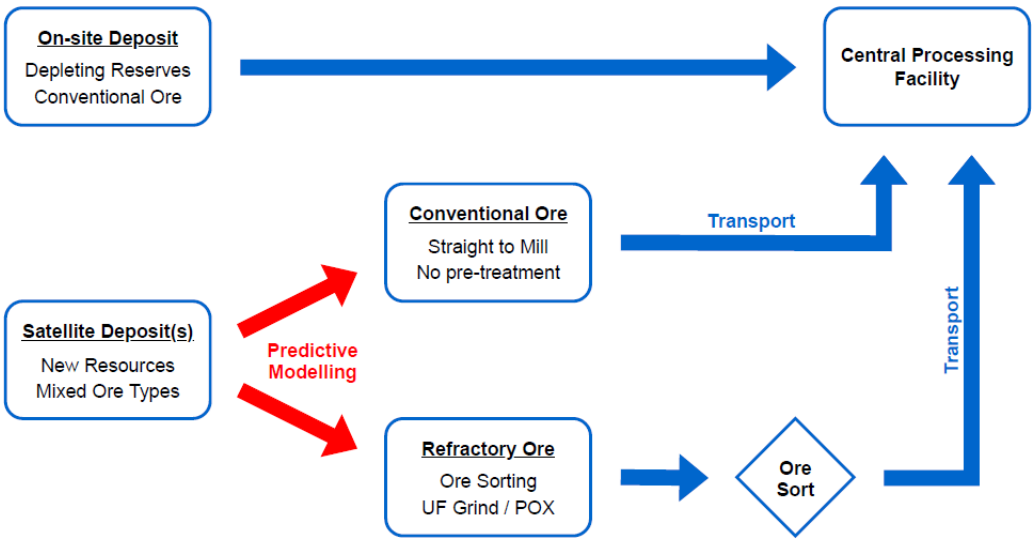

Figure 4.4.2. Schematic flow chart showing the developed regionalized framework strategy for handling conventional and refractory gold ore sources at a central processing facility. Abbreviations: UF = ultrafine, POX = pressure oxidation.

The overall framework is such that geometallurgical attributes are used to develop an MLP model capable of predicting recoveries from geochemical and mineralogical data collected early in the value chain in order to classify extracted ore into two feed types. These predicted proportions are then fed into the DES model to establish effective operational policies and related control strategies using mass balance. To maximize plant throughput and mitigate stockout risk, the tactical decision has been made to implement both stockpiling and blending practices in response to geological uncertainty caused by the varied ore feeds. The general architecture and data flows for the quantitative framework are depicted in Figure 4.4.3. As previously noted, this integrative approach can be used in the development of simulation-based digital twins. Similar to recent work by Wilson et al. (2021b), the proposed framework is currently intended for offline design and/or early implementation purposes, and can thus be termed a 'digital model', a subtype of the digital twin paradigm (Resman, et al., 2021; Singh, et al., 2021). However, it would be possible to integrate the models into a mine control system, whereby the framework could be gradually migrated to an online state.

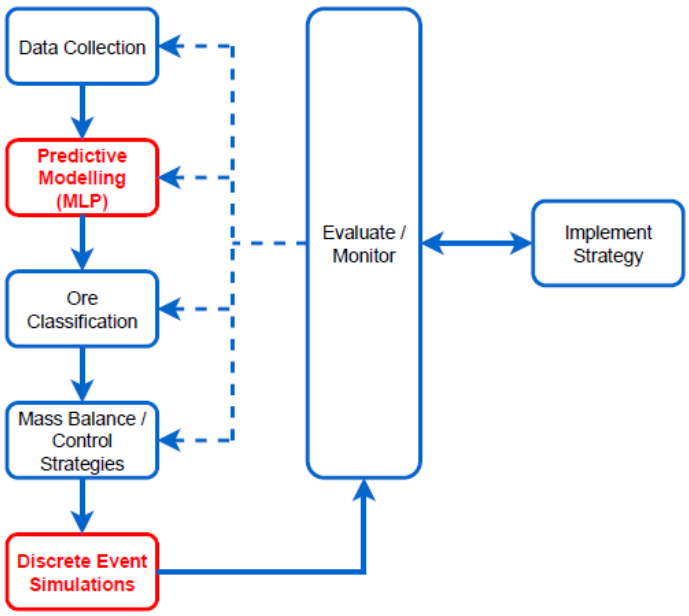

Figure 4.4.3. Flow chart showing the architecture and data flows for the developed quantitative framework (modified after (Wilson, et al., 2021b)).

The current set of calculations focuses on a conceptual integrated gold mill originally designed for the processing of free-milling gold ores via conventional cyanide leaching. The underground mining operation is relatively small, providing on the order of 692.2 kt @ 4.5 g/t Au for 100 koz of gold production per annum. With reserves in decline year over year, the mine is only forecasted to remain in production for another ~5 years. However, recent definition of a sizable satellite orebody (15.55 Mt @ 4.5 g/t Au for 2.25 Moz) has significantly increased the resource base of the current operator. The company is thus considering upgrades to the current plant infrastructure to increase throughput and extend its operating life by bringing the new deposit online.

A potential limiting drawback is the mixed nature of the new resources; gold here occurs as native free grains in quartz-carbonate vein sets, coarse to fine inclusions in disseminated pyrite, and both physically and chemically locked in disseminated fine-grained arsenian pyrite and arsenopyrite. The ore is mainly concentrated within a series of evenly spaced parallel subvertical structures within and adjacent to a broad shear zone spanning a major regional contact zone between mafic volcanic and sedimentary rock units. Detailed mineralogical, gold deportment and metallurgical testwork indicate that ~70% of the ore is refractory, with recoveries ranging from 30 to 99% by standard cyanidation. However, further testing has shown improved recoveries (>97%)

for the refractory ore using a combination of concentrate flotation, ultrafine grinding and pressure oxidation.

Distal to the contact zone, the nature of gold mineralization is clear; whereas ore hosted within the mafic volcanics is generally free-milling, sediment-hosted refractory gold is strongly associated with As-bearing sulfides and related minerals. Unfortunately, the vast majority of the deposit occurs within the sedimentary units to the west of the main lithologic contact. Conventional and refractory ores are thus best delineated using mineral distributions and geochemical signatures that can define irregular domains of arsenic enrichment that are not clear upon visual inspection, i.e. ore type and grade calls are extremely difficult for the mine geologist. It would be both unproductive and unsustainable to perform expensive and time-consuming characterization testwork at the stope face following each round of blasting. Instead, the company has opted to undertake a major ore characterization program using drill core samples for geochemical, mineralogical and corresponding metallurgical response determinations. This data could then be used for predictive modelling of future ore block recoveries using data collected from drill core samples during routine definition drilling programs; this would allow for expedited decision-making earlier in the value chain, thereby improving mine planning.

However, given the high capital costs to upgrade the metallurgical plant, it remains unclear how the processing facility will respond to the varied ore types from multiple sources. Moreover, the operator is considering an ore sorting pre-concentration step for the refractory ore prior to transport, which adds further complexity to the overall mass balance. There are also questions as to how to effectively design operating policies that will stabilize plant throughput against the significant potential for geological variability both within and between mining blocks from the new heterogenous orebody. The overall concept for the calculations is summarized in Figure 4.4.4; average ore compositions expected at the central mill facility include a 40–60% mass pull for refractory type ore resulting from the sorting process (see details in Section 4.4.4). For the sake of clarity, the producing mine and new satellite deposit are herein referred to as Mines I and II, respectively.

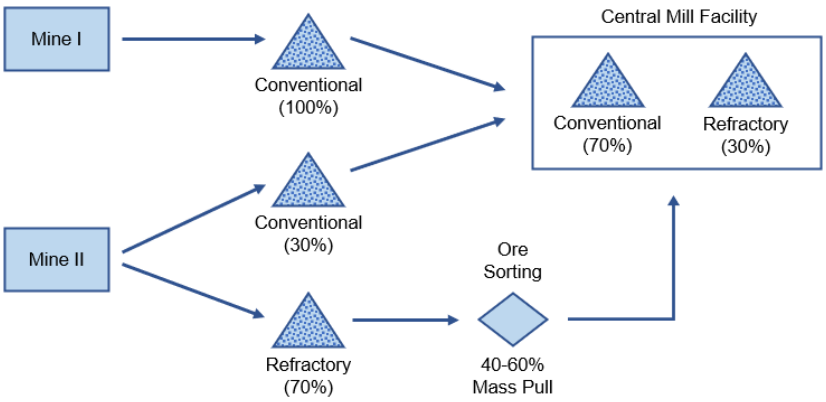

Figure 4.4.4. Diagram illustrating the problem concept for the current set of sample calculations. Mine I refers to the producing mine with which the mill is currently integrated; Mine II refers to the satellite deposit under consideration. Expected ore compositions are only approximate, and do not account for geological uncertainty.

This work implements stockpiling and blending practices using alternate modes of operation that can balance the ore feeds from the two mines in response to geological uncertainty. Ore type proportions for mining blocks from Mine II are based on predictive ML modelling of gold recoveries (using MLP regression), which are then combined with extracted ore from Mine I and fed into the DES portion of the framework to simulate system response. Adjustments can then be made to the available operational policies and related control strategies to maximize throughput and mitigate identified operational risks, e.g. ore stockouts.

4.4.3 Multilayer Perceptron Regression Modelling

With the selected model architecture and hyperparameter tuning (see Section 4.4.1), the model yielded its best performance with a training length on the order of 500 epochs, i.e. iterations through the entire training ($n = 240$ samples) and validation ($n = 60$ samples) sets. Plots of coefficient of determination (R^2 score) and root mean squared error (RMSE) values show diminishing returns or reversals around this point for both training and validation subsets (Figure 4.4.5). Overall, the extremely high R^2 scores (>99%) and low RMSE values (<1.0) indicate that the model has performed very well on the current dataset. Moreover, the agreement between the training and validation metrics suggests that it is not overfitting to statistical noise, and should thus generalize well to new data.

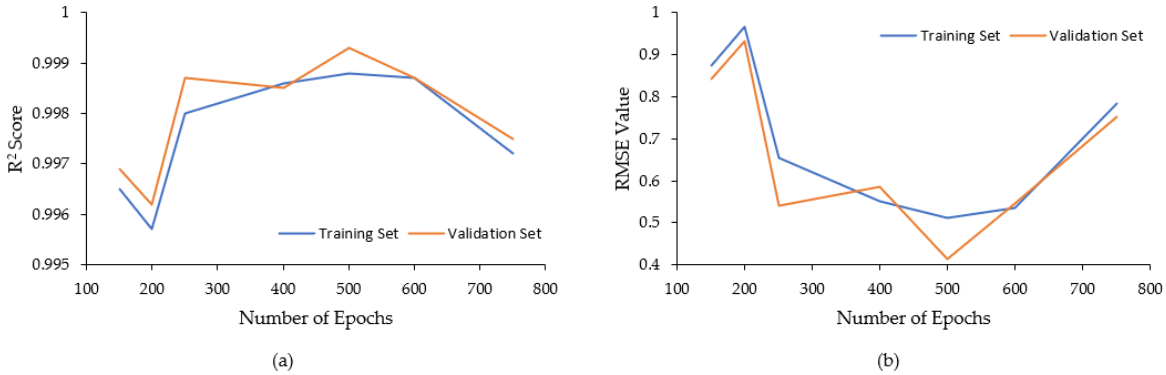

Figure 4.4.5. MLP regression model performance metrics for training and validation subsets, including (a) coefficients of determination (R^2) and (b) root mean squared error (RMSE) values. Note the reversal at 500 epochs for both metrics.

The model also performed quite well on the testing set, with R^2 and RMSE values of 0.82 and 7.07, respectively. This indicates reasonable generalization to unseen datasets derived from similar geological environments and sampling protocols. Predictions from the final model (training length of 500 epochs) are shown with respect to the withheld observed (i.e. labeled) recoveries in Figure 4.4.6, and comparative descriptive statistics are summarized in Table 4.4.4. The predictive power of the model appears best in the mid to upper recovery ranges (~65–95%), which is positive as the most difficult and critical ore type classifications would occur in this span.

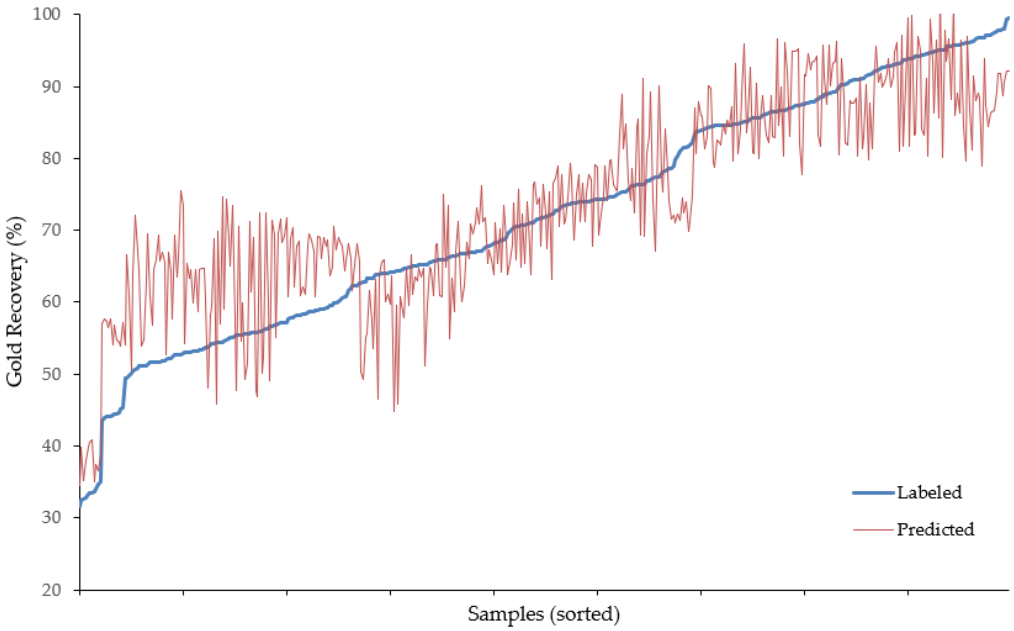

Figure 4.4.6. Plot of predicted vs. labeled recoveries from MLP regression on the unseen test set. Samples are sorted based on the target labels to highlight residual distances; predictive power appears best in the mid to upper recovery ranges (~65–95%).

Table 4.4.4. Comparison of summary statistics for labeled and predicted gold recoveries from MLP regression (500 epochs) on the test set ($n = 450$ samples).

Metric	Labeled Values	Predicted Values
Min (%)	31.54	34.45
Max (%)	99.51	100.00
Median (%)	71.80	72.24
Mean (%)	72.11	73.42
St. Dev. (%)	16.19	13.87

The decreased accuracy and higher error observed for the test set is not surprising, especially considering the relatively small training set size; in practice, a robust predictive model should be built on much larger datasets to improve confidence, particularly with the significant variability inherent to geological-based data. However, this exercise has shown the powerful predictive capability of MLP regression models for structured datasets common to the mining industry. Regardless, the exact nature of the ML model is not what is important here. The key is that the presented model, despite performing rather well on the generated datasets, can be modified or replaced within the flexible DES framework to suit the needs or scope of the specific problem.

It is critical for any sort of predictive modelling tool that appropriate ore characterization is established prior to implementation. This will often require an upfront surplus of sampling and analyses in order to adequately understand the nature of ore feeds; however, with sufficient time and validation of a robust predictive model, sampling frequency can likely be significantly reduced, in addition to more targeted analyses, both of which can result in long-term cost savings. Furthermore, with coupled analytical streams (e.g. geochemistry and mineralogy), additional savings may eventually be seen by employing other tools that could eliminate an analysis type altogether. For instance, with sufficient characterization, normative mineral phase calculations from geochemical data could possibly replace the need for mineralogical studies entirely.

In this study, the outputs of the MLP model, i.e. predicted recoveries, are used to determine relative proportions of conventional and refractory ore within each mining block from the new satellite deposit (Mine II). These proportions then serve as inputs for the DES framework in order to evaluate system-wide response to the varied ore feeds from both mines, under geological uncertainty.

4.4.4 Discrete Event Simulations

Ore type classifications for Mine II were based on the predicted recoveries made on the test set ($n = 450$ samples). Ore with >90% recovery was deemed free-milling, whereas lower recovery rates were considered of the refractory type; these are herein abbreviated as FMO and RTO, respectively. In the context of this study, the test set also corresponds to the first 150 mining blocks (~3 years of production) forecasted for extraction from Mine II, allowing for a minimum of 3 samples per block. In practice, a much greater number of samples would be required for appropriate ore characterization; however, this setup was deemed sufficient for demonstrative purposes. Due to the limited number of samples available for ore characterization, natural background noise, i.e. geological uncertainty, was added to the relative proportions of FMO and RTO via random number generation using a normal distribution with a standard deviation of 3%.

Simplified mid-range mine plans were generated for each of Mines I and II, corresponding to ~3 years of operations. Both mines are expected to produce similar ore tonnages, on the order of 500 kt/y, from similarly sized stopes averaging ~10 kt each. According to these rates, each mine plan comprises 150 mining blocks; tonnages were randomly assigned using a uniform distribution between 5 and 15 kt. For Mine I, all ore was assumed to be free-milling; for Mine II, the relative proportions of FMO and RTO were determined as above. Moreover, the portion of RTO from Mine II was subject to a random mass pull in the range of 40–60% (with an assumed two-fold grade increase) by also applying a uniform distribution.

Additionally, a total of 100 of these mine plans, i.e. statistical scenarios, were created for each of the mines in order to evaluate system-wide effects in response to a range of potential distributions. This approach is critical to proper risk assessment and to improve confidence in the design of robust operational policies and practices under geological uncertainty. Finally, the two sets of mine plans were then combined using weighted averages to reflect the overall ore feed that would be received at the central processing plant, assuming similar production rates at Mines I and II. In this manner, a 70–30 tonnage split of FMO and RTO (recall Figure 4.4.4) is expected as ore feed at the mill on average, bearing in mind that the refractory type ore has already undergone pre-concentration via ore sorting. The proposed mining rates allow for a ~25% reduction in corporate guidance levels for Mine I, thereby extending operating life and providing more time to replace

reserves through planned exploration. With the new production from Mine II, however, the result would be an approximate 50% increase in overall plant output to ~150 koz/y.

To handle the varied ore feeds, the proposed framework implements blending and stockpiling practices to mitigate the effects of unexpected changes in ore characteristics caused by geological uncertainty. These control strategies are described by two distinct operational modes, each governed by its own set of operating policies. Under Mode A, the mill receives 1,245 t/d of ore from Mine I and 755 t/d of ore from Mine II; under Mode B, the mill receives 1,370 t/d of ore from Mine I and 830 t/d of ore from Mine II. As summarized in Table 4.4.5, the overall mass balance is such that Mode A is anticipated to deplete the RTO stockpile by 100 t/d, whereas Mode B is expected to replenish RTO by 220 t/d. Though Mode B achieves a higher overall throughput, Mode A is generally the preferred plant configuration as it produces an additional ~10 koz Au/y based on increased grades associated with a higher proportion of ore-sorted, i.e. pre-concentrated, RTO. However, it is not sustainable to operate in Mode A indefinitely due to the rapid depletion of RTO using its assigned configuration rates. The decision to switch between modes is made at the end of 4-week production campaigns, and is based on a determined threshold. When stockpiled RTO drops below this critical level at the end of a campaign, the planned one-day shutdown provides an opportunity for the necessary retooling of key equipment to apply Mode B, which acts as a replenishment phase.

Table 4.4.5. Summary of the overall mass balance of FMO and RTO expected at the processing plant (expressed in t/d) under the available operational modes, ignoring geological uncertainty.

	FMO (Deposit Grade)				RTO (Upgraded)			
Mode	Mine I	Mine II	Into Mill	Balance	Mine I	Mine II	Into Mill	Balance
A	1245	155	1300	100	0	600	700	-100
B	1370	170	1760	-220	0	660	440	220

Plant configuration rates for each mode, i.e. the absolute and relative proportions of FMO and RTO, are assessed with respect to geological forecasts of the combined ore feed from the two mines using mass balancing. Following the approach of Navarra et al. (2019), a deterministic analysis of the proposed configuration rates indicates that Mode A should be applied 2.2 times as frequently as Mode B, for an average throughput of 2,062.5 t/d. However, this naïve approach ignores the risk of stockout caused by geological uncertainty. The primary aim of the framework

is to simultaneously maximize throughput and minimize target stockpile levels, meanwhile ensuring stable ore feed streams to mitigate stockout risk and avoid the disruption of continuous plant production. It is important to minimize stockpile levels as much as possible to reduce costs associated with excessive material handling and storage.

Similar to the previous case studies, the framework implements two control variables in the decision-making process, including a critical RTO level and the target total stockpile level, computed as the sum of available FMO and RTO. Deterministic calculations indicate minimum threshold values of 2,700 t and 5,940 t for these variables, respectively. The critical ore level is determined as a function of campaign length (27 days) and rate of change under Mode A (-100 t/d); target total stockpile level is determined as the maximum rate of change between available FMO and RTO under either mode (-220 t/d), also as a function of campaign duration. A negative threshold crossing for either of these variables represents a discrete event, which elicits a decision in the framework. Depending on the observed system response during simulations, these control variables can be adjusted by raising the threshold values as a form of operational buffer against geological uncertainty. Each simulation trial begins in Mode A as it is the more productive of the available operational modes; it is assumed that each combined ore feed block is processed to completion prior to loading the next parcel.

Representative graphical outputs from the DES framework are shown in Figure 4.4.7, demonstrating the fluctuations in FMO and RTO feed stockpiles over operating periods of 500 days (Figure 4.4.7a) and 250 days (Figure 4.4.7b). The application of Mode A is indicated when FMO levels are increasing and RTO levels are decreasing; Mode B is reflected by increasing RTO levels and diminishing FMO levels. The alternation of these modes is key to the stable functioning of the processing plant by providing relief to the system before it comes under stress via suitably selected threshold values (e.g. Figure 4.4.7a). When these critical levels are set too low, the system is repeatedly stressed by inadequate ore availability, thus requiring immediate recourse actions which are both less productive and unsustainable. Figure 4.4.7b illustrates a mine surging event caused by total depletion of FMO under Mode A ($t \cong 300$ days), wherein the additional ore is fed directly to the plant, in addition to three contingency mode segments caused by depletion of RTO

also under Mode A (t ≅ 360, 420, 480 days). The jagged nature of the line segments in both plots is indicative of the significant geological uncertainty in combined ore feeds from both mines.

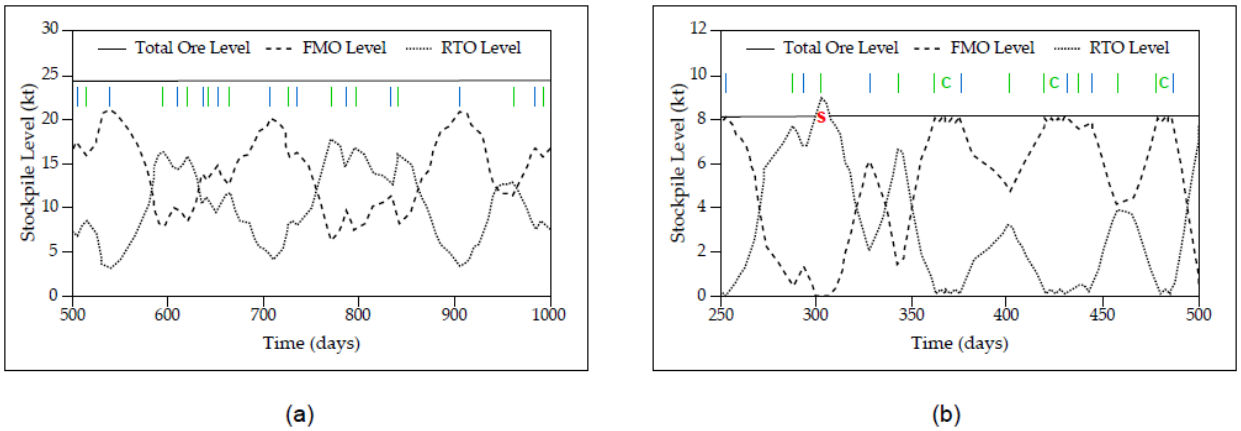

Figure 4.4.7. Representative graphical outputs from the DES framework, showing (a) stable plant operation with alternation between Modes A (green) and B (blue) over 500 operating days (critical RTO level = 8,100 t; target total ore level = 24,300 t), and; (b) system under stress with one mine surging event (red 'S') and three contingency modes (green 'C') triggered by inadequate FMO and RTO levels, respectively, over 250 operating days (critical RTO level = 2,700 t; target total ore level = 8,100 t).

To select appropriate values for the two control variables, a series of simulations were run with varied combinations of RTO and target total ore levels attempted. Data from an initial set of 6 simulations are summarized in Table 4.4.6; for these trials, the critical RTO level was held constant at 2,700 t (deterministic result) and the target total ore level was varied between 5,940 t and 12,150 t. This first pass was carried out on a single replication, i.e. one statistical realization or 'mine plan', in order to find a reasonable ore ratio range for further testing. In terms of throughput, it is clear that simulations 2, 3 and 4, corresponding to FMO:RTO ratios of 1.5, 2 and 2.5 (respectively), performed the best. Despite a decrease in throughput, simulation 5 (3:1 ore ratio) was also retained based on a lower stockout risk. While simulation 6 did not experience any stockouts, it was ignored from further trials as stockpile levels would become unmanageably large as the critical ore level is raised. It is also notable that in general, the proportion of time spent in the more productive Mode A appears to vary directly with the FMO:RTO ratio.

Table 4.4.6. Summary of modal time proportions, throughput rates and number of stockout events for simulations with varied ore type ratios using a constant critical RTO level of 2,700 t (deterministic result).

Sim	# Reps	Crit Ore Level (t)	Total Ore (t)	Ore Ratio	Mode A (%)	Mode A Cont (%)	Mode B (%)	Mode B Cont (%)	Shutdown (%)	Through-put (t/d)	No. of Stockouts
1	1	2700	5940	1.2	57.14	1.99	35.52	1.83	3.51	2046.30	15
2	**1**	**2700**	**6750**	**1.5**	**58.21**	**1.18**	**35.59**	**1.50**	**3.52**	**2055.13**	**13**
3	**1**	**2700**	**8100**	**2**	**62.88**	**1.28**	**32.09**	**0.22**	**3.52**	**2054.61**	**7**
4	**1**	**2700**	**9450**	**2.5**	**64.49**	**1.06**	**30.82**	**0.10**	**3.52**	**2054.49**	**5**
5	**1**	**2700**	**10800**	**3**	**64.08**	**2.15**	**30.23**	**0.04**	**3.51**	**2044.59**	**4**
6	1	2700	12150	3.5	64.27	2.03	30.19	0.00	3.51	2045.74	0

A second round of simulations then focused on raising the critical RTO level by factors of 2, 3 and 4 for each of the retained ore type ratios, i.e. FMO:RTO values of 1.5, 2, 2.5 and 3. These trials were executed using all 100 statistical replications in order to better gauge throughput rates and operational stockout risk over a range of distributions; the resulting data are summarized in Figures 8 and 9. Throughputs for all of the ore ratio configurations appear to stabilize at a minimum critical RTO level of 8,100 t (Figure 4.4.8a), and target total ore levels in the range of 20–30 kt (Figure 4.4.8b). While all of the ratios reached similar throughput rates, notably higher than the deterministic result of 2,062.5 t/d, the two lowest ratios managed these levels with substantially smaller total ore stockpiles (on the order of 5–10 kt).

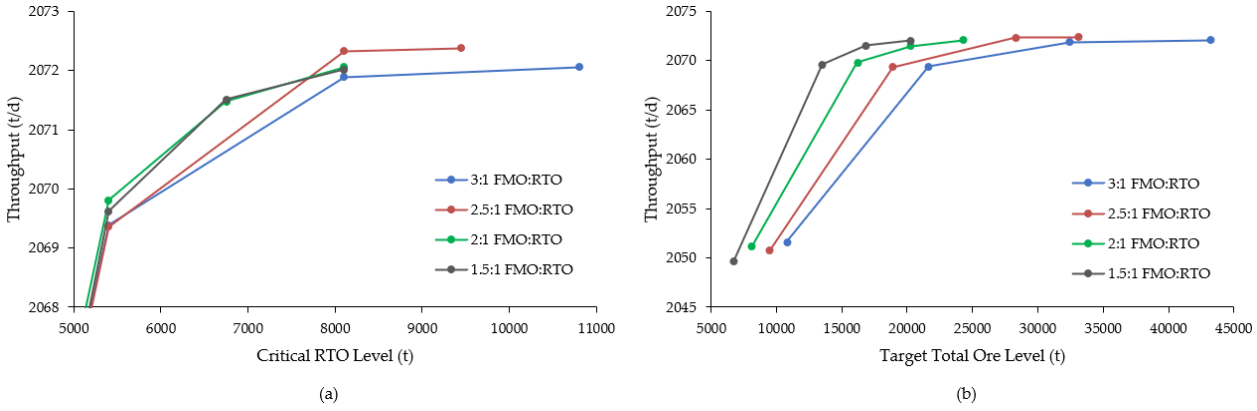

Figure 4.4.8. Plots of throughput rates (t/d) versus (a) critical RTO level, and (b) target total ore level for a variety of simulated ore type ratios over 100 statistical replications.

Considering the total tonnage from all 100 replications (~238.7 Mt) and the simulated average throughput rates, the resulting absolute numbers of operating days and ore stockout events were used to calculate the frequency of stockouts for each ore ratio. From these, monthly stockout probabilities were computed for each scenario, as shown in Figure 4.4.9. These trends show that a

2:1 ratio of FMO and RTO generally reduces operational stockout risk (on a monthly basis) to near zero with the smallest ore feed stockpile levels. As a result, the final selected model for this study implements threshold values of 8,100 t and 24,300 t for the critical RTO and target total ore control variables, respectively.

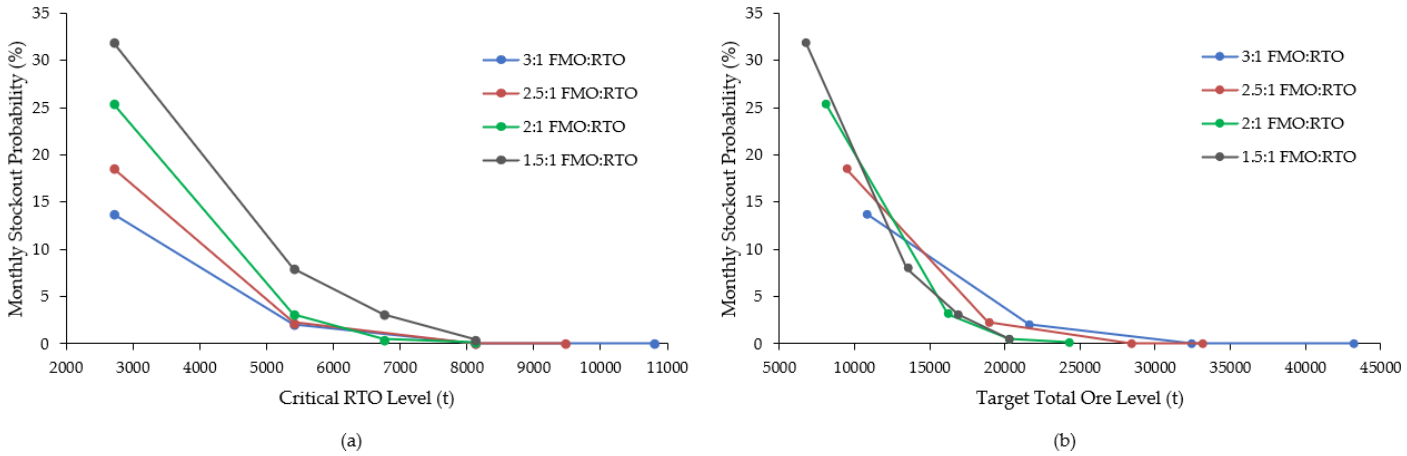

Figure 4.4.9. Plots of monthly stockout probability (%) versus (a) critical RTO level, and (b) target total ore level for a variety of simulated ore type ratios over 100 statistical replications.

A histogram of modal time proportions (Figure 4.4.10) compares the average performance of the final enhanced model vs. a naïve model that uses the deterministic values for both critical RTO (2,700 t) and target total ore (5,940 t) levels over 100 replications. It is evident that the enhanced model processes more ore under the more productive Mode A; moreover, this scenario results in less system stress resulting from ore feed depletions as evidenced by negligible application of contingency segments under either mode.

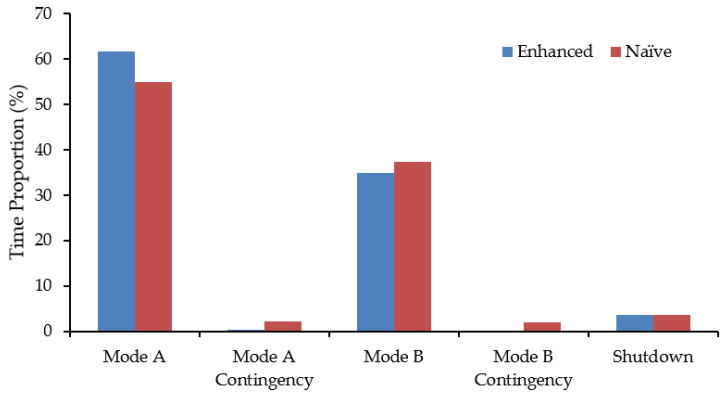

Figure 4.4.10. Histogram showing the relative modal time proportions of the final enhanced model vs. a naïve model that uses the deterministic values for critical RTO (2,700 t) and target total ore (5,940 t) levels over 100 replications.

The stability of the final model allows for the efficient processing of 447.5 koz of gold (averaged over the 100 statistical replications) in ~3.15 years, which is just under the target annual guidance level of 150 koz. By comparison, the naïve scenario would take an additional ~2 weeks to process a similar number of ounces, and would effectively be unsustainable due to chronic ore feed shortages. Armed with the confidence of stable system functioning using alternate modes of operation and the selected operational policies, a company is much better positioned to proceed with detailed project evaluation.

For demonstrative purposes, a high-level economic analysis using pre-tax net present value (NPV) was conducted to assess the value of bringing the new satellite deposit (Mine II) online. Under Option 1, the company simply continues to process the remaining ~500 koz of gold reserves at Mine I at a target annual guidance level of 100 koz; barring a significant resource expansion through underground exploration, the mine is thus projected to shut down in ~5 years. Under Option 2, guidance levels at Mine I are reduced to 75 koz Au/y, and Mine II is put into production at an equal guidance level for a target total of 150 koz Au/y. This would extend mine life at Mine I to just under 7 years, which also provides more opportunity to replace reserves. Once Mine I is fully depleted, guidance levels for Mine II would be increased to at least 150 koz Au/y to make up the difference.

To compare the two options, NPV was calculated as follows:

$$\mathrm{NPV} = \sum_{t=0}^{N} \frac{R_t}{(1+i)^t} \tag{4.4.1}$$

where N is the number of periods, t is the current time period, R_t is the net cash flow (i.e. revenue less costs), and i is the discount rate. Various gold prices from US$ 1,200/oz to US$ 1,900/oz were used as a form of sensitivity study to observe the relative tradeoff. For Option 1, it was assumed that 100 koz Au are produced per annum at an all-in sustaining cost (AISC) of US$ 850/oz. AISC is a non-GAAP (‘generally accepted accounting principles’) measure frequently employed in the gold sector to improve transparency with stakeholders and provide a better comparative valuation scale for companies and/or mining projects. The AISC measure includes all operating costs, general and administrative site and corporate expenses, freight, treatment/refining costs, royalties,

hedging effects, writedowns, sustaining capital (including near-mine exploration) and reclamation costs. The resulting NPV calculations for Option 1 are shown in Table 4.4.7.

Table 4.4.7. Summary of net present value (NPV) calculations for a range of potential gold prices under Option 1, assuming a production rate of 100 koz Au/y and all-in sustaining costs (AISC) of US$ 850/oz.

		Gold Price (US$/oz)							
Year	Metric[1]	$1,200	$1,300	$1,400	$1,500	$1,600	$1,700	$1,800	$1,900
1	PV	$31.818	$40.909	$50.000	$59.091	$68.182	$77.273	$86.364	$95.455
2	PV	$28.926	$37.190	$45.455	$53.719	$61.983	$70.248	$78.512	$86.777
3	PV	$26.296	$33.809	$41.322	$48.835	$56.349	$63.862	$71.375	$78.888
4	PV	$23.905	$30.736	$37.566	$44.396	$51.226	$58.056	$64.886	$71.716
5	PV	$21.732	$27.941	$34.151	$40.360	$46.569	$52.778	$58.988	$65.197
Total	NPV	$132.678	$170.585	$208.493	$246.401	$284.309	$322.217	$360.125	$398.033

[1] Dollar amounts for present value (PV) and NPV are shown in millions.

To evaluate Option 2, it is necessary to determine an approximate life-of-mine (LOM) for Mine II. Advanced deposit definition has identified 15.55 Mt @ 4.5 g/t Au for a total of ~2.25 Moz of contained gold in reserves and indicated resources. The subvertical mineralized zones are expected to be extracted via the longhole stoping mining method. Using Taylor's Rule (Camm & Stebbins, 2020), this corresponds to an estimated mine life of ~12.5 years, assuming recovery and dilution factors of 85% and 15%, respectively. However, this option requires significant capital investment to increase capacity at the central processing plant, and install an autoclave for the oxidative pretreatment of refractory ore. Community, permitting, distal exploration and non-sustaining capital costs are considered as 'profit and loss' (P & L) investments, and are not typically included in AISC disclosures. An initial investment of US$ 235M has thus been included at time $t = 0$ in the NPV calculations for Option 2, as shown in Table 4.4.8. This amount includes US$ 150M for a smaller industrial autoclave, and US$ 85M for the start-up costs at Mine II, in line with the upper range of average costs for an underground operation using longhole stoping with shaft access (Camm & Stebbins, 2020). In this scenario, both mines are operational for the first 7 years and the mill produces 150 koz Au/y at an assumed AISC of US$ 1,050/oz. Following depletion of gold reserves at Mine I, guidance levels at Mine II are increased for the remaining 6 years with the mill continuing to produce 150 koz Au/y at an assumed AISC of US$ 950/oz. Payback periods (in years) were also calculated based on cumulative NPV for each gold price.

Table 4.4.8. Summary of net present value (NPV) calculations for a range of potential gold prices under Option 2, assuming a production rate of 150 koz Au/y, and all-in sustaining costs (AISC) of US$ 1,050/oz for the first 7 years and US$ 950/oz for the final 6 years.

		Gold Price (US$/oz)							
Year	Metric[1]	$1,200	$1,300	$1,400	$1,500	$1,600	$1,700	$1,800	$1,900
0	PV	($235.000)	($235.000)	($235.000)	($235.000)	($235.000)	($235.000)	($235.000)	($235.000)
1	PV	$20.455	$34.091	$47.727	$61.364	$75.000	$88.636	$102.273	$115.909
2	PV	$18.595	$30.992	$43.388	$55.785	$68.182	$80.579	$92.975	$105.372
3	PV	$16.905	$28.174	$39.444	$50.714	$61.983	$73.253	$84.523	$95.793
4	PV	$15.368	$25.613	$35.858	$46.103	$56.349	$66.594	$76.839	$87.084
5	PV	$13.971	$23.285	$32.598	$41.912	$51.226	$60.540	$69.854	$79.167
6	PV	$12.701	$21.168	$29.635	$38.102	$46.569	$55.036	$63.503	$71.970
7	PV	$11.546	$19.243	$26.941	$34.638	$42.336	$50.033	$57.730	$65.428
8	PV	$17.494	$24.492	$31.489	$38.487	$45.484	$52.482	$59.480	$66.477
9	PV	$15.904	$22.265	$28.627	$34.988	$41.350	$47.711	$54.072	$60.434
10	PV	$14.458	$20.241	$26.024	$31.807	$37.590	$43.374	$49.157	$54.940
11	PV	$13.144	$18.401	$23.658	$28.916	$34.173	$39.431	$44.688	$49.945
12	PV	$11.949	$16.728	$21.508	$26.287	$31.067	$35.846	$40.625	$45.405
13	PV	$10.862	$15.207	$19.552	$23.897	$28.242	$32.587	$36.932	$41.277
Total	NPV	($41.650)	$64.900	$171.450	$278.001	$384.551	$491.101	$597.652	$704.202
Payback	(years)	n/a	9	6	4	3	2	2	2

[1] Dollar amounts for present value (PV) and NPV are shown in millions.

Figure 4.4.11 shows the relative tradeoff between Options 1 and 2 over the range of gold prices considered for the current study. The breakeven point for bringing Mine II online appears to occur at a gold price of ~US$ 1,450/oz, with a payback period of ~5 years. The sensitivity to gold price could be further reduced by expanding the resource/reserve base at Mine II, in addition to further increases in mill capacity. This economic assessment is fairly crude in nature and relies on a number of assumptions; in practice, a much more elaborate evaluation would be completed using detailed capital and operating costs, coupled with historic and updated operational data from the plant in question.

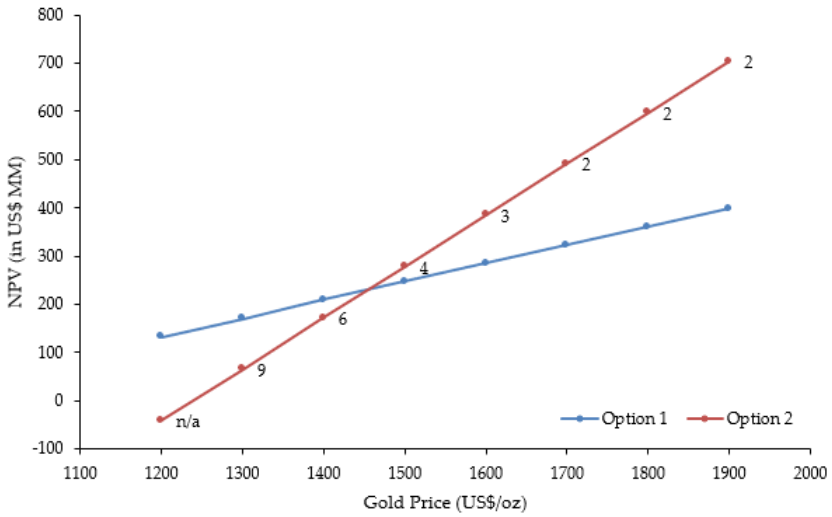

Figure 4.4.11. Plot showing the relative tradeoff between Options 1 and 2 for gold prices ranging from US$ 1,200/oz to US$ 1900/oz. The breakeven point for bringing Mine II online occurs at a price of ~US$ 1,450/oz, with a payback period of ~5 years (data labels).

4.4.5 Conclusions

As previously described, declining trends related to new gold discoveries are driving an emerging imbalance in the replacement of global gold reserves against forecasted production. However, technological advancements are improving not only the economic feasibility, but the overall sustainability of processing more complex and refractory ores to help fill the growing gap in supply and demand chains. Sensor-based sorting is one such method being evaluated or applied in the industry as it allows for the pre-concentration of target minerals based on physicochemical heterogeneities between ore and waste streams. This approach is particularly attractive for remote projects or satellite orebodies as it can significantly cut down on handling and transportation costs, in addition to improving cost and energy efficiencies at the processing plant. Moreover, environmental footprints are also greatly reduced by keeping a higher volume of ultimate waste at the mine site, thereby minimizing unnecessary tailings accumulations.

Refractory ore zones are relatively common in many gold mining districts, especially in deposits hosted along or proximal to major lithological contacts with sedimentary basins. However, often times these zones are cast aside due to the metallurgical implications, and only the free-milling ores are extracted for processing. As more efficient methods to improve the recovery of refractory gold and handle impurities of concern (e.g. arsenic) are developed, there will be increased opportunity to process these zones concurrently with conventional sources. An

interesting case could also be made to consolidate these untapped refractory zones from a collection of deposits within a mature or historic mining camp for processing at a centralized facility. Regardless, a processing plant receiving ores from multiple sources will undoubtedly face significant variations in ore feed attributes which must be considered in the design of operational policies. Computational intelligence tools are thus needed to assess mining system dynamics with respect to proposed new or modified control strategies that could mitigate operational risks presented by significant geological uncertainty.

This work explored a regional-based mine-to-mill strategy for the development of varied gold ore types from multiple sources using an integrated ANN and DES framework. In this approach, predicted outputs from the ANN model are used to classify ore feeds based on metallurgical response to standard cyanidation, which are then fed into the DES model to evaluate the system-wide response to geological uncertainty. The current quantitative framework provides a pathway to evaluate potential mineral processing routes using mass balance and alternate modes of operation. Adjustments can then be made to operating practices and parameters towards the development of effective operational policies. This study implemented stockpiling and blending as control measures to manage ore stockout risk caused by unexpected changes in ore feeds, i.e. geological uncertainty. A further level of complexity was also added by introducing uncertainty to the tonnages resulting from preconcentration of classified refractory ores (via ore sorting) into the mass balance. Results from sample calculations based on a conceptual scenario offer insight into the applicability of such a framework within a gold mining context, and warrant further study of similar strategies. As an example, computations carried out in parallel with and without preconcentration to evaluate system performance with respect to ore stocks and flows (and ultimately the resultant NPV) could make for interesting case studies to support or oppose the installation of an ore sorter at a given mining project. The real key is that the developed tool can improve confidence in stable mining system design, which allows for further detailed project evaluation and strategic decision-making.

Chapter 5

Discussion and Future Work

5.1 Integrated DES Frameworks for Mining System Evaluation

Geological variability and related uncertainty are inherent to all ore deposit types. These heterogeneities can range in intensity, and generally vary both within and between deposits and/or mining districts. This can lead to unexpected changes in ore feed attributes (e.g. grade, mineralogy, grain size distribution), thereby affecting the mining and extractive processes. All of these factors have a direct impact on the interplay of critical variables and integrated coordination of processes within the overall system. Given that ore feeds are exploited from complex and heterogeneous sources, it is clear that mining systems need to be flexible, with the ability to respond to changes and communicate with all related processes (both up and downstream). The availability of alternate operational modes, each with its own set of instructions, is crucial to the sustained development of most orebodies, particularly as a project matures and evolves.

Regardless, significant variability in ore feed attributes is likely to be experienced at any mineral processing plant, particularly those receiving feeds from multiple or complex ore sources; it is thus critical that these variations are considered in the design of effective operational policies. As such, computational intelligence tools are needed to assess mining system dynamics with respect to proposed new or modified control strategies that could mitigate potential operational risks presented by significant geology uncertainty. As previously noted, this research fills a particular gap in the mining literature by focusing on generalizable DES framework development with the flexibility to incorporate different data types and quantitative methods to test novel control strategies in response to geological uncertainty along the mine-to-mill (or smelter) profile.

Moreover, the integration of predictive models calibrated from geometallurgical characterization can further accelerate key decision-making and related planning processes. However, the generation of robust predictive models requires extensive (and expensive) systematic sampling and analytical campaigns to properly characterize ore feeds and related downstream process responses; the degree of sampling is difficult to anticipate in advance, and ultimately depends on the variability of the source orebody. Nonetheless, the ability to integrate reliable

predictions of processability based on geometallurgical attributes into a DES framework earlier in the value chain is of key importance to assess the effects of heterogeneous ore feeds on system-wide performance. Tactical adjustments can then be made well in advance via new or modified operational policies, or the implementation of new control measures, e.g. blending and stockpiling practices, in order to mitigate the identified risk factors.

Mining projects represent complex industrial systems that are host to a variety of treatments and processes. From extraction to mineral separation, concentration, metallurgical processing and tailings storage/disposal, there are a large number of moving parts requiring both management and coordination. The interaction of these parts can be a major source of bottlenecks and cause severe deficiencies, making DES an ideal candidate as a modelling and simulation tool for any mining system. Results from a series of case studies highlight the power of a flexible and generalizable DES framework towards the evaluation of a wide array of mining system contexts across commodity markets, operation scales, integration scopes, mine life cycle timing and data process techniques. Common threads between these problems have motivated this research to generalize concepts underlying the integration of mining and downstream processes, in order to help drive the development of appropriate evaluation tools currently lacking in the industry.

This approach is especially important given current and forecasted global mining trends driven largely by technological advancement, climate change concerns and the clean energy transition. Various government agencies and international organizations continue to update lists of critical minerals year over year based on projected market supply and demand chains. Regardless of the source, commodities at the forefront of these compilations are generally geared towards:

- Electrification (dominated by Cu and Al);
- Battery production and storage (e.g. Li, Co, Ni, Mn, graphite);
- Renewable energy technology (e.g. Cs and other REEs for photovoltaic cells);
- Electronics and medical equipment (e.g. precious metals and REEs), and;
- Cross-cutting minerals applicable to a wide range of technologies (e.g. Cu, Cr, Mo); see World Bank Group (2020) for more details and examples.

Not only are these critical metals sourced from a wide variety of deposit types, but many are

typically extracted from complex ores subject to significant geological uncertainty caused by structural controls as described in Section 2.1. In addition to geological and geometallurgical controls, there are a number of other factors related to company structures and business models, financial health, and corporate asset management strategies that can also give rise to important levels of uncertainty. For example, underground deposits are seldom drilled off to completion prior to ore production due to high capital drilling costs. Infill drilling and detailed zone definition are thus usually completed at staged increments to improve confidence in resources and reserves, as well as ore characterization, as necessary to meet corporate guidance targets. This delays the acquisition of new information about the ore, which can affect production scheduling and downstream control strategies. Moreover, the discovery of new zones can lead to significant changes in the morphology of an orebody, re-prioritization of development, and also presents geotechnical challenges related to the new host rocks, in addition to unforeseen mineralogical and metallurgical considerations. Such timing-related factors are particularly taxing for smaller companies with less access to financial liquidity.

Similarly, other factors such as higher than expected costs, lower revenues, fluctuations in the commodity markets, and even investor relations can be strong drivers for derailing the original optimized mine plan; i.e. decisions can be made on multiple levels to satisfy different types of opportunities and risks in mining systems. This can also mean targeting new or additional commodities, ore types and/or materials in response to increased market demand and prices. For instance, with emerging technologies taking advantage of previously discarded elements, secondary processing streams for by-products are becoming more common across the industry (Keller & Anderson, 2018). The same concepts can also create new opportunities such as tailings retreatment applications (as detailed in Section 4.1), processing of historic mining waste through reclamation efforts (e.g. Hollinger open pit Au mine, Timmins, ON, Canada), and consolidation of untapped resources due to metallurgical complexities (as described in Section 4.4).

The main takeaway here is that information flows and resultant strategic, tactical and/or operational goals can quickly change due to a variety of structural controls. While we certainly cannot change the nature of the commodities in the ground, or control the current geopolitical, economic or socioenvironmental climate, our models and resulting plans must be ready to change

as a function of new incoming data sources. As a result, there is a clear need for computational tools that can be quickly adapted to test new approaches or strategies in mining systems in response to unexpected changes. The key is to ensure framework extensibility, thereby enabling for the subsequent incorporation of increasingly detailed models and submodels as project development, continuous improvement or re-engineering efforts progress with increased confidence under a multi-phase approach.

The approach used in this research provides a pathway for dealing with the types of mining-related issues discussed here. By integrating advanced quantitative methods into a generalized and flexible DES framework that can be tailored to meet specific needs and/or problem sets, uncertainty (geological or otherwise) in mining systems can be managed through testing and development of effective control strategies along the mine-to-plant profile. The methodology is demonstrated as a solution to stabilize and enhance plant performance in response to significant variability in ore feed attributes for an array of deposit types and related mining system problems, including: 1) tailings retreatment applications (Section 4.1); 2) chloride-rich oil sands processing (Section 4.2); 3) regionalized strategies for As-rich copper ores (Section 4.3), and; 4) regional development of refractory gold systems (Section 4.4). The ensuing discussion has embodied how a similar approach could also be applied to a host of other contexts spanning the mining spectrum, especially those stemming from current and forecasted mining trends for critical minerals needed to support technological advancement and a low-carbon future.

Several authors (e.g. Grammatikopoulos & Downing, 2020) have highlighted the pressing need to incorporate critical geometallurgical information garnered from process mineralogy into metallurgical process definition and flowsheet development. The computational tool presented here is an ideal candidate for the integration of such data into a simulation framework in order to test novel approaches or control strategies for the development of suitable operational policies. By simulating extended operating periods, system-wide response to unexpected changes in mass flows can be evaluated, and adjustments can be made where necessary. Not only does this improve confidence at each stage of design and implementation, but it also cuts down on trial and error processes which can translate into important cost and time savings.

However, as with any proposed methodology, there are a few areas within the current framework that deserve certain considerations for future work in order to further improve its flexibility and generalizability. For instance, the framework presently assumes that ore/material is mined to completion from a single parcel at a time. This needs to be extended to handle parallel inputs, possibly each with its own set of operational modes. This has significant value on multiple levels: 1) at the deposit scale, it is feasible that different areas of a mine have entirely different geometallurgical characteristics, each with their own ore classes that need to be balanced, and; 2) the same concept holds true at the regional scale, as in the described cases of a centralized processing facility for copper smelting (Section 4.3), and refractory gold processing (Section 4.4). Similarly, each of these regionalized studies only focused on system performance at a single plant being fed from multiple ore sources; future work could also consider a whole network of mines and processing facilities. An even more elaborate scheme could incorporate geospatial attribute data for predictive 3D modelling of distinct geometallurgical units and subsequent ore block classifications. As indicated by Navarra et al. (2019), such scenarios could especially benefit from a supervisory control framework.

Moreover, this research has touched on the use of such integrated models as a suitable approach to develop dynamic simulation-based digital twins (as described in Sections 4.2 and 4.4). Currently intended for design and implementation purposes, the present framework would technically be considered a digital model as data flows between the 'physical' and virtual realms are made manually in an offline state. However, armed with updated ore characterization and operational data from an active mining project, the model could eventually evolve into a full digital twin (automatic two-way data transfers) by incorporation into a mine control system. This will no doubt become increasingly important with modern trends driving advances in mining automation in this accelerated age of Industry 4.0 and cloud-based internet of things (IoT) systems.

5.2 The Evolution of Sustainable Project Development

The term sustainable development is intended to encompass three main pillars focused on economic, social and environmental aspects that can be used to gauge corporate performance and responsibility. Though the concept first surfaced in the late 1960s to early 1970s, the term was not popularized until the late 1980s to early 1990s, finally gaining broad international recognition at

the 1972 UN Conference on the Human Environment held in Stockholm, Sweden (Sustainable Development Commission, 2011). However, the approach did not take hold in the mining industry until the Mining Association of Canada (MAC) put forth the Towards Sustainable Mining (TSM) initiative, now widely recognized as a sustainability standard to help build capacity within the global mining industry (Canadian Trade Commissioner Service, 2021).

In the early going, many major mining companies began to develop sustainable development corporate policies, but the primary focus long remained on economic factors to drive managerial decision-making. However, there has since been a seismic shift in global socio-environmental and geopolitical awareness, particularly over the past decade. This is evidenced by well-developed health and safety programs (social) that focus on 'zero harm' messaging and initiatives now common at most established mining project sites, in addition to operational teams dedicated to environmental monitoring and planning tasks. Moreover, increased project start-up trends are mostly related to permitting delays as a function of the required environmental testwork and transparent community engagement now legislated by many governing bodies; there are certainly still lapses in less developed areas of the world, but the overall improvement is undeniable.

With declining trends in the rates, sizes and grades of new mineral discoveries, this imbalance is expected to drive significant increases in energy consumption across the mining sector in order to meet future supply targets via processing of more complex and refractory ores. This is especially significant given the current state of climate change and related pressure from community stakeholders and governing bodies to reduce greenhouse gas emissions and transition away from fossil fuels to a clean energy-based economy. The industry has already started to adapt with renewable energy supply serving mine sites globally having grown from just 600 MW in 2015 to 4.9 GW in 2020 (Igogo, et al., 2020; Kirk & Cannon, 2020). Research and development efforts have even begun to focus on the notion of using 100% renewables to support operations via a combination of wind, solar and geothermal energy sources, as well as battery and process storage processes. In addition to the clear environmental benefits of a reduced carbon footprint, this approach may prove paramount to the feasibility of smaller remote projects that commonly face significant scheduling and cost barriers associated with power grid installation and/or fuel delivery limitations (Wilson, et al., 2022b). Collections of remote satellite deposits could even potentially

benefit from highly flexible and scalable plant operations with mobilization capabilities, or other regional-based strategies. Regardless of the approach or business model, it is clear that energy efficiencies will be increasingly pivotal in future decision-making processes for mining systems.

Moreover, with global mining rates accelerating due to new technologies (e.g. automation) and favourable market conditions allowing for large-scale low-grade open pit operations, there will undoubtedly be mounting pressure and scrutiny to improve current best practices in waste management. Tailings generation and related storage systems are accumulating at record pace, which can pose risks to both human health and the environment through dam failures or acid rock drainage (ARD) due to potentially harmful by-products from 'dirtier' sulfide ore sources. Continued research and development of tailings retreatment applications is one approach to help curb these effects. Currently, the two end-member goals are for the recovery of metals that were initially lost (or not targeted) to tailings streams, and incorporation into the production of industrial materials. The case study presented in Section 4.1 focused on the latter direction to highlight the potential of substituting tailings residues for the clay component in cement clinker. By integrating geostatistical modelling into the proposed DES framework, effective control strategies and related operational policies were developed in order to successfully manage the significant uncertainty associated with poorly documented abandoned tailings of mixed/unknown origin.

Another important concern is that of ARD associated with surface waste rock dumps at both active and historic mine sites (Vaziri, et al., 2021). However, with many commodities at record prices, much of this previously mined rock could potentially meet lowered economic cut-off grades. This presents an opportunity for miners to profit from essentially 'free' ore as part of the site remediation process. Furthermore, there is increasing interest in the strategic domaining and segmentation of waste materials for secondary processing, depending on plant and market conditions (Peña-Graf, et al., 2021). Similar to collections of satellite orebodies left unexploited due to the metallurgical implications associated with complex and/or refractory ores (as detailed in Section 4.4), there is also an opportunity for the potential consolidation of abandoned waste dump resources in mature or historic mining camps. Although, regionalized strategies similar to those described in Sections 4.3 and 4.4 will likely be critical to improve overall efficiencies towards the development of sustainable business models. Moreover, technological advancements,

such as sensor-based ore sorting, will also likely be necessary to enhance the economics around such projects, in addition to the benefits of improved material management (e.g. buffering capacity of nearby host-rock successions), reduced transport and smaller environmental footprints. Regardless, the added uncertainty to mass and energy flows with the insertion of any pretreatment process can make it difficult for miners to properly evaluate potential system-wide performance. As such, suitable tools that can simulate the coordination of these inputs and outputs as a function of geological variability are critical to the development of effective operational policies that are aligned with strategic management goals.

Ultimately, standard business models in the mining industry must continue to evolve in order to maintain the social license to operate (SLO) with not only community stakeholders, but also the younger generations of potential investors which place increasingly significant weight on sustainable and responsible growth models. While framed in a different context, all of these factors remain within the realm of mining system dynamics. As such, the basis of this thesis, i.e. the importance of flexible quantitative frameworks for the testing of novel control strategies, still holds. In order to develop more holistic/synergistic mining approaches, computational tools will need to be increasingly generalizable.

A systems approach using integrated DES frameworks will be crucial to model and simulate the interactions of key processes and variables within an ever growing number of potential subsystems, parameters, and KPIs that will need to be closely monitored to measure system-wide performance. As highlighted in this thesis, DES is a powerful tool for the development of effective operational policies and related control measures that can stabilize system performance against significant geological (or other types of) uncertainty, and should thus play a major role in future modelling and simulation efforts within the continually evolving mining landscape.

Chapter 6

Summary and Final Conclusions

6.1 Summary

The key objective of this research was to develop a generalizable methodology to test novel control strategies along the mine-to-plant profile using integrated DES frameworks. The fundamental advantages of this approach are the flexibility of the framework to incorporate varied data types and quantitative methods, as well as the extensibility to include more detailed models and/or submodels as project development progresses. By combining interdisciplinary expertise, the technique is capable of assessing potential operational risk factors by coupling dynamic geometallurgical attributes with target downstream process parameters for the development of effective operating policies and control strategies. As discussed in Chapter 5, this type of systems modelling approach can lead to improved overall efficiency and system stability, and therefore project sustainability. In a broader context, this thesis responds to a particular need for ML-assisted operational decision-making processes in the mining space in order to help drive future innovation. The flexibility of the proposed methodology allows for the framework to be molded around a given problem set, thus avoiding difficult negotiations with a highly specified simulation model.

To highlight the utility of a flexible and generalizable integrated DES framework towards modelling complex mining system dynamics, this research adapts the approach to a series of four case studies that span a variety of contexts across the mineral value chain. Each of these studies has been published separately in peer-reviewed journals; refer to the 'Contribution of Authors' section in the front matter of this thesis for publication details. In Section 4.1, geostatistical variability modelling via the turning bands method is integrated into a DES framework to evaluate tailings retreatment applications; in this work, the notion of using poorly documented tailings residues of mixed origin as a potential substitute for the clay portion in cement clinker production is evaluated. Section 4.2 explores the incorporation of predictive modelling of process variables using partial least squares (PLS) regression to assess system response for the extraction of bitumen from variably chloride-rich oil sands. A regionalized framework strategy for the processing of As-rich porphyry copper sulfide ores using simplified Monte Carlo simulation is developed in the

Chilean context in Section 4.3. Finally, an integrated artificial neural network and discrete event simulation framework for the regional development of refractory gold systems is presented in Section 4.4; this study uses multilayer perceptron (MLP) regression modelling to predict recovery response to standard cyanidation in mixed sulfide-rich gold ores for geometallurgical classification (i.e. domaining) purposes. In each case, suitable control strategies and related operational policies were developed using a combination of stockpiling and blending practices coupled with alternate modes of operation to stabilize and enhance overall plant performance in response to significant levels of uncertainty caused by geological and/or geometallurgical controls.

Following the work of Navarra et al. (2019), the DES framework was extended to accept different data types, include additional ore types, track rejected waste material, and stabilize the return to normal mining conditions (i.e. mining rates) following a required mining surge as a recourse action to ore stockouts. Moreover, the developed methodology has bridged different data processing techniques with the DES framework in a way not previously reported in the literation; as such, the flexible framework acts as a "wrapper" that can integrate any selected quantitative method suitable to the context or problem at hand. This thesis is among the first works to incorporate advanced quantitative methods, such as geostatistical modelling, PLS and MLP regression, into DES along the mine-to-plant profile. This is of high impact to the industry as it allows for the assessment, and importantly the mitigation, of potential operational risk factors caused by significant geological and/or geometallurgical controls through development of effective control strategies and related operational policies. Furthermore, the proposed framework is shown to represent a "digital model", an initial step along the pathway towards development of simulation-based digital twins; these types of advanced computational intelligence tools are becoming increasingly important in the age of Industry 4.0 and related Internet-of-Things systems.

6.2 Final Conclusions

1. Most mining projects are subject to significant spatio-temporal variability and uncertainty, driven by structural controls (e.g. geology, geometallurgy, corporate asset management), which can evolve during the course of exploitation as new characterization data is acquired, or as strategic goals are modified.

2. Declining trends in the rates, sizes and grades of new discoveries across many sectors are creating an imbalance in global supply and demand chains that will necessitate the exploitation and processing of more complex and/or refractory ore sources. This is especially pertinent for minerals critical to technological advancement and the clean energy transition. Particular opportunities are gaining traction, such as the consolidation of untapped/discarded ore sources due to mineralogical and/or metallurgical complexities, especially in mature or historic mining camps.
3. Process efficiencies and reduced environmental footprints are becoming increasingly important not only to the mining industry, but government and community stakeholders at large. New and/or modified approaches to mining could play a major role in meeting global demand as well as improving best practices towards waste management and site remediation, e.g. segmentation of tailings, secondary mining of waste rocks and tailings.
4. In the age of big data, influxes of information are accelerating in mining systems due to instrumentation advances in geology/geophysics, geochemistry, process mineralogy, sensor installations, among others. There is a critical need for advanced computational tools that can help optimize the coordination of inputs and outputs (i.e. mass, energy or information flows) within and between process streams as a function of updated incoming characterization data.
5. The integration of quantitative methods into extensible and adaptable DES frameworks is critical for the design, testing and validation of novel control strategies in the mine-to-plant profile, and allows for a multiphase approach that can support decision-making in the advancement of mining development projects. This generalized approach is particularly suitable for complex mining systems in the re-adjustment stages of the mining life cycle in order to assess and manage potential operational risks.
6. The incorporation of ML-assisted operational decision-making into a DES framework demonstrates a pathway for the development of dynamic simulation-based digital twins, which are quickly gaining interest in the age of Industry 4.0 and related IoT systems.

References

Abaidoo, C. A., Osei Jnr, E. M., Arko-Adjei, A. & Prah, B. E. K., 2019. Monitoring the Extent of Reclamation of Small Scale Mining Areas Using Artificial Neural Networks. *Heliyon,* 5(4), pp. 1–21.

Abdi, H., 2003. Partial least squares (PLS) regression. In: M. Lewis-Beck, A. Bryman & T. Futing, eds. *Encyclopedia for Research Methods for the Social Sciences.* Thousand Oaks (CA): Sage, pp. 792–795.

Abdi, H., 2007. Singular value decomposition (SVD) and generalized singular value decomposition (GSVD). In: N. J. Salkind, ed. *Encyclopedia of Measurement and Statistics.* Thousand Oaks (CA): Sage, pp. 907–912.

Abdi, H., 2010a. The method of least squares. In: N. J. Salkind, D. M. Dougherty & B. Frey, eds. *Encyclopedia of Research Design.* Thousand Oaks (CA): Thousand Oaks, pp. 705–708.

Abdi, H., 2010b. Partial least square regression and projection on latent structure regression (PLS regression). *Computational Statistics,* 2(1), pp. 97–106.

Abdi, H. & Williams, L. J., 2013. Partial least squares methods: Partial least squares correlation and partial least squares regression. In: B. Reisfeld & A. Mayeno, eds. *Methods in Molecular Biology: Computational Toxicology.* New York (NY): Springer Verlag, pp. 549–579.

Abuntori, C. A., Al-Hassan, S. & Mireku-Gyimah, D., 2021. Assessment of Ore Grade Estimation Methods for Structurally Controlled Vein Deposits – A Review. *Ghana Mining Journal,* 21(1), pp. 31–44.

Abzalov, M., 2016. Chapter 17 – Introduction to Geostatistics. In: Y. Dilek, F. Pirajno & B. Windley, eds. *Applied Mining Geology, Volume 12.* Springer Nature, pp. 233–237.

Adams, M. D., 2016. Overview of the Gold Mining Industry and Major Gold Deposits. In: *Gold Ore Processing – Project Development and Operations.* Cambridge (MA): Elsevier B.V., pp. 25–30.

AER, 2015. *Alberta's Energy Reserves 2014 and Supply/Demand Outlook 2015–2024, Statistical Series ST98–2015,* Calgary (AB): Alberta Energy Regulator (AER).

AER, 2016. *Operating criteria: Resource recovery requirements for oil sands mine and processing plant operations (AER Directive 082),* Calgary (AB): Alberta Energy Regulator (AER).

Afidenyo, J. K., 2008. *Microbial Pretreatment of Double Refractory Gold Ores.* Kingston (ON): M.A.Sc. Thesis – Queen's University.

Aitcin, P., 2016. Portland cement. In: P. Aitcin & R. Flatt, eds. *Science and Technology of Concrete Admixtures.* Philadelphia (PA): Woodhead Publishing, pp. 27–51.

Al-Bakri, A. Y. & Sazid, M., 2021. Application of Artificial Neural Network (ANN) for Prediction and Optimization of Blast-Induced Impacts. *Mining,* 1(3), pp. 315–334.

Algeer, R., Snowdon, L., Huang, H., Oldenburg, T. & Larter, S., 2016. Is water washing an important petroleum system process? *Proceedings of the AAPG Annual Convention and Exhibition.* Calgary, Canada, June 19–22, American Association of Petroleum Geologists (AAPG).

Ali, D. & Frimpong, S., 2020. Artificial intelligence, machine learning and process automation: existing knowledge frontier and way forward for mining sector. *Artif. Intell. Rev.,* Volume 53, pp. 6025–6042.

Allen, A. E., 2005. Influence of nitrate availability on the distribution and abundance of heterotropic bacterial nitrate assimilation genes in the Barents Sea suring summer. *Aquat. Microbio. Ecol.,* 39(1), pp. 247–255.

Almeida, P. & Carrasquilla, A., 2017. Integrating Geological Attributes with a Multiple Linear Regression of Geophysical Well Logs to Estimate the Permeability of Carbonate Reservoirs in Campos Basin, Southeaster Brazil. *AAPG Search and Discovery,* 10930(2017), pp. 1–47.

Alpagut, M. A. & Çelebi, N., 2003. System dynamics applications in the mining industry. In: G. Ozbayoglu, ed. *Proceedings of the 18th International Mining Congress and Exhibition of Turkey (IMCET).* Antalya (TU): Chamber of Mining Engineers of Turkey, p. 6.

Alpaydin, E., 2014. *Introduction to Machine Learning – 3rd Edition.* Cambridge (MA): The Massachusetts Institute of Technology Press.

Alruiz, O., Morrell, S., Suazo, C. & Naranjo, A., 2009. A novel approach to the geometallurgical modelling of the Collahuasi grinding circuit. *Minerals Engineering,* 22(12), pp. 1060–1067.

Altiok, T. & Melamed, B., 2007. *Simulation Modeling and Analysis with Arena.* Boston (MA): Academic Press.

Alvear, G. R. F., Nikolic, S. & J, M. P., 2014. ISASMELT for the recycling of E-scrap and copper in the U.S. case study example of a new compact recycling plant. *JOM,* 66(5), pp. 823–832.

Amato, F., Havel, J. & Gad, A.-A., 2015. Remotely Sensed Soil Data Analysis Using Artificial Neural Networks: A Case Study of El–Fayoum Depression, Egypt. *ISPRS Int. J. Geo-Inf.,* 4(2), pp. 677–696.

Asamoah, R. K., 2021. Specific Refractory Gold Flotation and Bio-Oxidation Products: Research Overview. *Minerals,* 11(93), pp. 1–14.

Ataee, O., Moghaddas, N. H., Lashkaripour, G. R. & Nooghabi, M. J., 2018. Predicting shear wave velocity of soil using multiple linear regression analysis and artificial neural networks. *Scientia Iranica A,* 25(4), pp. 1943–1955.

Atreya, H. N. & Sridhar, S., 2019. *Using Discrete Event Simulation as a Step Towards Creating a Digital Twin.* Gothenburg (SE): Department of Industrial and Materials Science, Chalmers University of Technology.

Awuah-Offei, K., Osei, B. A. & Askari-Nasab, H., 2012. Improving truck-shovel energy efficiency through discrete event modeling. In: *Proceedings of the 2012 SME Annual Meeting and Exhibit.* Seattle (WA): Society for Mining, Metallurgy & Exploration Inc. (SME), pp. 1–6.

Azizi, A., Shafaei, S., Rooki, R., Hasanzadeh, A. & Paymard, M., 2012. Estimating of gold recovery by using back propagation neural network and multiple linear regression methods in cyanide leaching process. *Materials Science: An Indian Journal,* 8(11), pp. 443–453.

Baek, J. & Choi, Y., 2019. Deep Neural Network for Ore Production and Crusher Utilization Prediction of Truck Haulage System in Underground Mine. *Applied Sciences,* 9(4180), pp. 1–21.

Baker, M. S., Buteyn, S. D., Freeman, P. A., Trippi, M. H. & Trimmer, L. M. III, 2017. *Compilation of geospatial data for the mineral industries and related infrastructure of Latin America and the Caribbean: U.S. Geological Survey Open-File Report 2017–1079 [Data set],* Reston (VA): U.S. Geological Survey.

Bakker, M., Alvear, G. & Kreuh, M., 2009. *ISASMELT TSL – Making a splash for nickel.* Sudbury (ON), Canadian Institute of Mining, Metallurgy and Petroleum, pp. 181–193.

Bao, Z., 2001. *Geochemistry of the Sediment-hosted Disseminated Gold Deposits in Southwestern Guizhou Province, China (Ph.D. Thesis),* Chicoutimi (QC): Université du Québec à Chicoutimi.

Baron, J. Y., Choi, Y. & Jeffrey, M., 2016. Double-Refractory Carbonaceous Sulfidic Gold Ores. In: *Gold Ore Processing – Project Development and Operations.* Cambridge (MA): Elsevier B.V., pp. 909–918.

Barson, D., Bachu, S. & Esslinger, P., 2001. Flow systems in the Mannville Group in the east-central Athabasca area and implications for steam-assisted gravity drainage (SAGD) operations for in situ bitumen production. *Bulletin of Canadian Petroleum Geology,* 49(3), pp. 376–392.

Bata, T., Schamel, S., Fustic, M. & Ibatulin, R., 2019. *AAPG Energy Minerals Division Bitumen and Heavy Oil Committee Annual Commodity Report – May 2019,* Tulsa (OK): American Association of Petroleum Geologists (AAPG).

Bateman, R., Ayer, J. A. & Dubé, B., 2008. The Timmins-Porcupine Gold Camp, Ontario: Anatomy of an Archean Greenstone Belt and Ontogeny of Gold Mineralization. *Economic Geology,* Volume 103, pp. 1285–1308.

Bengio, Y. & Glorot, X., 2010. *Understanding the difficulty of training deep feed forward neural networks.* Sardinia (IT).

Binney, W. P., 1987. Paper 86–24: A sedimentological investigation of the Maclean channel transported sulfide ores. In: R. V. Kirkham, ed. *Buchans Geology, Newfoundland.* Ottawa (ON): Geological Survey of Canada, pp. 107–147.

Boschert, S. & Rosen, R., 2016. Digital Twin – The Simulation Aspect. In: P. Hehenberger & D. Bradley, eds. *Mechatronic Futures.* Cham (CH): Springer International Publishing, pp. 59–74.

Both, C. & Dimitrakopoulos, R., 2021. Integrating Geometallurgical Ball Mill Throughput Predictions into Short-Term Stochastic Production Scheduling in Mining Complexes. *International Journal of Mining Science and Technology,* pp. 1–37.

Brook Hunt, 2010. *Global Copper Concentrate & Blister/Anode Markets to 2022 (2010 Edition).* Addlestone (UK): Wood Mackenzie Ltd.

Bubnicki, Z., 2005. *Modern Control Theory*. Berlin (DE): Springer-Verlag (Springer Science + Business Media).

Bulmer, J. T. & Starr, J., 1974. *Syncrude Analytical Procedures for Oilsands and Bitumen Processing.* Edmonton (AB): Alberta Oil Sands Technology and Research Authority.

Burrows, A., Partington, P., Sakala, J. & Mascrenhas, P. H., 2012. ISASMELT at Mufulira – Increased flexibility on the Zambian Copperbelt. In: *Proceedings of the Fray International Symposium – Metals and Materials Processing in a Clean Environment, Volume 1: Sustainable Non-Ferrous Smelting in the 21st Century.* Cancun (MX), pp. 217–226.

Caballero, C. D., Etcheverry, J. C., Ortiz, J. B., Saavedra, O. M., Rosales-Vera, M., Jaques, D. S. & León, M. G., 2016. *Improvements to the Operation and Design of the Fluidized Bed Roaster – Ministro Hales Division.* Kobe (JP), pp. 921–932.

Camm, T. W. & Stebbins, S. A., 2020. *Simplified cost models for underground mine evaluation: A handbook for quick prefeasibility cost estimates.* Butte (MT): Mining Engineering Department – Montana Technological University.

Canadian Trade Commissioner Service, 2021. Canada sets a world standard for sustainable mining. *CanadExport*, 12 April 2021.

Candente Copper Corp., 2019. *Leverage with large resource and exploration upside [PowerPoint presentation].* [Online]
Available at: https://candentecopper.com/site/assets/files/5575/2019-02-dntcp.pdf

Carvalho, F. P., 2017. Mining industry and sustainable development: Time for change. *Food and Energy Security,* 6(2), pp. 2048–3694.

Carvalho, T. P., Soares, F., Vita, R., Francisco, R., Basto, J. P. & Alcalá, S., 2019. A systematic literature review of machine learning methods applied to predictive maintenance. *Computers & Industrial Engineering,* 137(106024), pp. 1–10.

CER, 2020. *Canada's Energy Future 2020: Energy Supply and Demand Projections to 2050 (EF2020),* Ottawa (ON): Canada Energy Regulator.

Chaudhary, S., Yadav, S., Kushwaha, S. & Shahi, S. R. P., 2020. A Brief Review of Machine Learning and its Applications. *SAMRIDDHI: A Journal of Physical Sciences, Engineering and Technology,* 12(SUP 1), pp. 218–223.

Chen, C., Zhang, L. & Jahanshahi, S., 2010. Thermodynamic modeling of arsenic in copper smelting processes. *Metallurgical and Materials Transactions B,* 41(6), pp. 1175–1185.

Chenini, I. & Khemiri, S., 2009. Evaluation of ground water quality using multiple linear regression and structural equation modeling. *Int. J. Environ. Sci. Tech.,* 6(3), pp. 509–519.

Chilès, J. P. & Delfiner, P., 2012. *Geostatistics: modeling spatial uncertainty, 2nd Edition.* New York (NY): Wiley.

Chilès, J. P. & Lantuéjoul, C., 2005. Prediction by conditional simulation: models and algorithms. In: M. Bilodeau, F. Meyer & M. Schmitt, eds. *Space, Structure and Randomness.* New York (NY): Springer, pp. 39–68.

Christiansen, W. N., Hofstra, A. H., Zohar, P. B. & Tousignant, G., 2011. *Geochemical and stable isotopic data on barren and mineralized drill core in the Devonian Popovich Formation, Screamer sector of the Betze-Post gold deposit, northern Carlin trend, Nevada: U.S. Geological Survey Open-File Report 2010–1077,* Reston (VA): U.S. Geological Survey.

Cisternas, L. A., Lucay, F. A. & Botero, Y. L., 2019. Trends in Modeling, Design, and Optimization of Multiphase Systems in Minerals Processing. *Minerals,* 10(22), p. 1–28.

COCHILCO, 2017. *Sulfuros primarios: desafios y oportunidades (Registro Propiedad Intelectual No. 2833439; Ministerio de Mineria – Gobierno de Chile).* [Online] Available at: https://www.cochilco.cl/Listado Temtico/sulfuros primarios_desafios y oportunidades.pdf

Couillard, M. & Mercier, P. H. J., 2016. Analytical electron microscopy of carbon-rich mineral aggregates in solvent-diluted bitumen products from mined Alberta oil sands. *Energy & Fuels,* 30(7), pp. 5513–5524.

Coursol, P., Mackey, P. J. & Diaz, C., 2010. Energy Consumption in Copper Sulphide Smelting. In: *Proceedings of the Copper 2010 Conference (Hamburg).* Clausthal-Zellerfeld (DE): GDMB, pp. 649–668.

d'Andréa-Novel, B. & De Lara, M., 2013. *Control Theory for Engineers – A Primer*. Berlin (DE): Springer-Verlag (Springer Science+Business Media).

Darling, P., 2011. Chapter 1.1 – Mining: Ancient, Modern, and Beyond. In: P. Darling, ed. *SME Mining Engineering Handbook (3rd Edition).* Englewood (CO):Society for Mining, Metallurgy, and Exploration, Inc. (SME), pp. 3–9.

Datta, L., 2020. A Survey on Activation Functions and their relation with Xavier and He Normal Initialization. *arXiv: 2001.06632,* pp. 1–17.

Defreyne, J., Brace, T., Miller, C., Omena, A., Matos M. & Cobral, T., 2008. Commissioning UHC: A Vale copper refinery based on CESL technology. In: C. A. Young, P. R. Taylor, C. G. Corby & Y. Choi, eds. *Hydrometallurgy 2008: Proceedings of the 6th International Symposium.* Littleton (CO): Society for Mining, Metallurgy, and Exploration (SME), pp. 357–366.

Deniz, V., 2020. Application of multiple linear regression (MLR) analysis for concentration of chromite tailings by the flotation. *Physicochem. Probl. Miner. Process.,* 56(4), pp. 579–589.

Deutsch, C. V. & Journel, A. G., 1992. *GSLIB: Geostatistical software library and user's guide,* New York (NY): Oxfored University Press.

Deutsch, C. V. & Journel, A. G., 1998. *GSLIB: Geostatistical Software Library and User's Guide,* New York (NY): Oxfored University Press.

Dreisinger, D., 2006. Copper leaching from primary sulfides: Options for biological and chemical extraction of copper. *Hydrometallurgy,* Volume 83, pp. 10–20.

Dubé, B., Mercier-Langevin, P., Ayer, J., Atkinson, B. & Monecke, T., 2017. Chapter 2: Orogenic Greenstone-Hosted Quartz-Carbonate Gold Deposits of the Timmins-Porcupine Camp. In: T. Monecke, P. Mercier-Langevin & B. Dubé, eds. *Reviews in Economic Geology, Volume 19 – Archean Base and Precious Metal Deposits, Southern Abitibi Greenstone Belt, Canada.* Littleton (CO): Society of Economic Geologists (SEG).

Duchi, J., Hazan, E. & Singer, Y., 2011. Adaptive subgradient methods for online learning and stochastic optimization. *The Journal of Machine Learning Research,* Volume 12, pp. 2121–2159.

Dumakor-Dupey, N. K. & Arya, S., 2021. Machine Learning – A Review of Applications in Mineral Resource Estimation. *Energies,* 14(4079), pp. 1–29.

Du, Q., Yasin, Q. & Ismail, A., 2018. *A comparative analysis of artificial neural network and rock physics for the estimation of shear wave velocity in a highly heterogeneous reservoir.* Anaheim (CA).

Edwards, J. S. & Alvear, G. R. F., 2007. Converting using ISASMELT technology. In: A. E. M. Warner, C. J. Newman, A. Vahed, D. B. George, P. J. Mackey & A. Warczok, eds. *Proceedings of the Copper 2007 Conference: The Carlos Diaz Symposium on Pyrometallurgy – Volume III (Book 2).* Montreal (QC): Canadian Institute of Mining, Metallurgy and Petroleum, pp. 17–28.

Egaña, M. & Ortiz, J. M., 2013. Assessment of RMR and its uncertainty by using geostatistical simulation in a mining project. *Journal of GeoEngineering,* 8(3), pp. 83–90.

Egarievwe, S. U., Coble, J. B. & Miller, L. F., 2016. Analysis of how well regression models predict radiation dose from the Fukushima Daiichi Nuclear Accident. *Int. J. Appl. Phys. Math.,* 6(4), pp. 150–164.

Egbe, J. G., Ewa, D. E., Ubi, S. E., Ikwa, G. B. & Tumenayo, O. O., 2017. Application of multilinear regression analysis in modeling of soil properties for geotechnical civil engineering works in Calabar South. *Nigerian Journal of Technology,* 36(4), pp. 1059–1065.

Ekblad, A., 2005. Forest soil respiration rate and delta C-13 is regulated by recent above ground weather conditions. *Oecologia,* 143(1), pp. 136–142.

Emery, X., 2008. A turning bands program for conditional co-simulation of cross-correlated Gaussian random fields. *Computers & Geosciences,* 34(1), pp. 1850–1862.

Emery, X., Arroyo, D. & Porcu, E., 2016. An improved spectral turning-bands algorithm for simulating stationary vector Gaussian random fields. *Stochastic Environmental Research and Risk Assessment,* 30(1), pp. 1863–1873.

Emery, X. & Lantuéjoul, C., 2006. TBSIM: A computer program for conditional simulation of three–dimensional Gaussian random fields via the turning bands method. *Computers & Geosciences,* 32(1), pp. 1615–1628.

Emery, X. & Peláez, M., 2011. Assessing the accuracy of sequential Gaussian simulation and cosimulation. *Computers & Geosciences,* Volume 15, pp. 673–689.

Emmert-Streib, F., Yang, Z., Feng, H., Tripathi, S. & Dehmer, M., 2020. Introductory Review of Deep Learning for Prediction Models with Big Data. *Front. Artif. Intell.,* 3(4), pp. 1–23.

Enayatollahi, I., Bazzazi, A. & Asadi, A., 2013. Comparison Between Neural Networks and Multiple Regression Analysis to Predict Rock Fragmentation in Open-Pit Mines. *Rock Mechanics and Rock Engineering,* pp. 1–9.

ERCB, 2009. *Alberta's energy reserves 2008 and supply/demand outlook 2009–2018,* Calgary (AB): Energy Resources Conservation Board (ERCB).

Eskandari, H., Rezaee, M. R. & Mohammadnia, M., 2004. Application of Multiple Regression and Artificial Neural Network Techniques to Predict Shear Wave Velocity from Wireline Log Data for a Carbonate Reservoir, South-West Iran. *Recorder,* 29(7).

Esri, Garmin, GEBCO, NOAA, National Geographic, DeLorme, HERE, Geonames.org, GIS User Community, 2021. *World Ocean Base [basemap].* [Online]
Available at: https://www.arcgis.com/home/item.html?id=67ab7f7c535c4687b6518e6d2343e8a2
[Accessed 19 March 2021].

Evans, L. C., 2010. *An Introduction to Mathematical Optimal Control Theory*. Berkeley (CA): University of California.

Fahle, S., Prinz, C. & Kuhlenkötter, B., 2020. Systematic review on machine learning (ML) methods for manufacturing processes – Identifying artificial intelligence (AI) methods for field application. *Procedia CIRP,* Volume 93, pp. 413–418.

Feizi, F., Karbalaei-Ramezanali, A. A. & Farhadi, S., 2021. Application of multivariate regression on magnetic data to determine further drilling site for iron exploration. *Open Geosciences,* Volume 13, pp. 138–147.

Filippou, D. & Demopoulos, G. P., 1997. Arsenic immobilization by controlled scorodite precipitation. *JOM,* Volume 49, pp. 52–55.

Flores, G. A., Risopatron, C. & Pease, J., 2020. Processing of complex materials in the copper industry: Challenges and opportunities ahead. *JOM,* Volume 49, pp. 3447–3461.

Forti, V., Baldé, C. P. & Bel, G., 2020. *The Global E-waste Monitor 2020: Quantities, flows and the circular economy potential,* Bonn/Geneva/Rotterdam: United Nations University (UNU)/United Nations Institute for Training and Research (UNITAR)/International Telecommunication Union (ITU) & International Solid Waste Association (ISWA).

Fowler, M. & Riediger, C., 2000. Origin of the Athabasca tar sands. In: D. Barson, R. Bartlett, F. Hein, M. Fowler, S. Grasby, C. Riediger & J. Underschultz, eds. *Hydrogeology of heavy oil and tar sand deposits: Water flow and supply, migration and degradation – Field Trip Notes (GSC Open File 3946).* Calgary: Geological Survey of Canada, pp. 117–127.

Franklin, J. M., Gibson, H. L., Jonasson, I. R. & Galley, A. G., 2005. Volcanogenic Massive Sulfide Deposits. In: J. W. Hedenquist, J. F. H. Thompson, R. J. Goldfarb & J. P. Richards, eds. *Economic Geology 100th Anniversary Volume.* Littleton (CO): Society of Economic Geologists, Inc., pp. 523–560.

Freyssinet, P. H., Butt, C. R. M., Morris, R. C. & Piantone, P., 2005. Ore-Forming Processes Related to Lateritic Weathering. In: J. W. Hedenquist, J. F. H. Thompson, R. J. Goldfarb & J. P. Richards, eds. *Economic Geology 100th Anniversary Volume.* Littleton (CO): Society of Economic Geologists, Inc., pp. 681–722.

Fustic, M., Ahmed, K., Brough, S., Bennett, B., Bloom, L., Asgar-Deen, M., Jokanola, O., Spencer, R. & Larter, L., 2015. Reservoir and bitumen heterogeneity in Athabasca oil sands. *AAPG Search and Discovery, Article #20296, 15p.*

Gbadam, E., Awuah-Offei, K. & Frimpong, S., 2015. Investigation into Mine Equipment Subsystem Availability & Reliability Data Modeling Using DES. In: S. Bandopadhyay, ed. *Application of computers and operations research in the mineral industry.* Englewood (CO): Society for Mining, Metallurgy & Exploration, Inc.

Gentle, J. E., 2003. *Random Number Generation and Monte Carlo Methods, 2nd Edition.* New York (NY): Springer Science + Business Media, Inc.

Glaessgen, E. H. & Stargel, D. S., 2012. *Proceedings of the 53rd Structures, Structural Dynamics, and Materials Conference: Special Session on the Digital Twin – The digital twin paradigm for future NASA and U.S. Air Force Vehicles.* Honolulu (HI), American Institute of Aeronautics and Astronautics (AIAA).

Glencore Technology, 2018. *First chalcopyrite copper concentrate leaching using Albion Process technology [PowerPoint presentation].* [Online]
Available at:
https://www.albionprocess.com/en/downloads/LatestNews/Hydroprocess%20Glencore%20Technology%202018%20-%20Preso.pdf

Glencore Technology, 2021. *Copper/Nickel smelter installations [Fact sheet].* [Online]
Available at: https://www.isasmelt.com/en/installations/Documents/isasmelt-Installations.pdf

Glencore, 2015. *ISASMELT High Productivity Clean Smelting [Brochure].* [Online]
Available at: https://www.isasmelt.com/en/ download/Brochures/isasmeltbrochure.pdf

GlobeNewswire, 2021. *Osisko Development Announces Ore Sorting Test Results Significantly Increase Concentrator and Mill Grades While Reducing Carbon Footprint, Water and Land Use.* [Online]
Available at: https://www.globenewswire.com/en/news-release/2021/04/22/2215030/0/en/Osisko-Development-Announces-Ore-Sorting-Test-Results-Significantly-Increase-Concentrator-and-Mill-Grades-While-Reducing-Carbon-Footprint-Water-and-Land-Use.html
[Accessed 10 November 2021].

Gómez-Hernández, J. J. & Journel, A. G., 1993. Joint Sequential Simulation of MultiGaussian Fields. In: A. Soares, ed. *Geostatistics Tróia '92 (Volume 1).* Dordrecht (NL): Kluwer Academic Publishers (Springer), pp. 85–94.

Goodfellow, I., Bengio, Y. & Courville, A., 2016. *Deep Learning.* Cambridge (MA): Massachusetts Institute of Technology Press.

Goovaerts, P., 1997. *Geostatistics for Natural Resources Evaluation.* New York (NY): Oxford University Press.

Goulard, M. & Voltz, M., 1992. Linear coregionalization model: tools for estimation and choice of cross–variogram matrix. *Mathematical Geology,* 24(3), pp. 269–286.

Gou, M., Zhou, L. & Wei Ying Then, N., 2019. Utilization of tailings in cement and concrete: A review. *Science and Engineering of Composite Materials,* 26(1), pp. 449–464.

Gowest Gold Ltd, 2015. *NI 43-101 Technical Report and Prefeasibility Study for the Bradshaw Gold Deposit, Timmins, Ontario,* Toronto (ON): TSX Group Inc..

Grammatikopoulos, T., 2018. *High Definition Mineralogy by QEMSCAN: From Exploration to Processing.* Québec (QC): Centre de Recherche sur la Géologie et l'Ingénierie des Ressources Minérales – Université Laval.

Grammatikopoulos, T. & Downing, S., 2020. The Disruptive Role of Process Mineralogy in Geology and Mineral Processing Industry. *Aspects in Mining & Mineral Science,* 5(2), pp. 571–579.

Gray, M. R., Eaton, P. E. & Le, T., 2008. Inhibition and promotion of hydrolysis of chloride salts in model crude oil and heavy oil. *Petroleum Science and Technology,* 26(16), pp. 1934–1944.

Gray, M. R., Xu, Z. & Masliyah, J., 2009. Physics in the oil sands of Alberta. *Physics Today,* 62(3), pp. 31–35.

Greasley, A., 2020. *Architectures for Combining Discrete–event Simulation and Machine Learning.* Lieusaint (FR).

Greberg, J., Salama, A., Gustafson, A. & Skawina, B., 2016. Alternative process flow for underground mining operations: Analysis of conceptual transport methods using discrete event simulation. *Minerals,* 6(3), p. 65.

GRID–Arendal, 2019. *Global Tailings Portal.* [Online]
Available at: https://tailing.grida.no/#header [Accessed 24 July 2020].

Guarnera, B. J. & Martin, M. D., 2011. Chapter 4.6 – Valuation of Mineral Properties. In: P. Darling, ed. *SME Mining Engineering Handbook (3rd Edition).* Englewood (CO):Society for Mining, Metallurgy, and Exploration, Inc. (SME), pp. 219–226.

Hanniala, P., Mäkinen, T. & Kytö, M., 1991. Flash technology for converting. In: J. Vereecken, ed. *EMC '91: Non-Ferrous Metallurgy – Present and Future.* Dordrecht (NL): Springer Science+Business Media B.V., pp. 191–203.

Hedstrom, L., Holmstrom, A., Hammerschmidt, J., Charistos, A. & Mattich, C., 2016. Processing the arsenic rich MMH copper concentrate into a high quality calcine by fluidized bed roasting. In: *Proceedings of the XXVIII International Mineral Processing Congress (IMPC 2016), Quebec (QC).* Montreal (QC): Canadian Institute of Mining, Metallurgy and Petroleum (CIM), pp. 2344–2353.

Hein, F. J., 2006. Heavy oil and oil (tar) sands in North America: An overview & summary of contributions. *Natural Resources Research,* Volume 15, pp. 67–84.

Hein, F. J., Cotterill, D. K. & Berhane, H., 2000. *An atlas of lithofacies of the McMurray Formation, Athabasca oil sands deposit, northeastern Alberta: Surface and subsurface: AEUB/AGS Earth Sciences Report 2000–07,* Edmonton (AB): Alberta Energy and Utilities Board/Alberta Geological Survey.

Hein, F. J., Langenberg, C. W., Kidston, C., Berhane, H., Berezniuk, T. & Cotterill, D. K., 2001. *A comprehensive field guide for facies characterization of the Athabasca oil sands, northeast Alberta (with maps, air photos, and detailed descriptions of seventy–eight outcrop sections): AEUB/AGS Special Report 13,* Edmonton (AB): Alberta Energy Utilities Board/Alberta Geological Survey.

He, K., Zhang, X., Ren, S. & Sun, J., 2015. *Delving deep into rectifiers: Surpassing human–level performance on imagenet classification.* Santiago (CL).

Hermann, W. & Berry, R. F., 2002. MINSQ – a least squares spreadsheet method for calculating mineral proportions from whole rock major element analyses. *Geochemistry: Exploration, Environment, Analysis,* Volume 2, pp. 361–368.

Hern, T. & Long, C., 1991. Viewing some concepts and applications in linear algebra. *Visualization in Teaching and Learning Mathematics,* Volume 19 (MAA Notes), pp. 173–190.

Herrington, R., 2011. Geological Features and Genetic Models of Mineral Deposits. In: P. Darling, ed. *SME Mining Engineering Handbook (3rd Edition).* Englewood (CO): Society for Mining, Metallurgy, and Exploration, Inc., pp. 83–104.

Hornik, K., 1991. Approximation capabilities of multilayer feedforward networks. *Neural Networks,* Volume 4, pp. 251–257.

Hoskuldsson, A., 1988. PLS regression methods. *Journal of Chemometrics,* 2(1), pp. 211–228.

Huerta, M., Leiva, V., Liu, S., Rodriguez, M. & Villegas, D., 2019. On a partial least squares regression model for asymmetric data with a chemical application in mining. *Chemometrics and Intelligent Laboratory Systems,* 190(1), pp. 55–68.

Hurley, P. & Pritchard, R., 2005. Cement. In: P. Worsfold, A. Townshend & C. Poole, eds. *Encyclopedia of Analytical Science, 2nd Ed.* New York (NY): Elsevier Ltd., pp. 458–463.

Hu, Y. X., Liu, X. R., Xu, H. & Ge, H., 2010. Multiple linear regression prediction models to predict the uniaxial compressive strength and the elastic modulus of Pengguan complex. *Geotech. Investig. Surv.,* Volume 12, pp. 15–21.

Hyvarinen, O. & Hamalainen, M., 2005. HydroCopperTM – A new technology producing copper directly from concentrate. *Hydrometallurgy,* Volume 77, pp. 61–65.

Igogo, T., Lowder, T., Engel–Cox, J., Newman, A. & Awuah-Offei, K., 2020. *Integrating Clean Energy in Mining Operations: Opportunities, Challenges, and Enabling Approaches (Technical Report NREL/TP-6A50-76156,* Golden (CO): National Renewable Energy Laboratory.

IMT, 2013. *Ilustre Municipalidad de Taltal.* [Online]
Available at: https://web.archive.org/web/20130725152531/http://www.taltal.cl/contenido/44/historia [Accessed 16 July 2020].

International Mining, 2021. *COREM, Steinert ore sorting tests present opportunities for Cartier at Chimo gold project.* [Online]
Available at: https://im-mining.com/2021/04/09/corem-steinert-ore-sorting-tests-present-opportunities-for-cartier-at-chimo-gold-project/ [Accessed 10 November 2021].

Jalloh, A. B., Kyuro, S., Jalloh, Y. & Barrie, A. K., 2016. Integrating artificial neural networks and geostatistics for optimum 3D geological block modeling in mineral reserve estimation: A case study. *Int. J. Min. Sci. Technol.,* Volume 26, pp. 581–585.

James, G., Witten, D., Hastie, T. & Tibshirani, R., 2013. *An Introduction to Statistical Learning with Applications in R.* New York (NY): Springer Science+Business Media.

Jang, H. & Topal, E., 2014. A review of soft computing technology applications in several mining problems. *Appl. Soft Comput.,* Volume 22, pp. 638–651.

Johnson, R. A. & Wichern, D. W., 2007. *Applied Multivariate Statistical Analysis (6th Edition)*. Upper Saddle River (NJ): Pearson Prentice Hall.

Jordens, A., Marion, C., Grammatikopoulos, T., Hart, B. & Waters, K. E., 2016. Beneficiation of the Nechalacho rare earth deposit: Flotation response using benzohydroxamic acid. *Minerals Engineering,* Volume 99, pp. 158–169.

Journel, A. G., 1974. *Simulation conditionelle de gisements miniers – théorie et pratique, Thèse de Docteur Ingénieur.* Nancy (FR): Université de Nancy.

Journel, A. G. & Huijbregts, C. J., 1978. *Mining Geostatistics.* New York (NY): Academic Press.

Jung, D. & Choi, Y., 2021. Systematic Review of Machine Learning Applications in Mining: Exploration, Exploitation, and Reclamation. *Minerals,* 11(148), pp. 1–20.

Kaminsky, H. A. W., 2008. *Characterization of an Athabasca oil sands ore and process streams.* Edmonton (AB): PhD Thesis, Department of Chemical and Materials Engineering, University of Alberta.

Kaplan, U. E. & Topal, E., 2020. A New Ore Grade Estimation Using Combined Machine Learning Algorithms. *Minerals,* 10(847), pp. 1–17.

Kaur, H., Eaton, P. & Gray, M. R., 2012. The kinetics and inhibition of chloride hydrolysis in Canadian bitumen. *Petroleum Science and Technology,* 30(10), pp. 993–1003.

Keller, P. C. & Anderson, C. G., 2018. The Production of Critical Materials as By Products. *Aspects in Mining & Mineral Science,* 2(2), pp. 1–14.

Kern, M., Tusa, L., Leibner, T., van den Boogaart, K. G. & Gutzmer, J., 2019. Optimal sensor selection for sensor-based sorting based on automated mineralogy data. *Journal of Cleaner Production,* 234(2019), pp. 1144–1152.

Kingma, D. P. & Ba, J. L., 2015. *Adam: A Method for Stochastic Optimization.* San Diego (CA).

Kirk, T. & Cannon, C., 2020. *Sunshine for Mines: A Brighter Vision for Sustainable Resources.* [Online] Available at: https://rmi.org/sunshine-for-mines-a-brighter-vision-for-sustainable-resources/ [Accessed 28 February 2022].

Kleijnen, J. P. C., 2012. Chapter 18 – Design and Analysis of Monte Carlo Experiments. In: J. E. Gentle, W. K. Hardle & Y. Mori, eds. *Handbook of Computational Statistics.* New York (NY): Springer Science + Business Media, pp. 529–547.

Knuth, D. E., 1998. *The Art of Computer Programming – Volume 2 / Seminumerical Algorithms.* 3rd ed. Berkeley (CA): Addison Wesley Longman, Inc..

Koch, P.-H. & Rosenkranz, J., 2020. Sequential decision-making in mining and processing based on geometallurgical inputs. *Minerals Engineering,* 149(106262), pp. 1–10.

Kojo, I., Lahtinen, M. & Miettinen, E., 2009. Flash converting – Sustainable technology now and in the future. In: J. Kapusta & T. Warner, eds. *International Peirce-Smith Converting Centennial (San Francisco, CA).* Pittsburgh (PA): The Minerals, Metals & Materials Society (TMS), pp. 383–395.

Kojo, I. & Storch, H., 2006. Copper production with Outokumpu flash smelting: An update. In: F. Kongoli, ed. *Proceedings of Advanced Processing of Metals and Materials (Sohn International Symposium) – Volume 8: International Symposium on Sulfide Smelting (San Diego, CA).* Warrendale (PA): Minerals, Metals and Materials Society, pp. 225–238.

Kordosky, G., 2002. Copper recovery using leach/solvent extraction/electrowinning technology: Forty years of innovation, 2.2 million tonnes of copper annually. *Journal of the South African Institute of Mining and Metallurgy,* 102(8), pp. 445–450.

Krige, D. G., 1951. A statistical approach to some basic mine valuation problems on the Witwatersrand. *Journal of the Chemical and Metallurgical Society of South Africa,* Volume 52, pp. 119–139.

Krige, D. G., 1952. A statistical analysis of some of the borehole values in the Orange Free State goldfield. *Journal of the Chemical and Metallurgical Society of South Africa,* Volume 53, pp. 47–64.

Kusebauch, C., Gleeson, S. A. & Oelze, M., 2019. Coupled partitioning of Au and As into pyrite controls formation of giant Au deposits. *Science Advances,* 5(5), pp. 1–8.

Kusiak, A., 2017. Smart manufacturing must embrace big data. *Nature,* 544(7648), pp. 23–25.

Landro, N., Gallo, I. & La Grassa, R., 2021. Combining Optimization Methods Using an Adaptive Meta Optimizer. *Algorithms,* 14(186), pp. 1–15.

Lantuéjoul, C., 2002. *Geostatistical simulation: models and algorithms.* Berlin (DE): Springer.

Lashari, S. Z., Takbiri-Borujeni, A., Fathi, E., Sun, T., Rahmani, R. & Khazaeli, M., 2019. Drilling performance monitoring and optimization: a data-driven approach. *J. Pet. Explor. Prod. Technol.,* Volume 9, pp. 2747–2756.

Leach, D. L., Sangster, D. F., Kelley, K. D., Large, R. R., Garven, G., Allen, C. R., Gutzmer, J. & Walters, S., 2005. Sediment-Hosted Lead-Zinc Deposits: A Global Perspective. In: J. W. Hedenquist, J. F. H. Thompson, R. J. Goldfarb & J. P. Richards, eds. *Economic Geology 100th Anniversary Volume.* Littleton (CO): Society of Economic Geologists, Inc., pp. 561–607.

L'Ecuyer, P., 2015. *Random Number Generation and Quasi–Monte Carlo.* [Online] Available at: https://doi.org/10.1002/9781118445112.stat04386.pub2 [Accessed 24 April 2020].

L'Ecuyer, P., 2017. History of Uniform Random Number Generation. In: W. K. V. Chan, A. D'Ambrogio, G. Zacharewicz, N. Mustafee, G. Wainer & E. Page, eds. *Proceedings of the 2017 Winter Simulation Conference.* Las Vegas (NV): Association for Computing Machinery, pp. 202–230.

Leite, E. P. & de Souza Filho, C. R., 2009. Artificial neural networks applied to mineral potential mapping for copper-gold mineralizations in the Carajás Mineral Province, Brazil. *Geophys. Prospect.,* Volume 57, pp. 1049–1065.

Lektauers, A., Pecherska, J., Bolshakov, V., Romanovs, A., Grabis, J. & Teilans, A., 2021. A Multi-Model Approach for Simulation-Based Digital Twin in Resilient Services. *WSEAS Transactions on Systems and Control,* Volume 16, pp. 133–145.

Lidberg, S., Aslam, T., Pehrsson, L. & Ng, A. H. C., 2020. Optimizing real-world factory flows using aggregated discrete event simulation modelling. *Flexible Services and Manufacturing Journal,* Volume 32, pp. 888–912.

Li, X., Wu, B. & Zhu, J., 2018. Hazards of organic chloride to petroleum processing in Chinese refineries and industrial countermeasures. *Progress Petrochem Sci,* 2(3), pp. 204–207.

Li, Z. & Peters, S. G., 1998. *Comparative Geology and Geochemistry of Sedimentary-Rock-Hosted (Carlin-Type) Gold Deposits in the People's Republic of China and in Nevada, USA: U.S. Geological Survey Open-File Report 98–466,* Reston (VA): U.S. Geological Survey.

Li, Z., Zhang, X., Clarke, K. C., Liu, G. & Zhu, R., 2018. An automatic variogram modeling method with high reliability fitness and estimates. *Comput Geosci,* Volume 120, pp. 48–59.

Londono, Y., Mikula, R., Eaton, P. & Gray, M. R., 2009. Interaction of chloride salts and kaolin clay in the hydrolysis of emulsified chloride salts at 200-350 C. *Petroleum Science and Technology,* 27(11), pp. 1163–1174.

Long, J., Hoskins, S. & Reid, K., 2020. *United States Patent Application Publication.* United States, Patent No. US 2020/0102505 A1.

Luo, L., Zhang, Y., Bao, S. & Chen, T., 2016. Utilization of iron ore tailings as raw material for Portland cement clinker production. *Advances in Materials Science and Engineering,* Volume 2016, pp. 1–6.

Lystrom, D. J., Rinella, F. A., Rickert, D. A. & Zimmermann, L., 1978. *Multiple Regression Modeling Approach for Regional Water Quality Management,* Athens (GA): U.S. Environmental Protection Agency.

Mackey, P. J., 2013. Copper smelting technologies in 2013 and beyond (Plenary paper). In: R. Bassa, R. Parra, A. Luraschi & S. Demetrio, eds. *Proceedings of the Copper 2013 Conference (Santiago, CL).* Santiago (CL): Instituto de Ingenieros de Minas de Chile.

Maestre, F. T., 2004. On the importanceof patch attributes, environmental factors and past human impacts as determinants of perennial plant species richness and diversity in Mediterranean semiarid steppes. *Div. Distr.,* 10(1), pp. 21–29.

Maheswari, C., Prinyanka, E. B., Thangavel, S., Ram Vignesh, S. V. & Poongodi, C., 2020. Multiple regression analysis for the prediction of extraction efficiency in mining industry with industrial IoT. *Production Engineering,* Issue 4.

Marinković, J., 2008. Multivariate Statistics. In: W. Kirch, ed. *Encyclopedia of Public Health.* Dordrecht (NL): Springer Publishing, pp. 973–976.

Marsden, J. & House, I., 2006. *The Chemistry of Gold Extraction.* Englewood (CO): Society for Mining, Metallurgy & Exploration.

Marsland, S., 2015. *Machine Learning: An Algorithmic Perspective – 2nd Edition.* Boca Raton (FL): CRC Press (Taylor & Francis Group, LLC).

Masliyah, J. H., Czarnecki, J. & Xu, Z., 2011. *Handbook on Theory and Practice of Bitumen Recovery from Athabasca Oil Sands, Volume 1: Theoretical Basis.* Cochrane (AB): Kingsley Knowledge Publishing.

Matheron, G., 1973. The intrinsic random functions and their applications. *Advances in Applied Probability,* 5(1), pp. 439–468.

Mayhew, K., Mean, R., Miller, C., Thompson, J., Barrios, P., Koenig, C., Omaynikova, V. & Wagner, O., 2011. Teck – Aurubis: An integrated mine to metal approach to develop high arsenic copper deposits using the CESL process. *Proceedings of the Perumin 2011 Conference*, Arequipa (PE).

McCoy, J. & Auret, L., 2019. Machine learning applications in minerals processing: A review. *Miner. Eng.,* Volume 132, pp. 95–109.

McKinsey & Company, 2021. *Refractory gold ores: Challenges and opportunities for a key source of growth.* [Online] Available at: https://www.mckinsey.com/industries/metals-and-mining/our-insights/refractory-gold-ores-challenges-and-opportunities-for-a-key-source-of-growth [Accessed 10 November 2021].

Mean, J. R., 2011. *Triple bottom line thinking for a high arsenic bearing copper–gold project in northern Peru: Assessing the viability of an integrated mine, mill, and hydrometallurgical refinery (Unpublished master's thesis),* Burnaby (BC): Simon Fraser University.

Melzer, T., 2004. *SVD and its application to generalized eigenvalue problems.* Vienna (AT): University of Technology.

Meng, Q., Yuan, Z., Feng, Q. & Ou, L., 2017. The Effect of Quartz on the Flotation of Fine Wolframite with Octyl Hydroxamic Acid. *Minerals,* 7(10), pp. 1–13.

Mercier, P. H. J., Kingston, D., Kung, J., Woods, J. R., Kotlyar, L. S., Tu, Y., Smith, T., Ng, S., Moran, K., Sparks, B. D. & McCracken, T., 2007. *Development of an innovative method for assessment of oilsands ore processability by measurement of paramagnetic signatures – Final Report to CONRAD Bitumen Production Research Group (ICPET Report #PET-1570-06S),* Ottawa (ON): National Research Council Canada – Institute for Chemical Process and Environmental Technology.

Mercier, P. H. J., Patarachao, B., Kung, J., Kingston, D., Woods, J., Sparks, B. D., Kotlyar, L., Ng, S., Moran, K. & McCracken, T., 2008. X-ray diffraction (XRD)-derived processability markers for oil sands based on clay mineralogy and crystallite thickness distributions. *Energy & Fuels,* 22(5), pp. 3174–3193.

Metals Focus, 2020. *Gold Focus 2020,* London (GB): Metals Focus.

Mevik, B.-H. & Wehrens, R., 2007. The pls package: Principal component and partial least squares regression in R. *Journal of Statistical Software,* 18(2), pp. 1–24.

Mudd, G. M., 2007. Global trends in gold mining: Towards quantifying environmental and resource sustainability? *Resources Policy,* Volume 32, pp. 42–56.

Murphy, K. P., 2022. *Probabilistic Machine Learning – An Introduction.* Cambridge (MA): The Massachusetts Institute of Technology Press.

Nageshwaraniyer, S., Kim, K. & Son, Y. J., 2018. A mine-to-mill economic analysis model and spectral imaging-based tracking system for a copper mine. *J. S. Afr. I Min. Metall.,* 118(1), pp. 7–14.

Narendran, T. V. & Weinelt, B., 2017. *Digital Transformation Initiative – Mining and Metals Industry,* Cologny/Geneva (CH): World Economic Forum.

Navarra, A., Alvarez, M., Rojas, K., Menzies, A., Pax, R. & Waters, K., 2019. Concentrator operational modes in response to geological variation. *Minerals Engineering,* 134(1), pp. 356–364.

Navarra, A., Grammatikopoulos, T. & Waters, K., 2018. Incorporation of geometallurgical modelling into long-term production planning. *Minerals Engineering,* 120(1), pp. 118–126.

Navarra, A., Kuan, S. H., Parra, R., Davis, B. & Mucciardi, F., 2016. Debottlenecking of conventional copper smelters. *Proceedings of the International Conference on Industrial Engineering and Operations Management*, Kuala Lumpur (MY), pp. 2395–2406.

Navarra, A., Rafiei, A. & Waters, K., 2017a. A systems approach to mineral processing based on mathematical programming. *Canadian Metallurgical Quarterly,* 56(1), pp. 35–44.

Navarra, A., Marambio, H., Oyarzun, F., Parra, R. & Mucciardi, F., 2017b. System dynamics and discrete event simulation of copper smelters. *Minerals & Metallurgical Processing,* 34(2), pp. 96–106.

Navarra, A., Wilson, R., Parra, R., Toro, N., Ross, A., Nave, J.-C. & Mackey, P. J., 2020. Quantitative methods to support data acquisition modernization within copper smelters. *Processes,* 8(11), pp. 1–22.

Nazari Ostad, M., Emami Niri, M. & Darjani, M., 2018. 3D modeling of geomechanical elastic properties in a carbonate–sandstone reservoir: a comparative study of geostatistical co-simulation methods. *Journal of Geophysics and Engineering,* 15(4), pp. 1419–1431.

Nazari, A., Radzinski, R. & Ghahreman, A., 2017. Review of arsenic metallurgy: Treatment of arsenical minerals and the immobilization of arsenic. *Hydrometallurgy,* 174(2017), pp. 258–281.

Nelson, M. G., 2011. Chapter 6.1: Evaluation of Mining Methods and Systems. In: P. Darling, ed. *SME Mining Engineering Handbook (3rd Edition).* Englewood (CO): Society for Mining, Metallurgy, and Exploration, Inc. (SME), pp. 341–348.

Ng, W. S., Wang, Q. & Chen, M., 2020. A review of preg-robbing and the impact of chloride ions in the pressure oxidation of double refractory ores. *Mineral Processing and Extractive Metallurgy Review,* pp. 1–28.

Nie, W., Fang, J., Wen, S., Feng, Q., He, Y. & Yang, X., 2021. Estimation and improvement of recovery of low grade copper oxide using sulfide activation flotation method based on GA-BPNN. *Processes,* 9(583), pp. 1–14.

Nikolić, I. P., Milošević, I. M., Milijić, N. N. & Mihajlović, I. N., 2019. Cleaner production and technical effectiveness: Multi-criteria analysis of copper smelting facilities. *Journal of Cleaner Production,* Volume 215, pp. 423–432.

Nikolic, S., Edwards, J. S., Burrows, A. S. & Alvear, G. R. F., 2009. ISACONVERT – TSL Continuous Copper Converting Update. In: J. Kapusta & T. Warner, eds. *Proceedings of the International Peirce-Smith Converting Centennial (TMS Annual Meeting), San Francisco (CA).* Warrendale (PA): The Minerals, Metals & Materials Society (TMS), pp. 407–414.

Niu, W., Lu, J. & Sun, Y., 2021. A Production Prediction Method for Shale Gas Wells Based on Multiple Regression. *Energies,* 14(1461), pp. 1–11.

NOAMI, 2004. *National Orphaned/Abandoned Mines Initiative (NOAMI).* [Online] Available at: http://www.abandoned–mines.org/en/ [Accessed 24 July 2020].

Norouzi, S. & Ebrahimi, M. R., 2020. *A Survey on Proposed Methods to Address Adam Optimizer Deficiencies.* [Online] Available at: http://www.cs.toronto.edu/~sajadn/sajad_norouzi/ECE1505.pdf [Accessed 1 December 2021].

Nussbaumer, R., Mariethoz, G., Gravey, M., Gloaguen, E. & Holliger, K., 2018. Accelerating Sequential Gaussian Simulation with a Constant Path. *Computers & Geosciences,* Volume 112, pp. 121–132.

Ochromowicz, K. & Chmielewski, T., 2011. Solvent extraction in hydrometallurgical processing of Polish copper concentrates. *Physicochemical Problems of Mineral Processing,* 46(2011), pp. 207–218.

Oh, H. J. & Lee, S., 2010. Application of artificial neural network for gold-silver deposits potential mapping: A case study of Korea. *Nat. Resour. Res.,* Volume 19, pp. 103–124.

Olper, M., Maccagni, M., Matusewicz, R. & Reuter, M. A., 2008. Simplified copper production from primary concentrates: The direct electrorefining of white metal/copper matte. *Canadian Metallurgical Quarterly,* 47(3), pp. 369–376.

Omotoso, O. E. & Mikula, R. J., 2003. High surface areas caused by smectitic interstratification of kaolinite and illite in Athabasca oil sands. *Appl. Clay Sci.,* 25(2004), pp. 37–47.

Órdenes, J., Wilson, R., Peña-Graf, F. & Navarra, A., 2021. Incorporation of geometallurgical input into gold mining system simulation to control cyanide consumption. *Minerals,* 11(1023), pp. 1–16.

O'Regan, B. & Moles, R., 2006. Using system dynamics to model the interaction between environmental and economic factors in the mining industry. *Journal of Cleaner Production,* 14(1), pp. 689–707.

Ortiz, J. M., 2020. *Introduction to sequential Gaussian simulation – Annual Report 2020 (Paper 2020–01),* Kingston (ON): Predictive Geometallurgy and Geostatistics Lab (Queen's University).

Palomino, D. & Carrascal, L. M., 2007. Habitat associations of a raptor community in a mosaic landscape of central Spain under urban development. *Landscape Urban Planning,* 83(1), pp. 268–274.

Pamparana, G., Kracht, W., Haas, J., Diaz-Ferran, G., Palma-Behnke, R. & Roman, R., 2017. Integrating photovoltaic solar energy and a battery energy storage system to operate a semi-autogenous grinding mill. *Journal of Cleaner Production,* 165(1), pp. 273–280.

Paravarzar, S., Emery, X. & Madani, N., 2015. Comparing sequential Gaussian and turning bands algorithms for cosimulating grades in multi-element deposits. *Comptes Rendus Geoscience,* 347(1), pp. 84–93.

Patarachao, B., Mercier, P. H. J., Kung, J., Woods, J. R., Kotlyar, L. S., Sparks, B. D. & McCracken, T., 2010. Optimizing XRF calibration protocols for elemental quantification of mineral solids from Athabasca oil sands. *Advances in X–ray Analysis,* Volume 53, pp. 220–227.

Patterson, L. M. & Muntean, J. L., 2011. Multi-element geochemistry across a Carlin-type gold district Jerritt Canyon, Nevada. In: *Great Basin evolution and metallogeny – Geological Society*

of Nevada Symposium 2010 Proceedings. Reno (NV): DEStech Publications, Inc., pp. 1119–1151.

Pawar, R. J., 2003. Chapter 5 – Introduction to Geostatistics. In: M. Nikravesh, F. Aminzadeh & L. A. Zadeh, eds. *Developments in Petroleum Science, Volume 51.* Elsevier Science B.V., pp. 85–95.

Pell, R. J., Ramos, L. S. & Manne, R., 2007. The model space in partial least squares regression. *Journal of Chemometrics,* 21(1), pp. 165–172.

Peña-Graf, F. A., Grammatikopoulos, T., Kabemba, A. & Navarra, A., 2021. Integrated feed management of mineral processing plants with application to chromite processing. *Canadian Metallurgical Quarterly,* 60(3), pp. 130–136.

Peña-Graf, F., Órdenes, J., Wilson, R. & Navarra, A., 2022. Discrete Event Simulation for Machine-Learning Enabled Mine Production Control with Application to Gold Processing. *Metals,* 12(225), pp. 1–22.

Perez, K., Wilson, R., Jeldres, R. I., Toro, N., & Navarra, A., 2021. Environmental, economic and technological factors affecting Chilean copper smelters – A critical review. *Journal of Materials Research and Technology,* 15(2021), pp. 213–225.

Pham, Q. T. & Phan, T. K. D., 2016. Apply Neural Network for Improving Production Planning at Samarang Petrol Mine. *International Journal of Intelligent Computing and Cybernetics,* 9(2), pp. 126–143.

Phengsaart, T., Ito, M., Azuma, A., Tabelin, C. B. & Hiroyoshi, N., 2020. Jig separation of crushed plastics: the effects of particle geometry on separation efficiency. *Journal of Material Cycles and Waste Management,* 22(3), pp. 787–800.

Poole, D. L. & Mackworth, A. K., 2017. *Artificial Intelligence: Foundations of Computational Agents, 2nd Edition*. Cambridge (MA): Cambridge University Press.

Poole, D. L., Mackworth, A. K. & Goebel, R., 1998. *Computation Intelligence: A Logical Approach.* New York (NY): Oxford University Press.

Potdar, K., Pardawala, T. & Pai, C., 2017. A comparative study of categorical variable encoding techniques for neural network classifiers. *International Journal of Computer Applications,* 175(4), pp. 7–9.

Pradenas, L., Zúñiga, J. & Parada, V., 2006. CODELCO, Chile Programs its Copper-Smelting Operations. *INFORMS Journal on Applied Analytics,* 36(4), pp. 296–301.

Prevost, Y., Bedard, M. & Levac, C., 2013. Forty years of operation of the Noranda reactor process. In: R. Bassa, R. Parra, A. Luraschi & S. Demetrio, eds. *Proceedings of Copper 2013, International Copper Conference, Vol. III – The Nickolas Themelis Symposium on*

Pyrometallurgy and Process Engineering. Santiago (CL): Instituto de Ingenieros de Minas de Chile (IIMCh), pp. 265–277.

Price, T., Harris, C., Hills, S., Boyd, W. & Wraith, A., 2009. Peirce–Smith converting: Another 100 years? In: J. Kapusta & T. Warner, eds. *Proceedings of the International Peirce–Smith Converting Centennial (TMS Annual Meeting), San Francisco (CA).* Warrendale (PA): The Minerals, Metals & Materials Society (TMS), pp. 181–197.

Qaeze, F., Guillaume, R. & Thierry, C., 2015. *A Collaborative Planning Model to Coordinate Mining and Smelting Furnace.* Albi (FR).

Qiu, G., Luo, Z., Shi, Z. & Ni, M., 2011. Utilization of coal gangue and copper tailings as clay for cement clinker calcinations. *Journal of Wuhan University of Technology – Materials Science Edition,* 26(6), pp. 1205–1210.

Quelopana, A. & Navarra, A., 2021. Integration of strategic open–pit mine planning into hierarchical artificial intelligence. *Journal of the Southern African Institute of Mining and Metallurgy*, 121(12), pp. 643–652.

Reich, M., Kesler, S. E., Utsunomiya, S., Palenik, C. S., Chryssoulis, S. L. & Ewing, R. C., 2005. Solubility of gold in arsenian pyrite. *Geochimica et Cosmochimica Acta,* 69(11), pp. 2781–2796.

Resman, M., Protner, J., Simic, M. & Herakovic, N., 2021. A Five-Step Approach to Planning Data-Driven Digital Twins for Discrete Manufacturing Systems. *Applied Sciences,* 11(3639), pp. 1–25.

Riveros, P. A., Dutrizac, J. E. & Spencer, P., 2001. Arsenic disposal practices in the metallurgical industry. *Canadian Metallurgical Quarterly,* 40(4), pp. 395–420.

Robben, C. & Wotruba, H., 2019. Sensor-Based Ore Sorting Technology in Mining – Past, Present and Future. *Minerals,* 9(523), pp. 1–25.

Roy, S., Adhikari, G. R., Renaldy, T. A. & Jha, A. K., 2011. Development of Multiple Regression and Neural Network Models for Assessment of Blasting Dust at a Large Surface Coal Mine. *Journal of Environmental Science and Technology,* Volume 4, pp. 284–301.

S&P Global, 2021. *Gold price increase drives surge of smaller discoveries.* [Online] Available at: https://www.spglobal.com/marketintelligence/en/news–insights/research/gold–price–increase–drives–surge–of–smaller–discoveries

Saldaña, M., Neira, P., Flores, V., Moraga, C., Robles, P. & Salazar, I., 2021. Analysis of the Dynamics of Rougher Cells on the Basis of Phenomenological Models and Discrete Event Simulation Framework. *Metals,* 11(1454), pp. 1–20.

Saldaña, M., Toro, N., Castillo, J., Hernandez, P. & Navarra, A., 2019. Optimization of the heap leaching process through changes in modes of operation and discrete event simulation. *Minerals,* 9(7), p. 421.

Schlesinger, M., King, M., Sole, K. & Davenport, W., 2011. Chapter 8 – Batch converting of copper matte. In: M. Schlesinger, M. King, K. Sole & W. Davenport, eds. *Extractive Metallurgy of Copper (5th Edition).* Oxford (UK): Elsevier Science, pp. 127–153.

Schmidt, J., Marques, M. R. G., Botti, S. & Marques, M. A. L., 2019. Recent advances and applications of machine learning in solid-state materials science. *Computational Materials,* 5(83), pp. 1–36.

Schodde, R., 2011. *Recent trends in gold discovery.* Perth (AU), Paydirt Media, pp. 1–19.

Seedorff, E., Dilles, J. H., Proffett, J. M. Jr., Einaudi, M. T., Zurcher, L., Stavast, W. J. A., Johnson, D. A. & Barton, M. D., 2005. Porphyry deposits: Characteristics and origin of hypogene features. In: J. W. Hedenquist, J. F. H. Thompson, R. J. Goldfarb & J. P. Richards, eds. *Economic Geology 100th Anniversary Volume.* Littleton (CO): Society of Economic Geologists (SEG), pp. 251–298.

Seppa, H., 2004. A modern pollen climate calibration set from northern Europe: developing and testing a tool for palaeoclimatological reconstructions. *Journal of Biogeography,* 31(1), pp. 251–267.

SERNAGEOMIN, 2018. *Geoquimica Depositos Relaves Chile.,* Santiago (CL): Servicio Nacional de Geologia y Mineria (SERNAGEOMIN).

Shanks, P. W. C. & Thurston, R., 2012. *U.S. Geological Survey Scientific Investigations Report 2010-5070-C: Volcanogenic massive sulfide occurrence model.* Reston (VA): U.S. Geological Survey.

Shen, Y., Song, Z. & Kusiak, A., 2021. Enhancing the generalizability of predictive models with synergy of data and physics. *Measurement Science and Technology,* 33(3), pp. 1–11.

Shishvan, M. & Benndorf, J., 2014. Performance optimization of complex continuous mining system using stochastic simulation. In: H. J. Rodrigues, S. C. Mota, G. J. Miranda, A. Araujo & J. Folgado, eds. *Engineering Optimization.* Hoboken (NJ): Taylor and Francis, pp. 273–278.

Siegel, A. F., 2017. Chapter 12 – Multiple Regression: Predicting One Variable from Several Others. In: A. F. Siegel, ed. *Practical Business Statistics (7th Ed.).* Cambridge (MA): Academic Press, pp. 355–418.

Sillitoe, R. H., 1995. Exploration of porphyry copper lithocaps. In: J. L. Mauk & J. D. St. George, eds. *Proceedings of the Australasian Institute of Mining and Metallurgy Pacific Rim (PACRIM '95) Congress, Auckland (NZ).* Melbourne (AU): Australasian Institute of Mining and Metallurgy (AusIMM), pp. 527–532.

Sillitoe, R. H., 2000. Gold-rich porphyry deposits: Descriptive and genetic models and their role in exploration and discovery. *Reviews in Economic Geology,* Volume 13, pp. 315–345.

Sillitoe, R. H. & Perello, J., 2005. Andean copper province: Tectonomagmatic settings, deposit types, metallogeny, exploration, and discovery. In: J. W. Hedenquist, J. F. H. Thompson, R. J. Goldfarb & J. P. Richards, eds. *Economic Geology 100th Anniversary Volume.* Littleton (CO): Society of Economic Geologists (SEG), pp. 845–892.

Singh, M., Fuenmayor, E., Hinchy, E. P., Qiao, Y., Murray, N. & Devine, D., 2021. Digital Twin: Origin to Future. *Applied System Innovation,* 4(36), pp. 1–19.

Sobottka, T., Kamhuber, F., Faezirad, M. & Sihn, W., 2019. Potential for Machine Learning in Optimized Production Planning with Hybrid Simulation. *Procedia Manufacturing,* Volume 39, pp. 1844–1853.

Sonesten, L., 2003. Catchment area composition and water chemistry heavily affects mercury levels in perch (Perca fluviatilis L.) in circumneutral lakes. *Water Air Soil Pollution,* 144(1), pp. 117–139.

Spanos, T., 2008. Environmetrics to evaluate marine environment quality. *Environ. Monit. Assess.,* 143(1), pp. 215–225.

Srivastava, N., Hinton, G., Krizhevsky, A., Sutskever, I. & Salakhutdinov, R., 2014. Dropout: A Simple Way to Prevent Neural Networks from Overfitting. *Journal of Machine Learning Research,* Volume 15, pp. 1929–1958.

Stokes, C., Masselink, G., Revie, M., Scott, T., Purves, D. & Walters, T., 2017. Application of multiple linear regression and Bayesian belief network approaches to model life risk to beach users in the UK. *Ocean & Coastal Management,* 139(2017), pp. 12–23.

Strang, G., 1993. The fundamental theoremof linear algebra. *The American Mathematical Monthly,* 100(9), pp. 848–855.

Suazo, C., Kracht, W. & Alruiz, O., 2010. Geometallurgical modlling of the Collahuasi flotation circuit. *Minerals Engineering,* 23(2), pp. 137–142.

Sustainable Development Commission, 2011. *History of Sustainable Development.* [Online] Available at: http://www.sd–commission.org.uk/pages/history_sd.html
[Accessed 31 March 2022].

Tabelin, C. B., Park, I., Phengsaart, T., Jeon, S., Villacorte-Tabelin, M., Alonzo, D., Yoo, K., Ito, M. & Hiroyoshi, N., 2021. Copper and critical metals production from porphyry ores and E-wastes: A review of resource availability, processing/recycling challenges, socio-environmental aspects, and sustainability issues. *Resources, Conservation and Recycling,* 170, pp.1–35.

Tarshizi, E., 2015. Using Discrete Simulation & Animation to Identify the Optional Sizes and Locations of Mine Refuge Chambers. In: S. Bandopadhyay, ed. *Application of computers and*

operations research in the mineral industry. Englewood (CO): Society for Mining Metallurgy & Exploration Inc. (SME).

Taskinen, P., Akdogan, G., Kojo, I., Lahtinen, M. & Jokilaakso, A., 2018. Matte converting in copper smelting. *Mineral Processing and Extractive Metallurgy,* 128(1), pp. 1–16.

Tenenhaus, M., 1998. *La regression PLS: Théorie et pratique.* Paris (FR): Éditions Technip.

Thella, J. S., 2018. *The influence of mineralogy and surface chemistry on flotation of Cortez complex carbonaceous double refractory gold ore,* Brisbane (QLD): University of Queensland [PhD Thesis].

Tieleman, T. & Hinton, G., 2012. Lecture 6.5 – RMSProp: Divide the Gradient by a Running Average of Its Recent Magnitude. *COURSERA: Neural Networks for Machine Learning,* 4(2), pp. 26–31.

Tomra Sorting GmbH, 2021. *XRT Sorting Technology Adds Value to Your Sulphide–Associated Gold Mining.* [Online]
Available at: https://www.tomra.com/en/sorting/mining/segments/non–ferrous–metal–sorting/gold/sulphide–associated–gold [Accessed 10 November 2021].

Trefethen, L. N. & Bau III, D., 1997. *Numerical Linear Algebra.* 1st ed. Philadelphia (PA): Society for Industrial and Applied Mathematics (SIAM).

Tripodi, E., Rueda, J., Cespedes, C., Vega, J. & Gomez, C., 2019. Characterization and geostatistical modelling of contaminants and added value metals from an abandoned Cu-Au tailing dam in Taltal (Chile). *Journal of South American Earth Sciences,* 93(1), pp. 183–202.

Tunsu, C., Menard, Y., Ekberg, C. & Petranik, M., 2019. Recovery of critical materials from mine tailings: A comparative study of the solvent extraction of rare earths using acidic, solvating and mixed extractant systems. *Journal of Cleaner Production,* 218(1), pp. 425–437.

U.S. Geological Survey, 2021. *Mineral Commodity Summaries 2021,* Reston (VA): U.S. Department of the Interior.

Upadhyay, S. P. & Askari-Nasab, H., 2018. Simulation and optimization approach for uncertainty-based short-term planning in open pit mines. *International Journal of Mining Science and Technology,* Volume 28, pp. 153–166.

Vagenas, N., 1999. Applications of discrete-event simulation in Canadian mining operations in the nineties. *International Journal of Surface Mining, Reclamation and Environment,* 13(1), pp. 77–78.

Van Gosen, B. S., Verplanck, P. L., Seal, R. R., Long, K. R. & Gambogi, J., 2017. Rare-earth elements. In: K. J. Schulz, J. H. DeYoung, R. R. Seal & D. C. Bradley, eds. *Critical mineral resources of the United States – Economic and environmental geology and prospects for future*

supply: U.S. Geological Survey Professional Paper 1802. Reston (VA): U.S. Geological Survey, pp. 1–31.

Vann, J., Bertoli, O. & Jackson, S., 2002. An overview of geostatistical simulation for quantifying risk. In: S. M. Searston & R. J. Warner, eds. *Proceedings of the Quantifying Risk and Error Symposium.* Perth (WA): Geostatistical Association of Australasia, pp. 1–12.

Vaziri, V., Sayadi, A. R., Mousavi, A., Parbhakar-Fox, A. & Monjezi, M., 2021. Mathematical modeling for optimized mine waste rock disposal: Establishing more effective acid rock drainage management. *Journal of Cleaner Production,* Volume 288, pp. 1–9.

Verly, G. W., 1993. Sequential Gaussican Cosimulation: A Simulation Method Integrating Several Types of Information. In: A. Soares, ed. *Geostatistics Tróia '92 (Volume 1).* Dordrecht (NL): Kluwer Academic Publishers (Springer), pp. 543–554.

Villanueva, M., Calderón, C., Saldaña, M. & Toro, N., 2020. *Modelling a SAG grinding system through multiple regressions.* Brno (CZ), Scopus.

Wackernagel, H., 2003. *Multivariate Geostatistics: An Introduction with Applications (3rd Edition).* Springer Science & Business Media.

Wallace, D., Tipman, R., Komishke, B., Wallwork, V. & Perkins, E., 2004. Fines/water interactions and consequences of the presence of degraded illite on oil sands extractability. *Canadian Journal of Chemical Engineering,* 82(4), pp. 667–677.

Wang, C., Harbottle, D., Liu, Q. & Xu, Z., 2014. Current state of fine mineral tailings treatment: A critical review on theory and practice. *Minerals Engineering,* 58(1), pp. 113–131.

Wang, J. S. & Han, S., 2015. Feed-Forward neural network soft–sensor modeling of flotation process based on particle swarm optimization and gravitational search algorithm. *Comput. Intell. Neurosci.,* Volume 6, pp. 1–10.

Wang, S., Davenport, W., Siegmund, A., Yao, S., Gonzales, T., Walters, G. & George, D., 2016. Copper Smelting: 2016 World Copper Smelter Data (Paper PY1–1). In: *Proceedings of the Copper 2016 Conference.* Tokyo (JP): The Mining and Materials Processing Institute of Japan.

Wang, X., Qin, W., Jiao, F., Yang, C., Cui, Y., Li, W., Zhang, Z. & Song, H., 2019. Mineralogy and Pretreatment of a Refractory Gold Deposit in Zambia. *Minerals,* 9(406), pp. 1–16.

Wang, Y. X., Zhang, T. A., Zhang, Y. H., Lyu, G. Z. & Zhang, W. G., 2019. Mineral transformation in treating low–grade bauxite using the calcification–carbonization process and preparing cement clinker with the obtained residue. *Minerals Engineering,* 138(1), pp. 139–147.

Watt, L. & Kapusta, J., 2019. The 2019 Copper Smelting Survey. In: *Proceedings of the Copper 2019 Conference (Phillip Mackey Honorary Symposium), Vancouver (BC).* Montreal (QC): The Canadian Institute of Mining, Metallurgy and Petroleum.

Wightman, D. M. & Pemberton, S. G., 1997. The Lower Cretaceous (Aptian) McMurray Formation: An overview of the McMurray Area, Northeastern Alberta. In: G. S. Pemberton & D. P. James, eds. *Petroleum Geology of the Cretaceous Lower Mannville Group: Western Canada: Canadian Society of Petroleum Geologists Memoir 18.* Calgary (AB): Canadian Society of Petroleum Geologists (CSPG), pp. 312–344.

Wilkomirsky, I., Parra, R., Parada, F., Balladares, E., Etcheverry, J. & Diaz, R., 2020. Partial Roasting of High-Arsenic Copper Concentrates. *Metallurgical and Materials Transactions B,* Volume 51, pp. 2030–2038.

Wilson, R., Toro, N., Naranjo, O., Emery, X. & Navarra, A., 2021a. Integration of geostatistical modeling into discrete event simulation for development of tailings dam retreatment applications. *Minerals Engineering,* 164(2021), p. 106814.

Wilson, R., Mercier, P. H. J., Patarachao, B. & Navarra, A., 2021b. Partial Least Squares Regression of Oil Sands Processing Variables Within Discrete Event Simulation Digital Twin. *Minerals,* 11(689), pp. 1–30.

Wilson, R., Perez, K., Toro, N., Parra, R., Mackey, P. J. & Navarra, A., 2021c. Mine–to–smelter integration framework for regional development of porphyry copper deposits within the Chilean context. *Canadian Metallurgical Quarterly,* pp. 1–15.

Wilson, R., Mercier, P. H. J. & Navarra, A., 2022a. Integrated Artificial Neural Network and Discrete Event Simulation Framework for Regional Development of Refractory Gold Systems. *Mining,* 2(1), pp. 123–154.

Wilson, R., Reynolds, A. & Navarra, A., 2022b. Dynamic Renewable Energy–Driven Framework Development for Mineral Processing Circuits. In: MetSoc, ed. *Proceedings of the 61st Annual Conference of Metallurgists (COM 2022).* Montreal (QC): Springer Nature.

Winstin, W. & Goldberg, J., 2004. The EOQ with uncertain demand: the (r, q) and (s, S) models. In: *Operations Research: Applications and Algorithms (Section 16.6).* Boston (MA): Cengage Learning, pp. 895–902.

Wolstenholme, E. F. & Holmes, R. K., 1985. The design of colliery information and control systems. *European Journal of Operational Research,* 20(2), pp. 168–181.

World Bank Group, 2020. *Minerals for climate action: the mineral intensity of the clean energy transition,* Washington (D.C.): The World Bank Group.

World Gold Council, 2021. *World Gold Council.* [Online]
Available at: https://www.gold.org/ [Accessed 8 November 2021].

Wotruba, H. & Robben, C., 2020. Sensor-based ore sorting in 2020. *Automatisierungstechnik,* 68(4), pp. 231–238.

Wuest, T., Weimer, D., Irgens, C. & Thoben, K.-D., 2016. Machine learning in manufacturing: advantages, challenges, and applications. *Production & Manufacturing Research,* 4(1), pp. 23–45.

Xiao, D., Li, H. & Jiang, G., 2019. *Spectral and BP Neural Network Research on Classification of Iron Ore.* Wuhan (CN).

Xie, W., Zeng, Q., Zhou, L., Lan, T., Wang, R., Wu, J., 2022. Ore Genesis of the Baishitouwa Quartz–Wolframite Vein–Type Deposit in the Southern Great Xing'an Range W Belt, NE China: Constrains from Wolframite In–Situ Geochronology and Geochemistry Analyses. *Minerals,* 12(515), pp. 1–33.

Yadav, A., Yadav, K. & Sircar, A., 2021. Feedforward Neural Network for joint inversion of geophysical data to identify geothermal sweet spots in Gandhar, Gujarat, India. *Energy Geoscience,* 2(3), pp. 189–200.

Yamamoto, J. K., 2005. Correcting the smoothing effect of ordinary kriging estimates. *Mathematical Geology,* 37(1), pp. 69–94.

Yang, Y., Li, C., Liu, S., Min, H., Yan, C., Yang, M. & Yu, J., 2020. Classification and identification of brands of iron ores using laser–induced breakdown spectroscopy combined with principal component analysis and artificial neural networks. *Anal. Methods,* Volume 12, pp. 1316–1323.

Young, J., 2001. Portland Cements. In: K. H. J. Buschow, R. W. Cahn, M. C. Flemings, B. Ilschner, E. J. Kramer, S. Mahajan & P. Veyssiere, eds. *Encyclopedia of Materials: Science and Technology, 2nd Ed..* New York (NY): Elsevier Ltd., pp. 7768–7773.

Zhang, W., Wang, W. & Wu, F., 2012. The Application of Multivariable Optimum Regression Analysis to Remote Sensing Imageries in Monitoring Landslide Disaster. *Energy Procedia,* 16(2012), pp. 190–196.

Zhao, S., Kotlyar, L. S., Sparks, B. D., Woods, J., Gao, J. & Chung, K., 2001. Solids contents, properties and molecular structures of asphaltenes from different oilsands. *Fuel,* Volume 80, pp. 1907–1914.

Zhu, G., Cao, Y., Wang, Y., Wang, X., Miller, J. D., Lu, D. & Zheng, X., 2020. Surface chemistry features of spodumene with isomorphous substitution. *Minerals Engineering,* Volume 146, p. 106139.